EPFL

Thèse n°9911

Deconstructing and Reconstructing the Complexity of Tau pathology

Présentée le 31 mars 2023

Faculté des sciences de la vie
Laboratoire de neurobiologie moléculaire et neuroprotéomique
Programme doctoral en neurosciences

pour l'obtention du grade de Docteur ès Sciences

par

Galina LIMORENKO

Acceptée sur proposition du jury

Dr B. Schneider, président du jury
Prof. H. Lashuel, directeur de thèse
Prof. P. Paganetti, rapporteur
Prof. E. Wanker, rapporteur
Prof. P. De Los Rios, rapporteur

École polytechnique fédérale de Lausanne

2023

xx

Dedicated to my mum Lilija, grandmas Alla and Liudmila

TABLE OF CONTENTS

xx

ACKNOWLEDGEMENTS

“I’m sciencing as fast as I can!”
Professor Hubert Farnsworth

Rick Sanchez: “*Any of your, uh, scientists working on anything new?”*
Teenyverse President: “*All of them. That's their job.”*

I love my job, and there is never enough time to do all the experiments and have all the discussions. Good science is a collective effort, and I have been very privileged to be a part of a wonderful team, driven in their work, focused on bringing the best practices to the field, and deeply caring about the community and patients.

Professor Hilal Lashuel has played important roles in my academic upbringing, both as a supervisor and a mentor. LMNN team members have been an extended professional family – past and present, namely: Anne-Laure Mahul-Mellier, Bryan Frey, Driss Boudeffa, Enzo Morro, Marie Rodriguez, Melek Firat Altay, Nadine Ait-Bouziad, Nathan Riguet, Niran Maharjan, Pedro Magalhães, Rajasekhar Kolla, Sonia Donzetti, Theodora Paganaki, Yllza Jasiqi. I’d like to extend my gratitude to the collaborators: EPFL core facilities and super-helpful staff; AbbVie team; Neuroscience PhD program staff; EPFL admin and media staff, and all others that I have had pleasure of working with.

This journey could not have been possible without love and support of my parents Lilija Limorenko and Vitalijus Galvrilovas, grandmothers Alla Lachmickaja and Liudmila Limorenko.

Special thanks to Christopher Dennett, with whom every day can be wrapped up in carcinization and soothing sounds of J-pop. I am grateful to all my friends and members of different scientific, neurodiverse and skeptic communities that have been important parts of my support systems.

And, of course, my piggos Rick Sanchez, Morty, Beth, Jerry and Summer Smith, Evil Rick, Birdperson, Krombopulos Michael and Amy, and Gaia The Sentient Planet have been instrumental in reminding me that sleep and carrots are important.

Motivation, enthusiasm and discipline is what gets me out of bed and into a lab coat. I hope to continue representing the values of open scientific enterprise, promoting diversity and inclusion within the scientific community, and bringing science to wider public.

xx

ABSTRACT (ENGLISH)

This thesis consists of four Chapters unified by a singular theme – how do we develop disease models that faithfully reproduce the pathology seen in patients suffering from neurodegenerative disorders associated with the Tau protein, such as Alzheimer's disease? To answer this question, we must first understand the underlying mechanisms leading to the formation and progression of Tau pathology in detail. Next, it is necessary to scrutinize the models that are being used for the research and development of therapies and drugs. And finally, it is important to discover novel approaches to study the pathological mechanisms that are occurring in the brain and develop models that are accurate and will have a high potential to lead to successful translation of the laboratory findings to the patients.

In Chapter 1 "*To target Tau pathologies, we must embrace and reconstruct their complexities*" and Chapter 2 "*Revisiting the grammar of Tau aggregation and pathology formation: How new insights from brain pathology are shaping how we study and target Tauopathies*" we present the in-depth review of the Tau investigation field, and the in vitro and in cell models available. We review how our understanding of Tau aggregation and pathology formation has evolved over the past few decades, and present an analysis of new findings and insights from recent studies illustrating the biochemical, structural, and functional heterogeneity of Tau aggregates. Our analyses identify specific knowledge gaps and call for 1) embracing the complexities of Tau pathologies; 2) reassessment of current approaches to investigate, model and reproduce pathological Tau aggregation as it occurs in the brain; 3) more research toward a better understanding of the natural cofactors responsible for triggering Tau aggregation and pathology formation; and 4) developing improved approaches for in vitro production of the Tau aggregates and fibrils that recapitulate and/or amplify the biochemical and structural complexity and diversity of pathological Tau in Tauopathies. We discuss the importance of adopting new experimental approaches that embrace the complexity of Tau aggregation and pathology as an important first step towards developing mechanism- and structure-based therapies that account for the pathological and clinical heterogeneity of Alzheimer's disease and Tauopathies.

In Chapter 3 "*ClearTau: a novel efficient method for production of pathology-resembling co-factor-free Tau fibrils*" we present a novel, quick, cheap method for producing completely co-factor-free fibrils. We show that Tau fibrils generated using this method – ClearTau fibrils - exhibit amyloid-like features and morphological properties more reminiscent of the properties of the brain-derived Tau fibrils compared to the in vitro Tau fibrils produced by standard methods of preparation. The ClearTau fibrils retain the ability to bind RNA, share some structural/morphological features with brain-derived pathological fibrils and induce efficient seeding of Tau aggregation in vitro, in biosensor cells, and human neurons. As a proof of

concept, we use the ClearTau assay as a platform for screening Tau aggregation modulator compounds. Finally, the generation of ClearTau fibrils also paves the way for a more systematic analysis of Tau post-fibrillization PTMs and fibril interactome without interference from heparin or heparin-induced polymorphisms. Our novel method for in vitro ClearTau fibril production represents a crucial milestone for developing accessible, cheap, and high-fidelity tools for studying the Tau fibrillization processes relevant to neurodegenerative diseases. Furthermore, these advances open new opportunities to investigate the pathophysiology of disease-relevant Tau aggregates and will facilitate the development of Tau pathology-targeting and modifying therapies and PET tracers that can distinguish between different Tauopathies.

Finally, in Chapter 4 "*What exactly are Tau biosensor assays sensing? In-depth characterization of the commonly used cellular model thought to report on the Tau seeding propensity*" we are closely interrogating the widely-used cellular model. We ask three key questions: a) does TauRD cellular assay truly report the aggregation-triggering propensity of the transduced Tau seeds; b) can it determine the differences between the various types of Tau seeds; and c) what cell physiological processes are implicated in the output generation of the TauRD system? Ultimately, we seek to answer the question of whether this and similar systems can be reliably used as a characterization technique for Tau seeding propensity, and give recommendations on what is needed to improve it. We extensively characterized and assessed the TauRD system using observational, functional, and interventional assays, including imaging, CLEM, and biochemistry. Our findings suggest that a) the TauRD system does not explicitly report on the human pathology-relevant seeding propensity of the Tau seeds; b) the TauRD system does not faithfully distinguish between different types of seeds, and c) the formation of the expected output is heavily dependent on the cellular proteostasis functioning. We show how cells are responding to the Tau fibrillar seeds, and how it impacts their physiology.

Collectively, this work presents a) the in-depth review of current knowledge and state of the art of Tau research; b) identifies shortcomings and gaps in research; c) presents a novel in vitro model to study Tau aggregation and d) scrutinizes the widely-used Tau cellular model and dives deep into the mechanisms of cell responses to Tau fibrillar seed.

We believe that the development of models that faithfully reproduce the disease aspects in vitro and in cells is essential to develop effective diagnostics and therapies to treat neurodegenerative diseases.

RÉSUMÉ (FRANÇAIS)

Cette thèse se compose de quatre chapitres réunis sous un thème singulier : comment développer des modèles de pathologies reproduisant fidèlement celle observée chez les patients souffrant de troubles neurodégénératifs associés à la protéine Tau, comme la maladie d'Alzheimer ? Pour répondre à cette question, nous devons d'abord comprendre en détails les mécanismes sous-jacents conduisant à la formation et à la progression de la pathologie Tau. Ensuite, il est nécessaire d'examiner de près les modèles utilisés pour la recherche et le développement de thérapies et de médicaments. Enfin, il est important de découvrir de nouvelles approches pour étudier les mécanismes pathologiques qui se produisent dans le cerveau et de développer des modèles qui précis qui auront un fort potentiel à mener une transposition réussie des résultats de la recherche dans le contexte des patients.

Dans le chapitre 1 "Pour cibler les pathologies Tau, nous devons étreindre et reconstruire leurs complexités" et le chapitre 2 "Revisiter la grammaire de l'agrégation de Tau et de la formation de pathologies : Comment les nouvelles connaissances issues de la pathologie cérébrale influencent la manière dont nous étudions et ciblons les tauopathies", nous présentons un examen approfondi du champ d'investigation de Tau et des modèles in vitro et cellulaires disponibles. Nous examinons l'évolution au cours des dernières décennies de notre compréhension de l'agrégation de la protéine Tau et de la formation de pathologies , et nous présentons une analyse des nouveaux résultats et des idées issues d'études récentes illustrant l'hétérogénéité biochimique, structurelle et fonctionnelle des agrégats de Tau. Nos analyses identifient des lacunes spécifiques dans les connaissances et appellent à 1) déchiffrer les complexités des pathologies Tau ; 2) réévaluer les approches actuelles pour étudier, modéliser et reproduire l'agrégation pathologique de Tau telle qu'elle se produit dans le cerveau ; 3) intensifier les recherches en vue de mieux comprendre les cofacteurs naturels responsables du déclenchement de l'agrégation de la protéine Tau et de la formation de la pathologie ; et 4) mettre au point de meilleures méthodes de production in vitro d'agrégats et de fibrilles de protéine Tau qui reproduisent et/ou amplifient la complexité et la diversité biochimiques et structurelles de la protéine Tau pathologique dans les tauopathies. Nous discutons de l'importance d'adopter de nouvelles approches expérimentales qui tiennent compte de la complexité de l'agrégation et de la pathologie de la protéine Tau. Il s'agit d'une première étape importante vers le développement de thérapies fondées sur les mécanismes et la structure qui tiennent compte de l'hétérogénéité pathologique et clinique de la maladie d'Alzheimer et des tauopathies.

Dans le chapitre 3 "ClearTau : une nouvelle méthode efficace pour la production de fibrilles Tau sans cofacteur ressemblant à une pathologie", nous présentons une nouvelle méthode rapide et bon marché/abordable pour produire des fibrilles en l'absence de cofacteur. Nous

montrons que les fibrilles Tau générées par cette méthode - les fibrilles ClearTau - présentent des caractéristiques de type amyloïde et des propriétés morphologiques qui rappellent davantage les propriétés des fibrilles Tau dérivées du cerveau que celles produites in vitro par des méthodes de préparation standard. Les fibrilles ClearTau conservent la capacité de lier l'ARN, partagent certaines caractéristiques structurelles/morphologiques avec les fibrilles pathologiques dérivées du cerveau et induisent un ensemencement efficace de l'agrégation de Tau in vitro, dans des cellules biocapteurs et des neurones humains. Comme preuve de concept, nous utilisons le test ClearTau comme plateforme pour cribler les composés modulateurs de l'agrégation de Tau. Enfin, la génération de fibrilles ClearTau ouvre également la voie à une analyse plus systématique des PTMs post-fibrillation de Tau et de l'interactome des fibrilles sans interférence de l'héparine ou des polymorphismes induits par l'héparine. Notre nouvelle méthode de production in vitro de fibrilles de ClearTau représente une étape cruciale dans le développement d'outils accessibles, bon marché et de haute fidélité pour l'étude des processus de fibrillation de Tau pertinents pour les maladies neurodégénératives. En outre, ces avancées ouvrent de nouvelles possibilités d'étudier la physiopathologie des agrégats de Tau pertinents/d'intérêt pour les maladies et faciliteront le développement de thérapies ciblant et modifiant la pathologie Tau et de traceurs TEP capables de distinguer les différentes tauopathies.

Enfin, dans le chapitre 4 "Qu'est-ce que les tests de biocapteurs Tau détectent exactement ? Caractérisation approfondie du modèle cellulaire couramment utilisé et censé rendre compte de la propension à l'agrégation de Tau", nous interrogeons de près le modèle cellulaire largement utilisé. Nous posons trois questions clés : a) le test cellulaire TauRD rend-il vraiment compte de la propension à déclencher l'agrégation des seeds de Tau transduites ; b) peut-il déterminer les différences entre les divers/différents types de seeds de Tau ; et c) quels processus physiologiques cellulaires sont impliqués dans la génération de la sortie du système TauRD ? En fin de compte, nous cherchons à savoir si ce système et d'autres similaires peuvent être utilisés de manière fiable comme technique de caractérisation de la propension au seeding de Tau, et à formuler des recommandations pour l'améliorer. Nous avons largement caractérisé et évalué le système TauRD en utilisant des tests d'observation, fonctionnels et interventionnels, y compris l'imagerie, le CLEM et la biochimie. Nos résultats suggèrent que a) le système TauRD ne rend pas explicitement compte de la propension au seeding de Tau, pertinente pour la pathologie humaine ; b) le système TauRD ne fait pas fidèlement la distinction entre les différents types de seeds, et c) la formation du résultat attendu dépend fortement du fonctionnement de la protéostase cellulaire. Nous montrons comment les cellules réagissent aux seeds fibrillaires de Tau, et comment cela a un impact sur leur physiologie.

Collectivement, ce travail présente a) un examen approfondi des connaissances actuelles et de l'état de l'art de la recherche sur la protéine Tau ; b) identifie les lacunes et les insuffisances de la recherche ; c) présente un nouveau modèle in vitro pour étudier l'agrégation de la protéine Tau et d) examine minutieusement le modèle cellulaire Tau largement utilisé et plonge dans les mécanismes des réponses cellulaires aux seeds fibrillaires de Tau.

Nous pensons que le développement de modèles qui reproduisent fidèlement les aspects de la maladie in vitro et dans les cellules est essentiel pour mettre au point des diagnostics et des thérapies efficaces pour traiter les maladies neurodégénératives.

xx

CHAPTER 1

To target Tau pathologies, we must embrace and reconstruct their complexities

Galina Limorenko[#] and Hilal A. Lashuel[#*]

Laboratory of Molecular and Chemical Biology of Neurodegeneration, Brain Mind Institute, École Polytechnique Federal de Lausanne (EPFL), CH-1015 Lausanne, Switzerland.

* Corresponding Author: hilal.lashuel@epfl.ch

# Equal Contribution

Keywords

Microtubule-associated protein Tau, Tau, Heparin, Tau aggregation, Tau fibrillization, PHF, Tau PTMs

Neurobiology of Disease 2021 Dec;161:105536.

doi: 10.1016/j.nbd.2021.105536.

Abstract

The accumulation of hyperphosphorylated fibrillar Tau aggregates in the brain is one of the defining hallmarks of Alzheimer's disease (AD) and other Tauopathies. However, the primary events or molecules responsible for triggering Tau aggregation and pathology formation remain unknown. The discovery of heparin as an effective inducer of Tau aggregation *in vitro* was instrumental to enabling different lines of research into the role of Tau aggregation in the pathogenesis of Tauopathies. However, recent proteomics and cryogenic electron microscopy (cryo-EM) studies have revealed that heparin-induced Tau fibrils generated in vitro do not reproduce the biochemical and ultrastructural properties of disease-associated brain-derived Tau fibrils. These observations demand that we reassess our current approaches to investigate the mechanisms underpinning Tau aggregation and pathology formation. In this review article, we present an up-to-date analysis of 1) how our understanding of the Tau-heparin interactions has evolved over the years, 2) the various structural and mechanistic models of the heparin-induced Tau aggregation, 3) the similarities and differences between pathological and heparin-induced Tau fibrils; and 4) emerging concepts on the biochemical and structural determinants underpinning Tau pathological heterogeneity in Tauopathies. Our analyses identify specific knowledge gaps and call for 1) embracing the complexities of Tau pathologies; 2) reassessment of current approaches to investigate, model and reproduce pathological Tau aggregation as it occurs in the brain; 3) more research towards a better understanding of the natural cofactors responsible for triggering Tau aggregation and pathology formation; and 4) developing improved approaches for *in vitro* production of the Tau aggregates and fibrils that recapitulate and/or amplify the biochemical and structural complexity and diversity of pathological Tau in Tauopathies. This will result in better and more relevant tools, assays, and mechanistic models, which could significantly improve translational research and the development of drugs and antibodies that have higher chances for success in the clinic.

To target Tau pathology, we must embrace and reconstruct its complexity

Galina Limorenko and Hilal A. Lashuel*

Laboratory of Molecular and Chemical Biology of Neurodegeneration, BMI, EPFL, Switzerland

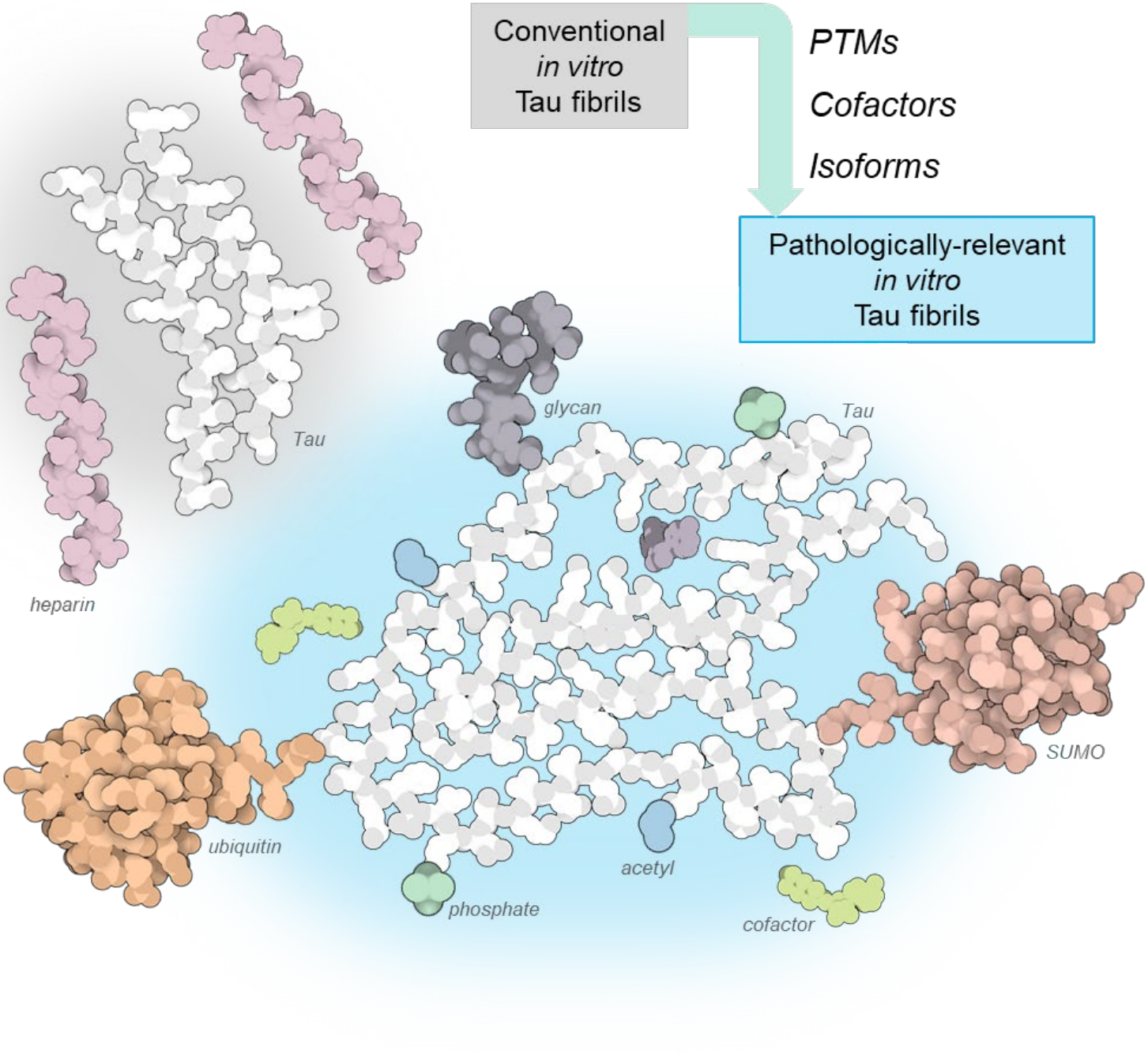

Introduction

The Microtubule-Associated Proteins (MAPs) are predominantly involved in the cytoskeletal dynamics, and MAP Tau is also the major component of neurofibrillary tangles (NFTs) found in the brain of Alzheimer's disease (AD) and other Tauopathies' patients. Within NTFs, Tau protein isoforms exist mostly in an aggregated, heavily modified, and fibrillar forms, including hyperphosphorylated paired helical fibrils (PHFs) and straight fibrils (SFs) in AD [1-3]. In the central nervous system (CNS), Tau is present in six isoforms (Figure 1 A) due to alternative splicing of the *MAPT* gene [4], all of which belong to the intrinsically-disordered protein (IDP) class. IDPs are highly soluble proteins that do not maintain a stable structure under normal conditions but fold or adopt partial structures upon interacting with other proteins, ligands, membranes, or organelles. The longest Tau isoform 4R2N is one of the largest IDPs known [5]. Under physiological conditions, the shortest Tau isoform 3R0N is predominantly found during brain development [6,7].

Tau isoforms contribute to a plethora of varied molecular and cellular functions in neurons and other cells (for a recent review see [8]). In neuronal cells, under normal conditions, Tau is predominantly localized to axonal compartment [9] and is involved in axonal [10] and synaptic functions [11,12] as well as in neurovascular coupling processes [13]. By virtue of its MT-binding profile, Tau was found to carry out important roles in cytoskeletal maintenance [14], mitochondrial transport [15], trafficking of cargo along microtubules [16], cell signalling [17], and maintenance of chromatin organization [18,19]. Tau is also involved in many cellular processes and pathways, such as stress responses [20] and cell proliferation [21].

Tau sequence can be subdivided into functionally distinct regions, where the N-terminal projection domain is involved in the microtubule (MT) spacing [22] and plasma membrane association [23], modulated by the N-terminal inserts [24] (Figure 1). Mid-domain is rich in prolines and is known to bind proline-dependent kinases [25]. MTBR and the C-terminal domains are involved in the regulation of MT stability and are implicated in Tau aggregation [26], among other functions

Tau 4R2N is the most often used full-length isoform in Tau studies. It contains 441 amino acids (~45.9 kDa) [27], occupies an effective volume of ~56 nm^3 [28], and has a radius of gyration of approximately 6.6 nm, as measured by small-angle X-ray scattering [29]. Tau amino acid sequence is subdivided into several regions (Figure 1 B): the N-terminal region (1-44), the inserts N1 (45-74) and N2 (75-103), the mid-domain (104-150), the proline-rich regions P1 (151-198) and P2 (199-243), the microtubule-binding region (MTBR; 244-370) and the C-terminal region (371-441) [30]. The MTBR of 4R Tau comprises four repeat domains R1 (amino

acids 244-274), R2 (275-305), R3 (306-336), and R4 (338-370), in the 3R tau isoform R2 is missing. MTBR is the primary driver of Tau proteins' aggregation [31]. Tau isoforms in the CNS comprise either none, one or two N-terminal inserts (0N, 1N, 2N) in the presence or absence of the R2 [4] with molecular weights ranging from ~37 to 46 kDa (Figure 1 A). In the adult brain, approximately half of the expressed Tau isoforms contain one N-terminal insert, ~40% contain none, and around 10% contain two N repeats, whereas 3R and 4R-containing isoforms are expressed at approximately equal levels [32-35].

Figure 1. Tau sequences and isoforms. A. Tau isoform alignment. Six Tau isoforms are found in the central nervous system. They differ by differential inclusion of N1, N2, and R2. The PHF6* sequence motif is a constituent of R2, whereas PHF6 is a part of R3 repeats. B.

4R2N, K18, and K19 Tau sequences. Tau sequence is subdivided into several domains based on alternative splicing of MAPT gene, which gives rise to N-terminal sequence; inserts N1 (Exon 2) and N2 (Exon 3); mid-domain and proline-rich stretches P1 and P2 (Exon 7); microtubule-binding repeats R1, R2 (Exon 10), R3 and R4; and C-terminal region. The commonly used Tau fragment K18 is derived from 4R MTBR, whereas the K19 fragment is derived from 3R MTBR plus the flanking amino acids L243, I371, and E372 [30]. The numbering of amino acids is based on the full-length Tau 4R2N sequence used in [30] for consistency throughout this work. The colour scheme and numbering are preserved throughout the article.

Tau contribution to neurodegenerative disorders

Tau misfolding and aggregation have been implicated in several neurodegenerative disorders through a combination of gain of toxic functions and loss of normal functions mechanisms, due to the reduction of the available functional pool of soluble Tau molecules [36]. Several Tau mutations were associated with primary familial Tauopathies, such as frontotemporal dementia linked to chromosome 17q21 (FTDP) or PiD, however, no mutations have been found in sporadic secondary Tauopathies, such as AD [37]. The levels of soluble non-phosphorylated and phosphorylated Tau proteins in CSF of AD patients are commonly used as an early marker of the neurodegenerative disease inception and progression. Several studies had shown that the levels of specific Tau species in the CSF [38], or the level of Tau pathology in the brain using PET imaging (reviewed in [39]) correlated with the onset and progression of patients' cognitive decline [40]. This, combined with the failure of several amyloid-targeting therapies in the clinic [41,42], has led to a renewed interest in the role of Tau in the pathogenesis of Tauopathies and as a prime target for developing diagnostics and therapies for these devastating diseases.

AD is one of the leading causes of dementia with the largest impact on the health and economies of developed nations worldwide. Therefore, studies aimed at elucidating the mechanisms of Tau aggregation and pathology formation had predominantly focused on the recapitulation of the signatory twisted PHFs seen in AD patient brain-derived samples using full-length Tau isoform 4R2N. In 3R and 4R primary Tauopathies, including PiD [43] and CBD [44,45], respectively, however, the ratios of these isoforms are perturbed. This leads to variable incorporation of Tau isoforms into insoluble inclusions that contain either predominantly 3R or 4R aggregated and differentially modified Tau isoforms [46,47]. In general, Western blotting analyses of dephosphorylated insoluble brain fractions, containing high molecular weight Tau species and fibrils, from Tauopathy patients show six bands corresponding to all six Tau isoforms, three 3R or three 4R isoform bands [48,49]. Based on these patterns, Tauopathies are categorized into types (Figure 2) such as

a) ***mixed Tauopathies,*** *3R+4R*, that include AD, chronic traumatic encephalopathy (CTE), FTDP with mutations V337M and R406W showing all six Tau bands;

b) ***predominantly-4R Tauopathies***, such as PSP, CBD, and FTDP with mutation P301L showing three 4R bands, and

c) ***predominantly-3R Tauopathies*****,** such as PiD and FTDP with mutations G272V and Q336R showing three 3R bands.

Importantly, in most Tauopathies where the Tau isoform composition has been established, the band intensity of soluble Tau isoforms is roughly equal, signifying preferential recruitment of Tau isoforms into insoluble inclusions or upregulation of these isoforms' expression. Given their high solubility and conformational flexibility, it remains unclear what triggers Tau isoforms' aggregation in the first place.

Molecular and sequence determinants of Tau aggregation

Despite decades of active research, the primary events responsible for triggering the misfolding and fibrillization of Tau remain unknown. Much of the insight we have into the molecular and sequence determinants of Tau aggregation and pathology formation is based on 1) biochemical protein characterization and analyses of pathological Tau aggregates isolated from post-mortem brains from a small number of patients with Tauopathies; and 2) in vitro studies where Tau misfolding and aggregation is triggered using conditions that do not necessary mimic those occurring in the brain. These studies point to Tau mutations, post-translational modifications (PTMs), interactions with polyanions, or a combination of these factors as key determinants of Tau aggregation and the diversity of Tau pathology in AD and other Tauopathies.

PTMs of Tau

Tau is extensively post-translationally modified, and PTMs have differential influences on the Tau isoforms' aggregation propensities (reviewed in [50]). These modifications include phosphorylation, acetylation, deamination, methylation and dimethylation, nitration, O- and N-linked glycosylation, ubiquitination, SUMOylation, and proteolytic cleavage [51] (Figure 3 A), often with co-occurrence and cross-talk between different PTMs [52-55], (for a recent review on singular PTMs see [56]).

Taken together, a large body of careful investigations over several decades have established that Tau aggregation propensity is strongly influenced by a) the specific residue PTM positions and overall PTM patterns along Tau molecules; b) the impact of these PTMs on the local protein structure, c) the electrostatic profile and distribution of charges along Tau molecule and d) the cross-talk between different Tau PTMs leading to the synergistic, additive and subtractive effects on Tau aggregation (reviewed in [50]).

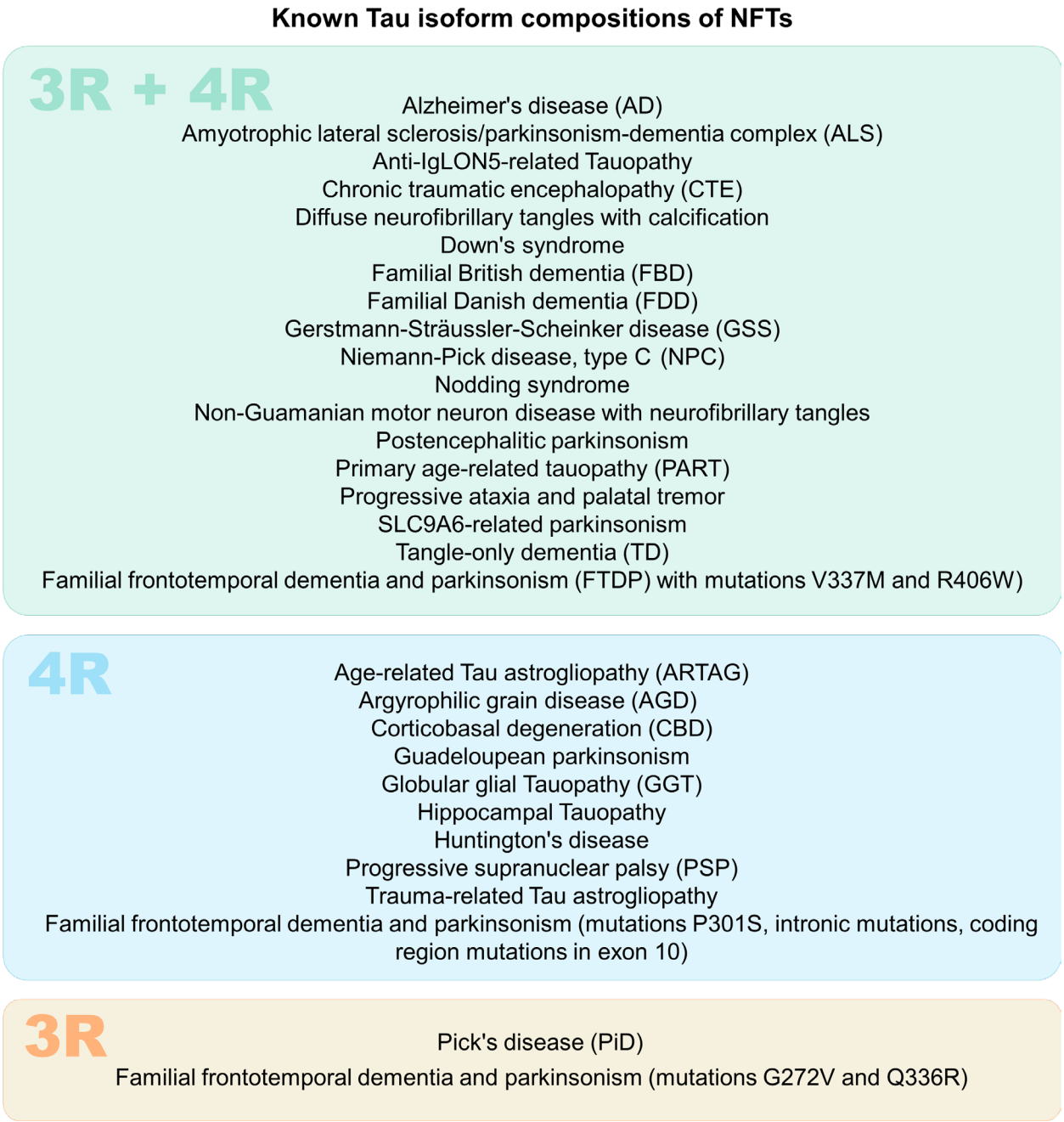

Figure 2. Isoform composition of known Tau pathologies. List of Tauopathies with known Tau isoform compositions defined as mixed Tauopathies (3R + 4R), predominantly 3R and predominantly 4R.

Cross-talk between Tau PTMs

Increasing evidence suggests that the Tau PTM code is a combinatorial code that involves the co-occurrence, spatial clustering (Figure 2 B), and cross-talk between multiple PTMs dependent on the type of disease pathology and the stage of its progression (Figure 2 C). The patterns of soluble Tau isoforms' PTMs change over the course of disease [57], however, they remain only a correlation to the underlying pathology and are not yet clearly established as its cause or consequence [58]. The complex interplay between multiple Tau PTMs appears to be tightly regulated in a hierarchical and spatio-temporal manner and is likely to occur during the various stages of fibril formation [54]. However, unravelling the complexity of the Tau PTM code is complicated by the fact that we cannot monitor changes in PTM patterns as they occur in the brain. Furthermore, thus far, most studies have focused primarily on mapping and cataloguing Tau PTMs rather than defining which PTMs co-occur on the same Tau molecule [58].

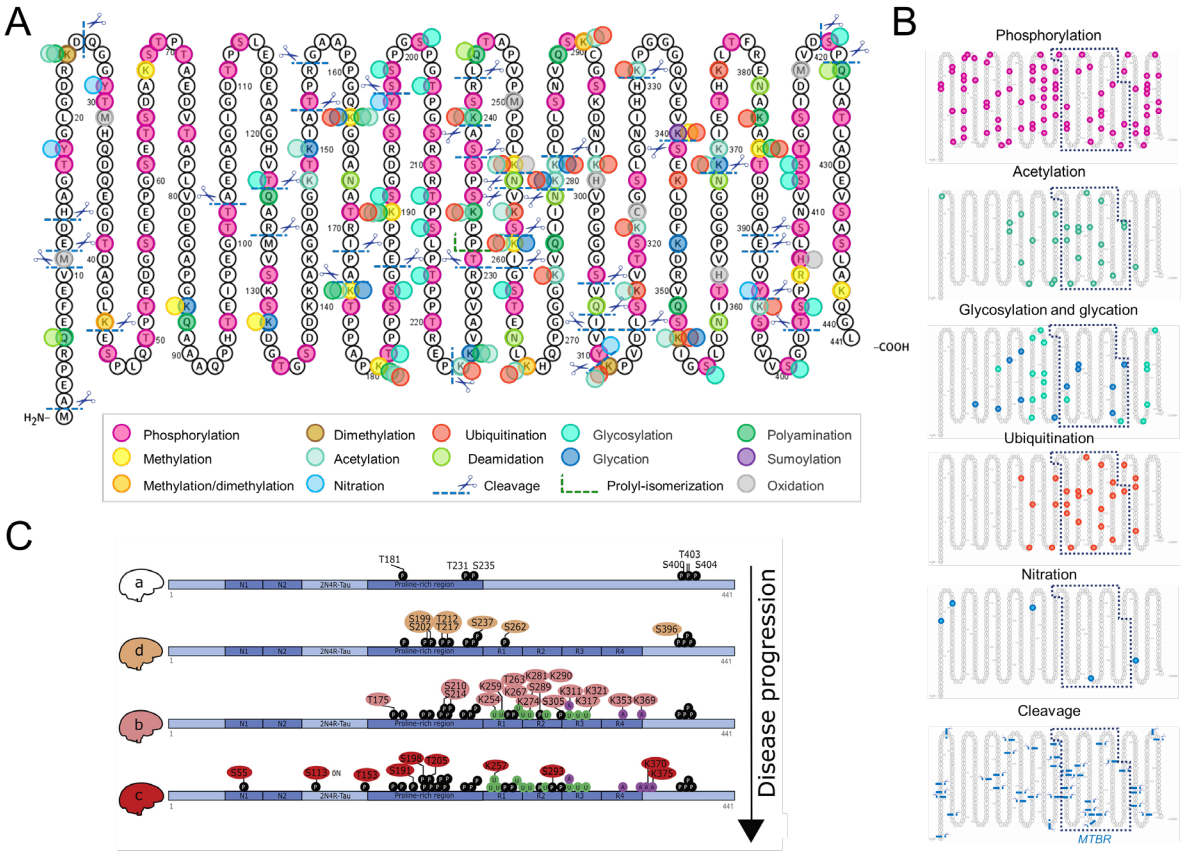

Figure 3. Tau post-translational modifications. A. Tau can be extensively modified on multiple sites at the monomer and fibril levels, producing complex PTM patterns that influence Tau's biophysical and biochemical properties. Different colours denote the different types of PTMs. Only experimentally verified (in vitro, in cells, or in vivo) modifications were included (as of December 2020). The sequence corresponds to the longest human Tau isoform 441.

B. Localization of individual sites of phosphorylation, acetylation, glycosylation and glycation, ubiquitination, nitration, and cleavage along Tau sequence. Note spatial clustering of the ubiquitination and acetylation sites in the mid- and MTBR domains. MTBR is enclosed by a dotted box. C. PTM diversity and differential pattern in AD progression from early (a) to late (b) stages (adapted from [57]).

Several studies have reported cross-talk between Tau phosphorylation and its proteolytic cleavage by different enzymes [59-63], as well as hypoacetylation [64]. Interestingly, out of the predicted 85 phosphorylation sites, only 55 were cumulatively modified in human samples [57]. Cross-talks between other PTMs were also observed, for example, between competing lysine-modification such as acetylation, methylation, glycation, SUMOylation, and ubiquitination (reviewed in [65]). O-GlcNAcylation of Tau has also been shown to influence its phosphorylation patterns, and *vice versa*, *in vitro* and in cellular systems [66-68].

In comparison to other Tau PTMs, the role of ubiquitination in regulating Tau aggregation and pathology formation remains understudied, despite the fact that it was one of first Tau PTMs to be linked to the neuropathology of Alzheimer's [69-71] and Down's syndrome with NFTs [72]. In AD patients, Tau was found both in monoubiquitinated [73] and polyubiqutinated forms [74]. Interestingly, AD-derived Tau polyubiquitination at K63 was detected on the soluble Tau [75], whereas ubiquitination at K48 was found on AD-derived insoluble Tau [74], suggesting that differentially-modified Tau species were targeted for degradation via different pathways. Immature Tau pretangles were consistently shown to be lacking in ubiquitination [76-78], whereas insoluble Tau fibrils were decorated with ubiquitin [70,79], in both mono- and polyubiquitinated forms [80,81]. Highly-ubiquitinated Tau was also detected in AD patients' CSF [82].

Functionally, there is still no consensus on what active roles, if any, Tau ubiquitination plays in the processes of Tau pathology and whether it contributes to initiation or development of Tau pathology, or is part of the cellular responses to cellular Tau aggregates. Recent work by Abreha et al. [83] revealed an unexpectedly large number of ubiquitination sites on Tau in AD patient samples. This AD ubiquitination map was further expanded to 27 residues out of possible 44 by the works of Wesseling et al. [57] and Kametani et al. [84], highlighting the enrichment of ubiquitinated sites in the Tau mid-domain and MTBR (Figure 3 B, Ubiquitination). In recent structural studies of brain-derived Tau filaments, extra electron densities were detected on the cryo-EM-resolved fibrils from AD and CBD patients' brains, which were reported to correspond to ubiquitin groups as determined by mass spectrometry [85]. Furthermore, significant changes in Tau peptide enrichment levels, including one-quarter of the peptides containing the KXGS motifs, harboured co-modifications of phosphorylation

and ubiquitination in AD patients' brains as compared to controls [83]. The ubiquitination of Tau is also regulated by other competing and non-competing PTMs. For example, SUMOylation at lysine 340 has been shown to increase Tau phosphorylation, which decreases Tau ubiquitination and subsequent degradation, thus leading to increased levels of sarcosyl-insoluble Tau in cells [86]. These studies further underscore the complexity of Tau PTMs' cross-talks and their potential role in the modulation of Tau clearance and aggregation propensities, and the formation of different types Tau fibril strains.

Tau aggregation in vitro requires interaction with cofactors

Tau proteins are highly soluble (Figure 4 A) and do not aggregate on their own *in vitro* [87]. The protein is predominantly positively charged in the mid- and the C-terminal regions, whereas, the N-terminus is predominantly negatively charged (Figure 4 B). The positively-charged regions flanking the MTBR were proposed to inhibit Tau assembly into fibrils through the electrostatic repulsion forces. This led to the hypothesis that neutralization or removal of the positive charge by binding of cofactors or Tau truncations, that eliminate positively charged regions, could accelerate Tau nucleation and fibrillization. Consistent with this hypothesis, several truncated Tau constructs of Tau self-assemble readily into the fibrils in the absence of the negatively-charged cofactors [88-90]. Furthermore, some non-specific hyperphosphorylation of Tau is sufficient to trigger its fibrillization in the absence of cofactors [91,92].

Indeed, initial attempts to induce efficient aggregation and fibrillization of full-length Tau isoforms *in vitro* in the absence of cofactors or modifications, on relevant time scales, had not been successful. Subsequent studies showed that anionic cofactors, such as heparin [93] (Figure 4 C), RNA [94], arachidonic acid [95] (Figure 4 D), free fatty acids [95], and polyglutamic acid [96,97], as well as molecules such as ethanol [98] or metal ions [99], could act as initiators and accelerate the aggregation of Tau monomers into higher-order assemblies and fibrils *in vitro.* However, the exact mechanisms of each Tau-cofactor interaction and the resulting fibril structures differ. The polysaccharide heparin is the most widely used Tau aggregation cofactor for reasons that will be explained below.

Tau aggregation mechanisms

Tau isoforms are highly soluble and exist in solution as an ensemble of disordered conformations (random coil) [28] with a presence of long-range contacts between N- and C-termini and along the Tau molecule ("paperclip" conformation) [100]. The mechanisms of Tau

oligomerization and fibrillization are complex and the molecular and cellular factors that govern these processes remain subjects of intense investigations and debate. In general, Tau aggregation commences by some sort of catalyst or cofactor-mediated 1) loss of long-range intramolecular Tau contacts, 2) conversion of disordered Tau monomers into nucleation- and aggregation-competent partially folded forms, loosely designated as “misfolded Tau”, that leads to 3) dimerization and oligomerization of Tau to form nucleus or “seed” [28,88] (Figure 5). Tau oligomerization may proceed through ON-pathways, leading to 4) formation of β-sheet-containing fibril polymorphs, or through OFF-pathways, resulting in the formation of various oligomeric structures or amorphous aggregates [101,102]. The OFF-pathway Tau oligomers may accumulate and re-enter the ON-pathway of fibrillization through monomer disassociation. Cofactor-induced ON-pathway aggregation kinetics are consistent with a nucleated polymerization mechanism and follow an S shape curve that is characterized by lag, exponential growth, and plateau phases [96,103-105] (Figure 5 A). The lag phase can be significantly shortened or eliminated by the addition of a preformed Tau aggregates, including preformed fibrils (PFFs), often referred to as nucleus or seed (Figure 5 B). Note that the *in vitro* preformed seeds are usually produced in the presence of cofactors, e.g. heparin, see below.

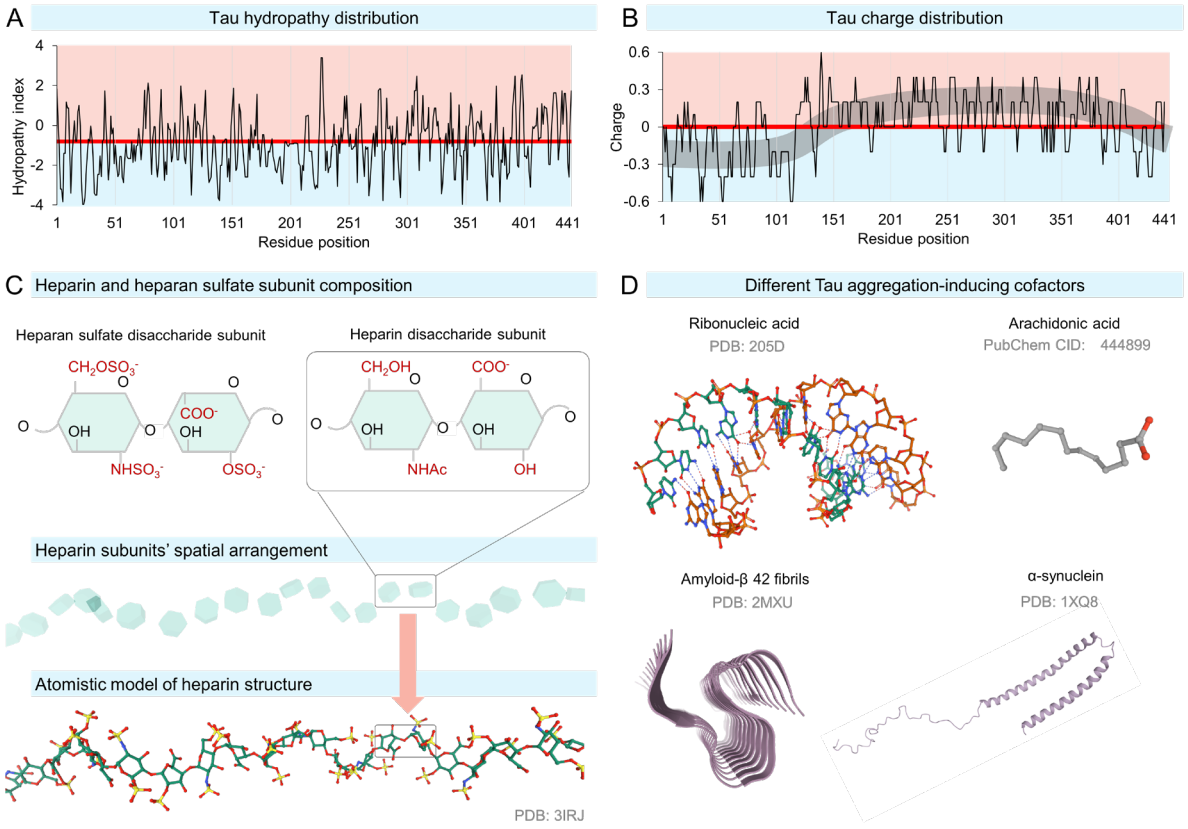

Figure 4. Tau hydrophobicity and charge distribution, and anionic aggregation cofactors. A. Hydropathic index distribution along the Tau 4R2N molecule. The red line denotes the grand average of hydropathy value of -0.868, red shading denotes more hydrophobic residues, blue shading denotes more hydrophilic residues. Estimations are based on the method by Kyte and Doolittle (1982) [106]. B. Schematic of charge distribution along the Tau molecule. The N- and C-termini are slightly negatively charged, whereas the mid-domain is predominantly positively charged. Red shading denotes positive charge, blue shading denotes negative charge, grey shading illustrates the predominance of positively charged residues along the Tau molecule. C. Disaccharide subunit compositions of heparan sulfate and heparin, schematic of the spatial arrangement of the heparin disaccharide subunits in the polysaccharide chain, and an atomistic representation of the heparin molecule. Structures were derived from PDB database [107], accession number 3IRJ. D. Different Tau *in vitro* aggregation-inducing cofactors including RNA (PDB: 205D), arachidonic acid (PubChem [108] CID: 444899), amyloid-β 42 fibrils (PDB: 2MXU), and partially folded α-synuclein (schematic adapted from [109]).

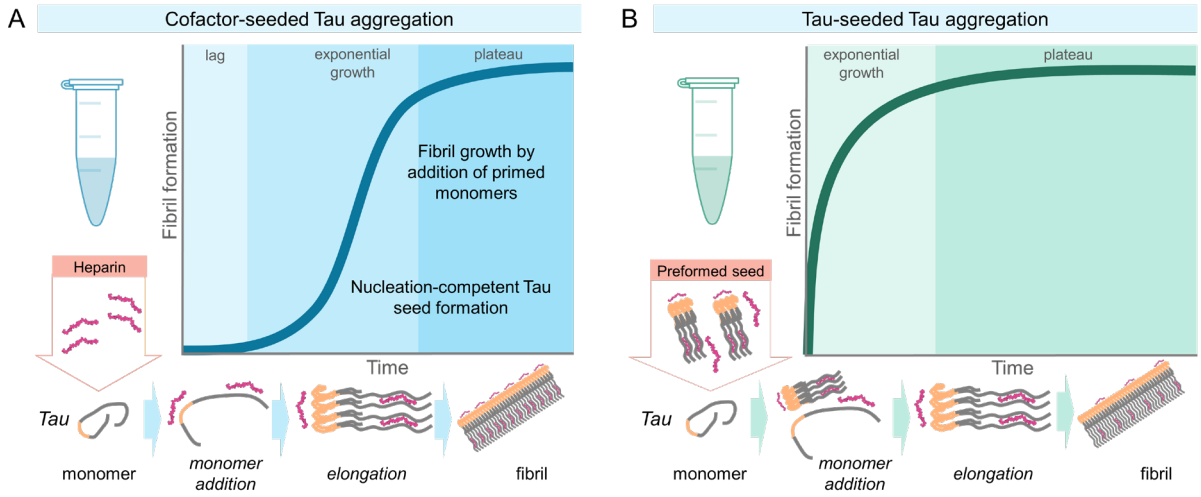

Figure 5. Schematics of kinetic curves of Tau aggregation reactions. A. Cofactor-induced Tau aggregation follows an S-shaped curve including the lag, exponential growth, and plateau phases. B. Preformed Tau nucleus-induced aggregation follows faster kinetics through the bypass of the lag phase.

Previous studies have shown that Tau misfolding and aggregation required loss of long-range contacts in the Tau molecule [100,110], as well as structural transitions of MTBR to folded β-sheet-forming conformations, driven by the PHF6* and PHF6 regions (Figure 1) [111]. The spontaneous aggregation of soluble full-length Tau was shown to be triggered and/or enhanced by the isomerization of proline 301 or in the presence of structure-destabilizing mutation P301L, as well as by other mutations (e.g., P301L, P301S, N296Δ, G303V, S305N, and V300I) in the Tau R2R3 fragment, that expose the shielded amyloidogenic motifs within MTBR, thus rendering the protein more prone to self-association and fibril formation [112]. Recently, Mirbaha et al. reported the existence of the two populations of the metastable inert

(Mi) and seed-competent Tau monomers (Ms) was proposed [113], however, others failed to replicate their findings [114] and further studies are needed to test this hypothesis.

How did we get from AD brain PHFs to heparin-induced Tau fibrils?

Tau found in the NFTs generally exhibits high levels of phosphorylation [115-117], however early on, following contradicting reports [118,119], it was unclear whether phosphorylation of Tau was sufficient or at all necessary for the formation of Tau fibrils. Therefore, to tease out the sequential order of the events associated with Tau fibril formation, researchers sought to decouple the processes of Tau phosphorylation and aggregation *in vitro* using recombinant non-phosphorylated Tau. However, because recombinant Tau isoforms aggregated painstakingly slow, the addition of cofactors was necessary to increase Tau aggregation rate *in vitro* [87].

Previously, proteinaceous brain amyloid deposits were found to contain polysaccharides, with the first report dating way back to 1855 [120], and subsequent studies showed that they were composed of heparan sulfate proteoglycans (HSPGs) [121]. Glycosaminoglycans (GAGs) had been identified in a variety of amyloid disorders as an integral part of the disease-specific deposits [122], including neurodegenerative disorders [123-129]. HSPGs are differentially expressed in AD brain [130] and had been found in NFTs and Aβ plaques in AD and other Tauopathies [123,124,131-138], predominantly associated with the early stages of disease progression [139]. The direct interactions of HSPGs and heparin with Tau and Aβ proteins were subsequently confirmed *in vitro* using biochemical and biophysical approaches [93,138,140-151].

Since the first report by Goedert *et al*. in 1996 [93] showed that heparin and HS were capable of inducing PHF-like formation of 3R, and fibril formation of non-phosphorylated recombinant 4R Tau isoforms *in vitro*, heparin has become one of the most widely used Tau aggregation cofactors for all six Tau isoforms. Under *in vitro* conditions, heparin induced the aggregation of all full-length Tau isoforms, with the shortest lag time found for isoform 4R2N, and the fastest aggregation kinetics found for isoform 4R1N, followed by 4R2N, 4R0N, with 3R isoforms showing the slowest aggregation rate [152]. PTMs such as phosphorylation and glycation were shown to modify the aggregation propensity of all Tau isoforms in the presence of heparin [153]. Other GAGs (e.g. chondroitin sulfate, dermatan sulfate, hyaluronic acid, dextran) were also found to induce Tau fibrillization depending on the extent of their sulfation [142,154], however, none had entered mainstream use mainly due to practical reasons, such as consistent and cheap production and availability, as well as due to lesser relevance to human pathology.

The presence of cofactors associated with the patient-derived Tau fibrils did not escape the detection by the high-resolution ultrasensitive techniques such as cryo-EM. The detection of unknown cofactor densities in the cryo-EM structures of CTE [155], CBD [44], PSP, GGT, GPT, and ADG, FTDP with mutations +3/+16, ARTAG and limbic-predominant neuronal inclusion body 4R Tauopathy (LNT, a subset of PSP) [156] (preprint at the time of writing) (Figure 6). Tau protofilament folds suggested their potential roles in regulating Tau fibril formation and/or maturation *in vivo*. Although the nature of the molecules that occupied these densities is yet to be determined, it is likely they could have been incorporated during the fibril formation. It remains unclear whether the presence of specific cofactors in combinations with PTMs is necessary for Tau-linked pathology formation, maturation and neurodegeneration in Tauopathies.

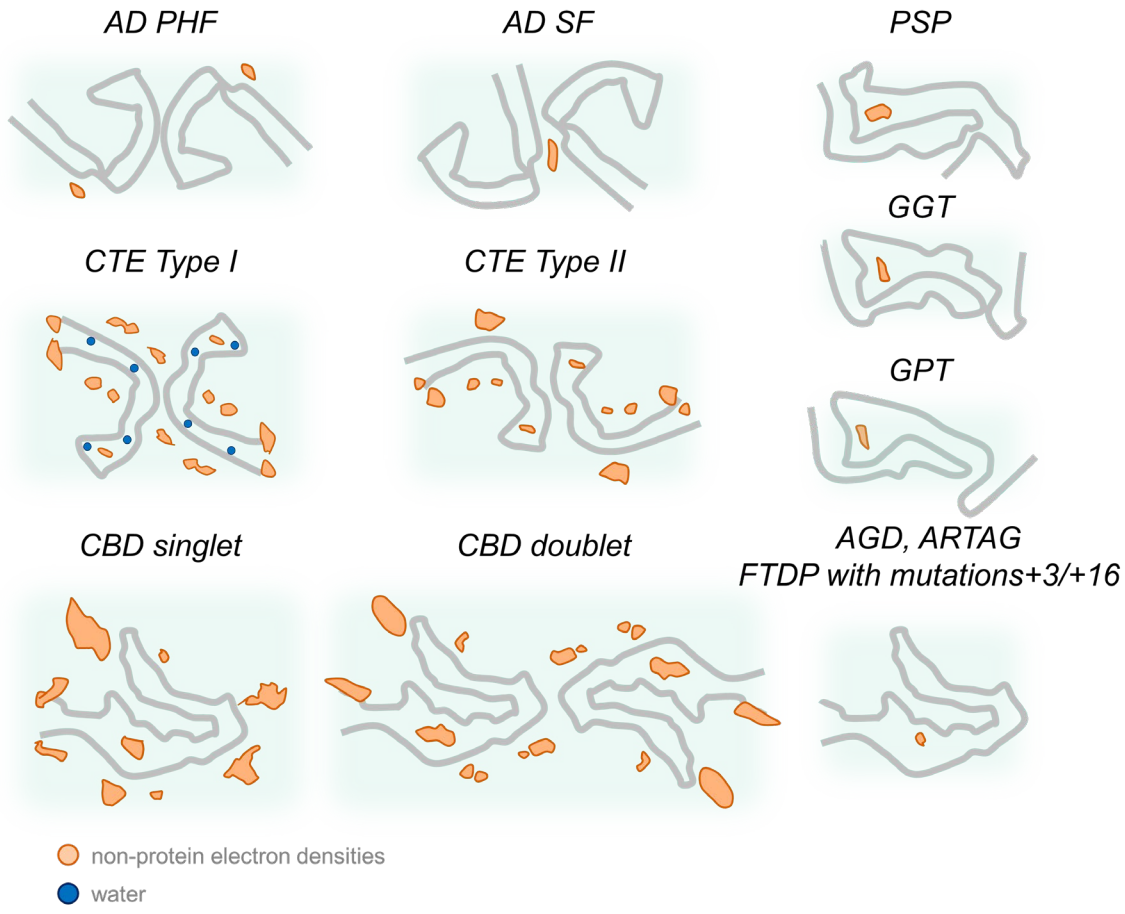

Figure 6. Non-proteinaceous electron densities associated with cores of Tau fibrillar structures derived from Tauopathies. PDB codes for AD, CTE, and CBD: 6NWP, 6NWQ, 6VHA, 6VH7, 6VI3, 6VHL, 6TJO, 6TJX. Structures for PSP, GGT, GPT, and ADG, FTDP with mutations +3/+16, ARTAG adjusted from [156].

Recent studies suggest that Tau interactions with cofactors is not restricted to early aggregation events and point to important roles of these interactions in the regulation of Tau fibril growth and seeding activity. Fichou *et al.* [114] demonstrated that the sequential seeding reactions of monomeric Tau by the heparin-induced Tau fibrillar seed, as well as by the mouse brain-derived fibrillar seed, were significantly diminished in the absence of supplementation with the cofactor (polyuracyl RNA). Similarly, Dinkel *et al*. [157] found that replenishment of RNA was necessary for the sequential cycles of template-assisted Tau fibril growth, which was abolished by the depletion of the cofactor *in vitro*. Furthermore, the molecular weight and sulfation patterns of heparin and other GAGs play large roles on interactions with Tau and their impacts on fibrillization catalysis [142,158,159].

Interestingly, cofactors may not be necessary to aggregate some forms of Tau *in vitro*, for example its shorter fragments containing PHF6 motif [88-90]. One report showed that full-length Tau aggregated using sequential seeding reactions over prolonged periods of time [160]. Similarly, a recent report by Chakraborty et al. reported that Tau aggregated in the absence of cofactors under mechanical agitation mechanism using polytetrafluoroethylene beads, albeit only after long incubation times [161]. It is important to note that these conditions also included the use of protease inhibitor tablets which generally contain aprotinin, bestatin, calpain I, calpain II, chymostatin, E-64, leupeptin, alpha-marcoglobulin, pefabloc SC, pepstatin, TLCK-HCL and trypsin inhibitor molecules. Functionally these fibrils showed higher RNA-sequestering properties than heparin-induced fibrils *in vitro*, likely through higher positive charge density which is neutralized by the negatively-charged heparin.

Do heparin-induced Tau fibrils resemble bona fide patient-derived PHFs?

The amyloid-like properties of recombinant Tau fibrils, coupled with the ease with which they can be reproducibly prepared, led to the use of heparin as the main initiator of Tau aggregation and fibril formation. Thus, the great majority of studies on the mechanisms of Tau oligomerization and fibril formation, as well as drug discovery efforts targeting Tau aggregates are based on the use of heparin [162]. But how closely do heparin-induced Tau fibrils resemble *bona fide* patient-derived PHFs? Could they be used as an authentic proxy for an accurate representation of disease-relevant Tau fibrillization mechanisms, or in the development and assessment of Tau targeting molecules such as aggregation inhibitors and positron emission tomography (PET) tracers?

In vitro aggregation studies have consistently shown that heparin-induced fibrils generated *in vitro* exhibit morphological features that are drastically different from those observed in PHFs

isolated from the AD brain (Figure 7, Table 1). Differences are found on several levels, such as Tau isoform composition [163], the number of the protofilaments comprising fibril [164], varying fibrillar morphology (size, shape) [165,166], biochemical properties such as solubility, PTMs, as well as immunoreactivity to different Tau antibodies and enzymatic digestion resistance profiles [167,168]. These differences highlight the gap between how we have been studying Tau aggregation in the laboratory and how the process of Tau fibrillization and pathology formation occur in the brain. Furthermore, thus far, *in vitro* studies have mainly focused on investigating one Tau isoform at a time, which does not reflect what occurs in the human brain where Tau fibrils comprise a mixture of different isoforms. The compositional differences of patient-derived fibrils should influence the choice of which Tau isoform to use in *in vitro* studies aimed at elucidating the mechanisms of Tau aggregation and fibril formation concerning the different Tauopathies. For example, in AD, all 4R and 3R Tau isoforms are detected in the high-order Tau twisted (PHFs) and straight (SFs) fibrils as a part of NFTs [48]. Despite this, it is predominantly modeled using singular 4R2N, 4R0N, or 4R1N Tau isoforms, rather than a mixture of 3R and 4R isoforms, which may be more desirable. For the predominantly 4R primary Tauopathies, classified as sporadic FTDP-Tau [169], such as PSP or CBD [170], 4R Tau isoforms are used, and for 3R Tauopathies, such as PiD, predominantly 3R2N is used, and foetal 3R0N is rarely employed to model Tau aggregation. Given the significant sequence overlap between the different isoforms, they are expected to interact with each other at different stages along the pathway to fibril formation, and could dramatically influence the kinetics of aggregation and equilibrium between the different aggregation states of Tau.

Furthermore, it was found that Tau isoforms were differentially modified in AD patients with complex patterns of PTMs depending on the stage of Tau pathology progression (see Figure 2 B) [57]. Thus, combinations of Tau isoforms' PTMs must be recapitulated *in vitro* for appropriate representation of pathological aggregates formed. Production of homogeneous site-specifically modified Tau isoforms is possible through chemical synthetic and semisynthetic strategies [171].

Finally, although the patient-derived Tau fibrils are heavily modified, the significance and contribution of PTMs to Tau fibrillization and the final structural properties of Tau filaments and aggregates are still unclear. More specifically, it remains unclear which PTMs found in the PHFs occur before or after the fibrillization process onset. This is primarily due to our ability to detect the PTMs only cross-sectionally, as snapshots at the times of sampling in humans.

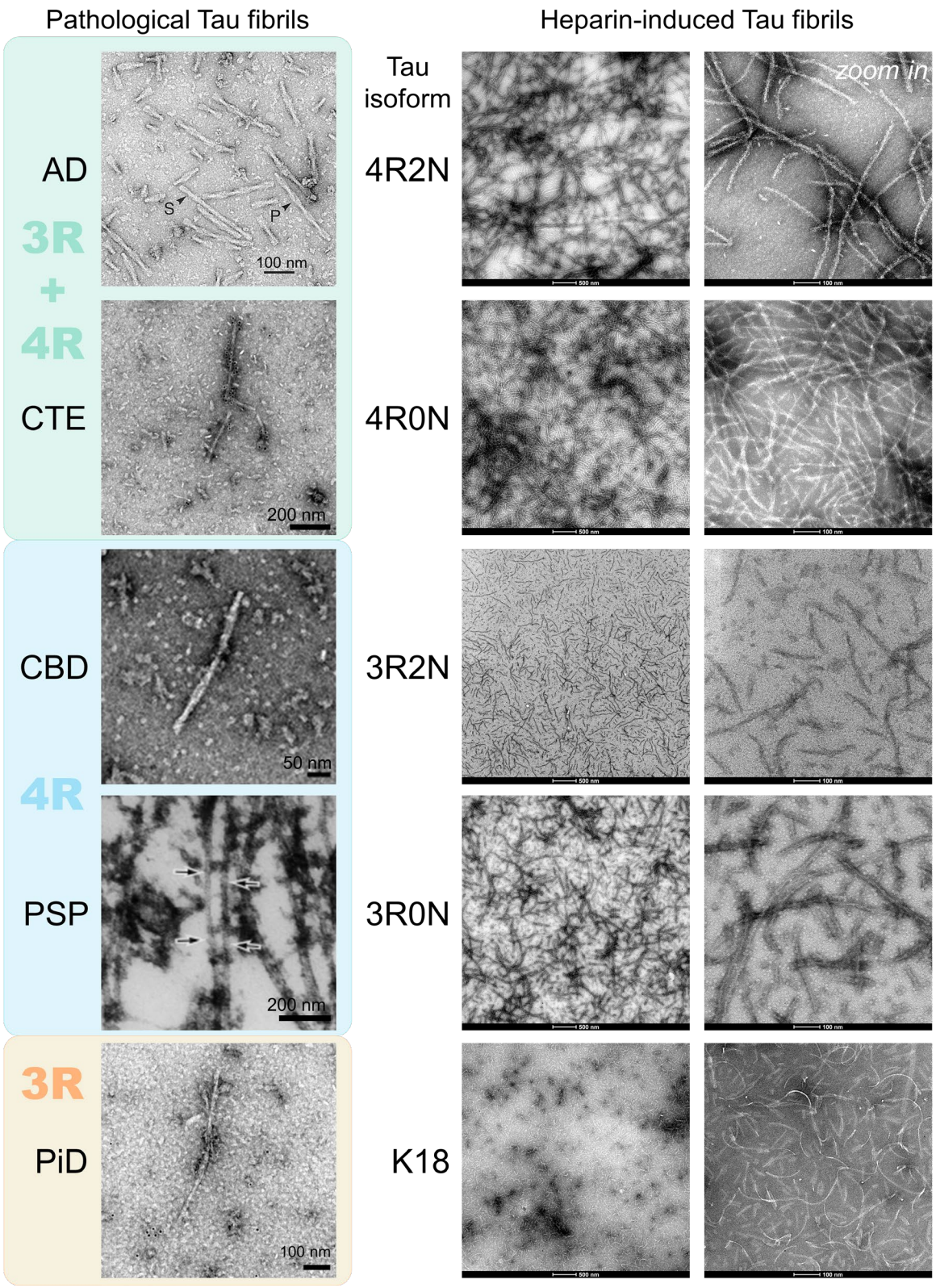

Figure 7. Examples of pathological and heparin-induced Tau fibrils. Negative staining electron microscopy images of Tau fibrils isolated from the human brain (4R+3R Tauopathies AD and CTE, 4R Tauopathies CBD and PSP, 3R Tauopathy PiD) and heparin-induced Tau fibrils composed of isoforms 4R2N, 4R0N, 3R2N, 3R0N and truncated Tau K18. Note heparin-

induced fibrils predominantly show long, flexible, single-protofilament fibrils (images courtesy of Lashuel lab). The image for a case from AD is from [172], CTE is from [155], CBD is from [44], PSP is from [173], PiD is from [43].

This limitation can currently be circumvented by longitudinal *in vivo* cerebral microdialysis of Tau in the extracellular fluid (ECF) in animal models [174-178], as well as in humans [179], albeit only for a limited time. In humans, high-precision and low-throughput longitudinal identification of ECF- and neuronally-derived Tau species may be achieved through a) intraoperative sampling during brain surgery [180] and molecular characterization by the mass spectrometry-coupled surgical tools, such as "iKnife" [181,182]; b) integrating neuroprosthetic implants with Tau biosensor nanomaterials [183,184], as well as through c) post-operative sampling of the residual material on the surgical tools, known as protein residue testing.

Table 1. General differences between pathological and heparin-induced Tau fibrils

	Pathological fibrils	*Heparin-induced fibrils*
Isoform composition	Multiple	Single
PTMs	Extensive	Naked
Protofilament composition	Double	Single or double
Twisting	Consistent	Variable
Protofilament interface	Consistent	Variable

The early biophysical studies of AD patient-derived PHFs using X-ray diffraction and Fourier transform infrared spectroscopy suggested that they did not contain extensive β-sheet [28,185]. However, subsequent careful studies confirmed the presence of β-sheet structures using biophysical techniques [111,172,186-189]. Less than thirty percent of the Tau sequence adopts β-sheet structures, whereas most of the molecule tends to maintain its disordered conformation. The heparin-induced Tau fibrils were also found to possess β-sheet arrangements of the Tau PHF6* and PHF6 domains, as probed by Fourier transform infrared spectroscopy, X-ray, and electron diffraction [172], fluorescence spectroscopy using pyrene maleimide labeling, and EPR [190], as well as solid state NMR [191]. Nevertheless, depending on the recombinant Tau isoform used to generate the Tau fibrils *in vitro*, the amino acid arrangements still differ from the pathological Tau fibrils they are employed to model (see Figure 7, Pathological and Heparin-induced fibrils).

Ultrastructure of Tau fibrils

At the dawn of the Tau cryo-EM

Until recently, it has not been possible to directly determine to what extent recombinant Tau aggregates produced *in vitro* recapitulate the key features of pathological Tau fibrils at the atomic level. However, recent advances in cryo-EM [43,44,155,164,189] (reviewed in [192] and [163]) techniques and data analyses have enabled the atomic-level determination of the ultrastructural composition of the ordered regions within Tau fibrils. The structures emerging from these studies provided unprecedented insights into the structural diversity of Tau fibrils isolated from human brains with different pathologies, and more recently of the heparin-induced Tau fibrils (Figure 8). More recently, the initial Tau fibril structures that were solved by cryo-EM were derived from AD patient brain in 2017 [189], followed by the fibrils derived from PiD in 2018 [43], CTE patients [155] and *in vitro* heparin-induced Tau fibrils [164] in 2019, as well as CBD in 2020 [44]. Recently, novel Tau fibril structures have been resolved including fibrils derived from PSP (non-peer-reviewed at the time of writing [156,193]), GGT, AGD, ARTAG, inherited FTDP-Tau with splice mutations at the nucleotide positions +3/+16 in the intron 10 of *MAPT* gene, FBD, and FDD (non-peer-reviewed at the time of writing [156]). Furthermore, Tau fibril structures from prion-protein amyloid diseases GSS associated with the F198S mutation, and prion-protein cerebral amyloid angiopathy (PrP-CAA) with Q160X truncation were also solved [194], thus opening up new avenues of exploring Tau contributions to amyloid diseases such as Huntington's, Lewy body dementia or fatal familial insomnia (Figure 2).

Structural features of pathological Tau fibrils

The Tau fibril structures derived from multiple Tauopathies are providing novel insights into versatility and heterogeneity of the structural landscape that can be occupied by the Tau molecular conformations, as well as conservation of the structures across different diseases. AD patient-derived PHFs are comprised of a mixture of 3R and 4R Tau isoforms and are formed from two Tau protofilament β-strands, in each strand the distance between stacked Tau molecules containing β-sheet conformation is ~4.7 Å and a helical twist of the angle -1 ° per 4.7 Å rise [189]. The two protofilaments symmetrically interface and hydrogen-bond at amino acids ^{332}PGGGQ^{336} (see Figure 8 B). In contrast, two Tau AD SFs' protofilaments are hydrogen-bonded through residues 317–324 on the first protofilament, and residues 312–321 on the second protofilament. This asymmetry balances the kink in the non-planar β-sheet-containing stacked Tau molecules and neutralizes the higher-order Tau fibril twist, as

determined by cryo-EM [189]. The interface can also be potentially altered by the PTMs of the protofilaments, such as ubiquitination of AD and CBD protofilaments [85].

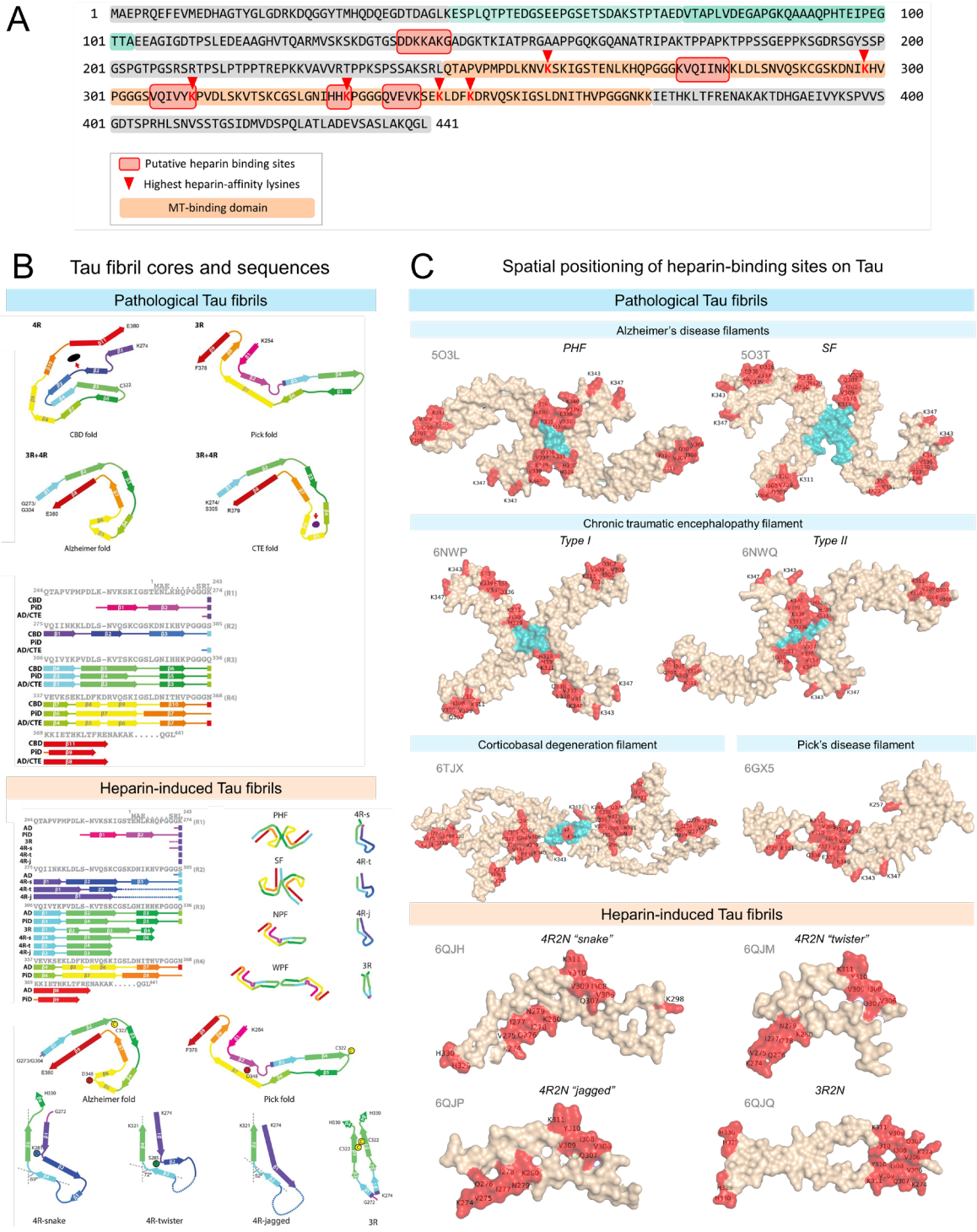

Figure 8. Pathological and heparin-induced Tau fibril core structures and sequence interactions with heparin. A. Sequences of electrostatically-driven heparin-binding sites on Tau molecule B. Core structures and Tau sequence alignments of pathological and heparin-induced fibrils (adapted from [44] and [164]). C) Spatial representation of highest affinity heparin-

binding sites on the Tau pathological and heparin-induced Tau fibril cores (red). The inter-protofilament interfaces are marked in cyan. PDB [107] codes are in grey.

Tau fibril structures determined from other Tauopathies presented a startling variety at the levels of single-molecule folding, singlet fibril ultrastructure, as well as inter-fibril interactions in the doublets [156]. The GGT Tau fold was similar to PSP, and comprised residues 272-379, further forming three distinct ultrastructures comprising singlet fibril or two doublet structures, differing in the interfacing residues between the single fibrils. Interestingly, the core fold structures of two types of fibrils derived from the frontal cortex of case PSP-F2 (named GPT by the authors) were different but resembled both the PSP and GGT Tau folds. Because this case of PSP-F2 harboured fibrils that were intermediate between PSP and GGT, it prompted the authors to classify it as LNT disease. Tau fibril core fold derived from AGD was formed by amino acids 273-387 (type I) and 279-381 (type II) and could assemble into three types of fibrils comprised from singlet or doublet fibrils. Interestingly, in one case of AGD, both AD-type PHFs and SFs could be found, whereas in another AGD case AD-type PHFs and CTE-type I fibrils could be detected. Similarly, in ARTAG cases AGT Tau fold was found forming type I and type II fibrils, as well as AD-type PHFs and SFs. In inherited FTDP-Tau with mutations +3/+16 in intron 10 of *MAPT* gene, only AGD fold was detected. The FBD and FDD both contained AD-type PHFs, with FBD also showing AD-type SFs and CTE-type I fibrils.

In primary prion amyloidoses PrP-CAA (Q160X) and GSS (F198S), Tau fibrils were composed of 3R and 4R Tau isoforms, similar to AD-type fibrils [194]. Both diseases contained Tau fibrils of AD-type PHFs, whereas PrP-CAA (Q160X) in addition contained AD-type SFs. Interestingly, using mass spectrometry, the fibrils were found to be post-translationally modified. Notably, fibrils were ubiquitinated on the residues K311 and K317 in both diseases, as well as on K254 and K267 in GSS (F198S); acetylated on K311 in both diseases, and M11 and K369 in PrP-CAA (Q160X), and N255 in GSS (F198S); and phosphorylated at T153, T175, T217, T181, S202, T217, T231, S235, S238, S262, S285, S289, S396, S400, S404 in both diseases, and on S185, S199, T212, S214, S305, S320, S324, S356, S422 and S433 in PrP-CAA (Q160X). Deamidation was found on residues Q6, Q167, R170, R242, Q244, N255, N265, N286, Q307, R327, and N381 in both diseases, with additional residues Q162, N279, N296, Q351, N410, and Q424 in PrP-CAA (Q160X), and residues Q165 and N368 in GSS (F198S).

Although AD-derived Tau fibrils [189] were found to resemble the CTE-derived fibrils [155], the CTE folds were found to harbour non-proteinaceous electron densities in the loop structure (see Figure 6). Recent work showed that PSP-derived Tau fibrils [193] were composed of the 4R Tau

isoforms, and included core-forming amino acids 268-395, similar to CBD fibrils [44]. Despite these similarities, however, the fold structures differed by the surface exposure of the amino acid residues. Whereas in CBD fold K281, K290, K298, and K370 were buried in the hydrophobic core, these residues were exposed on the surface of the PSP fold. Conversely, lysine residues 317, 321, 340, and 375 were exposed on the surface of CBD, but buried within the PSP fold. Interestingly, both the PSP and CBD filament structure harboured enclosed non-proteinaceous densities within the core folds, however, the amino acids in proximity to these densities differed between the two (see Figures 6 and 8).. In PSP, the likely negatively charged cofactor interacted with lysine 317, and in CBD fold cofactor interacted with K290, K294, and K370. These differences in the distribution of lysine residues in the core and surfaces of different Tau fibrils suggest that they are likely to exhibit different ubiquitination or acetylation signatures. These data illustrate the high flexibility and versatility of the same Tau sequence to adopt a range of polymorphic conformations, with differential availability of the residues to be post-translationally modified or interact with the cofactor molecules.

These findings have enormous implications and cautions against classifying Tauopathies based only on one most abundant, and easily detectable Tau fibril structure. These data demonstrate that 1) multiple Tau fibril conformers could coexist in one Tauopathy; 2) the same Tau fibrillar structures could be detected in different Tauopathies, as well as other primary amyloidoses; and 3) the extensive Tau PTM landscapes differed between conditions. Therefore, the Tau pathologies may not necessarily be driven by the unique Tau fibril structures, but rather by the biochemical compositional changes within the brain, which may be more closely related from one patient case to another, thus giving the rise to the similar Tau fibrillar structures as a result.

Paradoxically, the patient brain-derived Tau fibrils are much more structurally homogeneous [189] than Tau fibrils produced under controlled conditions *in vitro* [164]. This suggests the possibility of tightly controlled and conserved sequences of events leading to the formation of the Tau fibrils in specific ultrastructural conformations. For a more in-depth comparison of cryo-EM Tau fibrils from patient brains and *in vitro* produced Tau fibrils see the recent excellent review by Scheres *et al*. [163].

Structural features of heparin-induced Tau fibrils

In the presence of heparin, Tau formed fibrils of variable morphologies depending on the experimental conditions (see Figure 7) [195,196]. This heterogeneity was reflected in the cryo-EM structures recently reported by Zhang *et al.* [164]. From the three biophysically-determined

models of the lateral arrangement of Tau molecules within the core of the heparin-induced 4R Tau PHF fibrils, namely left-handed β-helix, right-handed β–helix, and intersheet-hairpin [190], only the right-handed β–helix model seemed to correspond to "4R-jagged" structure determined by cryo-EM [164]. Parsimoniously, based on structures hypothesized by [190] (three fibril core arrangements) and determined by [164] (three core arrangements of 4R Tau fibrils, see Figure 8 B, Heparin-induced Tau fibrils) at least six different amino acids arrangements in the core of the heparin-induced 4R Tau fibrils may exist, with a high possibility of the existence of yet-uncharacterized other β-sheet-containing polymorphs. Heparin-induced 4R2N Tau fibrils were found to exhibit dimensions (width = 20 nm) and helical twists (every ~80 nm) that are reminiscent of PHFs (non-twisted fibrils observed had widths of ~15 nm) [93]. However, reports of variable structures in the mixture ensued.

Previously, using electron microscopy, Xu *et al.* [197] reported that 4R2N Tau forms ribbon-like fibrils with center depressions (RCDs) and multi-striated ribbons (MSRs) with variable degrees of helical twisting and widths in the range from 5 nm to 25 nm, and ~7.2 ± 0.6 nm for non-twisted fibril segments. These fibrils showed widths between 18.9 to 28.9 nm in the narrowest and 10.9 to 14.2 nm in the widest parts of the fibrils, with the twist periodicity of 82.7 ± 4.6 nm. A recent ultrastructural cryo-EM study [164], which revealed the *de novo* atomic-level structures of heparin-induced Tau fibrils, showed the presence of at least three polymorphic helicoid 4R2N Tau fibril structures that consist of two protofilament strands, where the fibril width and helical periodicity of the twists differed from AD patient-derived PHFs (Figure 8 B). Fibrils designated by authors as "twister" were nearly uniformly 8 nm wide with twists spaced at around 25 nm; "jagged" fibrils were 5 to 9 nm in width and twists spaced by ~45 nm; and "snake" fibrils, the most abundant polymorphs, were between 4 and 10 nm wide with twists spaced by 65 nm. The "hose" fibrils were predominantly devoid of twists. Similar to AD brain-derived Tau fibrils, where transitions from PHF to SF structural arrangements could be seen along the singular fibril [198], the transitions from one type of fibril to another were observed in heparin-induced Tau fibrils [164]. These observations suggest that Tau fibrils, like other amyloid fibrils, are dynamic and could still undergo significant remodelling on their own or upon association with other fibrils.

Similarly, in truncated Tau K18 fibrils (Figure 1 B, K18), the R2 and R3 regions were found to be a part of the in-register parallel β-sheets, however, the R4 region appeared to remain disordered [199]. In AD PHFs and SFs, only Tau residues 306-378 constitute the fibril core, whereas the remaining residues comprise the "fuzzy coat " of Tau fibrils [189]. It is of note that at their C-termini Tau K18 and K19 fragments (Figure 1 B, K18 and K19) also lack the six

residues determined to constitute the AD (4R; 308-378) [189] and PiD (3R; 254-378) [43] fold cores, seven residues that are part of CTE fold core (4R; 274/305-379) [155] and eight residues that are part of CBD Tau fold core (4R; 274-380) [44]. These observations suggest that while these fragments are ideal to investigate some aspects of Tau aggregation, the structure of the fibrils they form may not accurately represent that of the disease-relevant Tau fibrils.

Previous studies on the interactions between Tau and heparin helped to illuminate the potential mechanisms of heparin-induced Tau fibrillization, and determine the heparin-interacting Tau residues [93,142,200,201]. As demonstrated in (Figure 8 A and C), many high heparin affinity sites on Tau constitute pathological Tau fibril core folds and are buried within the structures found in AD, PiD, CTE, and CBD. Previous studies suggested that heparin bound to or had a high affinity for the residues (^{306}VQIVYK^{311}, ^{336}QVEVK^{370}, K^{343}, K^{347}) (Figure 8 C) immediately adjacent to the residues mediating inter-protofilament interfaces, that governed the formation of the paired fibrils in AD-derived PHFs (^{332}PGGGQ^{336}) and SFs (^{317}KVTSKCGS^{324}, ^{312}PVDLSKVTSK^{321}), CBD-derived fibrils (^{343}KLDFKD^{348}), CTE-derived type I (^{324}SLGNIH^{329}) or type II (^{331}KPGGGQVE^{338}) fibrils. In contrast, in the heparin-induced Tau structures, the highest affinity sites are exposed on the surfaces of the fibril core on fibril surfaces.

Reconciling the biochemistry (PTM profile) and structural properties of brain-derived Tau filaments

One clear difference between pathological and heparin-induced Tau fibrils is that the majority of *in vitro* Tau fibrils are produced from recombinant and non-modified forms of the single Tau isoform. This is in stark contrast to the highly modified and hyperphosphorylated patient-derived Tau PHFs and fibrils, that require the action of multiple and tightly-controlled enzymatic processes.

Monomeric Tau is extensively post-translationally modified, with phosphorylation and truncation occurring at multiple sites along the Tau sequence [52] (see Figure 3). However, the initial cryo-EM studies did not detect the PTMs on the solved Tau fibrils [44,155,189]. This was puzzling, given the abundant evidence for extensive PTMs in these samples as assessed by Tau PTM-specific antibodies or mass spectrometry [57,85]. From a technical perspective, this could be explained by the small sampling size of Tau fibrils containing certain PTMs in sufficient amounts that could be determined from cryo-EM 3D reconstructions. It is also possible that the pool of non-modified Tau molecules was likely larger at the times of sampling, resulting in selective solving of only some specific Tau 3D conformations. Finally, application

of helical symmetry during 3D reconstruction improves densities in 3D reconstruction that follow proposed symmetry, but average out densities that are deviating from symmetry, either due to low sampling or flexibility of PTM affected domains. Finally, increasing evidence suggests that Tau could be modified after it forms fibrils [202,203]. Under these conditions, it is unlikely that all molecules in the fibrils would be accessible to modification by enzymes. This again makes it difficult to resolve PTMs by cryo-EM that are otherwise detectable by mass spectrometry.

Some progress towards deciphering the Tau PTM code has been achieved in a recent study by Arakhamia et al [85], which described the Tau fibril structure from AD and CDB with observed extra densities not attributed to amino acid residues. The investigators used cryo-EM in combination with mass spectrometry and the detected non-protein densities in the cryo-EM structures that were assigned the most likely PTM, such as ubiquityl group. Their findings highlight a dramatic effect of ubiquitin modifications on the high-order structure of the SFs from AD and doublet fibrils from CBD patient brain-derived material [85]. Interestingly, the density on the fibrils attributed to PTMs influenced the higher-order interprotofilament interfaces by the virtue of the positions of these modifications facing outwards from the core, rather than impacting molecular arrangements and intraprotofilament packing. This suggests that these modifications likely occurred after or during fibril formation, which is consistent with the prominent role of ubiquitination in targeting proteins for degradation [75] as well as contributing to the Tau fibril formation process [52]. It is therefore logical to expect the large impact of multiple PTMs on the Tau residues comprising or close to the core of fibrils occurring at the level of the monomeric Tau molecules before fibrillization onset. This work underscores the importance of studying the presence and roles of PTMs in the formation of Tau PHFs and fibrils and/or their morphological diversity (strains) at the ultrastructural level. It is important to note, however, that mass spectrometry techniques are only capable of detecting solubilized single molecules or small complexes, but not fibrils. In addition, the PTMs were extensively detected on or around residues forming the core of the fibrils (see Figure 3 B), which means that these PTMs may not be derived from the fibrils themselves, but rather from the soluble fraction, as well as non-fibrillar aggregates. Thus, novel approaches to mapping and characterization of PTMs present directly on the fibrils, as well as the detection of less abundant fibril polymorphs are urgently needed. Together, these observations suggest that Tau PTM patterns have the potential to impact not only the propensity and kinetics of Tau aggregation, but also the structural characteristics and polymorphisms of the fibrils generated in AD and other Tauopathies, and potentially heparin-induced Tau fibrils *in vitro*.

The missing links

Pathology-relevant Tau aggregation inducers

Thus far, most biophysical and biochemical Tau studies have primarily relied on heparin as a Tau aggregation inducer. However, the increasing evidence, including recent cryo-EM data, suggests that other cofactors may be involved in triggering and promoting Tau aggregation, leading to the pathology formation in the brain. Despite these technological achievements, several scientific questions persist upon analyses of the novel cryo-EM data of Tau fibril structures harbouring the cofactor molecule densities (see Figure 6) [193]. First and foremost, what are the natures of the negatively-charged cofactors within the PSP and CBD Tau fibrils, as well as the densities attributed to the cofactors on the surface of PSP fibrils, close to residues K280-K281 and H362 [156]? Establishing this will be crucial to understanding what triggers Tau aggregation in the first place, what regulates fibril remodeling and polymorphisms, and could lead to breakthrough developments of the in vitro methods for studying Tau aggregation. Next, what is the topological and the symmetry arrangement of the cofactor molecules within the filaments, as well as cofactor-to-Tau molecule stoichiometry? This will help establish the precise sequence of folding of Tau, and whether the cofactors are truly incipient to Tau conformational transitions. Notably, the cofactor densities in PSP and CBD were not associated with the amino acids of regions PHF6* (275-280) and PHF6 (306-311), previously shown to be driving the misfolding and aggregation of Tau in vitro [204]. It is possible the molecular processes that govern Tau misfolding and aggregation under pathological conditions differ profoundly to what has thus far been modelled *in vitro*. It should be noted that care must be taken to rule out any artefacts during the sample processing for cryo-EM, image acquisition and computational structure reconstruction that could be erroneously interpreted as cofactor densities present in the brain.

The large structural differences between heparin-induced and brain-derived Tau fibrils underscore the critical importance of revisiting the biochemical properties of Tau pathologies with an emphasis on defining the non-proteinaceous components of pathological Tau aggregates in different Tauopathies. These efforts will spearhead the identification of novel cofactors that may be responsible for triggering Tau aggregation and/or the formation of different conformers of Tau fibrils. Once identified, similar approaches to those used to interrogate Tau-heparin interactions will then be applied to systematically dissect their mode of interactions with Tau at different stages on the pathway to Tau fibrillization and pathology formation.

Challenges in investigating the role of PTMs in Tau pathology formation and diversity

Tau isoforms are large proteins and can be modified on more than 40 sites along the molecule (see Figure 3) [51,205]. Thus far no robust, streamlined, and reproducible methods exist to introduce more than a handful of PTMs to Tau *in vitro*. To address these limitations, our group [171,206,207] and others [208-210] developed new semi-synthetic methods that enable the site-specific introduction of single or multiple PTMs to Tau monomers before fibrillization and showed that PTMs heavily influence fibril formation and structural properties of the final aggregates. Furthermore, our work showed that hyperphosphorylation of the MTBR inhibited rather than promoted Tau fibrillization *in vitro* and seeding activity in cells [207]. These findings support the hypothesis that some of the Tau PTMs found in the AD brain may represent post-aggregation events, possibly reflecting cellular responses to clear, disassociate, or degrade Tau fibrils.

Secondly, in human pathology, Tau PTM patterns are known to be disease-specific and change in the course of the disease progression [57], therefore the precise patterns of the Tau PTMs are specific to that particular disease and its stage, or even an individual patient [211]. The choices of Tau PTM patterns to introduce to the recombinant protein should be informed by the data from human patients. These are predominantly acquired from post-mortem brain samples or liquid biopsies from living patients, such as CSF and blood plasma [212,213]. The PTMs profiles are generally identified using immunohistochemistry, mass spectrometry, and other biochemical methods, each not without the limitations, thus requiring complementary validation. For example, no single Tau antibody is capable of detection of all circulating Tau species, therefore a combination of antibodies targeting different regions must be used. Even the most commonly used total Tau and phosphorylated Tau detection assay (INNOTEST, Innogenetics, Ghent, Belgium) was shown to have high intra- and inter-laboratory detection variability, where re-analysis of data led to re-classification of subjects from normal to abnormal biomarker designation in 29% (due to intralaboratory variability) and 22% (due to interlaboratory variability) of cases attributed to phosphorylated Tau detection variability [214]. We believe that the presence of PTMs within or near the epitopes of many of the Tau antibodies will influence their ability to detect Tau or capture the true diversity of the Tau proteome in biological samples.

Thirdly, Tau can be processed in CSF, and it is predominantly detected in fragmented forms both in neurodegenerative disease patients and healthy controls [215-222], making it difficult to trace the isoform origin, and impossible to know the full pattern and co-occurrence of the PTMs on a single Tau molecule. The levels of detection of Tau are also known to be subject to hourly

fluctuations [223], and the detection of specific Tau species is known to have high patient-to-patient variability [38]. Taken together, which precise Tau PTMs or PTM patterns are detected in patients' CSF samples and how they change during the course of disease progression remains unknown. Addressing this knowledge gap will also require the development and application of methods that allow for profiling Tau PTMs at the single-molecule levels.

Finally, the PTM patterns may both contribute to the process of fibril formation when introduced to Tau monomers before fibrillization or occur during or after fibril formation. This distinction may significantly impact Tau fibril structure on the molecular, protofilament, and fibril levels, especially when PTMs occur during fibril formation. This presents new challenges as there are no existing methods that allow the site-specific introduction of multiple PTMs (other than phosphorylation) post-fibrillization of Tau. Also, the presence of multiple PTMs on Tau fibrils or oligomers could significantly alter their interactome and binding to ligands, as well as influence their seeding activity [38], underscoring the critical importance of investigating the PTM-dependent Tau interactome. Taken together, it is abundantly clear that Tau PTMs must be given serious consideration for use from both the experimental tool perspective, as well as the relevance of *in vitro* studies for human pathology.

The Grand Challenge: Reconstructing the spectrum of Tau pathologies.

Like Lewy pathologies in Parkinson's disease and amyloid plaques in AD [224], clinical and histological manifestations of Tau pathologies are highly heterogeneous and variable both between and within different Tauopathies [225-228]. This is not surprising as Tau pathological aggregates occur in different cell types (e.g., neurons, glia, and astrocytes) and brain regions. This is clearly reflected in the spectrum of different Tau aggregate morphologies observed in different tauopathies and are often described based on their appearance, e.g., neurofibrillary tangles, pretangles, coiled bodies, diffuse cytoplasmic granular, globular glia inclusions, and astrocytic plaques [228]. Such neuropathological diversity is not limited to primary Tauopathies but has also been observed in other NDDs such as human prion diseases. For a comprehensive overview of the cellular and molecular determinants of the heterogeneity and complexity of pathological Tau aggregates and inclusions, see Chung et al. [225].

The primary Tauopathies PSP and PART, and secondary Tauopathies AD and CTE show mature Tau NFTs in neuronal cells. AGD pathology also shows granular inclusions in the neurons. Neuronal Tau pretangles are detected in PSP, CBD, and GGT, whereas distended neurons are found in PiD, CBD and AGD. PiD, a predominantly-3R Tauopathy, shows distinct rounded inclusions called Pick's bodies in neurons, as well as astrocytic and Pick-body-like

pathologies in oligodendroglia (Figure 9 A-C). Glial astrocytic Tau pathologies are morphologically diverse, ranging from ramified cells in AGD and PiD, thorny cells in CTE and ARTAG, tufted cells in PSP, as well as presence of Tau plaques in CBD, and globular Tau inclusions in GGT. AD and PART do not generally show extensive astrocytic pathology. Interestingly, AD, CTE, ARTAG and PART are not characterised by the oligodendroglial pathologies, in contrast to PSP, CBD and AGD, which show coiled bodies, and GGT, which is characterised by the globular inclusions.

The molecular and cellular drivers underlying this neuropathological heterogeneity remain unknown. The distribution of Tau isoforms in pathological Tau aggregates has emerged as one of the defining and distinguishing features of Tauopathies. For example, NFTs in AD are composed primarily of 4R and 3R Tau, whereas the spherical Tau inclusions found in Pick's disease are composed mainly of 3R Tau. Although, Cryo-EM studies have revealed different core structures of Tau filaments from different Tauopathies, such structural differences or Tau isoform composition are not sufficient to explain the morphological heterogeneity and staining patterns (Tau antibodies and Thioflavin S) of Tau aggregates and inclusions within the same Tauopathy. This is in part because current methods to isolate Tau filaments are crude and do not allow for cell-type-specific isolation of Tau filaments.

Previous studies have shown that the cellular milieu is a key determinant of protein aggregation and dramatically the final structure of fibrils and their seeding activity [229,230]. Therefore, it is reasonable to assume Tau aggregates or inclusions in different Tauopathies or subtypes of a specific tauopathy could reflect differences in the biochemical (PTMs) and ultrastructural properties of the Tau aggregates or even the biochemical composition of the inclusions (i.e., presence of other proteins and molecules). The following observations support this hypothesis; 1) detection of Tau filaments with different PTM patterns from same Tauopathy (CBD) [85]; 2) detection of multiple Tau filaments with distinct core and structural properties from the same Tauopathy [156]; and 3) detection of Tau oligomers with distinct patterns of Tau PTMs in different patients with typical AD [211]. One alternative, but not mutually exclusive explanation, is that some aspects of neuropathological heterogeneity in Tauopathies may reflect different stages of Tau pathology formation and maturation.

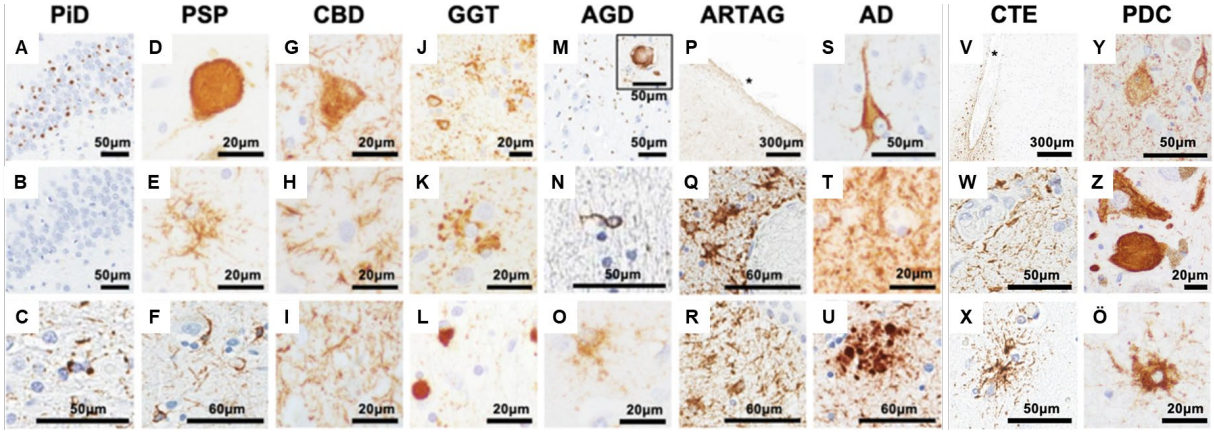

Figure 9. Examples of various tau inclusions in primary Tauopathies. (A-C) PiD. Neuronal Pick bodies stain positive for 3R tau (A) while negative for 4R tau (B). White matter oligodendroglial inclusions (C). (D-F) PSP. Neuronal globose tangle (D). Tufted astrocyte (E). Oligodendroglial coiled bodies (F). (G-I) CBD. Ballooned neuron (G). Astrocytic plaque (H). Neuropil tau threads (I). (J-L) GGT. GAIs (upper right) and neuronal pretangles (lower left) (J). Higher magnification of GAIs (K). GOIs (L). (M-O) AGD. Argyrophilic grains (inset shows ballooned neuron) (M). White matter oligodendroglial coiled body (N). Bush-like astrocyte (O). (P-R) ARTAG. Thorn-shaped astrocytes in subpial (P), perivascular (Q), and subependymal regions (R). (S-U) AD. NFT (S). Neuropil tau threads (T). Dystrophic neurites in a neuritic plaque (U). Immunoreactivity to RD3 (3R tau) (A), RD4 (4R tau) (B, M-O), and CP13 (pS202 tau) (C-L, P-U). Asterisks denote the crest of the gyrus. (V-X) CTE. Subpial tau at the depth of the cortical sulcus (V). Patchy perivascular tau (W). Thorn-shaped-like astrocytes (X). (Y-Ö) Guam PDC. Tau threads, extracellular tangle, and NFT (Y). Midbrain NFT and globose tangle (Z). Ramified astrocytes in periaqueductal gray matter (Ö). Immunoreactivity to CP13 (pS202 tau). Asterisks denote the crest of the sulci. Adapted from [225].

Bridging the gap between pathological and in vitro-formed Tau fibrils through embracing and reconstructing the complexity

Reconstructing the spectrum of Tau pathologies as they appear in human brains is a mission impossible. However, one way to bring us closer to this goal is to develop cellular and animal models that recapitulate many of the key features of the human pathology. Recent studies from our laboratory suggest that this possible [231]. Regardless of whether we are able to reconstruct Tau pathological diversity or not, a better understanding of the molecular and structural basis underlying the morphological this diversity is essential to guide the development of effective therapeutic and imaging agents that could target such diverse pathology. The failure to develop such agents could lead to underestimating the level of pathology or the development of therapies that target only a subset of the Tau aggregates, leaving other seeding-competent tau aggregates untouched. In this regard, the development of novel approaches for tackling neurodegenerative disorders, such as Tauopathies, is direly needed (Figure 10).

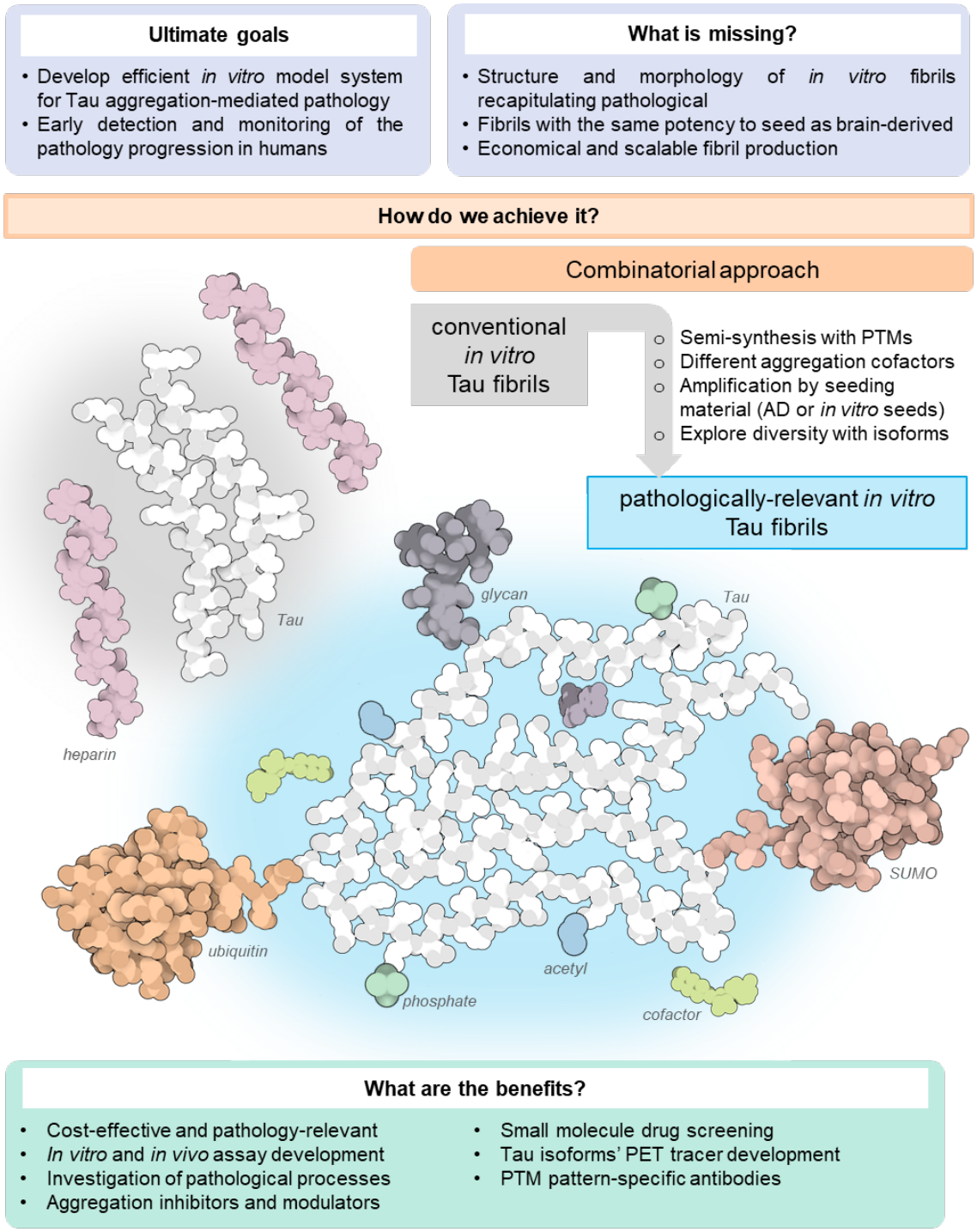

Figure 10. Bridging the gap between pathological and in vitro-formed Tau fibrils by embracing and reconstructing the complexity of the physiological and pathogenic Tau proteoforms and leveraging the latest advances in proteomics, chemical biology, and cryo-EM.

The combination of protein chemical synthesis and efficient in vitro tools that represent and mimic pathological processes of Tau aggregation with high fidelity have the potential for accelerated research into interventional therapies. Currently, no in vitro Tau fibrillization models accurately represent Tau aggregation processes, or model the formed fibrillar structures, derived from the human patient brain. The enormous complexity of the Tau biochemistry and biophysical properties contribute to the lack of translation of in vitro models to pathological structures, predominantly due to simplistic and reductionist approaches undertaken, that do not encompass the diversity of Tau protein isoforms and PTMs contributing to Tau aggregation. To develop better in vitro Tau aggregation models, these points must be considered, combined with a wider diversity of in vitro Tau aggregation cofactors. This will enable accurate and cost-effective modeling of pathology-relevant Tau aggregation processes and production of fibrils, which may be used for streamlined development of small molecule aggregation inhibitors; positron emission tomography tracers; as well as PTM-specific antibodies; contributing to better translation of laboratory findings into the clinic.

There is a pressing need to bridge the gap between the simplicity and utility of recombinant Tau, and the complexity of Tau in the brain. One way is to use a combination of enzymatic and protein synthesis approaches to introduce multiple PTMs to reproduce, to the extent possible, the PTM profile of Tau in the brain. One may argue that the large number of PTMs observed on Tau are difficult, if not impossible, to regenerate on one Tau molecule. However, we would like to stress that the commonly depicted combinatorial maps of Tau PTMs do not reflect the distribution of Tau PTMs on a single molecule, or PTMs observed on Tau fibrils. Rather, these maps give a summative representation of PTMs present on thousands of Tau molecules, which existed in different conformational states at the time of purification from different cells or brain tissues. Likely, the number of PTMs, as well as the PTM co-occurrence patterns, at the level of single Tau molecules are more constrained than we think. Therefore, it is crucial to revisit and reassess the PTM profile of different Tau preparations, aggregation states, different cell types, and brain regions with an emphasis on defining PTMs that co-occur on the same peptides/proteins. This will help narrow the number and diversity PTMs, thus making it possible to precisely reconstruct the relevant Tau species with PTM profiles that are similar to those seen in the brain. Although the recent advances in the chemical synthesis of Tau by our group and others have enabled for the first time the introduction of single or multiple PTMs site-specifically in different regions in Tau monomer [91,92,171,206,207], new methods are needed to enable site-specific modification of Tau oligomers and fibrils.

Future Directions:

1. Definition of pathological species across Tauopathies

Recent studies have shown that several types of Tau fibrils structure could coexist in Tauopathies. Further studies are needed to determine more precisely the relationship between these different Tau fibrils and whether they represent a continuum, interconverting structures, or distinct types of structures. Much of the knowledge we have about PTMs is derived from Tau aggregates isolated from the AD brain, mostly insoluble Tau. Therefore, there is a need to assess the PTM profiles of oligomers and fibrils from AD and other Tauopathies. This knowledge could provide novel insight into the key determinants of pathology formation in different Tauopathies and may pave the way for disease-specific diagnostics and therapeutic strategies.

2. Better sample preparation and disease stage stratification

We can isolate and characterize tau aggregates from human brains, but the limited quantities available using these methods and their heterogeneity limits their utility in large-scale drug discovery efforts and make them inaccessible to most research laboratories. Therefore, there is a need to continue to work aggressively to use the knowledge gained from the studies highlighted above to reverse engineer Tau pathological aggregates, determine whether they have conserved structures, and develop robust and reproducible methods to produce them at scale. More biochemical and structural studies using materials from patients that died at different stages of disease progression are essential. This work could pave the way for developing disease-specific biomarkers and diagnostics.

3. Focus on PTMs

We have made great progress in mapping the profile of PTMs associated with Tau pathology, but it remains unclear which of these PTMs 1) are associated with early and late stages of Tauopathies; 2) occur post-aggregation of Tau; 3) modify Tau cell-to-cell propagation and pathology spreading. Addressing these knowledge gaps is crucial for the development of effective small molecule and antibody-based strategies to image or target pathological Tau aggregates in the brain. Further, investigating the cross-talk between different Tau PTMs or the mechanisms that govern their competition for the same residues could unlock new avenues for targeting different aspects of Tau aggregation, propagation, and toxicity.

4. Pathology-relevant cofactors

More in-depth characterization of the biochemical composition of pathological aggregates beyond just their protein contents could provide novel insight into non-proteinaceous molecules that could be responsible for triggering Tau misfolding and aggregation across Tauopathies. These may include a wide range of molecule types, such as other interacting proteins, polysaccharides, nucleosides and nucleic acids, fatty acids and metal ions. Currently the major hindrances to characterisation of the native Tau fibril-interacting cofactors include unsuitable purification and biochemical detection protocols, further compounded by the small amount of pathological Tau material accessible to investigators. One way to reconcile this would be to utilise multiple approaches to investigate pathological Tau material, for example combining gentle biochemistry approaches with ultra-sensitive techniques such as mass spectrometry and cryo-EM, that can use minuscule amounts of the analytes. Further studies are also needed to investigate the interplay between PTMs and aggregation-inducing cofactors. This area has received very little attention, although previous studies have shown that a single mutation is sufficient to alter the interaction of Tau molecule with cofactors, e.g., RNA [157,232]. Addressing this knowledge gap could also pave the way for developing new methods for investigating the disease-relevant mechanisms of Tau aggregation and assays to screen for modifiers of Tau pathology formation and toxicity.

5. Revisit the relevance of heparin-induced Tau aggregation

Heparin-induced Tau fibrils are used in a wide variety of *in vitro*, in cell culture treatments, and *in vivo* studies. These conditions are also used to generate tools and reagents that are used to develop diagnostics tools and therapies for AD and tauopathies. Whether heparin is an integral part of the Tau fibrils is an important question to ask for several reasons. Heparin may impact the structural properties of Tau fibrils and their interactions with proteins and small-molecule ligands or antibodies. Based on the known properties of heparin within other experimental systems and its functions *in vivo*, the presence of heparin or abnormal levels of heparin in Tau fibril preparations may alter their biochemical and structural properties, as well as binding to small molecules and other proteins. This could explain why it has been very challenging to develop Tau-imaging agents or advance many of the small molecule modifiers of Tau aggregation into the clinic using assays that rely on heparin-induced recombinant Tau fibrils. This also has significant implications for the use of heparin-induced Tau aggregates to explore the relationship between Tau aggregation, neurodegeneration and pathology spreading. The presence of heparin in Tau fibril preparations may also lead to unexpected

effects when injected into the model animal brain, or upon cell culture treatments. Previous studies show that heparin molecules could potentially

1) elicit immune cell responses [233] non-contingent on the presence of Tau;

2) impact cardiovascular system cells and components, resulting in vasodilation [234];

3) interact with extracellular matrix constituents impacting Tau fibril spread and cellular uptake [158,235];

4) activate differential signaling pathways within cells [236-241];

5) stimulate aberrant modifications of Tau monomers [242] or fibrils, or

6) interact with Tau-targeting compounds and obfuscate their effects on Tau aggregation, as was found for leuco-methylthioninium molecule (TauRx Therapeutics) [243].

6. Novel methodological approaches

The aggregation mechanisms under conditions that mimic the complexity of Tau aggregation in the brain and the coexistence of multiple Tau isoforms are still unclear. We need new ways where we can study the aggregation of Tau isoforms as mixtures and not as individual species under the conditions closely recapitulating the brain milieu. Furthermore, we need to reconcile the PTM and structural data of Tau fibrils. Although mass spectrometry analyses of pathological Tau aggregates usually show a large number of PTMs that are distributed throughout the sequence of Tau including regions in the core of the fibrils, such PTMs are rarely seen in the cryo-EM structures. This is due to the methods interrogating different states of the Tau molecules – soluble Tau in mass spectrometry, insoluble Tau in cryo-EM. Therefore, we need new integrative approaches, such as nanobodies to Tau PTMs that can be combined with cryo-EM, and better fibril dissociation into monomers and solubilization approaches to apply mass spectrometric analyses to the material faithfully derived from the pathological Tau aggregates. Together, these advances will pave the way for more systematic studies on the roles of PTMs in regulating Tau aggregation, pathology formation, and diversity.

Achieving these goals will require concerted and collaborative efforts between scientists from different disciplines, new mechanisms to fund, recognize and reward team science, and rapid integration of new insights from patients into basic and translational research [224].

xx

CHAPTER 2

Revisiting the grammar of Tau aggregation and pathology formation: How new insights from brain pathology are shaping how we study and target Tauopathies

Galina Limorenko[#] and Hilal A. Lashuel[#*]

Laboratory of Molecular and Chemical Biology of Neurodegeneration, Brain Mind Institute, École Polytechnique Federal de Lausanne (EPFL), CH-1015 Lausanne, Switzerland.

Corresponding Author: hilal.lashuel@epfl.ch

# Equal Contribution

Keywords

Microtubule-associated protein Tau, Tau, Heparin, Tau aggregation, Tau fibrillization, PHF, Tau PTMs

Chemical Society Reviews. 2022 Jan 24;51(2):513-565.

doi: 10.1039/d1cs00127b.

Abstract

Converging evidence continues to point towards Tau aggregation and pathology formation as central events in the pathogenesis of Alzheimer's disease and other Tauopathies. Despite significant advances in understanding the morphological and structural properties of Tau fibrils, many fundamental questions remain about what causes Tau to aggregate in the first place. The exact roles of cofactors, Tau post-translational modifications, and Tau interactome in regulating Tau aggregation, pathology formation, and toxicity remain unknown. Recent studies have put the spotlight on the wide gap between the complexity of Tau structures, aggregation, and pathology formation in the brain and the simplicity of experimental approaches used for modeling these processes in research laboratories. Embracing and deconstructing this complexity is an essential first step to understanding the role of Tau in health and disease. To help deconstruct this complexity and understand its implication for the development of effective Tau targeting diagnostics and therapies, we firstly review how our understanding of Tau aggregation and pathology formation has evolved over the past few decades. Secondly, we present an analysis of new findings and insights from recent studies illustrating the biochemical, structural, and functional heterogeneity of Tau aggregates. Thirdly, we discuss the importance of adopting new experimental approaches that embrace the complexity of Tau aggregation and pathology as an important first step towards developing mechanism- and structure-based therapies that account for the pathological and clinical heterogeneity of Alzheimer's disease and Tauopathies. We believe that this is essential to develop effective diagnostics and therapies to treat these devastating diseases.

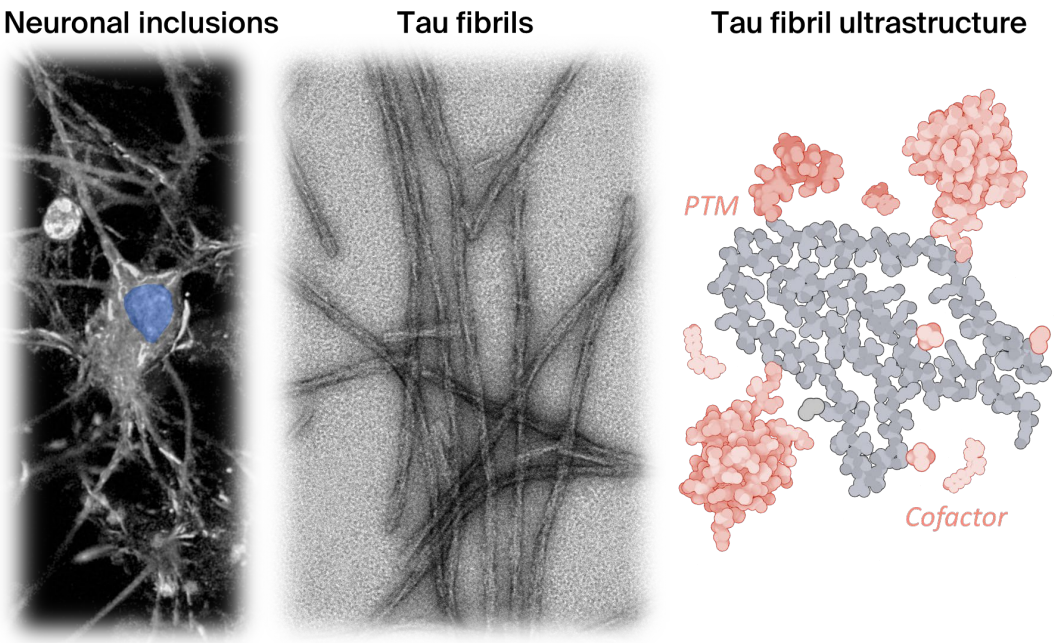

Introduction

The microtubule-binding protein Tau is an intrinsically disordered protein, which is expressed as six isoforms in the adult human central nervous system (Figure 1 A). In cells, Tau is most prominently associated with dynamic regulation and stabilization of cytoskeletal and mitotic microtubules through direct binding to tubulin dimers [244], however other non-canonical functions of Tau have been proposed [245] (Figure 1 B). In neurons, it is important to regulate axon outgrowth and maintenance of axonal cytoskeletal integrity and transport [246]. However, factors such as mutations [247], post-translational modifications (PTMs) [248], interaction with other molecules [249,250] (Figure 1 C), and changes to the biochemical composition of surrounding milieu (e.g. pH, drug compounds) [251] may result in weaker interaction between Tau and its natural partners or its dissociation from microtubules (reviewed in [252]). This is thought to lead to Tau accumulation, which creates conditions that favor its aggregation and formation of the β-sheet rich fibrillar aggregates found in the brains of individuals with Alzheimer's disease (AD) and other neurodegenerative diseases (NDDs). Hyperphosphorylated and fibrillar Tau is found in the form of paired helical filaments (PHFs) and straight filaments (SFs) in cytoplasmic neurofibrillary tangles (NFTs) and dystrophic neurites, which represents one of the two main hallmarks of Alzheimer's disease (AD), in addition to amyloid plaques. Tau aggregates, both fibrils, and oligomers are also found in the brain of individuals that suffered from other neurodegenerative diseases (NDs), which include Pick's disease (PiD) and progressive supranuclear palsy (PSP), collectively known as Tauopathies [253-260]. Several structures of brain-derived Tau fibrils have been recently solved using cryo-electron microscopy (cryo-EM), and the list currently includes Tau folds from AD, Pick's disease (PiD), chronic traumatic encephalopathy (CTE), corticobasal degeneration (CBD), progressive supranuclear palsy (PSP), argyrophilic grain disease (AGD), primary age-related tauopathy (PART), familial British dementia (FBD), familial Danish dementia (FDD), globular glial tauopathy (GGT), and author-coined limbic-predominant neuronal inclusion body 4R tauopathy' (LNT) [261] (for recent reviews see [156,163,262]).

Increasing evidence points to Tau aggregation (oligomerization and fibril formation) and post-translational modifications (PTMs) as central events in the pathogenesis of AD and Tauopathies, which made Tau an appealing target for drug discovery and development [263-265]. However, the molecular and cellular factors that trigger Tau misfolding and aggregation and drive the spreading of Tau pathology in the brain remain unknown. Furthermore, the functional significance of Tau aggregation is still unclear. Whether it is a pathogenic gain-of-function (GOF) linked to the formation of cytotoxic Tau species or represents a neuroprotective process

that sequesters soluble toxic forms of Tau, or a balance of both, remains to be elucidated. These processes are also accompanied by the loss of physiological function(s) (LOF) due to the depletion of soluble and functional Tau proteins. It is likely that both GOF and LOF mechanisms contribute to the development and progression of Tauopathies. However, the relative contributions of each to the various stages of disease development remain unknown.

Crucially, which forms of Tau are the primary initiators of these processes and how PTMs influence the course of Tau aggregation and pathology formation and spreading remain subjects of intense investigation and debate. In this review article, we will 1) review how our understanding of Tau aggregation and pathology formation has evolved over the past few decades; 2) present analysis of new findings and insights from recent studies illustrating the biochemical, structural and functional heterogeneity of Tau aggregates; and 3) discuss the importance of adopting new experimental approaches that embrace the complexity of Tau aggregation and pathology as an important first step towards developing mechanism- and structure-based therapies that account for the pathological and clinical heterogeneity of Alzheimer's disease and Tauopathies. We believe that this is essential to develop effective diagnostics and therapies to treat these devastating diseases.

Tau protein expression

Six major Tau isoforms are found in the central nervous system that differs based on the inclusion and exclusion of the exons 2, 3, and 10 of the MAPT gene, resulting in the Tau protein isoforms containing 0, 1, or 2 N-terminal segments, and differential exclusion of the second microtubule-binding repeat [266](Figure 1 A). On the level of protein expression, Tau is most abundant in the frontal and occipital cortices, followed by white matter, whereas its levels are significantly reduced in putamen and cerebellum in concordance with gene expression data [32]. The protein levels or distribution of 3R-Tau and 4R-Tau isoforms are approximately equal across brain regions, with 1N-Tau isoforms accounting for about 50%, 0N-Tau isoforms for ~40%, and 2N-Tau isoforms for ~10% of total Tau [32]. However, in neurodegenerative diseases, the ratio of Tau protein isoforms containing 3 or 4 microtubule-binding repeats is perturbed [267-272].

Cellular processes

The Tau proteins have been implicated in multiple cellular processes (Figure 1 D). It was long thought that the primary function of Tau was to stabilize microtubules. Still, more recently, the

focus shifted to its abilities to regulate the MT dynamics, more so than to stabilize them [273] (reviewed in [274]). Tau is involved in the insulin signaling pathway by inhibiting phosphatase and tensin homolog (PTEN) [275], nuclear functions such as stability of heterochromatin [245], and synaptic processes such as long-term depression [276,277] and potentiation [278] (reviewed in [279]). Depletion of functional Tau leads to impairments of the processes related to the subset of highly cycling and dividing brain cells, such as hippocampally-positioned neuronal precursors, involved in neurogenesis [280-283] and glial precursors to neuronal cells [284,285], as well as incomplete neuronal cell-cycle re-entry [286]. This resulted in the neurodegeneration that underlies impairment in memory, increased anxiety, and reduced learning ability [287,288]. Recent studies have also shown that Tau proteins are secreted and propagated from one cell to another. Although this process has been proposed to play central roles in the spreading of Tau aggregates, whether extracellular Tau also plays a physiological role in the brain remains unknown.

What happens upon complete depletion of Tau in neurons? Interestingly, complete mouse Tau knockout mice that do not express any Tau isoforms showed variable pathological phenotypes at an advanced age, manifesting in cognitive and motor deficits, which varied according to the genetic background of mice [289]. Another commonly used mouse line is hTau [290]. It is hemizygous for overexpression of all six human Tau isoforms on mouse Tau knockout background, and the litters result in the expected half of the mice to express human Tau only, and the other half to be complete mouse and human Tau knockout, providing the isogenic experimental controls. Tau proteins are ubiquitously expressed throughout tissues, and function in processes related to cell division and dynamic cytoskeleton reorganization. Consistent with this, hTau mice showed peripheral deficits in functions related to the highly cell-cycling, dividing, and metabolically-active secreting pancreatic cells in the Tau knockouts, and overexpression of human Tau in islet cells did not rescue the deficits in glucose homeostasis [291,292]. Also, impairment in memory, increased anxiety, and reduced learning ability were observed in these mice, which could not be rescued by the expression of human Tau isoforms [292]. Incomplete cell-cycle re-entry (CCR) of post-mitotic neurons was also observed in hTau mice in [286], suggesting that loss of physiological Tau could contribute to neurodegeneration via mechanisms independent of Tau aggregation (LOF) and formation of NFTs. Consistent with this hypothesis, aberrant CCR was implicated in the processes of neuronal loss in AD patients [287,288], and in mouse models [293,294], and was found to be independent of the Aβ plaque or NFT formation. Further, the ectopic cell CCR was found to require soluble Aβ oligomers-mediated activation of Tau kinases Fyn, PKA, and CCKII, which phosphorylated Tau at positions pY18, pS409, and pS416, respectively [295].

A

Tau Isoforms

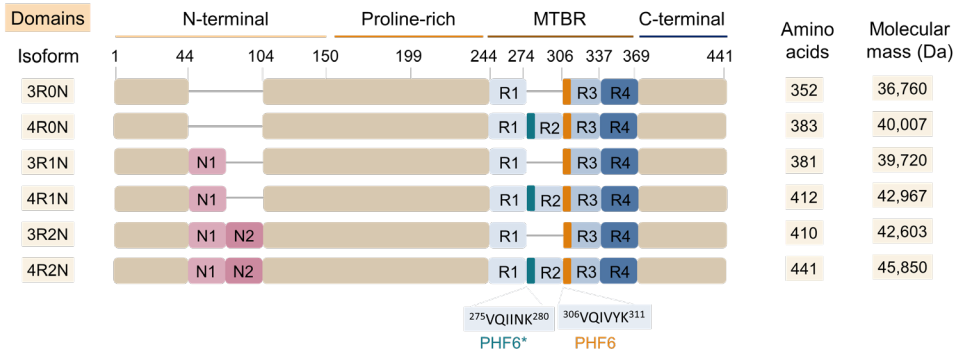

B

Major functional associations

N-terminal projection domain

- Associates with C-terminus and proline-rich region
- Inhibits fast kinesin-dependent axonal transport and influences cargo delivery
- Modulates binding of dynactin to microtubules
- Modulates binding to lipid membranes
- Influences microtubule spacing
- Contains phosphatase-activating domain

Microtubule-binding domain

- Mediates binding to microtubules and lipids
- Regulates microtubule polymerisation and stabilisation
- Mediates Tau aggregation processes that are influenced by multiple PTM patterns
- Constitutes cores of the pathological PHFs and SFs
- Mediates bundling and cross-linking of the actin filaments
- Activates cholinergic receptors

C

Interacting molecules

N-terminus | Proline-rich | MTBR | C-terminus

Proteins

AATF	BAG1	CASP6	CSNK1D	EGFR	GAR1	HSP90AA1	LRRK2	MAPT	NUDC	PLCG1	PRKCZ	S100B	SRP14	TUBA1A
ABCF1	BAG6	CASP7	CSNK2A1	EIF2S2	GNPNAT1	HSPA1A	MAP2	MARK1	NUFIP1	PLCG2	PRKRA	SCG3	SRPK1	TUBA1B
ABL1	BIN1	CASP8	CTSD	EIF2S3	GRB2	HSPA4	MAP2K7	MARK2	OGT	PPP1CA	PSEN1	SCLT1	SRPK2	TUBA4A
ACTA1	BRSK1	CCDC124	CUEDC2	EP300	GSK3A	HSPA5	MAP7D1	MARK3	OTUB1	PPP1CB	PSMB5	SERBP1	STAU1	TUBB1
ACTB	BRSK2	CDC37	DCTN1	EWSR1	GSK3B	HSPA8	MAPK1	MARK4	PA2G4	PPP1CC	PSMC2	SGK1	STIP1	TUBB3
ACTG1	C14orf166	CDCA8	DDX6	EZR	Gtf2e2	HSPB1	MAPK10	MASP1	PABPC1	PPP2CA	PTGES3	SIK1	STUB1	UBC
AHSA1	C19orf53	CDK1	DENR	F2	H1FX	HTRA1	MAPK11	MELK	PACSIN1	PPP2CB	PTK2B	SIRT1	STXBP1	UBE2D2
AK2	C7orf50	CDK2	DGUOK	FKBP1A	HAX1	KATNA1	Mapk12	METAP2	PARK2	PPP2R4	PWP2	SLC1A2	SYK	UBE2W
AKT1	C9orf78	CDK5	DNAAF2	FKBP3	HDAC6	KIAA1143	MAPK13	MTHFD1	PDAP1	PPP5C	RPL35	Slc6a8	SYNCRIP	UFD1L
AMPH	CALM1	CHEK1	DNAJA1	FKBP4	HGS	Kifc3	mapk14	NME2	PDIA2	PRKACA	RPS26	SMAD2	TCEB3	USP43
APOE	CAMK2A	CHEK2	DUSP1	FKBP5	HNRNPAB	Klc1	MAPK3	NMNAT2	PEG10	PRKCA	RPS6KA1	SNCA	TFEB	YBX1
APP	CAPN1	CKAP5	DYNLRB1	FUS	HNRNPD	Klc2	MAPK8	NMT1	PHGK	PRKCB	RPS6KA3	SNRNP70	TIA1	YWHAB
ARHGEF2	CAPN2	CLU	DYRK1A	FYN	HNRNPL	LCK	MAPK8IP1	NPEPPS	PIK3R1	PRKCE	RPS6KA5	SPICE1	TIGD6	YWHAE
ARMC1	CASP1	CREBBP	DYRK2	G3BP1	HNRNPUL1	LGMN	MAPK9	NSUN2	PIN1	PRKCG	RPS6KB1	SQSTM1	TRAF6	YWHAQ
ATXN2	CASP3	CSNK1A1	EDF1	G3BP2	HOOK3	LIMS1	MAPRE1	NUB1	PKN1	PRKCI	RRP7A	SRC	TTBK1	YWHAZ

RNA transcripts

AC006077.2-201	AL357033.3-201	CAPNS1-206	CSNK1E-206	FAM89B-202	HAPLN2-201	KHSRP-213	MPND-207	PHF10-201	PWWP2B-202	TCF15-201
AC008738.5-201	ALYREF-202	CCM2-219	CYBA-201	FAM89B-203	HES6-203	LIMCH1-211	NECTIN3-201	PPP1CA-203	RAB12-201	TGIF1-202
AC015813.7-201	ANKRD60-201	CDV3-203	CYHR1-209	FBLL1-201	HOXB3-208	LMO2-202	NKAIN4-203	PPP2CB-201	RAN-202	TRIP10-202
AC116565.1-201	B4GALT2-203	CHCHD4-202	DRD4-201	FEZF2-203	HRAS-203	MAF-203	NT5DC2-202	PPP2CB-204	SATB1-AS1-216	UBE2M-201
ACOT7-209	C11orf63-202	CMTM4-202	ECHS1-201	FOXD1-202	ILK-212	MAPK3-201	NT5DC2-203	PRELID2-202	SEPT3-204	Z97634.1-201
AES-202	C11orf68-202	CMTM4-204	FAM149A-205	GALR3-201	INO80B-201	MAPK3-202	NT5M-207	PRR5-216	SLC25A28-201	ZFYVE21-201
AL136373.1-201	C11orf84-201	CRIP2-201	FAM149A-215	GIPC1-205	INO80B-203	METRNL-201	OLFM1-208	PRR5-217	SSSCA1-205	ZNF358-202
AL356512.1-201	CACNG8-202	CSNK1E-204	FAM19A5-203	HAGHL-201	INO80B-WBP1-202	MPND-201	PABPN1-201	PTF1A-201	TAF5L-202	ZNRF2P1-201

Other

Anionic lipids | Sulfated polysaccharides | DNA | Metals

D

Gene Ontology terms (molecular function, biological process, cellular component)

actin binding
activation of cysteine-type endopeptidase activity involved in apoptotic process
amyloid fibril formation
apolipoprotein binding
astrocyte activation
axolemma
axon
axon cytoplasm
axon development
axonal transport
axonal transport of mitochondrion
cell body
cell projection
cell-cell signaling
cellular response to brain-derived neurotrophic factor stimulus
cellular response to heat
cellular response to nerve growth factor stimulus
cellular response to reactive oxygen species
central nervous system neuron development
chaperone binding
cytoplasm
cytoplasmic microtubule organization
cytoplasmic ribonucleoprotein granule
cytoskeleton
cytosol
dendrite
dendritic spine
DNA binding
double-stranded DNA binding
dynactin binding
enzyme binding
extracellular region
generation of neurons
glial cell projection
growth cone
histone-dependent DNA binding
Hsp90 protein binding
identical protein binding
internal protein amino acid acetylation
intracellular distribution of mitochondria
learning or memory
lipoprotein particle binding
main axon
membrane
membrane raft
memory
microglial cell activation
microtubule
microtubule binding
microtubule cytoskeleton
microtubule cytoskeleton organization
microtubule lateral binding
microtubule polymerization
minor groove of adenine-thymine-rich DNA binding
mitochondrion
negative regulation of establishment of protein localization to mitochondrion
negative regulation of gene expression
negative regulation of kinase activity
negative regulation of mitochondrial fission
negative regulation of mitochondrial membrane potential
negative regulation of tubulin deacetylation
neurofibrillary tangle
neurofibrillary tangle assembly
neuron projection
neuron projection development
neuronal cell body
nuclear periphery
nuclear speck
nucleus
phosphatidylinositol binding
phosphatidylinositol bisphosphate binding
plasma membrane
plus-end-directed organelle transport along microtubule
positive regulation of axon extension
positive regulation of cellular protein localization
positive regulation of diacylglycerol kinase activity
positive regulation of microtubule polymerization
positive regulation of neuron death
positive regulation of protein localization to synapse
positive regulation of superoxide anion generation
protein binding
protein homooligomerization
protein kinase binding
protein phosphatase 2A binding
protein polymerization
protein-macromolecule adaptor activity
regulation of autophagy
regulation of calcium-mediated signaling
regulation of cellular response to heat
regulation of chromosome organization
regulation of long-term synaptic depression
regulation of microtubule cytoskeleton organization
regulation of microtubule polymerization
regulation of microtubule polymerization or depolymerization
regulation of mitochondrial fission
regulation of response to DNA damage stimulus
regulation of synaptic plasticity
response to lead ion
RNA binding
rRNA metabolic process
sequence-specific DNA binding
SH3 domain binding
single-stranded DNA binding
somatodendritic compartment
stress granule assembly
supramolecular fiber organization
synapse assembly
synapse organization
tubulin binding
tubulin complex

Figure 1. Tau sequences, functions, and interactome. A. In the adult human central nervous system, six Tau isoforms are highly expressed. Functional domains contain N-terminal inserts (N1, N2), a proline-rich region, four microtubule-binding repeat domains (R1 aa 244-274; R2 aa 275-305; R3 aa 306-336; R4 aa 337-368) and C-terminus. Amino acid numbering is based on the sequence of the full-length human 4R2N Tau (1-441). B. Major functions attributed to the Tau N-terminal projection domain, which include the N-terminal and first part of mid-domain, and microtubule regulation domain that includes the second part of mid-domain, MTBR, and remaining C-terminal residues. C. A partial list of known Tau interacting proteins. Protein binding partners for Tau 4R2N were established using searches through IntAct [296] and BioGRID databases [297] filtering for unique direct interactors verified experimentally. Notably, a specific binding region on Tau is established only for a tiny fraction of all interactors. Tau interacting RNA transcripts were predicted using RNAct database [298]. Other types of Tau-interacting molecule classes include DNA, lipids, and polysaccharides (IntAct [296]). D. Gene Ontology [299] terms associated with Tau query. Tau is associated with multiple molecular functions, biological processes, and cellular components.

Tau knockout neurons did not enter the CCR despite the activation of kinases. However, the expression of Tau restored the CCR, in contrast to the phosphorylation-resistant Tau mutants which failed to restore it [295].

In summary, depletion of Tau may lead to impairments of the processes related to the subset of highly cycling and dividing brain cells, such as hippocampally-positioned neuronal precursors, involved in neurogenesis [280,281] and glial precursors to neuronal cells [284,285].

Interactome

One way to gain insight into the functions of Tau in health and disease is through understanding its interactome network. Tau is involved in multiple interactions with a wide range of molecules, with different domains implicated in regulating these interactions (Figure 1 B). These include proteins, nucleic acids, lipids, and polysaccharides, many of which have been shown to regulate many aspects of Tau functions under physiological and/or pathological conditions [300-302](IntAct database [296], BIOGrid database [297], RNAct database [298]) (Figure 1 C). Tau interacts with more than 200 proteins (Figure 1 C, Proteins). This versatility and broadness of Tau interactions with proteins are highly complex and it differs between healthy and pathological human conditions [303]. Experimental approaches such as neuroproteomics[59], laser capture microdissection coupled with mass spectrometry [304,305], and interactome studies have been instrumental for the interrogation of Tau interactions with other molecules [303,306,307], and in organoid [308] and mouse models [309]. Tau was found to interact with DNA [310] and RNA [311], strongly suggesting that it has important regulatory roles in the nucleus [245,312], such as wide-scale chromatin reorganization, detected in AD brain [313], as well as through post-

transcriptional regulation of multiple gene transcripts (Figure 1 C, RNA transcripts). Tau interactions with other molecules are often heavily influenced and modulated by the extensive Tau PTMs [55]. One of the most prominent PTM-regulated Tau interactions is with tubulin, the subunits composing MTs. Hyperphosphorylation in the MTBR decreases Tau affinity for MTs and leads to an increased rate of its dissociation. This may lead to a higher rate of Tau self-association conducive to aggregation [314]. Further functional validations of the Tau interacting partners are necessary to understand the significance and extent of the molecular functions of Tau beyond its canonical association with the tubulin.

Tau contribution to neurodegenerative disorders

The presence and spreading of Tau-positive detection in the brain of normally-aging individuals is well-known, and is not in itself considered to be a functional Tau pathology, and may not be associated with cognitive impairment, however, could indicate the incipient pathology [315-318]. In older adults, Tau accumulates predominantly in medial temporal lobes and is concurrent with low cognitive deficits that accompany the normal aging processes [319,320]. Regional brain vulnerability to Tau pathology is well-known in humans and is thought to be stereotypical of different Tauopathies, for example in AD the pathology tends to follow the "subcortical to cortical" spreading pattern affecting the cortex at the later stages, whereas in PSP and CBD pathology is confined to the subcortical regions, with later stages affecting basal ganglia and cerebellum [170,321,322]. Entorhinal, temporal isocortices, and hippocampal formations are highly susceptible to Tau aggregate formation and neurodegeneration [321,323-334]. Brain circuits between these areas are anatomically connected and are implicated in memory formation, consolidation, and cognition. The aggregation of Tau observed in these neocortical regions temporally follows the deposition of amyloid-β, and correlates with the loss of cognitive abilities in Alzheimer's patients [335,336]. Non-neuronal and glial cell populations can also contribute to Tau-mediated pathology formation in mouse models [337,338], and microglia-expressed triggering receptor expressed on myeloid cells 2 (TREM2) gene variants contribute to the increased AD risk in humans [339]. Tau pathology is thought to proceed through the primary mechanism of direct Tau aggregation in the cell cycle-arrested non-neuronal oligodendrocyte [340] and astrocytic cells [341], through secondary pathology events such as gliosis and neuroinflammation via cytokine excretion [342,343], or glia-mediated Tau spreading [344].

Therefore, it is important to delineate the conditions which flip the switch of physiological-to-pathological Tau aggregation in the brain. These may include 1) regional vulnerability of the

brain circuits to Tau aggregation, 2) neuronal and non-neuronal cell type vulnerability, such as increased susceptibility of the excitatory presynaptic neurons [345], 3) emergence of particularly toxic Tau protein subpopulations due to PTMs or associations with cofactor molecules or other amyloidogenic proteins, such as amyloid-β [346], 4) local changes in the brain and CSF acidification levels [347,348], as well as 5) subcellular mislocalization of Tau protein from axonal to somatodendritic compartments [349] that may contribute to Tau displacement from microtubules in cells [350] and subsequent aggregation. It is yet not fully understood which mechanisms contribute substantially to the inception and progression of human Tauopathies.

In terms of the clinical manifestations of Tau pathologies, loss of cognition coupled with the regional brain Tau NFT distribution detected by live PET imaging may indicate the specific Tau-associated disease. These tests, combined with the post-mortem histochemical stainings and the biochemical properties of the isolated Tau, form the basis of the classification of the Tauopathy disorders, and their stages of progression [351].

Table 1. Tauopathies with known Tau isoform composition

3R+4R	**4R**
Alzheimer's disease (AD)	Age-related Tau astrogliopathy (ARTAG)
Amyotrophic lateral sclerosis/parkinsonism-dementia complex (ALS)	Argyrophilic grain disease (AGD)
Anti-IgLON5-related Tauopathy	Corticobasal degeneration (CBD)
Chronic traumatic encephalopathy (CTE)	Guadeloupean parkinsonism
Diffuse neurofibrillary tangles with calcification	Globular glial Tauopathy (GGT)
Down's syndrome	Hippocampal Tauopathy
Familial British dementia (FBD)	Huntington's disease
Familial Danish dementia (FDD)	Progressive supranuclear palsy (PSP)
Gerstmann-Sträussler-Scheinker disease (GSS)	Familial frontotemporal dementia and parkinsonism (FTDP, mutations P301S, intronic mutations, coding region mutations in exon 10)
Niemann-Pick disease, type C	
Nodding syndrome	
Non-Guamanian motor neuron disease with neurofibrillary tangles	**3R**
Postencephalitic parkinsonism	Pick's disease (PiD)
Primary age-related tauopathy (PART)	Familial frontotemporal dementia and parkinsonism (FTDP, mutations G272V and Q336R)
Progressive ataxia and palatal tremor	
SLC9A6-related parkinsonism	
Tangle-only dementia (TOD)	
Familial frontotemporal dementia and parkinsonism (FTDP, mutations V337M and R406W)	

The Tauopathies with the known biochemical Tau profile are classified into predominantly 4R-Tauopathies containing the 4R Tau isoforms in the insoluble protein brain fractions, such as PSP, CBD, and AGD, as well as gliopathies ARTAG and GGT. Predominantly-3R Tauopathies include the neuronopathy and gliopathy PiD and neuronopathy the behavioural variant of frontotemporal dementia (bvFTD) [351]. The Tauopathies defined by the presence of all six Tau isoforms include AD, CTE, PART, tangle-only dementia (TOD), dementia with Lewy bodies (DLB), and primary progressive aphasia (PPA) (Table 1). Also, co-occurrence of Tau pathology may be observed in the late stages of other proteinopathies, such as Huntington's disease [352], synucleinopathies [353], and amyotrophic lateral sclerosis (ALS) [354].

Following the findings that cognitive decline correlated with Tau pathology progression in patients [40] to a better extent than amyloid β pathology, the levels of Tau in CSF [38], as well as Tau PET imaging [39] in the brain have been studied as early biomarkers. This is especially prescient due to fact that the sporadic and secondary Tauopathies, such as AD, are not associated with specific mutations in the Tau-coding MAPT gene and therefore elude early screening. This is in contrast to familial Tauopathies (Table 1), such as autosomal dominant frontotemporal dementia and parkinsonism (FTDP) linked to chromosome 17q21 [355], or Tauopathies with a clear underlying genetic component, such as Pick's [356]. Therefore, early detection of incipient pathological Tau processes as diagnostics biomarkers, as well as therapeutic targets, has recently garnered much attention.

Spreading of Tau pathology

At the brain level, in AD the Tau pathology spreading follows the pathological stage-like manner (Figure 2 A), starting from entorhinal and transentorhinal cortices at stage I, progressing to hippocampal in stage II and transentorhinal cortical regions in stage III, followed by the cerebral and visual cortices in stage IV and later stages V and VI [321,357]. Evidence suggests that Tau pathology in AD is transmitted along the anatomically connected brain regions (reviewed in [358]). Computationally-aided integration of imaging and biochemical data would allow for reconstructing the AD connectome, which, combined with computer modeling approaches, have the potential to provide higher resolution and granularity to our understanding of stages of Tauopathy progression in the human brain [359].

On a cellular level, Tau pathology is thought to spread from one cell to the next through Tau proteoform release from the donor cell via multiple potential pathways, such as the direct

transport across membrane, exocytosis, endosome-, exosome-, and heparan sulfate proteoglycan (HSPG)-mediated release (Figure 2 B).

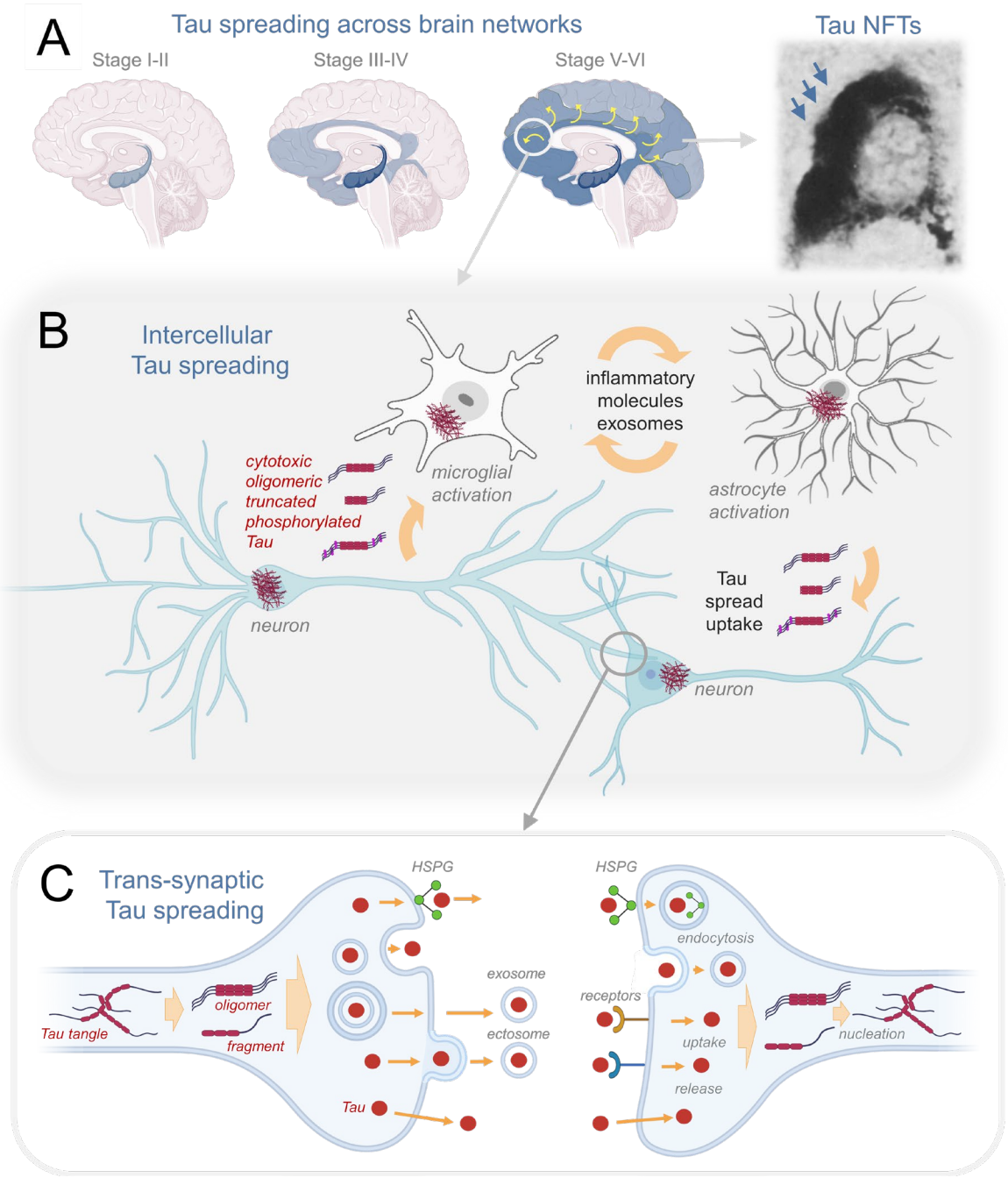

Figure 2. Tau aggregation mechanisms. A. Schematic representation of Braak stages of Tau pathology across brain networks as detected by immunohistochemistry of NFTs (reproduced from ref. [76] with permission from the Elsevier, copyright 1991). B Intercellular Tau pathology spreading between neuronal and neuronal, and neuronal and glial cells. C Trans-synaptic spreading of different pathogenic Tau proteoforms is thought to occur through their transport across membrane release, exocytosis, endosome-, exosome-, HSPG-mediated release from the affected donor cell. The uptake of putative pathological Tau species is thought to be

mediated by HSPG-, receptor-coupled mechanisms, endocytosis, and direct transport across the plasma membrane. The recipient cell may develop further Tau pathology through nucleation and seeding of the endogenous Tau.

A further transmission of Tau across synaptic cleft is thought to be followed by Tau uptake by recipient cell via direct transport, endocytosis, or receptor-, or HSPG-mediated uptake. In the recipient neurons Tau is thought to nucleate and initiate recruitment and aggregation of endogeneous Tau (Figure 2 C), first affecting the distal, followed by proximal dendrites, then cell soma, eventually reaching the axonal compartment [360]. It has been suggested that the spread of toxic Tau species underlying the pathologies may be mediated by one or a combination of a) a direct prion-like spreading mechanism of misfolded Tau across the cellular membrane with the recruitment of normal Tau in the receiving cell; b) exosome-mediated and c) trans-synaptic spreading of toxic Tau species (reviewed in [361,362]) (Figure 2 A). Thus far, however, the evidence for the prion-like Tau propagation is only circumstantial in humans, with most work to elaborate this hypothesis done in cellular and animal models (see recent reviews [263,363,364]). Which forms of Tau are secreted and propagated in the human brain remains unclear, although studies have identified several truncated [365,366] and post-translationally modified forms of the protein [57,211] in CSF and blood of Tauopathy patients.

Composition of neurofibrillary tangles

Besides the Tau proteins in fibrillized conformation, NFTs are composed of multiple other molecules, including proteins, carbohydrates, nucleic acids, and lipids. Formation and diversity of molecular composition of NFTs are established by 1) the molecules that drive the primary formation of NFTs, such as mutant proteins, or proteins in pathological conformations, such as fibrillar Tau, 2) recruitment of other molecules and cellular components through direct binding or diffusion, and 3) as a secondary formation due to accumulation of cellular waste products following cellular impairment and degeneration.

In addition to Tau, early biochemical and immunohistological profilings of NFTs from different diseases identified other associated molecular components. Although the exact molecular composition of pathological Tau aggregates remains unknown, several studies have highlighted their complexity and diverse composition. Cytoskeletal proteins such as MAP1B [367], MAP2 [368], neurofilament, and vimentin [369] were detected by immunohistochemistry in AD-derived NFTs early on. Further, in AD, extracellular NFTs contained amyloid-β, amyloid-P, extracellular signal-related kinase-2, glial fibrillary acidic protein (GFAP), and ubiquitin,

whereas intracellular NFTs contained apolipoprotein E (Apo E), basic fibroblast growth factor (bFGF), GFAP, heparan sulfate proteoglycan (HSPG), complement membrane attack complex C5b-9, neurofilament, synaptophysin, and ubiquitin. Other NFT-associated molecules included casein kinase II (CKII), glycogen synthase kinase-3 (GSK3), phospholipase C-δ, malondialdehyde, heme oxygenase-1, vitronectin, gangliosides C, anti-thrombin III, and lactotransferrin. Pick's bodies were shown to contain Apo E, advanced glycation end-products (AGEs), bFGF, chromogranin B, complements C1, C1q, C4, C2, C3, C5, C6 and C8, clathrin, membrane complement inhibitor CD59, clusterin, GFAP, synaptophysin, and ubiquitin (reviewed in [370]). NFTs in PSP contained enriched GFAP and ubiquitin, whereas CBD inclusions contained GFAP and marker for killer lymphocytes Leu-7 (reviewed in [371]). The proteomic profiling of NFTs using laser capture microdissection coupled to mass spectrometry revealed peptides derived from 542 proteins [372]. However, the list of these 542 proteins is not openly available. 41 polypeptides were identified in AD NFTs by mass spectrometry and included GAPDH and ubiquitin carboxy-terminal hydrolase L1 (UCH-L1) that colocalized with NFTs by immunostaining [373]. Another study identified 72 proteins within the NFTs, with biochemically-verified glyceraldehyde 3-phosphate dehydrogenase (GAPDH) as a major constituent [374]. S-glutathionylated GAPDH form was detected in the blood of Alzheimer's patients and is a pro-apoptotic molecule that was not present in blood under healthy conditions [375].

Given such complexity of NFTs and the implications of their biochemical diversity for targeting and imaging pathological Tau, it is crucial to revisit Tau pathology with more systematic approaches to dissect the molecular compositions of intracellular, extracellular, and ghost tangle NFTs. A better understanding of the proteomic compositions of individual NFTs could provide insight into biochemical changes associated with the formation and maturation of Tau pathology. The knowledge gained from these studies, combined with the structural insight gained from Cryo-EM could guide future efforts to develop diagnostic and therapeutic strategies that target specific Tau pathologies or capture their diversity in the brain. Furthermore, a better understanding of the molecular components of pathological Tau aggregates could also provide novel insight into natural cofactors responsible for triggering Tau pathology formation in different Tauopathies.

Tau aggregation

Under pathological conditions, Tau is observed in the aggregated state in the surviving cells of patients with Tauopathies (Figure 3 A).

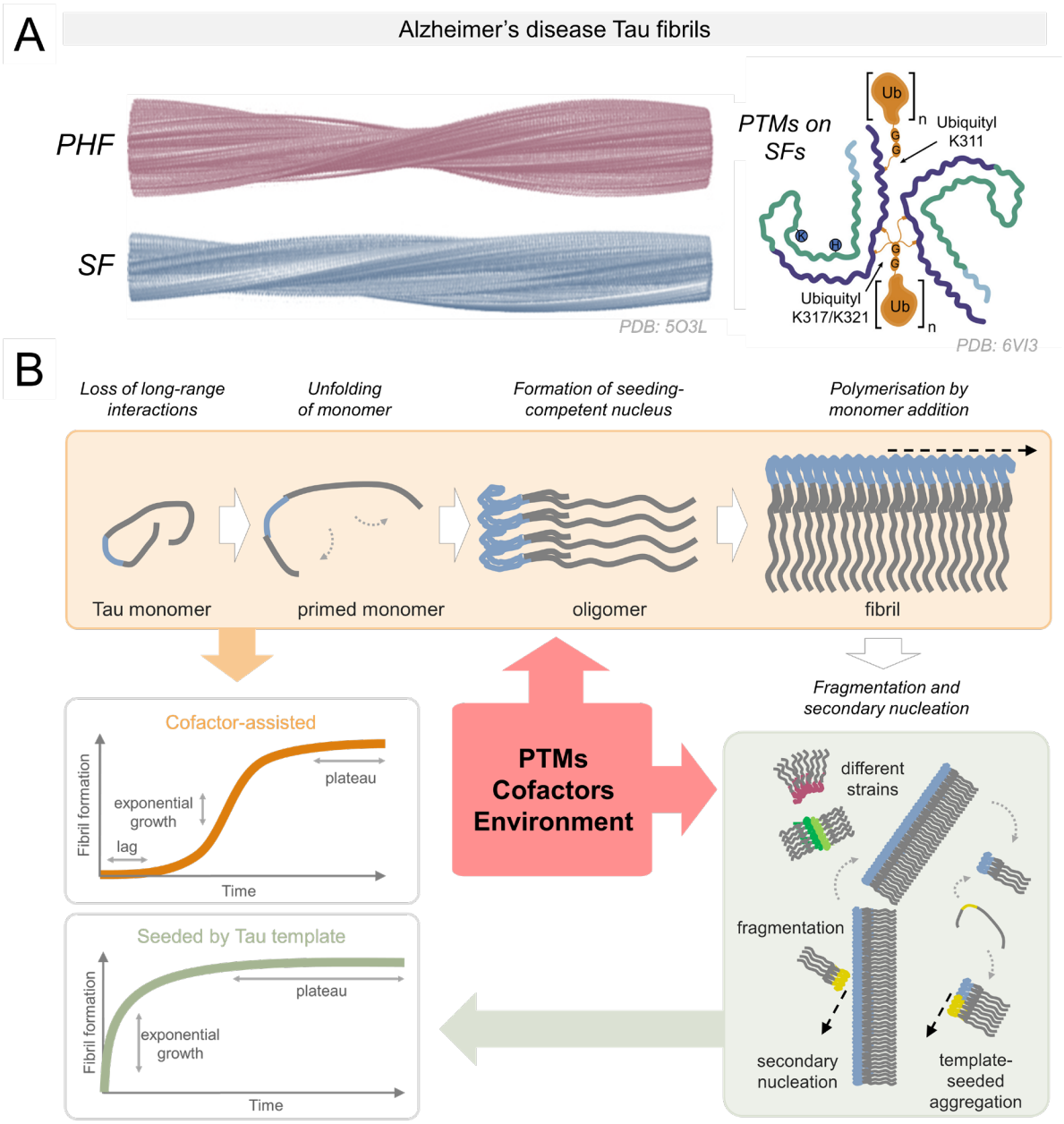

Figure 3. A. Alzheimer's disease derived-Tau fibrils in the paired helical filament (PHF) and straight filament (SF) structures (reproduced with modifications from ref. [189] with permission from the Macmillan Publishers Limited, part of Springer Nature, copyright 2017). SFs may be post-translationally modified (reproduced with modifications from ref.[85] with permission from the Elsevier, copyright 2020). B. Tau aggregation is thought to start by the loss of the long-range contacts on the soluble Tau monomers in semi-stable paperclip conformation. The formation of a seeding competent nucleus is necessary for the fibrillization to proceed. Secondary nucleation events and fragmentation of fibrils contribute to further Tau fibrillization that may result in Tau aggregates in various structural conformations. PTMs, cofactors, and environmental conditions can influence Tau fibrillization. Kinetics of cofactor-assisted Tau fibrillization generally follows the S-shaped curve kinetics, seeded Tau fibrillization follows exponential curve kinetics with the loss of the lag phase.

Therefore, there is considerable interest to understand the conditions and molecular processes contributing to Tau protein aggregation. In solution, all Tau isoforms are soluble and exist as an ensemble of disordered conformations, but are capable of acquiring secondary structure upon association with MTs [376], dimeric tubulin [377], or membranes [378]. The solubility of Tau proteins could be attributed to the high positive charge density surrounding the aggregation-prone microtubule-binding region, as well as long-range N-terminal interactions with the mid-domain and C-terminal domain. To aggregate and form β-sheet-rich fibrillar structures - Tau proteins must undergo conformational changes or interaction with other molecules that alter the charge distribution along the Tau molecule, leading to the formation of aggregation-competent intermediates (Figure 3 B). This can be mediated and influenced by negatively-charged cofactors, such as heparin [93]; changes in the environmental solvent conditions like the presence of osmolyte urea or trimethylamine N-oxide [379]; fluctuations of the proton density gradient pH [5]; the introduction of specific patterns of post-translational modifications [207,380], (reviewed in [56]), or other yet to be identified factors.

Biophysical concepts applied to Tau aggregation

Tau is thought to aggregate through the nucleation-dependent mechanism, surpassing the kinetic barrier by forming a seeding nucleus leads to a rapid elongation phase after the initial lag period through templated addition of monomers to the end of growing fibril [381] (see Figure 3 B). The priming of soluble semi-stable monomers existing in a paperclip conformation [100] into partially misfolded conformation is necessary for the formation of the seeding-competent Tau nucleus. The lag phase can be overcome upon the addition of the preformed fibrillar Tau seed or cofactor molecules. ΔK280, P301L, V337M, and R406W Tau mutants, found in FTDP-17 patients, were found to have higher aggregation propensity into paired helical filaments than wild type Tau [382].

Both Tau mutations detected in familial (P364S), and sporadic (G366R) FTDP-17 reduced MT polymerization activity of Tau, however, interestingly, only the protein with mutation detected in the sporadic case had higher aggregation propensity in vitro [383]. Specific mutations associated with FTDP-17 on the sites P301 and S320 were highly dependent on the residue substitutions in their propensity to be seeded by exogeneous preformed fibrils, or facilitate aggregation in cells [384]. Only the threonine substitution of proline 301 of 4R0N Tau resulted in an increase in the detergent-insoluble Tau upon overexpression in HEK293T cells, followed by K18 fibril seeding, whereas overexpressed mutants G303V, G304S, or S305N Tau remained in soluble fractions. Double mutants P301S/S320F and P301L/S320F, however,

were found to be highly potent to aggregate even without the addition of the preformed seed. These mutations likely work through destabilizing the semi-stable paperclip conformation of the Tau monomer,[100] leading to the formation of highly aggregation-prone intermediates that proceeded to the formation of insoluble Tau, however, the exact mechanisms are unknown.

Understanding of biologically relevant Tau protein aggregation is increasingly informed by the concepts commonly used in polymer science fields. Solubility and assembly properties of monomers under supersaturated conditions define the assembly characteristics, such as labile conditions favoring stochastic nuclei formation, or metastable phase, where ripening of nuclei into elongated structures is favored [385,386]. Conversion of Tau monomers must proceed through misfolded aggregation-competent conformations to form seeds upon transient association. Seed formation from Tau monomers is considered the rate-limiting step in the aggregation process. This process could be induced or promoted by mutations, cellular stress factors, e.g., oxidation stress, PTMs, or interaction with aggregation promoting cofactors or changes in the cellular environment leading to disruption of the long-range intramolecular interactions that stabilize the Tau monomers. On the other hand, in “noisy” biological systems, stable seeding nuclei may also assemble due to transient contacts of molecules of various conformations. Therefore, further polymerization can be thermodynamically unfavorable and these nuclei would not result in the formation of the fibrils [387]. This was observed for some meta-stable heparin-Tau complexes that did not polymerize without forming specific seed structures that overcame the fibril nucleation energetic barrier [232]. Once the templating, uniform surfaces of conformational species are established, the assembly proceeds predominantly by end-addition of Tau monomers independent of the action of heparin.

Determinants of Tau aggregation

Post-translational modifications (PTMs) of Tau

Tau protein aggregation can be extensively modulated by the patterns of post-translational modifications (PTMs) [50]. Tau can be phosphorylated, nitrated, acetylated, ubiquitinated, proteolytically cleaved, SUMOylated, deaminated, oxidated, glycosylated, and glycated, methylated, and demethylated on numerous residues [51,56]. Importantly, the patterns, co-occurrences, and interactions between PTMs may play key roles in Tau functions and the processes of aggregation [52-55].

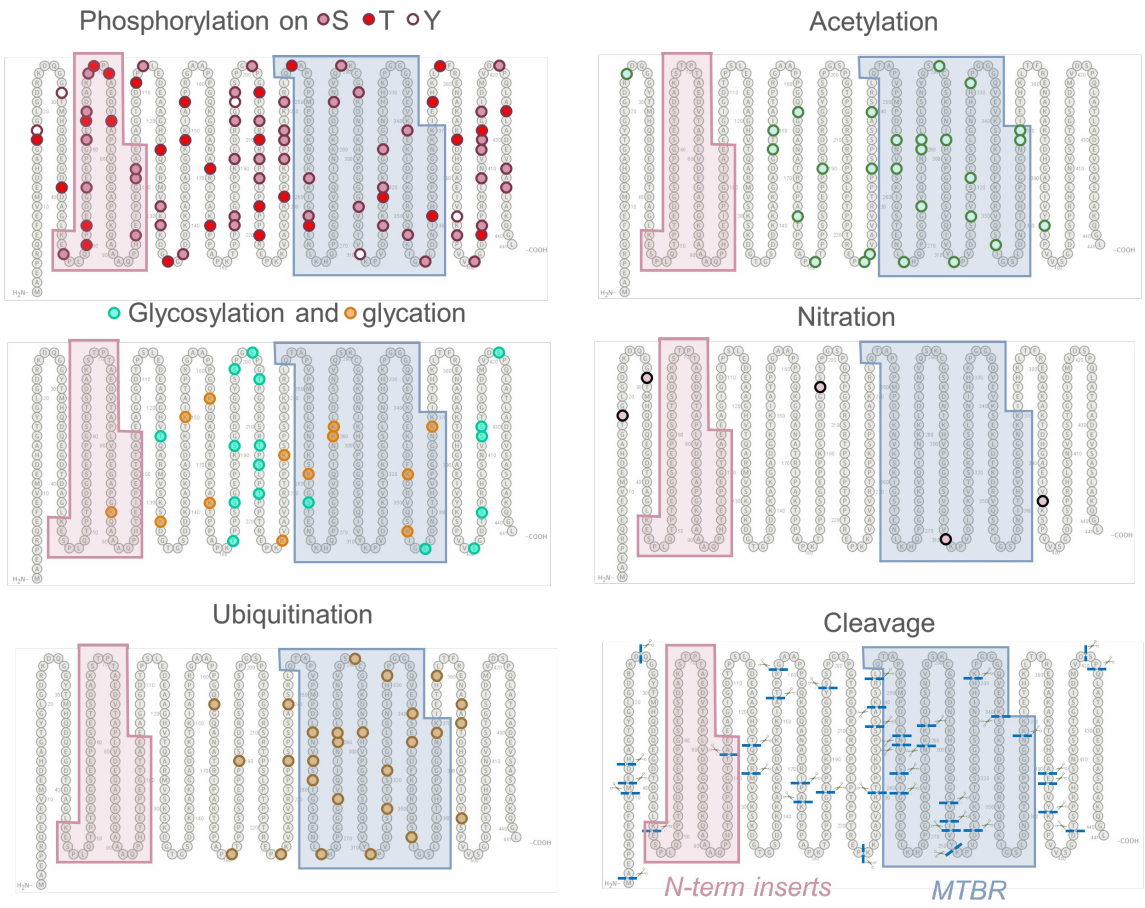

Figure 4. PTM patterns on Tau. Phosphorylation sites are distributed along the Tau molecule, whereas acetylation and ubiquitination sites are clustered around mid-domain and MTBR. Two cleavage sites, a single glycation site, and no acetylation, nitration, or ubiquitination sites are present in the N-terminal repeats.

In a recent study, Wesseling et al. [57] provided the first unbiased qualitative and quantitative profiling of the diversity of the Tau proteoforms and how it changes during AD progression. Although this study revealed that the cumulative number of the detected PTMs was much less than predicted, it still further highlighted the complexity of the Tau PTM patterns in pathological samples with the identification of 55 phosphorylation, 17 ubiquitination, 19 acetylation, and 4 methylation sites. However, several other types of Tau PTMs, which have been detected in the brains of Tauopathy patients were not investigated in this study, including nitration, oxidation, O-GlcNacylation, and glycation.

The high abundance of PTMs in pathological Tau aggregates, relative to soluble Tau, led to hypotheses implicating a central role of PTMs in triggering Tau aggregation and pathology

formation. The patterns of Tau PTMs evolve throughout the disease progression [57], however, the significance and relations to underlying pathology are not yet understood. It has become clear that the PTM occurrence patterns, cross-interactions, and spatial distribution contribute to the combinatorial Tau PTM code, functions of which are yet to be fully deciphered [58].

Phosphorylation

Phosphorylation is one of the most common Tau PTMs and may occur on several of the 85 tyrosine, serine, and threonine residues throughout the longest Tau isoform sequence (Figure 4, Phosphorylation). Physiologically, Tau phosphorylation patterns modulate Tau-MT interactions, generally decreasing the Tau binding affinity for tubulin subunits [388-391]. However, specific sites, such as pT50 were found to promote tubulin assembly in vitro and in cells [392]. Phosphorylation patterns differ between Tau derived from the brain and biological fluids of healthy individuals and neurodegenerative disease patients [54,57,84,393] Early studies detected higher phosphorylation levels of Tau in AD patients' brains by immunohistochemistry [394,395], as well as by nanoelectrospray mass spectrometry [396]. Immunolabelling by AT8 antibody detects Tau phosphorylated at mid-domain residues pS199/pS202/pT205/pS208 [397], which are present in all Tau isoforms (see Figure 1) and is extensively used to assess and quantify the Tau pathology in humans and animal models. Phosphorylation at these sites is also used for histological Braak staging of Tau pathology [321], and the diagnosis of AD in living patients. Which phosphorylation sites drive Tau aggregation and the role of different phosphorylation sites or patterns in regulating different aspects of Tau aggregation, pathology formation, interactions with other contributing factors, and spreading in the brain remain subjects of active research and debate [398]. Several strategies have been used to investigate the role of phosphorylation in regulating Tau functions in health and disease. However, many of the commonly used approaches have limitations that preclude deciphering the Tau phosphorylation code

Phosphorylation mimics

Pseudophosphorylation by amino acid substitution is the most widely used method to mimic the electrostatic and steric effects of a phosphate group and investigate the role of phosphorylation in regulating Tau structure and aggregation properties in vitro (Figure 5 A). Despite the popularity of this approach, however, it has several limitations (reviewed in [399]). Pseudophosphorylation requires introducing non-native amino acids into protein sequence, which could impact the Tau structure beyond the effects of the introduced charge. Also,

aspartic or glutamic acids do not encompass all true physical steric and charge attributes of the phosphate group. Previous studies from our lab and others have shown that phosphomimetics do not reproduce all aspects of phosphorylation [400,401] or the cross-talk between phosphorylation and other PTMs [402,403]. In addition, phosphorylation is a dynamic PTM, and phosphomimetic approaches are generally irreversible.

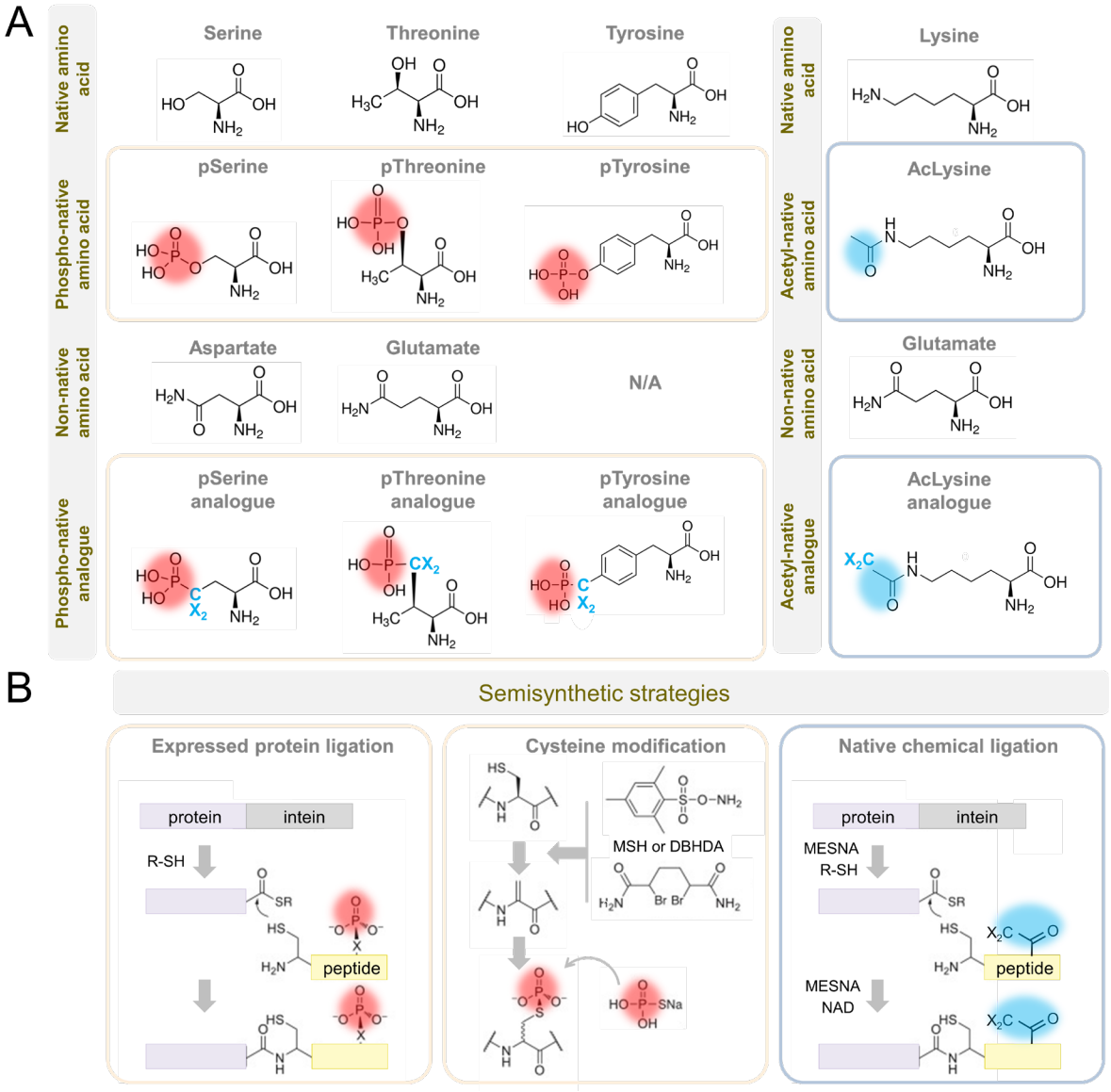

Figure 5. Strategies for in vitro mimics of phosphorylation and acetylation of Tau protein. A. Amino acid substitutions for phosphorylated serine and threonine include aspartic and glutamic acid, as well as phospho-analog residues, including phospho-tyrosine. Amino acid substitutions for acetylated lysine include glutamic acid, as well as acetylation, mimics B. Semisynthetic strategies include protein ligation and cysteine modification (reproduced with modifications from ref. [399] with permission from the Elsevier Ltd., copyright 2015). Abbreviations: DBHDA: 2,5-dibromohexane diacetamide, MESNA: 2-mercaptoethanesulfonate, MSH: O-mesitylenesulfonylhydroxylamine, NAD: nicotinamide

adenine dinucleotide, R-SH: thioester. Phospho-group is designated in red, acetyl group is designated in blue.

One alternative and commonly used approach to phosphorylate Tau involves the use of kinases that have been shown to phosphorylate Tau in vitro or in cells. However, the enzymatic phosphorylation suffers from a lack of specificity or differential affinity of kinases for specific residues. Almost all the kinases that phosphorylate Tau do so at multiple residues. This can lead to variable rates of phospho-group addition and result in samples containing a mixture of differentially phosphorylated proteins. Furthermore, our knowledge of Tau kinases is still limited, and not all desired residues or their combinations may be efficiently phosphorylated in vitro. Previously, the lack of knowledge about the enzymes involved in regulating phosphorylation at specific sites precluded studies from assessing whether phosphomimetics accurately reproduce the effect of phosphorylation. However, recent advances in protein synthesis of Tau and other proteins now make this possible, therefore providing means for assessing the suitability of using phosphomimetics to investigate phosphorylation in vivo.

Alternative approaches for precise and clean in vitro Tau phosphorylation include combinations of enzymatic, synthetic, and semisynthetic strategies (Figure 5 B) [404,405] that were successfully adapted to Tau [171,207]. These strategies provide homogeneous site-specifically modified proteins, including phosphorylations, nitrations, and acetylations, in large quantities for experimental application in vitro, in vivo, and for drug screening and development. In addition to paving the way for deciphering the Tau PTM code with great precision, these approaches will allow reproducing the complexity of Tau species as they exist in vivo. This is essential for developing accurate assays to quantify and monitor changes in total Tau or specific modified Tau species.

The complicated relationship of Tau phosphorylation and aggregation

The predominant focus of investigations of Tau isoforms' phosphorylations has been on the modulation of their aggregation propensity, which depends heavily on the spatial distribution of phospho-groups along the Tau molecule. Early studies showed that phosphorylated Tau readily formed AD-like fibrils in vitro [406,407]. Hyperphosphorylated Tau derived from AD brain cytosolic fraction fibrillized more efficiently in vitro compared to non-phosphorylated protein [408]. In vitro, full-length Tau readily formed fibrils upon kinase-mediated hyperphosphorylation of mid-domain residues pS202, pT205, pS208, but not S262 [91]. In another study [391], phosphorylation of mid-domain region residues pT181, pS199, pS202, pT205, pT212, pS214,

pT217, pT231, or pS262 only moderately increased Tau aggregation propensity. However, phosphorylation reduced tubulin binding and MT-assembly in a phosphosite-specific manner.

The C-terminal domain appears to play a crucial role in modulating Tau aggregation propensity. Mimicking of phosphorylation at residues S396 and S404 by mutating serines to glutamines was found to increase Tau aggregation [409]. A subsequent study by Haase et al. [410] using a pseudophosphorylation mutation strategy of selected serine or threonine residues to aspartic or glutamic acids found that N-terminally positioned mutations inhibited, and C-terminally positioned mutations promoted Tau aggregation, particularly the pseudophosphorylation of residue 422. The enzymatic phosphorylation of C-terminal residues pS396, pS404, pS409 or pS422 alone, or combined with the mid-domain residues greatly enhanced Tau aggregation in vitro [391]. In addition, FTDP-17 Tau mutations G272V, P301L, V337M, and R406W were found to increase the rate of Tau fibrillization in vitro when the C-terminal residues S396, S400, T403, and S404 were phosphorylated, compared to non-mutant protein, that also fibrillized when phosphorylated at these sites [390]. Taken together, additions of negative-charge bulky phospho-group before aggregation onset to N-terminal domain or MTBR tend to decrease Tau aggregation; phosphorylations of C-terminal residues tend to increase Tau aggregation; whereas mid-domain phosphorylations tend to be highly context-dependent concerning the modulation of Tau aggregation.

Conversely, phosphorylation at S262 was previously associated with the inhibition of full-length [411] or truncated Tau aggregation [207]. Also, in a Tau overexpression cell system, the phosphorylation pattern corresponding to AT8 antibody epitope did not result in the formation of high molecular weight Tau species, or observable PHF-like fibrils, even at high amounts of phosphorylated Tau reaching up to 8% of total cellular proteins [118]. Similarly, using eukaryotic Sf9 cellular Tau overexpression system coupled to native mass spectrometry of phosphorylated Tau in these cells, Drepper et al. found that even the highly-phosphorylated Tau fractions did not show self-assembly into the fibrils [412]. In addition, recent work from our group showed that phosphorylation of all five tyrosine residues, three N-terminal residues Y18, Y29, and Y197, or a single tyrosine residue Y310 in the MTBR greatly reduced Tau aggregation [380].

These observations suggest that the pattern of phosphorylation is a key determinant of Tau structure and aggregation. However, a more systematic investigation of the role of Tau phosphorylation using strategies that enable homogeneous and site-specific phosphorylation

or hyperphosphorylation is essential for elucidating the role of phosphorylation in the pathogenesis of Tauopathies.

Glycosylation

The non-canonical form of glycosylation is O-linked-N-acetylglucosaminylation (O-GlcNAcylation), which is added to protein residues by enzyme O-GlcNAc transferase (OGT), and removed by O-GlcNAcase (OGA). Early studies reported high levels of Tau glycosylation of Tau PHFs, but not normal Tau, in AD patient brains [413,414]. The levels of O-GlcNAcylation and OGT were lower in AD patients [415-417], which may be linked to the impairment of metabolic processes related to glycans. The knockout of OGT was further shown to increase Tau phosphorylation, aggregation and induce neurodegeneration in mice [417]. Interestingly, deglycosylation of PHFs in vitro promoted their conversion into straight filaments (SFs) [414], illustrating the profound influence of PTMs on the structure, dynamics, and morphology of the Tau fibrils. Tau can be O- and N-glycosylated on asparagine, serine, and threonine residues [418], thus competing with phosphorylation of the same serine and threonine sites (Figure 4, Glycosylation) [419]. Several sites modified by OGT were identified in vitro and included T123, S400, S409, S412, S413 [68,420].

An inverse correlation between Tau phosphorylation and O-GlcNAcylation levels [66,421] was found in AD patients' brains, implicating glucose metabolism impairment as a contributing factor to AD progression and pathology [422]. O-GlcNAcylation of Tau peptides at S400 was found to inhibit phosphorylation at the neighboring S396 and S404 sites [423]. In cells, different subsets of the overexpressed Tau molecules were found to carry O-GlcNAcylation and phosphorylation, suggesting a function-related balance between these PTMs [67]. In a HEK293 tau-BiFC cellular system, inhibition of OGT resulted in increased Tau phosphorylation at S199 and S396 [424].

On the other hand, NMR-based studies showed that phosphorylation was not blocked by O-GlcNAcylation [68]. Furthermore, more recent work using antemortem AD patient CSF samples found increased levels of total N-glycans, which correlated with an increase of total and phosphorylated Tau levels, especially in patients with subjective cognitive impairment, an early stage in AD pathology development [425]. This suggests that any offset of Tau phosphorylation by Tau glycosylation may have a negligible effect on the total levels of phosphorylated Tau detected in CSF.

It has been proposed that O-linked Tau glycosylation reduces Tau aggregation through the prevention of its phosphorylation on the same residues [66,426-428], pointing to the importance of the temporal sequence of Tau modifications. The deglycosylation of already hyperphosphorylated Tau derived from the cytosolic fraction of AD patients' brains, failed to induce its fibrillization [408]. Tau phosphorylation on the PHF-1 antibody epitope, which includes residues pS396/pS404, and spans over O-GlcNAc S400 residue was found to enhance Tau aggregation, whereas glycosylation of residues S400, S412, and S413 slowed Tau aggregation rate [429]. N-linked glycosylation may also contribute to the structural integrity of the AD-derived PHFs, as evidenced by the fact that deglycosylation by F/N-glycosidase F resulted in untwisting of the fibrils into thin filaments [82]. In addition, N-glycosylated Tau had a lower aggregation propensity and showed shorter and thinner fibrils than deglycosylated Tau [430]. Despite this, the impact of increased Tau O-GlcNAcylation may only be prominent in the physiological systems, and it may involve or require complex interactions with other Tau PTMs and/or cofactors. HEK293 Tau-BiFC cell-based studies showed that Tau aggregation was decreased by inhibition of OGA, and increased by inhibition of OGT (Lim, Haque et al. 2015), suggesting that this particular Tau PTM must be studied within the complex cellular context.

Glycation

Glycation is a non-enzymatic spontaneous reaction between free amino groups of molecules, such as proteins, with free reducing sugars leading to the formation of Amadori products, precursors to AGEs, and reactive oxygen species [431]. As opposed to functional glycosylation PTMs, glycation is irreversible, and glycated proteins tend to become defective and lose their functionality [432]. AGEs were found colocalized with Tau PHFs in NFTs in AD brain [433-435], and are associated with AD pathology [434,436]. AGEs may impact neuronal cell survival through increases in Tau phosphorylation and its dissociation from MTs [437].Glycation has not been reported to induce fibrillization of Tau in vitro [438], but may contribute to stabilization and accrual of the bundles of Tau fibrils [439]. [153]In vitro studies failed to show complete inhibition of heparin-induced aggregation of either full-length Tau or Tau fragments by glycation [440], or impact the polymerization and structure of MTs [441]. Another work found that glycation preceded and promoted phosphorylation of all six Tau isoforms, indirectly leading to enhanced aggregation [153], suggesting that Tau glycation may be an early PTM signifying incipient pathology.

Acetylation

Multiple lysine residues in the Tau sequence can be acetylated and are predominantly located around the proline-rich and MTB regions (reviewed in [65]) (Figure 4 Acetylation). Tau acetylation at K280 (AcK280) was immunohistochemically detected in brain tissue of AD, CBD, and PSP patients, mirroring the Tau hyperphosphorylation staining pattern [442]. In the recent study by Wesseling et al., high acetylation frequency was detected at the residues K535, K369, K370, and K375 located in the MTBR repeat R4, the region outside the fibrillar core fold [57].

Acetylation at K280 has been reported to be associated with the early stages of AD. It is thought to occur in CTE patients' brains before Tau hyperphosphorylation, suggesting that Tau acetylation might be an early marker of incipient Tau pathology [443]. Acetylation at K174 was also detected at early stages in AD patients by mass spectroscopy [444], whereas AcK274 and AcK281 were found at the later stages of the AD progression [445]. In vivo rodent experiments showed that AcK174, AcK274, and AcK281 disrupted synaptic homeostasis, suggesting that Tau acetylation on specific residues leads to hippocampus-associated memory loss at the early stages of dementia [446]. Contrary, Choi et al. [447] used AD patient-derived organoids and the rodent model of AD to show that the inhibitor of histone deacetylase 6, which was found to deacetylate Tau and modulate its clearance [64], reduced the synaptic defects and pathology associated with Tau. In addition, acetylation of potential and canonical degron motifs, including the Tau sequence KFERQ, may be required for enhanced protein recognition and degradation by autophagy systems [448]. This suggests that at least some residues and patterns of Tau acetylation may be protective. Acetylation may have cross-talk with other PTMs, such as phosphorylation. When acetylated on KXGS motifs that modulate Tau binding to MTs, the phosphorylation of these sites on Tau was reduced, and Tau MT-binding capacity was preserved, thus preventing Tau detachment and downstream aggregation [449]. Acetylation modifies lysine residues, which can also be ubiquitinated, methylated, glycated and SUMOylated. This introduces the modification conflicts, which in case of decreased ubiquitination due to acetylation resulted in a decrease of Tau turnover [450].

In vitro investigations of Tau acetylation at lysine residues predominantly focused on its connection to Tau aggregation. Furthermore, previous work predominantly utilized pseudoacetylation by lysine-to-glutamic acid substitution, which may not fully represent the effects of acetylation, or in vitro enzymatic acetylation, which may result in a non-specific and differentially-modified mixture of proteins [171,451]. Acetylation-mimic of residues K280 and K281

was found to promote Tau fibrillization [452,453] (see Figure 5 A). On the other hand, singular acetylation or mimic of K321, or in combination with other lysines, including K280 and K281, was found to decrease Tau fibrillization [449,454,455]. Using precise site-specific acetylation of K280 through protein semisynthesis (Figure 5 B) to obtain homogeneously-acetylated protein [171], our group showed that AcK280 greatly enhanced the rate of Tau fibrillization and promoted the formation of short fibrils [449,450]. Overall, Tau acetylation may be a promising PTM marker of the incipient Tau pathology. However, the underlying mechanisms linking it to Tau aggregation and pathology formation and spreading must be investigated further.

Ubiquitination

One of the most elusive Tau PTMs is ubiquitination despite being one of the earliest identified Tau PTMs linked to pathological profiles. Under normal conditions, Tau was shown to be ubiquitinated and proteolytically degraded by ubiquitin-proteasome system [456]. However, under pathological conditions ubiquitinated Tau was detected in PHFs following the occurrence of PTMs such as glycosylation and phosphorylation [70,71,76,457]. Tau with high levels of ubiquitination was detected in AD patients' CSF [82,83]. In AD patients, Tau was singly [73] or multiply ubiquitinated [74]. Differential patterns of Tau ubiquitination were detected in AD patient samples according to the stage of disease progression [57], and electron densities on AD brain-derived Tau fibrils detected by cryo-EM and cross-referenced by mass spectrometry were attributed to ubiquitin groups [85] (Figure 3 A).

The roles of ubiquitination in Tau fibril formation are still unclear. Ubiquitination is a complex PTM that remains understudied because of the lack of knowledge of the enzymes that regulate Tau ubiquitination in this domain. Tau is known to be ubiquitinated by E3 ligases such as axotrophin/MARCH7 [458], C-terminus of the Hsc70-interacting protein (CHIP) [459], and TNF receptor-associated factor 6 (TRAF6), which was also found to colocalize with sequestosome/p62 in the Alzheimer's brain-derived Tau aggregates [460]. The polyubiquitination of Alzheimer's brain-derived Tau by CHIP-Hsc70 complex was dependent on its hyperphosphorylated state only in the presence of E2 ligase HbcH5B [461], indicating the process specificity and interplay between PTMs. Thus far, only one deubiquitinating Tau enzyme OTUB1 has been identified in mice [462]. Further investigations must focus on at which stages of Tau aggregation and at what Tau sites ubiquitination occurs, and how it impacts fibril structure and clearance. This can be achieved using precision protein semisynthesis strategies successfully applied to study impacts of singular ubiquitination, as well as the impact of multiple additions of ubiquityl groups on α-synuclein aggregation properties [463,464].

Tau cleavage

Another prominent modification of Tau is the proteolytic cleavage of the protein, which occurs at multiple sites along the protein sequence (Figure 4, Cleavage, Figure 6 A). Several lines of evidence suggest that the generation of Tau fragments of different lengths plays an important role in driving Tau pathology formation and the pathogenesis of AD and other Tauopathies. Several Tau fragments have been detected in the brain and CSF both in healthy individuals and in neurodegenerative disease patients, including AD [63,216,218-220], PSP [217], CBD [221], and in traumatic brain injury (TBI) [215], reviewed in [365] (Figure 4 A). Tau 1–402 was used as an early CSF biomarker for early neurodegeneration processes accompanying AD [218]. A recent study [465], using brain microdialysis, and biochemical and cellular assays of interstitial brain fluid in mice to detect secreted Tau, demonstrated that Tau was predominantly present in truncated forms at different stages of pathology progression, as well as across brain regions.

Tau fragments resulting from truncations at positions D13 [466], E391, and D421 [202,467] were reported to promote Tau aggregation, accumulate in AD brains, and their levels correlated with the progression of disease [466]. 46 kDa fragment was detected using mass spectrometry and primary amino acid sequencing in AD and was determined to be a result of caspase-cleaved Tau at D421 [468]. Multiple Tau truncations were also found in PHFs [469], illustrating the heterogeneity of Tau forms present within the Tau aggregates found in the brain. Truncated Tau fragments were found in NFTs in AD (4R+3R Tau) [203,253,470-472], Pick's disease (PiD) (3R Tau) [473], PSP (4R Tau) [474], and other neurodegenerative disorders [475].

Several studies suggest that proteolytic Tau fragments may contribute directly to Tau neurotoxicity and the initiation of Tau pathology. The Tau 45–230 (~17 kDa) fragment produced by proteolytic cleavage by calpain-1 and thrombin between residues 45 and 230, lead to functional impairments in synapses and axonal transport in cells, as well as behavioral deficits in animals [476],[59,477]. The [478]Tau 26–230 (20–22 kDa) fragment could seed full-length Tau aggregation in vitro. In cells, it was enriched in mitochondria and impaired its activity [479], and induced cell death in differentiated human SH-SY5Y cell line [480], and primary neurons [481]. A 24 kDa C-terminal Tau fragment produced by calpain 1 cleavage between residues R242 and L243 showed higher aggregation capacity and lower affinity for MTs in vitro[482]. In the SH-SY5Y cell line, it showed enhanced propagation and seeding of Tau in the neighboring cells {Matsumoto, 2015 #29. Another 35 kDa Tau fragment, likely generated by cleavage between residues in the region of 182 and 194, and is present in 4R Tauopathies such as PSP and CBD [474]. Further investigations in the Chinese hamster ovary cell line showed that

overexpression of Tau 35 kDa led to its hyperphosphorylation, lower MT-binding affinity, induction of unfolded protein stress response, and aberrant insulin signaling [483]. Tau truncations produced by removing from 12 to 121 C-terminal residues were also found to increase Tau aggregation [409]. Finally, it has been widely known that truncated Tau fragment K18 has a higher propensity to aggregate compared to full-length Tau. These findings suggest that some of the Tau fragments are capable of acting as seeds that could initiate the aggregation of full-length Tau proteins.

Some Tau truncations resulted in subcellular mislocalization or misdirection of Tau thus impairing its normal functions. The 4R isoform of the Tau fragment 151-391 was displaced from axonal to nuclear compartment in human neuroblastoma cells and primary rat neuronal cultures [478]. Tau fragment 1-314 was found to detach from MTs and promote loss of hippocampal neurons concurrent with induction of mislocalization of full-length Tau to the somatodendritic compartment and synaptic impairment [484].

Other [481]Tau fragments 1–255 and 369–441 showed impaired MT-binding and polymerization, whereas fragments 1–368, 256–441, and 256–368, in addition, had higher aggregation propensities as compared to full-length Tau [365,485]. N-terminal fragment 1-13 resulted in degeneration of the axonal structures, whereas its counterpart Tau fragment 14–441 contributed to the formation of Tau aggregates [486,487].

[479,484,486,487]Other fragments seem to have no associated toxicity in cellular models, such as Tau 1–25 [480] and 125–230 [365], however, the functional or pathogenic roles of the most known enzyme-cleaved and pathology-associated Tau fragments remain understudies. These include Tau fragments 1–242 [482], 45–441 [476], 258–372 [488], 315–441 [484], 403–441 [218], 1–152, 1–197, 3–124, 3–230, 156–209, 156–441, 198–441, 210–230, 210–441, 231–441 and 422–441 [365]. Equally unclear are the functional or protective roles, if any, of some Tau fragments. Interestingly, some truncated species may enhance proteolytic and autophagic degradation of Tau and its turnover through specific interactions with co-chaperones and ubiquitin ligases [489]. [490]

Whether Tau cleavages found in pathological aggregates occur before, during, or after the onset of Tau aggregate formation [203,491] needs further investigation. Some studies have reported that Tau hyperphosphorylation preceded Tau cleavage in cell cultures and human AD brain [62,473,492], whereas others reported that NFT formation followed the Tau cleavage events [493]. Tau cleavage was also reported to precede Tau ubiquitination [73] and glycation [71] events in AD.

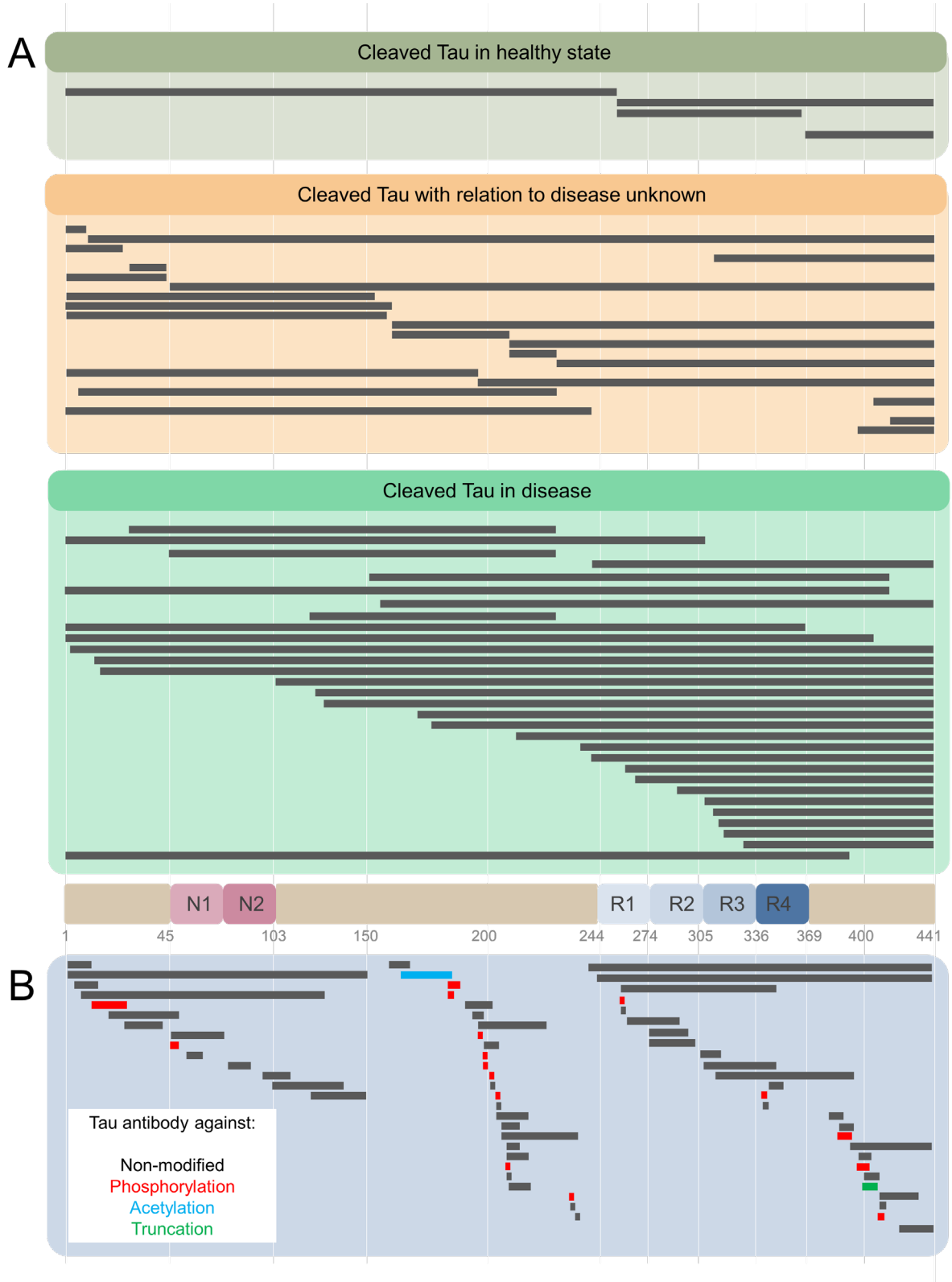

Figure 6. A. Enzymatic cleavage-generated Tau truncation products identified in healthy and Tauopathy patients [365]. B. Anti-Tau antibody list from www.alzforum.com database. Alzforum lists a total of 572 Tau antibodies, 45 laboratory-produced, and 527 commercial. 534 are human-reactive, 360 with listed epitopes identified, with unique sites mapped in the figure. Where epitope is unknown, antibodies are raised against full-length (6), C-terminus (18), and

N-terminus (14). The break in the Tau sequence coverage is at amino acids 150-159 in the proline-rich domain.

Early and late NFT formation-specific markers were associated with Tau cleavage by caspase-3, -6, -7, and -9 in the AD brain and correlated with the scores of cognitive decline [466,494-498]. Tau cleavage by calpains [499,500] was detected in AD and frontotemporal dementia with parkinsonism (FTDP) [480,501]. Despite these findings, multiple truncated Tau species were also detected in normal human hippocampal, cerebellar, entorhinal, prefrontal, and motor cortical brain regions across the age range of 18 to 104 years old [490], functions and significance of which alone, or in combination with other Tau PTMs, are yet to be determined (see Figure 6 A).

Taken together, these observations suggest that cleavage of Tau plays important roles in Tau aggregation, AD pathogenesis, and possibly in the disease progression and severity [497,502]. This also underscores the critical importance of mapping the Tau cleavage patterns in health and disease. They also suggest that Tau fragments play important roles in the pathogenesis of AD and other Tauopathies. Finally, the abundance of Tau fragments underscores the importance of reassessing their physiologic and pathogenic roles and the extent to which assays used to quantify total Tau can capture these various fragments. These studies should consider all six Tau parent isoforms, which could be cleaved at equivalent sequence positions but produce fragments of varying lengths and sizes.

Cross-talk between Tau PTMs and impacts on aggregation

Increasing evidence suggests that the Tau PTM code is a combinatorial code that involves the co-occurrence of and cross-interactions between multiple PTMs dependent on the type of neuropathology and the stage of its progression. Tau PTMs were found to cluster in specific regions of the protein in the brain samples of AD patients [57]. The cross talks between Tau PTMs were and are still being investigated in the context of Tau phosphorylation, primarily due to the unavailability and poor characterization of antibodies for other PTMs. For example, Tau cleavage and Tau dephosphorylation co-occurrences have been observed in hippocampal, cortical, and cerebellar granule neurons [59-61]. This could link the decreased cleavage of Tau hyperphosphorylated at the specific sites to impaired degradation of Tau. This may be followed by the accumulation and subsequent aggregation of Tau in neuronal and glial cells, leading to degeneration. Short Tau fragments containing MBD sequences such as the PHF6 motif were found to aggregate in vitro without the addition of cofactors [111,186],

whereas PTMs in this region, such as pY310, were found to reduce the fibrillization propensity of truncated K18 or full-length Tau [380]. Furthermore, Guillozet-Bongaarts et al. [62] reported that dephosphorylation of residue S422 was necessary for caspase-3 mediated cleavage at D421 in vitro, emphasizing the importance of cross-talk between Tau PTMs. A recent report [63] using Tau proteins truncated at various positions expressed in HEK-293T cells showed that Tau truncation after the first 50 amino acids reduced its phosphorylation at T205 and T231. Truncation after amino acid 150 enhanced its phosphorylation at T205, S212, S214, T217, T231, and S235 irrespective of the presence of the C-terminus. Truncation after amino acid 231 increased its phosphorylation at S262, S396, and S404 [63].

Cross-talks between other PTMs were also observed, for example between the lysine-targeting PTMs such as acetylation, methylation, glycation, SUMOylation, and ubiquitination (reviewed in [65]). Hyperphosphorylation was associated with hypoacetylation – less acetyl PTMs - of the four KXGS motifs present in MTBR, which increased Tau aggregation propensity [64]. AD patients' brain-derived co-phosphorylated and ubiquitinated Tau peptides containing KXGS sequences were enriched compared to control-derived samples [83]. In cellular system [86], Tau phosphorylation was increased by SUMOylation of K340. This was correlated with the decrease in Tau ubiquitination and degradation, resulting in enhanced levels of insoluble Tau. These findings suggest that Tau aggregation may be modulated by the synergistic effects of the multiple PTMs.

O-GlcNAcylation has also been shown to influence the site-specific phosphorylation pattern of Tau in vitro and in a cellular system [66]. The crosstalk between Tau phosphorylation and O-GlcNAcylation was confirmed in cells, where the lower levels of Tau phosphorylation correlated with increased glycosylation and higher nuclear localization of Tau [67]. Interestingly, an NMR study by Bourrée et al. [68] found that O-GlcNAcylation did not impact Tau phosphorylation by the rat brain extract or mitogen-activated protein kinase 1 enzyme. However, phosphorylation slightly increased Tau O-GlcNAcylation by the O-linked N-acetylglucosamine transferase enzyme through indirect cross-talk mechanisms which remain to be fully understood.

Spatially, phosphorylation events seem to accrue in the N-terminal and proline-rich Tau region during the Tau NFT aggregate formation and maturation, whereas acetylated and non-ubiquitinated regions seem to dominate in the MTBR overtime [57]. These studies further underscore the complexity of Tau PTMs' cross-talks in the modulation of Tau isoforms' normal functions, its aggregation propensities, and remodeling of the fibrils.

A complex interplay of multiple Tau PTMs in a tightly regulated spatiotemporal manner is likely to occur during the various stages of Tau aggregation and pathology formation [54]. The phosphorylation patterns of Tau oligomers were heterogeneous among AD patients and correlated with the severity of the disease progression in biophysical, biochemical, cell- and animal-based functional assays [211]. Further investigations of the Tau oligomer PTM landscapes are needed to understand their functional significance in vivo (reviewed in [503,504]).

Advantages and limitations of the current approaches investigating Tau PTM code

Mass spectrometry-based techniques and experimental design

Mass spectrometry-based proteomic approaches are increasingly used to capture the heterogeneity and co-occurrence of Tau PTMs. The high sensitivity and specificity of mass-spectrometry offer many advantages, but deciphering the PTM code of Tau using this technique requires careful experimental design. For example, recent work by Wesseling et al. [57] successfully used mass spectrometry to determine the PTM profiles in patient cohorts. However, the frequency and evolution of the PTM profiles within individual patients over time were impossible to establish due to the cross-sectional data collection. Another major gap in our knowledge of the Tau PTM code includes the lack of comprehensive profiling of Tau PTM co-occurrences in healthy young and aged non-demented subjects, which could inform us of their normal functions. As a statistical aggregate, the PTM occurrences and their relative frequencies are increased as the pathology progresses. The fine stratifications of patients are necessary to mitigate high interpatient variability and enable us to delineate specific Tau PTM patterns in the different regions of the molecule. Furthermore, the current methods of enzymatic digestions and mapping of PTMs do not allow to determine the co-occurrence of PTMs on the same Tau molecule, and therefore their interplays and functional significances. Future studies should be designed to allow the longitudinal profiling of Tau PTM patterns' evolution, determination of PTM patterns on the same Tau molecule, and PTM maps of the different soluble, oligomeric and fibrillar Tau species [58].

Similarly, most studies attempting to map and identify the naturally occurring Tau cleavage products in biofluids [212] rely on mass spectrometry-based experimental approaches [213] often in combination with immuno-enrichment of Tau species using antibodies, followed by the enzymatic digestion, labeling, and mass spectrometry analyses of fragments. Several antibodies, which cover virtually the whole sequence of the Tau molecule (www.alzforum.org) have been produced (Figure 6 B). However, the most often utilized Tau enrichment antibodies

tend to target the proline-rich middle domain (103-244), present in all six Tau isoforms, and peptides from which tend to be overrepresented in mass spectrometry hits [222,505]. Previously, N-terminally truncated Tau fragments found in AD samples by Derisbourg et al. [506] were identified by immuno-enrichment using Tau5 antibody against Tau amino acids 218-225. However, the possible range of the Tau species devoid of this region, such as nucleation-competent and aggregation-prone MTBR, or conformations where this region is inaccessible was not captured. Similarly, Portelius et al. [507] identified 19 tryptic Tau fragments in AD patients' CSF by nanoflow LC-ESI mass spectrometry using immunoprecipitation with antibodies BT2 (epitope 194-198), HT7 (159-163), AT120 (against phospho-threonine-181), or AT270 (phospho-dependent epitope 176-182), thus limiting the detection to Tau species containing the middle domain, whereas Tau is known to undergo extensive N-terminal [221,474,480,508] and C-terminal [509,510] truncations, similar to Cicognola et al. [366]. Unfortunately, the majority of currently available Tau antibodies are overwhelmingly targeting the unmodified Tau epitopes (Figure 4 B). Therefore, future studies aimed at the comprehensive mapping of the Tau PTM profile should employ approaches and a combination of antibodies that capture the diversity of Tau proteins and fragments in brain tissues and biological fluids.

Co-factor-induced Tau aggregation mechanisms determined in vitro

Heparin

In general, the unifying characteristic of the Tau aggregation inducers is a polymer with a net negative charge. Heparin and heparan sulfate (HS) remain the most commonly used glycosaminoglycan (GAG) polysaccharides to induce Tau aggregation in vitro and have shaped our current understanding of the mechanisms of Tau aggregation and pathology formation (Figure 7). With the advent of recombinant protein technologies for large-scale Tau production, in 1996 heparin was shown to act as an inducer for the aggregation of unmodified recombinant Tau [256]. It was soon after widely adopted to produce large amounts of Tau fibrils for in vitro, in cells, and in vivo experiments. Heparin-fibrillized Tau was used as a proxy for the Tau fibrils derived from pathological brain samples for biochemical, biophysical, and kinetic characterization, as well as for screening of Tau fibril-binding molecules. But it became clear that despite some similarities, the heparin-fibrillized Tau differs from pathological Tau fibrils in multiple ways [164]. These findings are not unique to heparin, but other Tau fibrillization cofactors such as RNA and lipids, which also induce the formation of polymorphic Tau fibrils with a physicochemical profile different to patient-derived Tau. Here we focus on heparin given that

it is the most widely used and accessible Tau fibrillization cofactor and formed the cornerstone of the experimental investigations of Tau fibrillization for nearly three decades.

GAGs are a large class of long anionic unbranched polysaccharides consisting of repeating disaccharide units [511]. Based on the compositional differences, GAGs comprise five classes of molecules, such as hyaluronic acid, predominantly associated with skin tissues, synovial fluid and articular cartilage [512]; chondroitin sulfate, which is a major component of perineuronal nets, changes in sulfation patterns of which were is linked to cognitive decline in AD [513], as well as dermatan sulfate, keratan sulfate, and HS, all of which play important structural and signaling roles in neural and other tissues [511,514-516]. Heparan sulfate proteoglycans (HSPGs) have been implicated in the Tau pathology and spreading at the stages of its release from the affected cell, as well as in facilitating the internalization of pathogenic forms by the neighboring cell (reviewed in [517]). Despite the popularity and ease of use of polysaccharides as cofactors for in vitro Tau fibrillization, the formed fibrils differ from pathological in several ways. The heparin-induced fibrils are highly heterogeneous, predominantly single protofibril, generally unmodified and composed out of the single Tau isoform, which contrasts with the highly conserved disease-specific Tau fibril fold. In addition, the heparin-induced fibrils are generated from recombinant unmodified proteins and thus lack the PTMs found on the patient brain-derived Tau fibrils [156,164]. Other concerns for the downstream applications in vitro, in cells and in vivo arise when using added heparin as a cofactor to fibrillize Tau. These may include interference with the Tau fibril-targeting compounds [243], disruption of the cellular uptake of Tau fibrils [158], and causing vasodilation or immune response in animals [233,234], all of which may contribute to the modification of Tau seeding propensity non-contingent on the inherent properties of the Tau seed itself.

Mechanisms of heparin-induced Tau aggregation

Kinetics of Tau aggregation and heparin-to-Tau stoichiometry

For Tau aggregation to proceed efficiently and on reasonable time scales [160], the aggregation-inducing cofactors must have a high affinity for Tau. Heparin displays properties of fast Tau protein binding and forms stable heparin-Tau complexes. Kinetic biolayer inferometry assays, using biotinylated monomeric full-length Tau immobilized on the biosensor and incubated with variable concentrations of heparin or synthetic heparinoid (SN7-13) solutions, demonstrated the high heparin affinity to Tau with ON rate constant of around 9*10^5 M-1 s-1 and the lower

OFF rate constant of 6*10^5 M-1 s-1 [235]. This is consistent with a previous report suggesting that heparin-Tau binding in the submicromolar range [200].

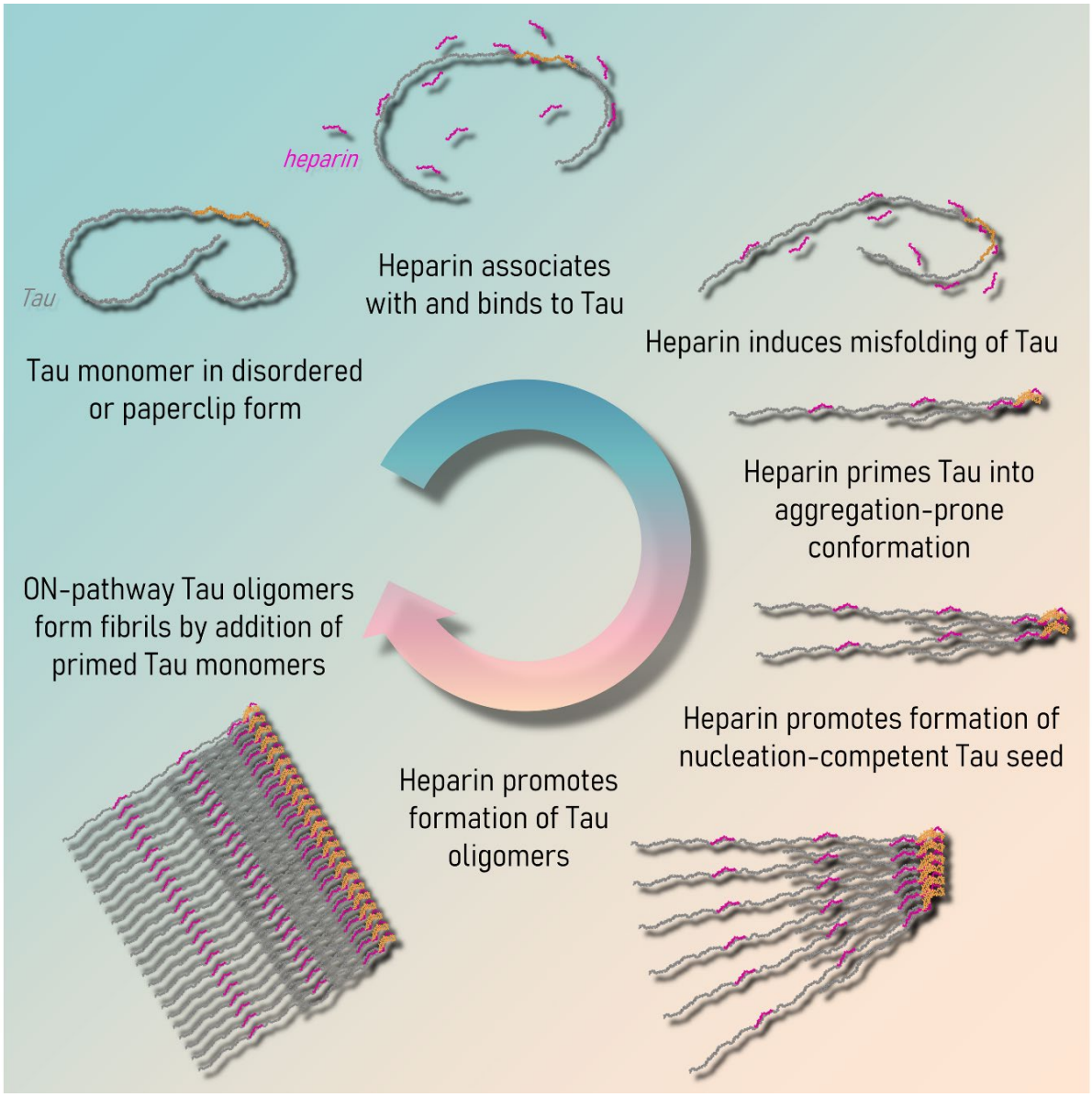

Figure 7. Hypothetical mechanism of heparin-induced Tau fibril formation. Tau exists in solution as a disordered monomer that could undertake the paperclip conformation. Negatively-charged heparin can bind to positively-charged regions on Tau and prime it into aggregation-prone conformation. Tau forms the nucleation-competent seed, ON-pathway oligomers, and fibrils upon the addition of primed monomers. Heparin molecules may tightly associate with Tau fibrils. Tau MTBR is designated with coral, N- and C-termini in grey, heparin molecule in magenta.

At physiological pH and in the presence of a reducing agent, such as dithiothreitol (DTT), the 4R Tau MTBR formed a stable complex with ~7 kDa heparin at a ratio of one-to-one [518,519] or

two Tau MTBR molecules per one 12 kDa heparin molecule [519]. These interactions were slower in the absence of reducing agents, which suggests that the formation of intramolecular cysteine bridge could stabilize Tau MTBR monomer and/or disrupt its interactions with heparin, thus preventing efficient 4R Tau MTBR fibrillization even in the presence of cofactors [101,520,521]. Interestingly, the lag phase was unaltered when the Tau MTBR to heparin molar ratio was either one-to-one or one-to-two. However, it decreased sharply at higher molar ratios of heparin. Conversely, the exponential growth rate increased with a decreasing ratio of heparin to Tau MTBR [519]. Quantitation of Tau MTBR and heparin-binding kinetics, based on calculations of the stoichiometry of the molecules and association and dissociation rate constants, suggested that the interaction between Tau MTBR and heparin occurs at the nucleation step. The exponential growth phase, which proceeds by the sequential addition of Tau MTBR monomers to seeding competent nuclei or fibrils, was reduced at lower heparin to Tau MTBR molar ratios and inhibited at higher ratios. This demarcates the narrow optimal range of heparin-to-Tau molecule ratios necessary for the efficient Tau fibrillization reactions. Furthermore, these studies show that the heparin association rate with Tau is higher than the dissociation rate. On average, more heparin molecules are likely to be associated with Tau than are released back into the solution.

The kinetics of heparin-induced Tau fibrillization was also dependent upon the length of heparin polysaccharide chains, with longer chains providing higher Tau-heparin binding and nucleation efficiency [522], likely due to a higher amount of the binding sites along the Tau molecule. However, due to the high complexity of the glycochemistry of the heparin, the quality of the commercial heparin products depends on the purification or synthesis methods, and the origin or the raw material. This might lead to high batch-to-batch variability and large heterogeneity in terms of the heparin molecular sizes [158].

Electrostatic charge contributions to heparin-Tau interactions

The heparin-protein interactions are primarily mediated by the iduronic acid epimerization of heparin, polysaccharide chain conformations, and negative charges of sulfate groups [523,524] (Figure 8 A). Polysaccharide sulfation patterns are key determinants of the specificity and the affinity of heparin-protein interactions [525,526]. In general, medium (MMW; ~5-12 kDa) to high (HMW; >12 kDa) molecular weight heparins induce Tau fibrillization. Heparin-Tau interactions have been determined to rely largely on the electrostatic, rather than covalent, van der Waals, or other forces. Heparin provides charge compensation for the lysine- and histidine-rich stretches [527] that form upon the in-register, parallel stacking of the Tau repeat regions R2 and

R3 [200]. The full-length Tau aggregation conditions most often feature a Tau-to-heparin ratio of four-to-one to achieve charge neutralization [528], a ratio within the range experimentally determined using kinetics assays (see below). For full-length TauΔ187 under physiological conditions, the charge was estimated to be approximately +13.5. For 11 kDa heparin, the charge was estimated at around -50, which is the equivalent of approximately Tau-to-heparin molar ratio of four-to-one, resulting in a charge balance of +54 to -50 [529].

Heparin-induced conformational changes of Tau

Heparin interactions with Tau alter the conformational landscape of the protein, resulting in the population of partially-structured Tau intermediates with an increased propensity for self-assembly and fibril formation. Upon heparin binding to Tau monomer, Tau undergoes conformational transitions characterized by the presence of two distinct Tau populations, one possessing the unstructured features of the IDP, another, however, showing compaction of MTBR and restructuring of the N- and C-termini upon heparin binding to Tau [110,201]. This dichotomy in Tau molecular states is opposed to the expected continuum of expanding-contracting Tau conformers under the conditions of the sole effect of charge redistribution along the Tau molecule by heparin. Under these conditions, the Tau conformations are expected to undergo progressive loss of intrinsic disorder and a gradual shift towards a more structured protein. However, this was not the case, as the Tau protein either retained most of its IDP character and long-range intramolecular contacts or collapsed into structured compact MTBR conformation.

In vitro chemical cross-linking performed at various time points during Tau aggregation showed that Tau formed stable dimers, tetramers, and higher-order assemblies in the presence of heparin [201]. This suggests that in addition to direct effects on Tau molecular conformation, heparin promotes Tau aggregation and fibril formation through stabilizing or increasing the formation of nucleation-competent Tau oligomers [530]. Heparin was shown to associate with the rigid core region of Tau PHFs composed of the MTBR. However, the N-terminal residues upstream of the N-terminal inserts N1 at amino acid position 45-74 and N2 75-103 were also important for Tau-heparin interactions [200,522,527,531]. Studies by electrochemical impedance spectroscopy and cyclic voltammetry showed that Tau monomers immobilized on the gold electrode surface by the N-termini had a lower capacity to bind heparin compared to the Tau molecules immobilized by cysteine residues 291 and 322 in the middle of the protein, which allowed the N- and C-termini mobility [532]. These studies indicate

that heparin binds tightly to several regions of Tau molecules and influences its conformational and aggregation properties.

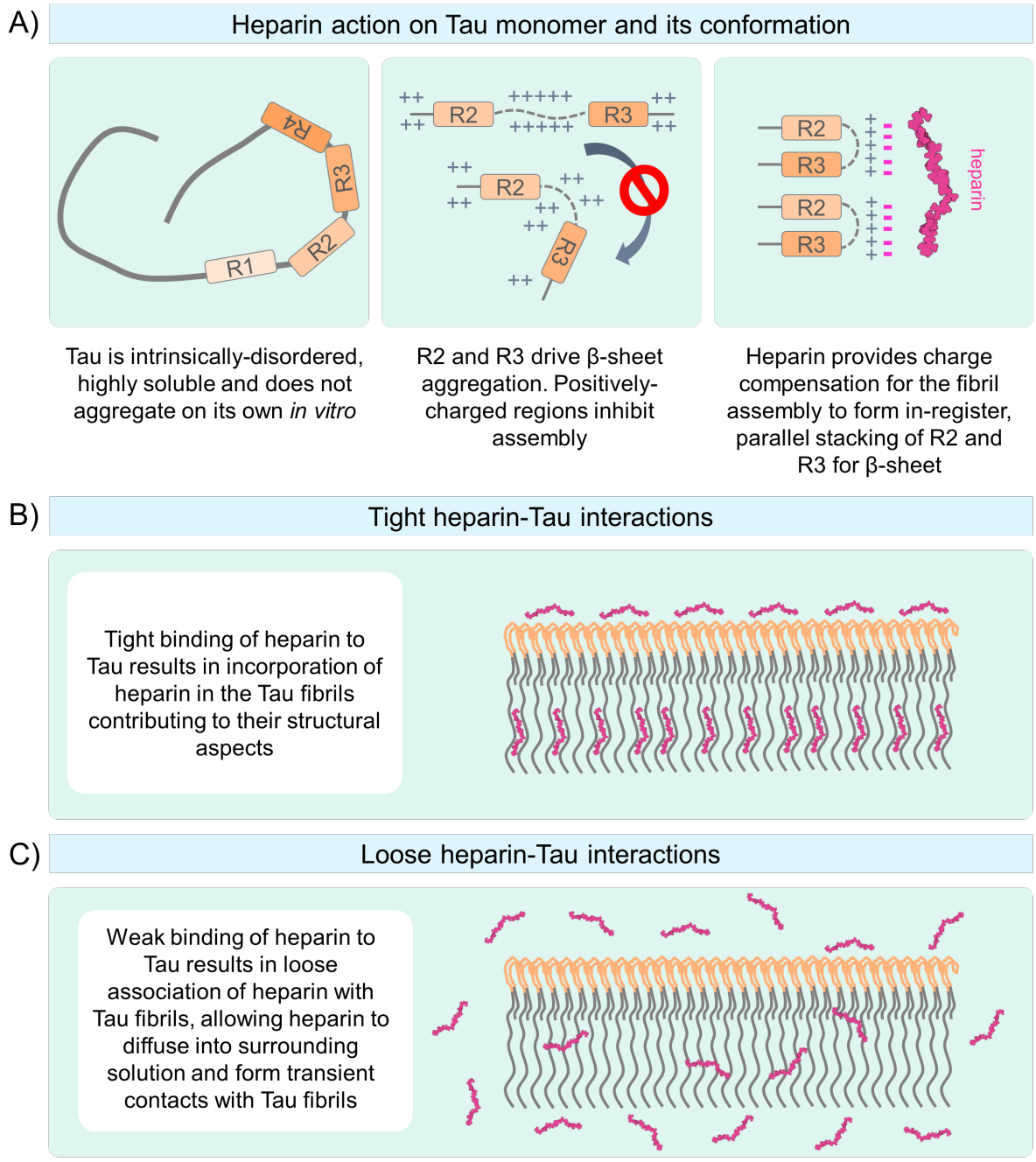

Figure 8. Heparin-induced Tau aggregation mechanisms. A) Proposed mechanism of charge neutralization by heparin around R2 and R3 regions of Tau molecule conducive to Tau aggregation. B) Tight interactions between heparin and Tau may lead to the incorporation of heparin into fibrils and contributions to their structure. C) Loose associations of heparin with Tau may lead to the release of heparin molecules into the surrounding medium.

Heparin-binding sites on Tau

Based on the experimental evidence from biophysical studies, several heparin-binding sites on Tau have been proposed. Using variable length Tau fragments, the minimal Tau fragment sequence competent of the heparin-induced assembly into the fibrils was determined to comprise 18 amino acid stretch 317KVTSKCGSLGNIHHKPGGG335, located in the R3 repeat [97]. This contains two basic lysine and two histidine residues, and cysteine residue, conducive to the formation of inter-peptide sulfur bridges, that may promote the formation of nucleation-competent peptide dimer in vitro [530,533,534]. Within this peptide, the triplet 329HHK331 was hypothesized as a likely heparin-binding site [535]. The K331 residue was identified to have a substantial low-molecular-weight (LMW) heparin-binding affinity (10 μM range), among other positively charged residues. In the same study, using NMR spectroscopy, the highest affinity heparin-binding sites were mapped to the stretches 139DKKAKG144 in the proline-rich domain; within the PHF6* (275VQIINK280) in the R2 and the PHF6 (306VQIVYK311) in the R3; and 336QVEVK370 in R3-R4 [200]. The individual positively-charged lysine residues along the Tau molecule also showed heparin-binding affinity, with the highest affinity for K257 within the R1; K298 within the R2; K311 in the PHF6 and K331 within the R3; as well as K343 and K347 within the R4. Notably, the heparin-binding affinity of Tau lysine residues could be modified by the charges of other residues in the vicinity, providing support for the strong impact of electrostatic forces in heparin-Tau interactions. Other studies also indirectly suggested the heparin-binding sites were present within the Tau MTBR [518].

Insights into PHF6 region as the backbone of Tau fibrils

Despite the wide use of Tau peptides harboring the PHF6 sequence as a representative for the pathological Tau fibril formation, stark differences exist in residue configurations within the Tau fibrillar core of in vitro and pathological Tau fibrils. Generally, the two stable β-sheet forming polymorphs include the front VIY and back QVK side residues of the PHF6 sequence VQIVYK. Crystal structures of fibrils composed of Tau fragments 305SVQIVY310 [536] and 274KVQIINKKL282 [537] formed steric zippers [538] with the residues of the same sequence on the opposing molecule. This may suggest that the homotypic association of the aggregation-driving sequences, including the PHF6, may be key to Tau aggregate formation. However, the cryo-EM structures of pathological Tau fibrils show much greater diversity in association side-chain partners of these regions. In AD-derived PHFs [189] VQIVYK sequence formed the heterosteric zipper with the sequence THKLTF, in PiD [43] VQIVYK β-sheet was opposed to GQVEVK, and in CBD folds [85] residues VIY of VQIVYK were opposite to DNIKHV, and on the

flip side of the sequence VQIVYK the residues QVK were opposite to GQVEVK. Both CTE Type I and II fibrils [155] were formed by the heterosteric zippers running in the opposite directions through phenol on oxygen atom Oε in VQIVYK and histidine on nitrogen atom Nδ in HKLTFR with the distances of the magnitude permissible for the hydrogen bond formation. In the heparin-fibrillized Tau polymorphs [539] only 3R2N fibrils showed a steric zipper between opposing VQIVYK - VQIVYK sequences, which also differed from crystal structures of these regions [536]. NMR studies of 4R0N fibrils showed the region VQIVYK constituting part of the β-sheet, among other regions yet to be mapped [540]. These high-resolution studies, as well as computational modeling [541], revealed the importance of π-stacking of the tyrosine rings for the stabilization of all known Tau fibrillar structures. The occurrence of PTMs in the regions that may lead to destabilization or prevent the formation of the bonds instrumental for the formation of stable Tau polymers could decrease the aggregation propensity of Tau [380].

Tau dimerization under reducing or oxidizing conditions

Induction of Tau aggregation by adding ~18 kDa heparin under reducing conditions [542] depended on cysteine residues within MTBR [88], illustrating the importance of this region for the binding of heparin to Tau. The formation of Tau dimers is thought to be an early event of the ON-pathway of Tau fibrillization. Dimerization of Tau through the covalent formation of cysteine-cysteine intermolecular sulfur bridges was observed under oxidizing conditions with 3R Tau isoforms, which in the presence of cofactors proceeded to form fibrils.

Table 2. Atomic distances between cysteine residues in Tau fibrils			
Disulfide bond distance [543]			~2.3 Å
		S ─ S distances (Å) between residues	
	PDB	**C291 ─ C291**	**C322 ─ C322**
Pathological Tau fibril fold			
Alzheimer's disease	5O3L	-	4.79
Corticobasal degeneration			
Type I	6TJO	4.80	4.86
Type II	6TJX	4.81	4.82
Chronic traumatic encephalopathy			
Type I	6NWP	-	4.72
Type II	6NWQ	-	4.90
Pick's disease	6GX5	-	4.85
Heparin-induced Tau fibrils			
4R2N "snake"	6QJH	4.80	4.76
4R2N "twister"	6QJM	4.72	-
		1. C322 ─ C322	**2. C322 ─ C322**
3R2N	6QJQ	3.70	5.13

However, the 4R isoforms were found to form an intramolecular sulfur bridge that compacted the monomers thus significantly delaying or preventing the formation of fibrils even in the presence of cofactors [101]. Under reducing conditions, however, the Tau dimers were not covalently linked and could form fibrils in the presence of cofactors [101]. The recent cryoelectron microscopy (cryo-EM) of Tau fibril structures support the formation of Tau fibrils under reducing conditions from both 3R and 4R Tau isoforms in patients and in vitro [43,155,164,189,544], as the distances between cysteine residues 291 or 322 observed are ~2.5 times larger than the disulfide bond [543] (Figure 9, Table 2).

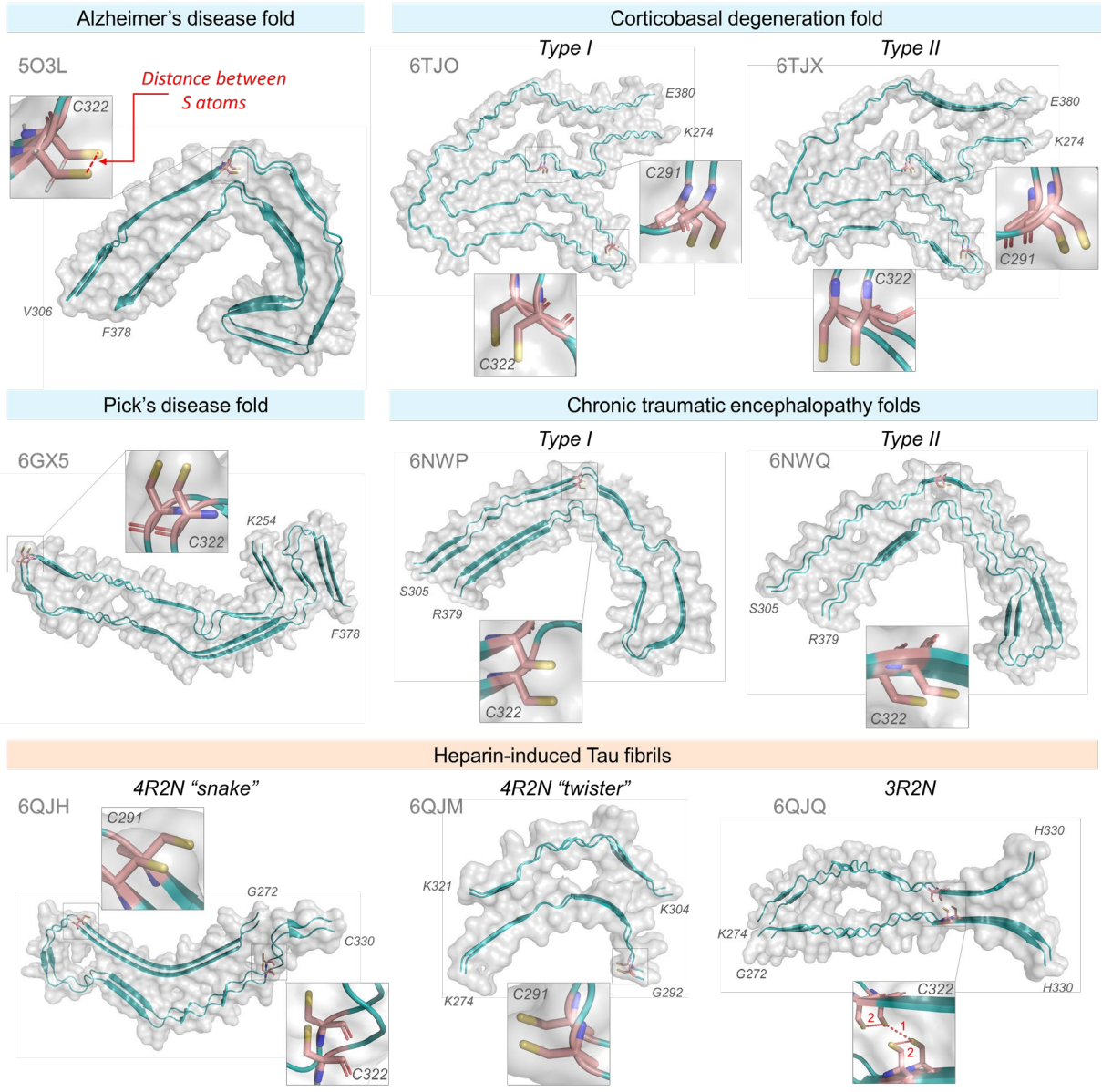

Figure 9. Cryo-EM structures of Tau fibrils and cysteine residue positions. Tau fibril structures available at Protein Data Bank [107], accession codes are in grey, structures were rendered using PyMOL software (The PyMOL Molecular Graphics System, Version 2.0 Schrödinger,

LLC [545]). Two molecule strands are shown for each structure. Atomic distances between sulfur atoms on adjacent cysteine residues (as depicted in Alzheimer's disease fold, red dashed line) were measured using the PyMOL [545] Measure tool and are summarized in Table 1. All distances between cysteine residues are significantly larger than the distance required for the formation of the disulfide bond at 2.3 Å [543].

Is heparin a major structural component of Tau fibrils?

The initial clues that heparin could be involved in the formation of Tau pathological aggregates (Figure 8 B) came from studies on patient brain-derived Tau PHFs. Heparinase enzyme treatment of AD patient brain-derived PHFs resulted in the loss of the PHFs' helical twist signature [546,547] [154] and a shift of PHFs' twist periodicity from 69.5±5 nm to 78.2±7.7 nm. Interestingly, this treatment decreased PHFs' immunoreactivity to the N-terminal antibody Tau14 (epitope recognition of amino acids 141-176) and phosphorylation-dependent antibody AT8 (pS199/pS202/pT205/pS208 [397]), but increased the detection by PHF-1 antibody (pSer396/pSer404) [546]. Curiously, the labeling of PHFs and SFs with Tau14 antibody was restricted to a subpopulation of fibrils and was nearly abolished by the heparinase treatment. This is puzzling when considering that part of the Tau14 epitope spans over amino acids 140KKAK143, which were previously identified as heparin-binding sites [154]. The authors surmised that the fibril untwisting could be attributed to increased conformational flexibility in the C-terminus and/or degradation of the heparin bound to sites near MTBR. Also, likely, the diminished accessibility of the heparinase enzyme to this domain on Tau fibrils could have contributed to the retention of the heparin molecules bound at this site, thus reducing the recognition by Tau14.

The heparinase-treated PHFs also showed altered biochemical properties, such as higher sodium-dodecyl-sulfate (SDS) solubility and reduced PHF-1 immunoreactive high molecular weight species by Western blotting. Although several in vitro studies have attempted to address the question of whether heparin is integrated into Tau fibrils [114,157,167,200,519,548], at this time no consensus has been reached. It is likely that heparin associates strongly with specific sites on Tau fibrils. Several aspects of the biochemical properties of heparin (e.g. molecular weight and sulfation patterns) and Tau molecules (e.g. isoform, modifications, mutations, and aggregation) have been shown to influence the interactions between these two molecules. Finally, the binding and the heparin-Tau association-dissociation equilibrium might maintain a stochastic component, i.e. not readily attributable to any predictive variable. All these observations motivated researchers to look increasingly closer at heparin-Tau interactions to disentangle the complex relationships between heparin and Tau.

Evidence for the heparin integration into Tau fibrils

Sibille et al. were the first to experimentally test whether heparin was integrated into the Tau fibrils using NMR spectroscopy, and found that HMW heparin interacted with the positively-charged regions flanking the MTBR of Tau monomers [200]. After Tau fibrillization reaction completion, followed by the depletion of residual heparin, no relaxation of the heparin-Tau interacting residues or detectable heparin free signal were seen, indicating that all heparin was tightly associated with Tau. In the case of a weak association of heparin with Tau, the expectations were to observe the gradual release of heparin into the solution, accompanied by the NMR shift of heparin-binding amino acids in Tau, which was not the case. This suggested that heparin was stably integrated into the surface of Tau fibrils in parallel with the direction of fibril growth, rather than being intercalated perpendicularly within β-sheets, in which case the β-sheet packing of amino acids would have been perturbed, or resulted in longer distances between packed molecules.

Electron paramagnetic resonance (EPR) studies showed that RNA induced the formation of Tau fibrils containing in-register stacking of in-parallel β-sheet-containing monomers, conformationally resembling heparin-induced Tau fibrils. However, RNA affinity for 3R MTBR fibrils was higher than heparin, which suggests other structural differences between Tau fibrils induced by heparin or RNA. Subsequent studies by Fichou et al. [114] (see below) showed that RNA was stably associated with the Tau fibrils, but could be displaced into the soluble fraction by the addition of heparin. No change in fibril morphology was detected after heparin addition and RNA displacement. The majority of fluorescein-conjugated heparin (around 80%) was directly shown to be associated with 3R or 4R MTBR fibrils, with a low amount remaining in the soluble fraction. These results show that the binding of these negatively-charged cofactors to the surfaces of Tau fibrils is mediated by electrostatic forces that are more pronounced in the case of heparin, most likely due to high negative charge density per heparin molecule [549]. The main limitation of this study was the use of truncated Tau proteins with non-native amino acid residues, which could limit the translation of these results to the full-length Tau isoforms. However, increasing evidence suggests that Tau fragments are present in appreciable amounts under physiological and pathogenic conditions [215-222].

So far, the most compelling evidence for heparin as a constituent of Tau fibrils came from the direct detection of spin-labeled heparin within Tau fibrils. Using continuous-wave EPR and biochemical approaches, Fichou et al. [114] showed that heparin (~15 kDa) and RNA (~900 base pairs) were integral parts of the in vitro formed Tau fibrils. Upon removal or heparin, using

enzymatic digestion by heparinase which removed around 20% of bound heparin, a fraction of the Tau fibrils depolymerized into the Tau monomers and dimers. Similarly, treatment with RNAse led to the removal of around 60-70% of bound RNA. The detection of spin-labeled heparin in the thioflavin-positive heparin/RNA-containing Tau fibril-containing fraction post-heparinase/RNAs treatment showed that some of the heparin/RNA bound were structurally integrated into Tau fibrils and were not easily accessible by enzymes. Nevertheless, in both cases, heparin and RNA cofactors were instrumental for maintaining the thioflavin-positive and continuous-wave electron paramagnetic resonance of paramagnetic spin spectra signatory of β-sheet arrangement within Tau fibrils. These observations suggest that these two cofactors contribute to the structural integrity of Tau fibrils. Interestingly, thus far no non-proteinaceous electron densities in cryo-EM imaging of Tau fibrils were attributed to heparin, possibly due to sample preparation procedures and reversible and dynamic nature of heparin-Tau contact. It remains unclear to what extent the level of heparin/RNA integration into the fibrils alters their morphology or stability. Also, whether the interactions happen before or after Tau fibril formation in vivo must be clarified.

Evidence against the heparin integration into Tau fibrils

A few studies have argued against the significant heparin integration into the Tau fibrils (Figure 8 C). Based on the mass-per-length analysis of scanning transmission electron micrographs, von Bergen et al. [167] failed to detect the expected increase of ~11% mass in fibrils formed by the Tau MTBR variant (lysine 280 deletion) in the presence of LMW heparin (6 kDa). Also, following the centrifugation of the Tau aggregation solution, fluorescently-labeled MMW heparin (16 kDa) was predominantly detected in the soluble fraction, with a low but detectable amount in the polymerized Tau protein pellet fraction containing the fibrils. Based on these observations, it was concluded that heparin was not incorporated into the fibril core [167], which is in line with the earlier findings [200] that heparin is likely to associate with the fibril surface residues, some of which may be lacking in fibrils composed of just Tau MTBR. However, this study had several limitations, including the use of 1) a mutant form of a Tau fragment (MTBR) that lacks one of the important lysines (K^{280}) for heparin interaction; 2) LMW heparin (6 kDa) that was likely to possess reduced Tau-binding affinity compared to the HMW heparin, and 3) large fluorescent tag on the heparin molecules which could affect their biochemical properties and binding to Tau. These issues might limit the extrapolation of the results from this study to the non-mutant Tau MTBR or full-length Tau and heparin interactions.

Using kinetic and steady-state analyses, Carlson et al. [548] suggested that heparin-to-Tau molar ratios were more important factors in Tau polymerization than the concentration of Tau molecules. These authors argued for an allosteric impact of heparin on Tau molecules resulting in a low thermodynamic barrier to nucleation [548]. Based on the classical model of allosteric regulators [550], the authors concluded that heparin was not integrated into the Tau fibrils. However, the data in the study did not directly demonstrate that on the structural level. Similarly, Ramachandran and Udgaonkar [519] estimated the heparin-to-Tau molecule stoichiometry at the end of fibril formation to be one-to-twenty. Based on the theoretical calculations using heparin-Tau dissociation constant and Tau and heparin molecules' concentrations values, they argued that heparin was only a minor constituent of the formed fibrils. Analyses of the heparin-induced full-length Tau or MTBR fibrils at three different heparin concentrations by AFM and FTIR spectroscopy showed no significant size or structural differences of fibrils between these three conditions [519]. One obvious limitation of this experimental design is the lack of independent controls, such as alternative inducer-generated fibrils or reassessment of the fibril biophysical properties after enzymatic heparin removal treatment.

In summary, kinetic, structural, and biochemical studies strongly suggest the possibility of tight heparin association with or integration into Tau fibrils under certain conditions in vitro. However, further investigations using complementary experimental techniques and quantitative approaches are warranted to determine the precise mechanisms of heparin-Tau fibril interactions (Figure 7 B and C) and whether these interactions occur at the monomer or fibril levels in the brain.

The tight binding of heparin or other cofactors to Tau fibrils has significant implications for using heparin-induced fibrils to investigate Tau fibril toxicity mechanisms of seeding activity in cells or in vivo as the Tau-non-contingent responses, due to the presence or release of these molecules may occur. In the case of heparin, this includes vasodilation of the blood vessels [234] and immune [233] or aberrant cell stress responses [236-240,551]. Also, the presence of heparin of other cofactors might directly impact the post-translational modifications of Tau fibrils [242], alter their surface properties, secondary nucleation events, and thus their seeding activity and spreading through extracellular matrix interactions [158,235]. Furthermore, the interference of the polysaccharide with the Tau-targeting molecules [243] cautions the use of the current systems in the development of Tau pathology targeting drugs and tracers.

Do Tau and heparin interact in patients' brains in vivo?

Although heparin moieties were detected within intracellular NFTs [123-129], it is still puzzling how the extracellular heparin and HSPGs might directly impact the fibrillization of predominantly intracellular Tau in vivo, which by definition requires direct exposure to these molecules. Physiological and pathological forms of Tau were demonstrated to be released into the ECS in the free form, as well as in ectosomes or exosomes, and internalized by the neighboring cells via bulk dynamin-mediated endocytosis or HSPG-dependent micropinocytosis [552] (reviewed in [553] and [554]). This forms the basis of the hypotheses on the pathological Tau propagation in the brain along the neuroanatomically connected regions (reviewed in [555] and [556]). However, the initiation events that spur the primary Tau conversion from physiological to pathological forms remain unknown.

Tau molecules in physiological conformation present in the ECS might have ample opportunities to encounter heparin, and other cofactors, especially in the events of heparin-mediated neuroinflammatory responses. Thus, one may speculate that during these events, heparin exerts conformational changes on Tau molecules, priming them into fibrillization-competent forms and/or tightly binding to Tau. The subsequent cellular intake of these primed Tau molecules or Tau-heparin complexes might cascade into the pathological Tau oligomerization, fibrillization, and formation of NFTs, concomitantly sequestering the functional pool of Tau molecules and inciting cellular stress responses. Further investigations are necessary to determine whether the ECS heparin mediates the Tau conformational changes from physiological to pathological forms in vivo. Addressing this question might be achieved using techniques such as microdialysis of ECS in the brain of model animals [175,177,557,558], or recovery of the material from the brain electrode implants of neurodegenerative disease patients undergoing the procedures such as deep brain stimulation. The Tau proteoforms and heparin molecules then can be determined by highly sensitive biophysical techniques, such as mass spectrometry [559] at different stages of Tau pathology formation.

Indirect heparin-mediated induction of Tau aggregation

Heparin activates Tau kinases

Interestingly, apart from the direct interaction of heparin with Tau to induce the formation of fibrils, heparin might also indirectly influence Tau's biochemical and biophysical properties through stimulation of Tau hyperphosphorylation by several Tau kinases. This is thought to

occur due to heparin-induced conformational changes that ultimately lead to increased exposure of phosphorylation sites on Tau [201].

Heparin was shown to greatly enhance Tau phosphorylation by p34/cdc28 serine-threonine kinase [560] and by protein kinase A at least on serine 156 [561]. However, the physiological relevance of modifications by these kinases is unknown. On the other hand, heparin enhanced Tau phosphorylation by protein kinase FA/glycogen synthase kinase-3α (GSK-3α) in vitro, which phosphorylated residues found in the AD pathology, such as serines 235, 262, 404, 324 and 356, and threonines 212 and 231 [242,562]. Similarly, heparin was shown to enhance Tau phosphorylation by stress-activated serine-threonine kinases (SAPK1γ, SAPK2a, SAPK2b, SAPK3, SAPK4) on the serines (S202, S396, S404, S422) and threonines (T181 and T205, T231 [563]) in vitro. Interestingly, Hasegawa et al. [142] showed that the heparin concentration required to induce Tau phosphorylation by MAP kinase, NCLK, and GSK3β on multiple serine residues, and notably on serine 262, was lower than the heparin concentration required to induce Tau fibrillization. This suggests possible precedence of heparin-induced Tau phosphorylation to fibrillization, however subsequent studies showed that cofactor-induced Tau fibrillization kinetics were complex and dependent on other factors in addition to heparin-Tau concentration stoichiometry [519,548]. Serine 262 is considered abnormally phosphorylated in AD [564,565]. However, our group [207] and others [91,411] showed that phosphorylation of serine 262 in combination with other residues inhibited, rather than promoted, heparin-induced Tau aggregation in vitro. It is still unclear whether and how the predominantly extracellular heparin or plasma membrane-associated molecules of HSPGs can directly impact Tau kinase-mediated downstream fibrillization of Tau in the intracellular milieu in vivo.

Taken together, cofactors such as heparin and others, known and unknown, seem to play a much larger role in the Tau fibril formation, their biochemical characteristics, and their impact on neuropathology formation and progression than is generally thought and should be investigated further.

Other Tau aggregation inducers and mechanisms

RNA

Tau was first discovered to directly bind to RNA molecules in 1984 by Schröder et al. [566], later corroborated by others [157,567]. RNA was also found in association with hyperphosphorylated Tau in NFTs, Pick bodies, and neuritic plaques [568,569], providing credence to the physiological

relevance of investigating RNA-induced Tau fibrillization. In 1996, Kampers et al. [94] showed that RNA induced Tau assembly into fibrils through the formation of the intermolecular cysteine 322 disulfide bridges, which led to the formation of Tau dimer intermediate before Tau fibrillization. Subsequently, RNA has been successfully used to induce and study Tau fibrillization mechanisms in vitro [570]. Nevertheless, the formation of disulfide-mediated dimer formation is not necessary for Tau fibrillization in the brain [101] as exemplified by their absence in the cryo-EM-solved fibrils from sporadic AD, Pick's, CBD, and CTE patients (see Figure 9). The presence of RNA catalyzed the conversion of soluble Tau into insoluble forms, likely through the charge balance to allow the tighter packing of the molecules [571]. Recently, the role of RNA-Tau interactions has received increased attention due to converging data implicating liquid-liquid phase separation as a key mechanism in the initiation of Tau aggregation and fibril formation. [567]

Liquid-liquid phase separation and Tau aggregation

Another recently proposed model for the aggregation of Tau involves liquid-liquid phase separation (LLPS) (reviewed in [572,573]). In biology, LLPS defines biophysical processes of condensation of biomolecules driven by transient interactions [574]. These condensates are involved in the formations of membrane-less organelles in cells, such as nucleoli, stress granules, and liquid droplets. Recent findings suggest that these condensates may be implicated in the protein aggregation processes in neurodegenerative diseases spurred interest among researchers to study LLPS processes further [575] which have been reviewed in [574]. RNA and heparin were found to induce LLPS of Tau into reversible condensed droplets that increased local Tau concentration, where Tau retained mobile conformations [567]. In cells, the transfer RNAs were the predominant RNA species that were associated with Tau droplets [567]. Wegmann et al. [576] showed that Tau condensation into droplets coincided with the formation of Tau fibrils in the presence of heparin or RNA cofactors in vitro, suggesting the possibility of the coacervate heparin-Tau complex formation as an intermediate to Tau fibrillization [577]. However, whether these two processes were independent was unclear.

Recent studies using turbidity assays with varying salt concentrations showed that in the presence of heparin, the formation of thioflavin-positive Tau aggregates occurred under a much wider range of NaCl concentrations, in contrast to complex coacervation, which occurred only in a small subset of the conditions [578]. These results indicated that canonical heparin-induced Tau fibrillization was preferential to electrostatically driven heparin-Tau coacervate complex formation. The two processes – Tau LLPS formation and fibrillization – were likely to

occur under overlapping conditions, but were independent processes. On the contrary, another study showed that LLPS-promoting conditions increased the fibrillization kinetics of Tau [579]. This was exacerbated by the presence of the disease-associated mutations ΔK280, P301L, and G272V, which, in their own right, did not influence the phase transition propensity of Tau compared to non-mutant protein. Under physiological buffer conditions and Tau concentration of 2 μM [479,580], resembling that of the protein levels in the neurons, Tau required molecular crowding agents such as polyethylene glycol to phase separate. However, the P301L mutation or AT8-positive phosphorylation at pS202/pT205/pS208 increased the formation of droplets [581].

These studies indicate that total Tau concentration and molecular crowding conditions, isoform composition and ratios, and the presence of pathological mutations can all impact Tau's propensity to phase separate. Nevertheless, whether the LLPS and ordered amyloid assembly of Tau fibrils are co-occurring or co-dependent processes has not yet been definitively demonstrated. Furthermore, the LLPS should be modeled under physiological conditions to provide useful insights into Tau biology. Although the Tau LLPS is an exciting new line of research into mechanisms leading to Tau fibrillization, thus far the lack of robust tools to study these delicate and dynamic biophysical processes in cells and in vivo restricted studies to explore the therapeutic potential of modulating these processes and investigating their role in the pathogenesis of AD and other neurodegenerative diseases (reviewed in [582]).

Lipids and membranes

Early studies showed the presence of lipids and membranes in association with the neuropathological lesions in neurodegenerative disease patients [583-585], and directly bound to Tau [23,586]. Therefore, Tau-lipid interactions and anionic lipid-mediated aggregation of Tau were subsequently extensively studied (reviewed in [587]). Lipid membranes promoted Tau self-assembly at the membrane surface [378,588]. MTBR was identified as a lipid-binding domain [589,590], with interactions specifically mediated by the PHF6 region [591]. Lipid membranes were found to induce a shift in full-length Tau molecular conformation towards β-sheet-containing structures, that formed stable oligomeric complexes [592].

Tau interactions with membranes could be modulated by Tau PTMs. Phosphorylation had differential effects on Tau interactions with lipid membranes in various systems. Phosphorylation of Y310 in the MTB region [380] reduced its affinity for lipids in vitro. In neuronal cells casein kinase 1 and GSK3β inhibition led to increased Tau association with the

membrane, whereas inhibiting protein phosphatase 2A, or mimicking phosphorylation in the N-terminal and proline regions, led to a decrease of Tau affinity for membranes [593]. Similarly, mimicking phosphorylation of 3R0N fetal Tau isoform on multiple residues significantly decreased its membrane association [594]. Membrane fraction-containing extracts of cell lines [595,596] and neuronal cultures [593] contained predominantly dephosphorylated non-aggregated Tau. On the other hand, oligomeric Tau phosphorylated by GSK3β in vitro had a higher affinity for di-palmitoylphosphatidylcholine (DPPC) or 1-palmitoyl-2-oleoylphosphatidylcholine (POPC) unilamellar vesicles, whereas phosphorylation of monomeric 4R1N did not affect its lipid-binding affinity [597]. During apoptotic cell death phosphorylated aggregated Tau was enriched in the plasma membrane-containing PC12 cell line extracts [598]. Tau phosphorylation by Fyn kinase resulted in its recruitment and enrichment at the membrane in neuronal cells [599], and oligomeric phosphorylated Tau was enriched at plasma membrane of human 4R0N-overexpressing murine neuronal N2a cell line [600]. As evident from the contradicting reports, the role of Tau phosphorylation and PTMs on its lipid interactions is dynamic and multifaceted, and must be investigated further in light of its impact on transmembrane Tau spreading (see Figure 3 A) [362,601].

From a Tau aggregation tool development perspective, unsaturated long-chain fatty acids, such as arachidonic acid (5,8,11,14-eicosatetraenoic acid (20:4)) and 9-palmitoleic acid (16:1), were found to efficiently promote full-length Tau assembly into long fibrils in vitro [95]. Arachidonic acid-induced Tau fibrils showed twists at the 88 ± 15 nm intervals, were thioflavin-positive and immunoreactive to PHF-specific Alz50 antibody [105]. Nevertheless, the lipids were not extensively adopted for in vitro Tau fibrillization assays, likely due to the difficulty of the post-fibrillization purification and lipid removal, as well as the heterogeneity of the fibrillar assemblies.

Interaction with other amyloid-forming proteins

Most neurodegenerative disorders are characterized by overlapping proteinopathy profiles [602]. In addition to Tau-containing NFTs, amyloid-β plaques are another pathological characteristic of AD [603]. It has been stipulated, primarily based on the results from preclinical AD models, that amyloid-β was associated, and may directly contribute to the initiation of Tau fibrillization [604-607]. Amyloid-β was found to exacerbate the AD-derived Tau-seeded pathology in the mouse brain, resulting in the extensive formation of NFTs and neuropil threads, and the pathology spread throughout the brain regions, possibly through the secondary nucleation mechanism [608]. Amyloid-β and Tau interconnections were recently reviewed by Ciccone et al [609].

Furthermore, the co-occurrence of Tau and α-synuclein in neuropathological inclusions has been observed in other neurodegenerative diseases since the early 1990s, including AD with Lewy bodies [610] and dementia with Lewy bodies (DLB) [611-613]. Only recently, however, the direct relationship between these proteins and Tau fibrillization has been investigated. Heterotypic induction of Tau fibrillization has been demonstrated upon co-incubation with pre-aggregated amyloid-β fragments [604] or monomeric α-synuclein, which bound Tau through its C-terminus [614]. The latter case also resulted in the formation of homotypic α-synuclein fibrils under a low concentration of α-synuclein monomers. In contrast, no α-synuclein fibrils were formed in the absence of Tau. α-synuclein oligomers were found to nucleate oligomeric Tau formation, but not β-sheet forming fibrils [615]. Tau K18 was found to form co-oligomeric complexes with α-synuclein [616], indicating that this region is important in Tau interactions with α-synuclein. α-Synuclein was also found to modulate the spread of Tau pathology in the mouse brain [617]. Fibrils composed from both Tau and α-synuclein monomers showed differential pathology propagation when injected into the mouse brain, where Tauopathy was induced at higher levels than synucleinopathy [618].

Both Tau and α-synuclein have been implicated in pathology spreading through anatomically connected brain regions in a protein strain-specific manner, resulting in distinct disease phenotypes in humans (reviewed in [619] and [620]). Presence of high levels of Tau in the AD-subtype of Parkinson's disease correlated with age, early cognitive impairment scores, grey matter reduction in the frontal cortex, and APOE ε4 allele status [621]. Increasingly, evidence suggests that heterotypic induction of Tau aggregation by other amyloidogenic proteins contributes to the co-occurrence of different proteinopathies found across neurodegenerative disorders [264]. These findings underscore the critical importance of conducting systematic studies to determine the key sequence, structural and cellular determinants of Tau interactions with other amyloid proteins and how they influence each other's aggregation, toxicity, and pathology spreading. The fact that the pathological aggregates of Tau, α-synuclein, and other amyloid proteins such as TDP-43 are heavily modified emphasizes the importance of conducting these studies in models that reproduce the biochemical complexity of disease-relevant pathological aggregates of these proteins.

How can the new biochemical and structural insights into physiological and pathogenic Tau inform drug discovery?

The Tau PTM patterns as drug targets

How the complex patterns of PTMs influence Tau aggregation and pathology formation remains unclear. However, it is becoming abundantly clear that the diversity and the distribution of Tau PTMs suggest that they play key roles in regulating Tau aggregation and pathology formation, and therefore require closer investigations. A large body of careful investigations over several decades has shown that Tau aggregation propensity depends heavily on the specific residue PTM positions, overall patterns along the Tau molecule, and their impact on the local protein structure (reviewed in [50]) (see Figure 3). However, most of these studies were based on investigating Tau PTMs one at a time. They did not account for the complex interplay between different PTMs, which is likely to be tightly regulated during pathology formation and maturation. Also, the patterns of PTMs may differ between different Tau proteoforms. In a recent study, Dujardin et al. [38] conducted a systematic study to investigate the relationship between the phosphorylation of different Tau species (soluble, oligomers, and seed-competent Tau) from 32 patients with AD and their seeding activity in cellular and animal models of Tauopathies. Their findings revealed striking patient-to-patient variation in the hyperphosphorylation profile of these different forms of Tau. The authors suggested that variations in PTMs may underlie the clinical heterogeneity of AD.

Together, multiple studies further underscore the complexity of Tau PTMs, the importance of cross-talk between the different PTMs in the modulation of Tau aggregation and seeding propensities, remodeling of the fibrils, and potentially disease progression and clinical heterogeneity of Tauopathies [622]. These observations underscore the importance of employing more precise tools and experimental approaches to 1) refine our knowledge of the distribution maps of the Tau PTMs in healthy individuals at different stages of aging and disease progression; 2) identify the pathology-driving or preventing PTM patterns; and 3) map co-occurring PTMs, as well as their Tau isoform origin. This will pave the way for elucidating the role of cross-talk between PTMs in regulating Tau functions, aggregation, pathology formation, and spreading during disease progression. The knowledge gained from these studies will also help guide more disease-relevant reductionist approaches by defining the precise chemical identity of the Tau proteoforms that should be used to model Tau aggregation and toxicity in vitro. Finally, the complexity of the Tau PTMs should be taken into consideration when developing therapeutic antibodies targeting specific domains of Tau, or antibody-based tools

used to quantify Tau species and pathological aggregates. In the section below, we provide an overview of previous studies to assess the therapeutic potential of targeting Tau PTMs to treat AD and other tauopathies. Although there are many studies on targeting Tau kinases in preclinical models, we will focus the discussion below on kinases and drugs that have been evaluated in clinical trials.

Phosphorylation

As mentioned above, Tau is known to be phosphorylated by at least 37 protein kinases (reviewed in [314]), which have variable specificity for Tau residues [623], and is subject to dephosphorylation by at least four phosphatases [624]. Because early studies implicated hyperphosphorylation as a pathogenic event that drives the initiation of Tau aggregation, several kinases were shown to phosphorylate specific residues on Tau and pursued as potential targets for the treatment of AD and other Tauopathies. In contrast, phosphatase enzymes are nonspecific and generally act upon many more client proteins other than Tau and have not been extensively investigated for applications in Tauopathy interventions and treatment. Most Tau kinases are known to phosphorylate multiple client proteins and have already been investigated for their involvement in other diseases. In many cases, the availability of inhibitors of these kinases, including some that were in the advanced development stages, facilitated their repurposing as potential therapeutics for AD and Tauopathies [625].

One promising kinase candidate is glycogen synthase kinase 3β (GSK3β) (reviewed in [626 627]), which phosphorylates Tau on at least 26 residues, and its levels are increased as the disease progresses [628,629]. Overactivation of GSK3β resulted in Tau hyperphosphorylation and led to neuronal death [630,631]. Lithium is a potent inhibitor of the GSK3β, inhibition of which was shown to lead to lower levels of hyperphosphorylated Tau in mice [632,633]. Lithium has also been shown to reduce GSK3β-mediated phosphorylation of Tau and to increase Tau binding to the microtubules and their assembly in neurons [634-636], in mice [637], and prevented NFT pathology formation [638].

Lithium salts are drugs commonly used for symptom management in bipolar and other psychiatric disorders [639]. Lithium has been studied as a modifying treatment for AD, mild cognitive impairment, and dementia [640,641]. However, its efficacy is still unclear. One important consideration is the toxicity, poor tolerance, and side effects of lithium, which led to discontinuation of the recent clinical trial (ClinicalTrials.gov Identifier: NCT00703677)

evaluating lithium for the treatment of tauopathies CBD and PSP. Epidemiological observations of lower incidence of dementia in populations with access to tap water containing higher long-term levels of lithium [642], although later contested [643], still spurred interest in the use of microdose lithium as a preventative measure to stave off dementia, as well as disease progression modifying treatment in Alzheimer's disease (ClinicalTrials.gov Identifier: NCT03185208, LATTICE trial, currently recruiting). Microdosing of lithium (NP03) at levels 400-fold lower than standard formulations is being considered for clinical trials in humans based on the preclinical studies [644]. The selective GSK3β inhibitor tideglusib (NP031112) [645] was also evaluated for the treatment of AD (ClinicalTrials.gov Identifiers: NCT00948259 and NCT01350362) and PSP (ClinicalTrials.gov Identifier: NCT01049399) [646]. However, it failed to show a clinically relevant modification of disease progression despite reducing brain atrophy in PSP [647], no levels of phosphorylated Tau were reported.

Another Tau-phosphorylating enzyme of interest is Src-family tyrosine kinase Fyn. It specifically phosphorylates the residue Y18, which was found in the Alzheimer's brain NFTs [648]. Despite promising preclinical data [649,650] and good drug penetration and tolerability profile (ClinicalTrials.gov Identifier: NCT01864655) [651], Fyn inhibitor saracatinib (AZD0530) showed no clinical efficacy in Alzheimer's patients with no significant changes in the CSF total or phosphorylated Tau (ClinicalTrials.gov identifier: NCT02167256) [652].

Other Tau kinases have also been considered potential targets for pharmacological agents with expected lowering of Tau phosphorylation and aggregation. These include cyclin-dependent kinase 5 [653], c-Abl tyrosine kinase (c-Abl) [654], lemur tyrosine kinase 2 (LTK) [655], dual specificity tyrosine-phosphorylation-regulated kinase 1A (Dyrk1A) [656], and thousand-and-one amino acid kinases (TAOKs) [657]. However, thus far few have proceeded beyond preclinical investigations, or their clinical efficiency is not yet known, for example for the c-Abl inhibitor Nilotinib (ClinicalTrials.gov Identifier: NCT02947893). Tau kinases that a) phosphorylate Tau in vitro or b) promote its phosphorylation by other kinases, and c) are implicated in the neuropathological profile of patients with Tauopathies are the potential targets for further investigations [658]. These include casein kinase 1 (CK1) [659], c-Jun amino-terminal kinase (JNK) [660], extracellular signal-regulated kinases 1 and 2 (Erk1 and Erk2) [661], adenosine-monophosphate activated protein kinase (AMPK) [662], cyclic AMP (cAMP)-dependent protein kinase (PKA) [663], protein kinase N1 [664], tau-tubulin kinases 1 and 2 (TTBK1 and TTBK2) [628,665], Ca2+/calmodulin-dependent protein kinase II (CaMKII) and microtubule-affinity regulating kinases (MARKs) [666]. Also, the rational targeting of the specific regulatory subunits of Tau phosphatases has been proposed as a viable strategy to selectively reduce pathology-

associated phosphorylation of Tau. Tau phosphatases that are implicated in Tauopathies include protein phosphatases 2A and 2B (PP2A and PP2B) [667,668], protein phosphatase 5 (PP5) [669], and calcyclin binding protein and Siah-1 interacting protein (CacyBP/SIP) [670]. Recently, we proposed that focusing on inhibiting Tau phosphorylation events that lead to its disassociation from MTs may offer an alternative and more effective strategy to prevent Tau aggregation by stabilizing its native conformations [207].

O-GlcNAcylation

Preclinical studies have shown that increasing Tau O-GlcNAcylation by inhibiting O-GlcNAcase (OGA) can slow aggregation and prevent neurodegeneration in rTg4510 [671,672], Tau-P301L [673], and JNPL3 [440] mouse models. Thiamet G is a potent inhibitor of OGA, and it was demonstrated to reduce Tau phosphorylation at T181, T212, S214, S262, S356, S404, and S409 after acute lateral ventricle injection in mouse brain [674]. Based on this, an OGA inhibitor compound MK-8719, the Thiamet G derivative [675,676], and ASN120290 [677] were developed, and both were granted the orphan drug status for the treatment of PSP, however, their clinical efficacies beyond Phase I trials remain unknown [678].

Acetylation

Salsalate, the derivative of salicylate, primarily a CBP/p300 inhibitor [679], was investigated in the preclinical studies in the PS19 mouse line overexpressing P301S-Tau. Salsalate reduced Tau acetylation at K174 by inhibiting acetyltransferase p300, and subsequently decreased neuronal loss in the hippocampus, thus reserving memory [444]. Subsequently, salsalate was investigated in Phase I clinical trial for PSP (ClinicalTrials.gov Identifier: NCT02422485). However, it was discontinued due to a lack of efficacy. Further investigations in early Alzheimer's patients are ongoing (ClinicalTrials.gov Identifier: NCT03277573).

Ubiquitination

Currently, no therapies are directed at lowering Tau ubiquitination levels or enhancing pathological Tau clearance. Possible strategies might include increasing Tau acetylation at the lysine residues, thus preventing their ubiquitination and Tau aggregation into PHFs that lead to the formation of NFTs. Furthermore, as the impairments of lysosomal and proteasomal protein degradation systems may result in a build-up of ubiquitinated Tau species [680,681], targeting these pathways to enhance protein clearance might have favorable effects in

clearing some of Tau pathology. It is important to stress, that there are no studies on the effect of site-specific mono- or poly-ubiquitination of Tau on its aggregation. Therefore, whether ubiquitination prevents or enhances Tau aggregations remains unclear and might depend on at what stages during aggregation and pathology formation Tau becomes ubiquitinated.

Tau aggregation inhibitors

Targeting Tau monomers: Initial efforts aimed at targeting Tau focused on trying to identify small molecules that stabilize the native state of Tau or prevent its aggregation. The dynamic, flexible structure of Tau and the multiple domains playing a role in the initiation of its self-assembly make targeting Tau monomers very challenging. Indeed, no drugs have been shown and validated to stabilize the native monomeric state of Tau.

Preclinical studies provide insights into the possible targets for inhibition of Tau aggregation and β-sheet-containing fibrillization intermediates or oligomers (reviewed in [682]). Small molecules, such as methylene blue [683], orange G [684], oleocanthal [685], "molecular tweezer" CLR01 [686], phthalocyanine tetrasulphonate [687], curcumin [688] and diazodinitrophenol [684], thiophene [689], and polythiophene [690] compounds have also been reported to inhibit Tau aggregation in vitro. Thus far, methylene blue derivative and curcumin are the only small molecule Tau aggregation inhibitors that have advanced to clinical trials, and none have been approved for clinical use [691]. The most prominent attempt to target Tau aggregation directly has centered on methylene blue. Phenothiazine compound methylene blue (methylthioninium chloride) was found to prevent Tau fibrillization, but not the formation of oligomeric Tau [692], likely through oxidation of cysteines [693,694]. Phenothiazine could also mitigate Tau-related neurodegeneration and pathology through autophagy induction [695], reduction of Tau phosphorylation by mitogen-associated kinase 4, reduction of synaptotoxicity [696], and upregulation of genes by NF-E2-related factor 2/antioxidant response element in mice [697]. Furthermore, due to its primary function as a redox cycler, the total impact of methylene blue is thought to be the result of stimulating the mitochondrial function, metabolism, and reduction of inflammatory responses. Its oldest application in toxicology includes treatment of methemoglobinemia [698-700], and against malaria from 1891 [701,702], psychiatric conditions such as depression [703,704], claustrophobia or fear [705], and ifosfamide-induced encephalopathy [706]. Despite such widespread use of methylene blue in various conditions, unfortunately, no epidemiological studies capturing incidence rates of dementia or AD have been done in these patient populations. Therefore, despite the possible direct effects of methylene blue on Tau fibrillization, it is likely to have pleiotropic effects on brain pathology. Recently, despite

promising preclinical data [707,708], the derivative of methylene blue in a reduced form, LMTX (hydromethanesulphonate; TRx0237) failed to show clinical efficacy in Phase III clinical trials (NCT01689246 and NCT01689233). However LMTX is being investigated as a monotherapy in early stage AD patients (NCT03446001).

Targeting aggregated and pathological Tau

Contrary to the extracellular localization of AD-associated amyloid-β aggregates, Tau-containing NFTs are predominantly intracellular. This represented a challenge to large antibody-based Tau-targeting strategies due to poor cell membrane penetrance and antibody uptake. However, the discovery that Tau pathology propagates in the brain by mechanisms of cell-to-cell Tau protein spreading [554,556] sparked a huge interest to develop antibodies and therapeutic agents targeting the propagating Tau proteoforms in the extracellular and transsynaptic space. The ultimate goal is to interfere with the propagation of Tau pathology to the different brain regions after its inception by direct sequestration and neutralization of the toxic and/or seeding competent Tau species [709].

Despite decades of research, it is still unclear which Tau proteoforms are driving Tau pathology. The reductionist biophysical concepts have dominated the Tau aggregation field and have been useful tools for informing on the kinetics of in vitro Tau aggregation, where the simple sigmoid aggregation curve has been used as a primary model. However, it must be stressed that they can only be applied to in vitro systems. The processes of Tau aggregation taking place under pathological conditions in cells likely involve multiple yet unidentified cofactors, complex PTMs, and pathological diversity, which could be driven by parallel or cell-type dependent mechanisms of aggregation.

The attempts to systematically identify toxic Tau species, such as oligomers or fibrils, from patient samples are confounded by the difficulties of their purification in high quality and large amounts necessary for downstream studies, in addition to the possibility that there are multiple toxic forms of Tau. Although in vitro approaches allowed investigators to produce large quantities of pure Tau fibrils, their biophysical, biochemical, and structural properties substantially differed from the brain-derived material. These factors complicate the rational design of antibodies targeting specific Tau proteoforms due to our limited knowledge of the relevance of these proteoforms to pathological processes, as well as the difficulties to reconstruct these proteoforms in vitro for the antibody design and screening. Therefore, the

exact species of Tau targeted by antibodies are not well defined [503], and their formation pathways and clinical relevance remain unknown.

The advent of super-resolution imaging techniques, such as cryo-electron microscopy (cryo-EM), allowed for a direct structure visualization of human brain-derived Tau fibrillar cores (Figure 10) [156,163] to inform rational design of the inhibitors for the β-sheet-containing Tau aggregation, that is considered to be pathology-associated, as opposed to amorphous Tau aggregates or precipitation [710]. Cryo-EM was also used to directly map the ligand-binding sites within the AD Tau fold [711]. It showed that fibril core residues comprise only the MTBR repeats R3 and R4, which is important in designing the antibodies with epitopes directed outside of these regions. However, this technique is limited to detecting around 28% of the Tau sequence that constitutes the solid core of fibrils, thus overlooking the less structured Tau domains that might bind ligands, promote Tau aggregation or regulate pathological Tau spreading, for example heavily post-translationally modified proline-rich and C-terminal regions. Furthermore, robust methodological approaches are yet to be developed to isolate the putatively pathological Tau intermediate species and oligomers from the human brain in large amounts and good enough quality for cryo-EM and related techniques.

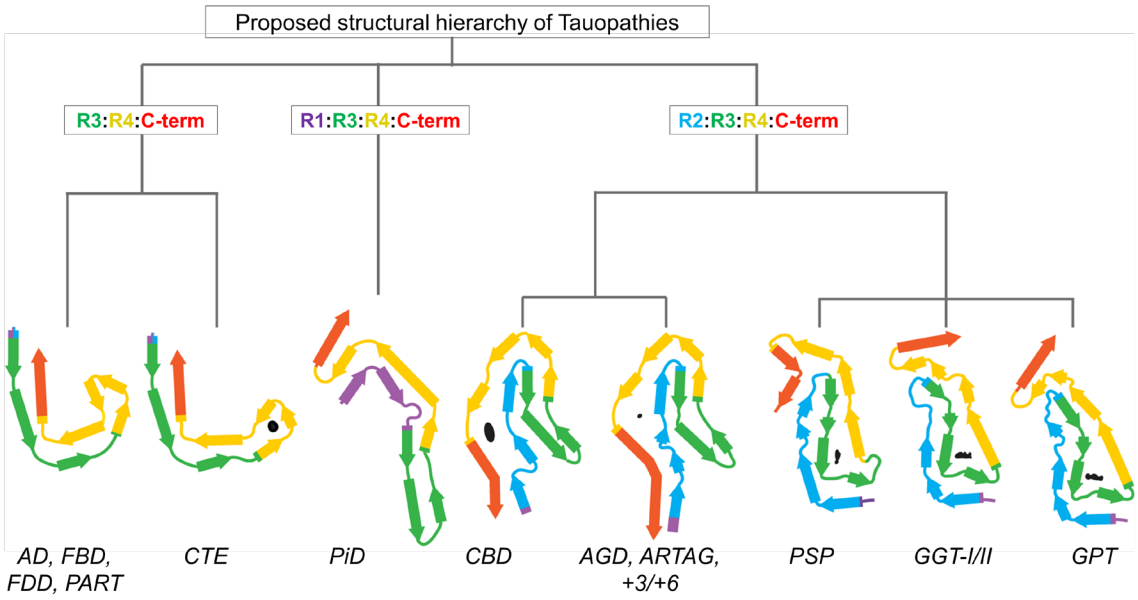

Figure 10. Proposed classification of Tauopathies based on the structural hierarchy of the Tau fold formations based on the similarity. Colors denote different Tau domains (reproduced with modifications from ref. [156] with permission from The Author(s), under exclusive licence to Springer Nature Limited, copyright 2021).

Immuno-based anti-Tau therapies

Passive and active anti-Tau immunotherapies are being actively investigated in both preclinical and human studies [678,712] (Figure 11). Extracellular Tau is a popular target for passive antibody therapies because it does not require cell penetration, and might prevent the cell-to-cell spread of pathological Tau. Antibody ABBV-8E12 targets the N-terminal Tau region, when administered peritoneally to P301S mice reduced brain atrophy and Tau pathology in hippocampus [713]. In humans, ABBV-8E12 (tilavonemab) was assessed in Phase II clinical trials for PSP (ClinicalTrials.gov Identifier: NCT03391765) but discontinued due to the lack of efficacy, and in an early AD trial, which has completed the Phase II (ClinicalTrials.gov Identifier: NCT03712787). Another anti-N-terminus antibody gosuranemab (BIIB092) was evaluated for PSP and other Tauopathies (ClinicalTrials.gov Identifier: NCT03068468); however, it was discontinued in 2019 due to failure to meet primary and secondary endpoints, and no efficacy was found for AD (ClinicalTrials.gov Identifier: NCT03352557, scheduled to end in 2024). Following encouraging results in Phase I (ClinicalTrials.gov Identifier: NCT02820896), semorinemab (RO7105705), which targets N-terminus of all Tau isoforms in both monomeric and oligomeric forms of Tau and is independent of phosphorylation, has been evaluated in Phase II clinical trial TAURIEL that was terminated in early 2020 due to lack of efficacy (ClinicalTrials.gov Identifier: NCT03828747). Another trial LAURIET assessing semorinemab in patients with prodromal and mild AD (ClinicalTrials.gov Identifier: NCT03289143) was reported in August 2021 meeting only one primary end-point out of two, and not meeting any secondary functional or cognitive endpoints. Several other passive immunotherapies targeting different regions of the Tau protein are currently under development, including the MC1-derived antibody zagotenemab in Phase II for AD (ClinicalTrials.gov Identifier: NCT02754830 and NCT03019536); JNJ-63733657, recognizing phosphorylated T217 in Phase II for AD (ClinicalTrials.gov Identifier: NCT03689153, NCT03375697, and NCT04619420); Lu AF87908, recognizing pS396, in Phase I for AD (ClinicalTrials.gov Identifier: NCT04149860); PNT001, recognizing cis-isomer of pT231, in Phase I for AD and TBI (ClinicalTrials.gov Identifier: NCT04096287 and CT04677829); and bepranemab, binding the residues 235–246, in Phase I for PSP (ClinicalTrials.gov Identifier: NCT03605082, NCT03464227, NCT04185415, and NCT04658199). Another Tau MTBR-targeting antibody E2814 is currently recruiting participants to be investigated in clinical trials commencing in 2021 (ClinicalTrials.gov Identifier: NCT04971733) within the Dominantly Inherited Alzheimer Network Trials Unit (DIAN-TU) program led by the Washington University School of Medicine [714]. Despite the lack of success in the clinic so far, the interest in the research and development

of the anti-amyloid Tau-targeting therapies is likely to increase following important, albeit controversial [715,716], by United States' Food and Drug Administration's approval [717] of amyloid-β targeting AD drug BIIB037 [718] (aducanumab, ClinicalTrials.gov Identifier: NCT02477800, NCT02484547). It is important to stress that many of these clinical trials have been driven by studies exploring antibodies targeting different regions in Tau and efficacy in preclinical models rather than precise targeting of disease-relevant pathogenic species. Differences in Tau aggregate conformations and biochemical properties between rodent and human brains could explain the failure to translate success in mice to the clinic. The large number of structural data emerging from brain-derived pathological aggregates from Tauopathies is helpful but may not be sufficient to guide disease-specific therapies and diagnostics as they lack information about the large segments of the protein flanking the core of the fibrils, and which could still play important role in the regulation of Tau pathogenic properties. Therefore, a combination of comprehensive structural and biochemical profilings of the Tau species and aggregates in the brain is essential to develop more effective therapies and diagnostics.

Active immunotherapies (vaccinations) for Tau include delivery of Tau sequence fragments to elicit the immune response of the recipient [712]. This should arguably prevent the pathology formation, or help clear existing Tau aggregates and inclusion through their recognition by the innate immune system. The furthest therapy along with in the development pipeline is AADvac-1, which is a Tau peptide consisting of residues 294-305 adjunct to keyhole limpet hemocyanin [719]. It was evaluated in the Phase II trial in AD (ClinicalTrials.gov Identifier: NCT02579252) with promising results that will further its evaluation in the Phase III trial. Another active Tau vaccination is ACI-35 which includes 16 copies of pS396 and pS404 Tau in a liposome carrier. This showed a robust immune response in P301L-Tau and wild-type mice, and produced antibodies that bound the NFTs, and reduced insoluble and soluble Tau levels in the brain homogenates [720]. In human subjects, redesign into ACI-35.030 resulted in a higher immune response compared to the original version. Currently, no investigations in the clinical settings are underway for this therapy.

Nanobodies

Another potentially promising approach to target Tau pathology propagation is using nanobodies such as single-chain variable fragments (scFvs) or intrabodies (iBs) to recognize, bind and intercalate into Tau fibrillar structures [721]. Nanobodies have the advantage of being much smaller in size than conventional multiple-chain antibodies, thus binding to epitopes with low accessibility due to steric hindrance, and can better penetrate across the blood-brain

barrier (BBB) and cell membrane. Several preclinical studies investigated the therapeutic potential of nanobodies. The strategy for the development of anti-Tau nanobodies was first published in 2002. A candidate nanobody targeting Tau domain 151-422 (scFv#2) was shown to penetrate the cell cytoplasm and the nucleus, and bind the intracellular Tau [722]. Another nanobody, scFv-RN2N, targeting 2N Tau isoforms, efficiently crossed the BBB, which could be enhanced by scanning ultrasound, in transgenic pR5 human Tau P301L mice [723]. Furthermore, the GSK3β-mediated Tau phosphorylation at mid-domain epitopes recognized by antibodies AT8 (pS202/pT205/pS208) and AT180 (pThr231) was inhibited, whereas C-terminal phosphorylation at S404 was not affected. On a phenotypic level, these mice showed a reduction of anxiety-like behavior in elevated plus-maze [723].

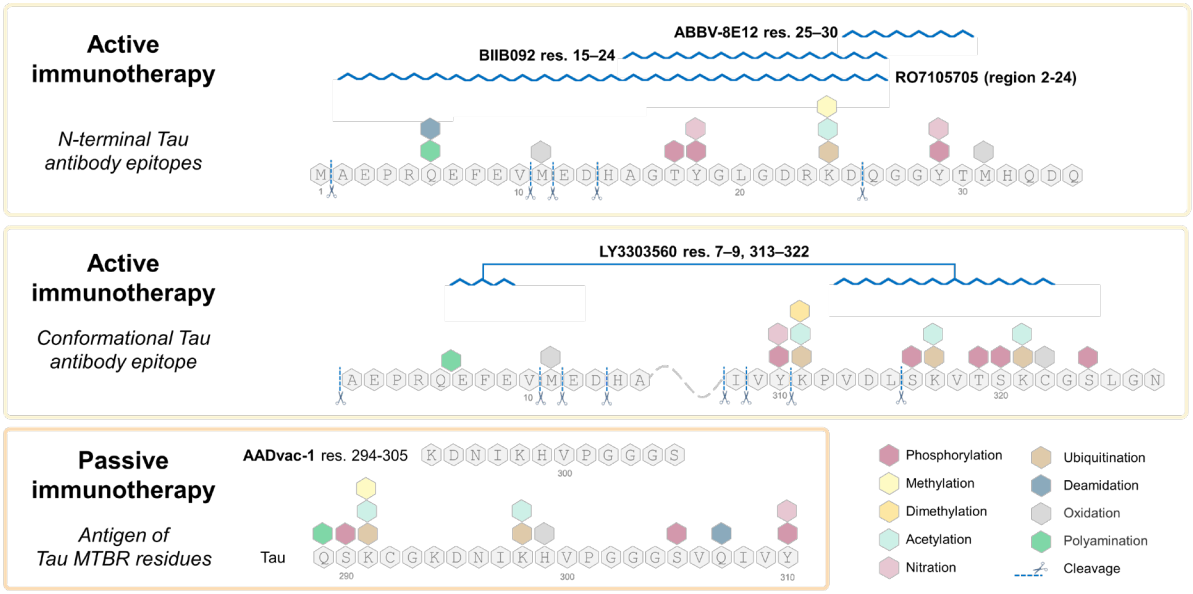

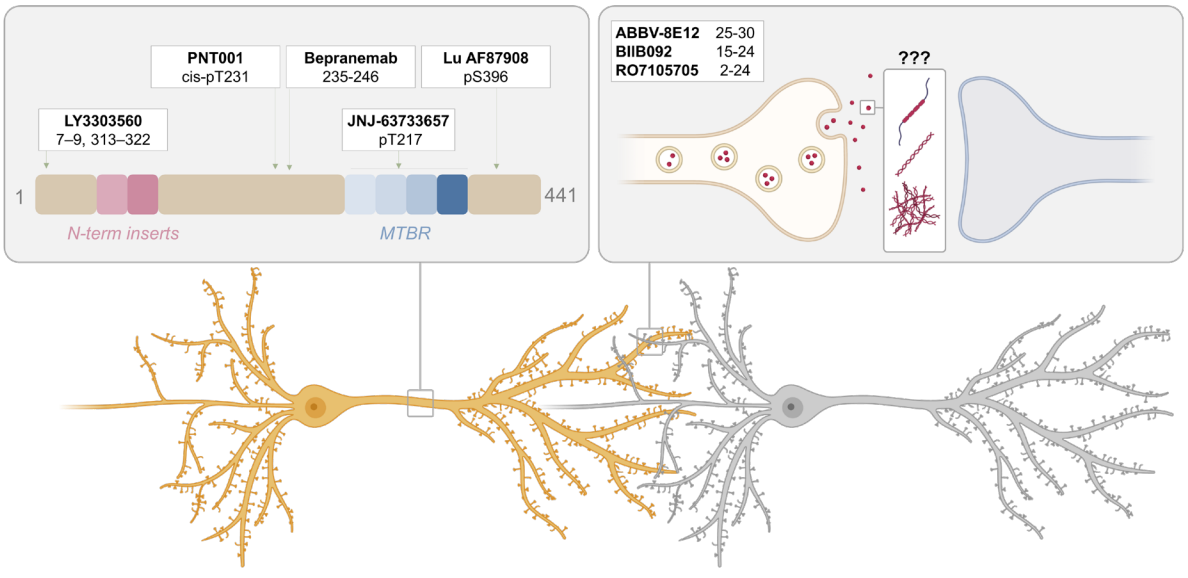

Figure 11. Active and passive Tau immunotherapies. Known epitopes of antibodies are aligned to the Tau sequence with highlighted PTMs. Putative intracellular and extracellular Tau targeting antibodies with epitope amino acid numbers where known.

Studies in rTg4510 and JNPL3 P301L Tau mice showed higher efficacy of iBs than scFvs derived from antibodies PHF1, CP13, and Tau5 when overexpressed in the brain [724]. Nanobodies prevented aggregation upon mutant 4R0N S320F Tau overexpression in HEK293T cells. However, the in vivo effects on the motor phenotypes of the mice were only modest, with no assessment of cognitive functions [724]. The latest efforts to develop new nanobodies targeting Tau showed their ability to reduce heparin-induced Tau aggregation in vitro and prevent Tau pathology propagation by templating when expressed in the mouse brain (preprint at the time of writing [725]). Further exploration of target engagement of the post-translationally modified Tau epitopes should be explored to determine the feasibility of recognition of the large PTMs, such as ubiquitin groups, by the small nanobodies.

PROTACs

Another approach to clearance of toxic Tau species is by using proteolysis targeting chimera proteins (PROTACs) [726]. These work through binding of the target molecule such as Tau or Tau aggregates by the ligand connected through the linker to the ligand-binding the ubiquitin ligase molecule [727]. Ubiquitin ligase then ubiquitinates the target molecule, therefore directing the entire complex for the degradation by the proteasome. Recent advances in rational protein engineering and evolution have allowed multiple target proteins to be directed for proteasomal clearance to ameliorate the cellular pathology they may cause. These include B-cell lymphoma 6 (BCL6) [728], focal adhesion kinase (FAK) [729], androgen [730] and estrogen [731] receptors, and Bruton's tyrosine kinase (BTK) [732] for cancer treatments, P300/CBP-associated factor and general control nonderepressible 5 (PCAF/GCN5) [733] and interleukin-1 receptor-associated kinase 4 (IRAK4) [734] for immunotherapies, as well as signal transducer and activator of transcription 3 (STAT3) [735].

The PROTAC approach for Tau clearance has been investigated in preclinical models. TH006 peptide was designed to recruit both Tau and ubiquitin ligase von Hippel-Lindau tumor suppressor protein (Vhl), and reduce Tau levels in 3xTg-AD mice and primary neuronal cultures [736]. PROTAC binding Tau and ubiquitin ligase kelch-like ECH-associated protein-1 (Keap1) efficiently reduced Tau levels in cellular SH-SY5Y human bone marrow cancer model and rodent Neuro-2a and PC-12 cell lines [737]. Small molecule PROTACs that recruited

ubiquitin ligase Cereblon were reported to degrade non-modified and phosphorylated Tau in human neuronal models harboring Tau mutations A152T or P301L[738]. Another PROTAC recruiting Cereblon was designed from the Tau PET tracer ^{18}F-T807 [739]. The compound QC-01–175 cleared Tau in FTLD patient-derived neurons, resulting in a higher resilience of cells to stress. Presumably, QC-01–175 selectively bound to and degraded the monomeric aberrant FTD-associated Tau variants, as the clearance of monomeric Tau in the neurons derived from healthy controls was insignificant. Another small molecule, C004019, designed to bind both monomeric Tau and Vhl ubiquitin ligase efficiently targeted it for degradation by the proteasome in cellular and mouse models [740]. C004019 was efficient at improving synaptic and cognitive deficits in hTau and 3XTg-AD mice. The reduction in the high molecular weight Tau observed was attributed to the shift in the equilibrium between soluble monomeric and oligomeric or aggregated Tau species. The Tau aggregates are not preferentially degraded by the proteasomal pathway [741,742]. A related approach to targeted Tau clearance involves the direct proteolysis of bound Tau, conceptually demonstrated by the artificial synthetic apocyclen-hybrid hydrolase I2-Cu(II) [743], which was designed to recognize the Tau hexapeptide PHF6, VQIVYK, present in MTBR R3 repeat. I2-Cu(II) cleaved the Tau fragments and prevented their aggregation in vitro, and reduced the overexpressed Tau-EGFP signal in the N2a cell line.

Conclusions and implications for targeting Tau

Converging evidence continues to point towards Tau aggregation as one of the central events in the pathogenesis of AD disease and other Tauopathies. The relative contribution of loss of functions vs. gain of toxic functions to the pathogenesis of Tauopathies remains unknown. However, it is clear that preventing Tau aggregation in the first place and neutralizing its seeding activity would also contribute to maintaining the normal level of Tau and thus minimize loss of Tau function. Therefore, targeting the process of Tau aggregation, instead of just specific Tau species only, remains a viable therapeutic strategy for treating Tauopathies.

Despite significant advances in understanding the morphological and structural properties of Tau fibrils, many fundamental questions about what causes Tau to aggregate in the first place and the role of cofactors, Tau PTMs, and Tau interactome in regulating Tau aggregation, pathology formation, and toxicity remain unknown. In this review article, we provide an overview of our current understanding of the sequence and molecular determinants of Tau aggregation and the various experimental approaches that have shaped our understanding of its mechanisms of aggregation and role in Tauopathies. Our analyses of the literature revealed

a widening gap between the complexity of Tau sequence, structure, and pathology in the brain, and the tools and model systems commonly used to investigate the mechanisms of Tau aggregation and toxicity in research laboratories. We also showed that many of the methods and assays to screen for modifiers of Tau aggregation and toxicity are carried out using unmodified Tau aggregates that do not share the same biochemical signatures or structural properties of pathological Tau. Currently, most experimental approaches do not take into account the diversity of Tau PTMs, the complexity of the Tau PTM patterns in their physiological and pathological forms, or the fact that the Tau PTM patterns change during disease progression. Therefore, it is not surprising that the conventional approaches have not borne tangible results in the clinic. We highlight the necessity to revisit the Tau aggregation processes, associated cofactors, and develop more suitable models that recapitulate the structural and biochemical diversity of pathological Tau. The extensive mechanistic studies and experimental approaches that have been used to investigate and gain insight into the role of heparin in regulating Tau aggregation are useful and can be extended to other newly discovered cofactors. One important consideration for Tau-targeting antibody-based therapies is defining the precise epitopes or conformational states the antibodies are engineered to recognize.

Tau is extensively modified, with cleavage, phosphorylation, ubiquitination, and O-GlcNAcylation potentially interfering and preventing the binding of antibodies raised and tested against non-modified forms of Tau protein produced in vitro by conventional approaches. This includes PTMs on the neighboring residues. Also, epitope masking and inaccessibility due to conformational changes in Tau might contribute to less recognition and binding by the antibodies. The design of Tau-specific antibodies should be informed by the data from patient-derived pathological Tau and using reagents that reproduce the key features of the relevant Tau proteoforms. This could be achieved using semisynthetic and synthetics strategies to produce precisely-post-translationally modified Tau, which is then fibrillized using a clean and efficient system with the addition of pathology-relevant cofactor molecules. This will allow to raise and optimize antibodies that have a higher potential to yield efficient Tau pathology modifying molecules that will be successful in clinical settings. One alternative approach is to develop cellular and animal models that recapitulate pathological Tau aggregation at the structural and biochemical levels. Today, it remains unknown whether Tau aggregates in cellular and animal models of Tauopathies possess the same core structure and morphological features of brain-derived Tau aggregates. More detailed biochemical and structural characterization of Tau aggregates in these models is essential to maximize the translation of preclinical success to more effective therapies in the clinic.

Several approaches have been employed to generate antibodies targeting different epitopes and aggregated forms of Tau species, and many are in clinical trials today. Given that many of these antibodies' design was not guided by precise information about the pathogenic Tau species in the brain, it should not surprise anyone that many of these antibodies will not succeed in clinical trials. However, the outcomes of these clinical trials will provide important insight into the potential of sequence and species-specific antibodies for the treatment of AD. They will also help guide future efforts to develop more effective antibodies and therapies. That being said, many steps could be introduced now to minimize failures or ensure that ineffective antibodies are identified early in the process, including 1) employing structure-based and computational approaches that leverage the availability of several cryo-EM structures of brain-derived Tau fibrils [744], 2) more comprehensive assessment of the biochemical properties (PTMs) of Tau species in the brain and the CSF; 3) evaluating the efficacy of antibodies in multiple animal models of Tau pathology formation and spreading, and 4) rigorous characterization of the specificity of the antibodies towards different pathologic Tau species. This could be achieved using expanded libraries of a) recombinant Tau species (monomers, oligomers, and fibrils) bearing pathologically relevant PTMs, and b) well-characterized soluble and insoluble Tau aggregate preparations isolated from brains of different patients with Tauopathies. This approach would determine the extent to which therapeutic antibodies can capture the diversity of pathological Tau species detected in vivo. Although cryo-EM studies of Tau fibrils suggest that the Tau fibrils in the brain are more homogeneous and possess structural features specific for each Tauopathy, it remains unclear if these studies are capturing the diversity of Tau fibrils, or mainly the dominant structures. In contrast, increasing evidence suggests that soluble oligomeric and seeding competent forms of Tau are highly heterogeneous in their size distribution and PTM patterns. Therefore, elucidating the structural properties of recombinant and brain-derived Tau oligomers is essential to any future efforts to improve the precision of therapeutic antibodies and their efficacy.

Although multiple factors may contribute to the failure of clinical trials, the considerations for the patient populations are somewhat unique for the structure-based Tau aggregation inhibitors. This is especially important given recent findings revealing a high level of heterogeneity in the PTM profiles and seeding activity of Tau aggregates from AD patients' brains [38]. Patient stratification based on the disease stage, informed by the robust peripheral biomarkers, may be crucial to determine the appropriate target population and the windows of therapeutic intervention for disease progress-modifying effects. This may involve the early and pre-/asymptomatic stages, where the Tau pathology is developing but has not yet fully

progressed and amassed in multiple brain regions. The clearance of the already-formed Tau fibrillar burden and prevention of its spreading is being targeted by immuno-based anti-Tau therapies discussed above.

Like targeted immunotherapies, it is crucial to know precisely which Tau species should be targeted by PROTACs. These target species may include 1) monomeric Tau to reduce the total Tau levels and maintain an equilibrium of Tau species in favor of soluble monomers, 2) monomeric Tau harboring disease-associated mutations, 3) small oligomers that can be efficiently cleared by the proteasome before exerting cytotoxicity or proceeding to form larger aggregates, or 4) seeding competent fibrillar Tau aggregates. Artificially designed hydrolases targeting specific Tau oligomeric and fibrillar species, and directly degrading them, represents a promising strategy to clear the incipient or established Tau pathology.

Although this review focuses on understanding the grammar of Tau aggregation and Tau aggregate-targeting therapies, we would like to re-emphasize that more investments are needed to understand how the loss of normal Tau due to misfolding, aggregation, and seeding contributes to neurodegeneration and clinical symptoms at different stages of disease progression. It is our opinion that the most effective therapies will be combination therapies that, firstly, prevent Tau misfolding and aggregation, and, secondly, neutralize existing bioactive Tau aggregates. The clinical heterogeneity of the AD and other Tauopathies combined with increasing evidence of the possible roles of other Tau-aggregation independent mechanisms in the pathogenesis of Tauopathies suggest that future therapies will involve personalized combination therapies based on molecular mechanisms associated with each disease subtype. Such therapies are more likely to be effective at slowing the progression of the Tauopathies at different stages of disease diagnosis. The sooner we embrace the concept of combination personalized therapies, the better.

Acknowledgements

We would like to thank Laura Gasparini, Somanath Jagannath, Rajasekhar Kolla, Senthil Kumar Thangaraj, Pedro Santana Magalhães and Theodora Panagaki for providing valuable critical assessment of the manuscript.

xx

CHAPTER 3

ClearTau co-factor-free fibrils: a novel efficient method for the production of pathology-resembling Tau aggregates

Galina Limorenko[1], Meltem Tatli[2], Rajasekhar Kolla[1], Sergey Nazarov[3], Marie-Theres Weil[4], David C. Schöndorf[4], Daniela Geist[4], Peter Reinhardt[4], Dagmar E. Ehrnhoefer[4], Henning Stahlberg[2], Laura Gasparini[4] and Hilal A. Lashuel[1] ✉

[1] Laboratory of Molecular and Chemical Biology of Neurodegeneration, Brain Mind Institute, School of Life Sciences, Ecole Polytechnique Fédérale de Lausanne, CH-1015 Lausanne, Switzerland.
[2] Laboratory of Biological Electron Microscopy, School of Basic Sciences, Institute of Physics, Dubochet Centre for imaging, Ecole Polytechnique Fédérale de Lausanne, CH-1015 Lausanne, Switzerland.
[3] Biological Electron Microscopy Facility, School of Life Sciences, Ecole Polytechnique Fédérale de Lausanne, CH-1015 Lausanne, Switzerland.
[4] Neuroscience Discovery, AbbVie Deutschland GmbH & Co KG, Knollstrasse, 67061 Ludwigshafen, Germany.

✉ email : hilal.lashuel@epfl.ch

Keywords: Tau, ClearTau, fibrils, aggregation, co-factor-free, heparin-free

Nature Communications. In review.
Patent application No. 22204800.1 (priority founding) 31st October 2022.

Abstract

Tau protein fibrillization is implicated in the pathogenesis of several neurodegenerative diseases collectively known as Tauopathies. For decades, investigating Tau fibrillization in vitro has required the addition of polyanions or other co-factors to induce its misfolding and aggregation, with heparin being the most commonly used. However, heparin-induced Tau fibrils exhibit high morphological heterogeneity and a striking structural divergence from Tau fibrils isolated from Tauopathies patients' brains at ultra- and macro-structural levels. To address these limitations, we developed a novel, quick, cheap method for producing completely co-factor-free fibrils. We show that Tau fibrils generated using this method – ClearTau fibrils - exhibit amyloid-like features and morphological properties more reminiscent of the properties of the brain-derived Tau fibrils. We believe that these advances open new opportunities to investigate the pathophysiology of disease-relevant Tau aggregates and will facilitate development of Tau pathology-targeting and modifying therapies and PET tracers that can distinguish between different Tauopathies.

Introduction

The microtubule-binding protein (MAP) Tau is an intrinsically disordered protein (IDP) that is most prominently associated with the dynamic regulation and stabilization of cytoskeletal and mitotic microtubules [244]. In neurons, Tau is also important for regulating axon outgrowth and maintaining axonal transport and cytoskeletal integrity [246]. However, factors such as post-translational modifications (PTMs) [248], mutations in the protein sequence [247], interaction with other proteins [249,250] and changes to the biochemistry of its surrounding environment, such as pH or the presence of drugs [251], may result in the lowered affinity, weaker interaction or full dissociation of Tau from microtubules (for a recent review see [252]). Tau may then accumulate and aggregate into higher molecular weight species, such as fibrils associated with pathology. Increasing evidence points to Tau aggregation and PTMs as central events in the pathogenesis of Alzheimer's disease (AD) and Tauopathies, events that investigators strive to faithfully model in the laboratory (for a recent review see [745]).

In addition to amyloid plaques composed of β-amyloid, a classic hallmark of AD, another prominent pathological feature of AD is hyperphosphorylated Tau which is found in neuronal cell bodies or neurites in the form of paired helical filaments (PHFs) and straight filaments (SFs) [746]. Tau aggregates and fibrillar structures are also found in the brain of individuals afflicted by other neurodegenerative diseases (NDs), collectively known as Tauopathies, which include Pick's disease (PiD) and progressive supranuclear palsy (PSP) [253-255,257-260,747]. Tau exists as six isoforms in the human central nervous system, designated 4R2N, 4R1N, 4R0N, 3R2N, 3R1N, and 3R0N. Where the Tau isoform compositions of the Tau fibrils are known [48], Tauopathies are classified into predominantly 3R (i.e., PiD), predominantly 4R (i.e, PSP), or mixed (3R + 4R; i.e., AD).

Full-length Tau isoforms are highly soluble and notoriously resistant to aggregation on their own, in contrast to other amyloid-forming proteins, such as α-synuclein [748], β-amyloid peptide [749] or amylin [750], which misfold, aggregate, and form amyloid fibrils simply by incubation at 37 °C. The molecular and cellular factors that trigger Tau misfolding and aggregation, and drive the Tau fibrillization processes remain unclear. Therefore, to study Tau fibrillization in vitro, investigators have adopted Tau aggregation systems using various negatively-charged co-factor molecules or protein modifications, such as truncations or phosphorylation, which are used to induce or accelerate the full-length Tau fibrillization process. Negatively-charged polysaccharide free-floating heparin (FFH) has thus far been the most commonly used Tau aggregation co-factor, although others including RNA, anionic lipids or small proteins are occasionally used (reviewed in [751]).

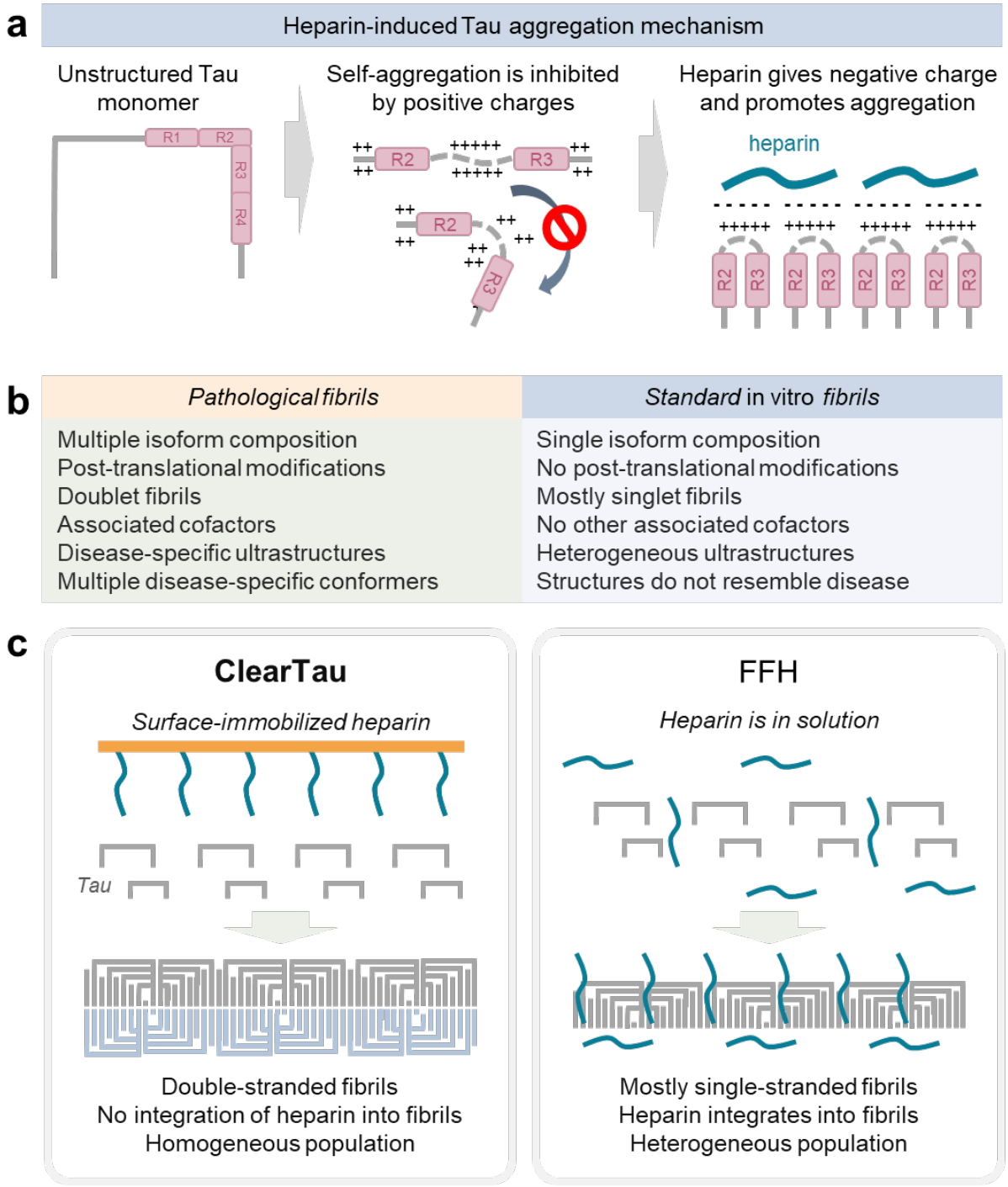

Figure 1. Heparin-induced Tau fibrillization. **a** Tau exists as an unstructured monomer in solution and is not prone to aggregation without co-factors. The positive charge density around repeat regions (amino acids 275-305, R2; 306-336, R3) prevents molecule folding and self-association. Heparin provides negative charges to compensate for the positive charge density on Tau and promote Tau folding into β-sheet-containing conformation conducive to fibrillization. **b** General features of the pathology-derived Tau fibrils and conventional FFH-induced Tau fibrils. **c** Schematic of the ClearTau and FFH-induced Tau fibrillization. In the ClearTau method, the heparin molecules are covalently immobilized on the aggregation vessel wall. The addition of Tau monomers up to the minimal composition buffer results in the

rapid formation of the Tau fibrils from all six Tau isoforms composed of doublet filaments. In the presence of FFH, the association of heparin with Tau filaments may interfere with the doublet fibril formation.

The mechanisms by which anionic co-factors induce Tau aggregation are thought to include electrostatic charge neutralization of highly positively-charged regions on Tau, promoting changes in the local and global Tau polypeptide shape [751]. This allows the folding of the aggregation-promoting Tau regions PHF6* and PHF6 into β-sheet-containing conformation (Figure 1a), leading to Tau fibrillization and assembly into higher-order Tau fibrils. In addition, structural and biophysical studies have shown a high affinity of specific positively-charged Tau residues for heparin, notably the interfibrillar interface-forming residues in the core of the fibril folds (Figure 1).

To be clinically relevant, in vitro Tau aggregation systems must recapitulate some of the morphological, biochemical, and structural features of Tau aggregates and fibrils found in human pathologies. Several high-resolution structures of Tau fibrils composed of different Tau isoforms have been recently solved using cryoelectron microscopy (cryoEM; see [262]), including Tau filaments isolated from post-mortem patient brain tissues. These structures combined with other experimental observations suggest that heparin or other co-factors used to induce Tau aggregation introduces several limitations that preclude biologically-relevant studies from elucidating the role of Tau aggregation in the pathogenesis of Tauopathies (Figure 1b). First, recent studies demonstrated that in vitro FFH-induced Tau fibrils differ from pathological patient-derived fibrils at the biochemical (lack of PTM pattern due to use of the unmodified isoforms) and structural (amyloid core conformation) levels [164]. In addition, the mature Tau fibrils in AD, corticobasal degeneration (CBD), and chronic traumatic encephalopathy (CTE) are composed of doublet Tau filaments with the interfilament interfaces differing between these disorders, which manifests in various twisted morphologies of the higher-order Tau fibrils. In contrast, conventional in vitro-produced Tau fibrils extensively comprise a single-filament and are structurally and morphologically divergent from any Tau fibrillar structures derived from ND patients' brains, recently illustrated by cryoEM-solved FFH-induced fibril structures [164]. Second, the addition of heparin to Tau results in heterogeneous fibril populations, whereas the ultrastructures of pathological Tau fibrils are consistent between patients and are a signatory of the specific Tauopathies (Figure 1b). Third, heparin and other co-factors have been shown to bind strongly and remain associated with the Tau fibril, which could interfere with their interaction with other small molecules and ligands (e.g., RNAs, small-molecule compounds) [200,243]. These properties preclude the use of FFH-induced Tau fibrils to

investigate the structural basis of Tau aggregation, cellular uptake, and toxicity or their use for the development and testing of Tau-targeting and binding molecules, as well as positron emission tomography (PET) tracers.

To address these limitations, we developed a novel in vitro protein fibrillization method to generate heparin-free Tau fibrils, ClearTau fibrils. This method uses surface-immobilized heparin to induce Tau misfolding and aggregation while preventing its tight association with and incorporation into the fibrils [26] (Figure 1c). Prior knowledge of the mechanisms involved in heparin-induced Tau fibrillization suggests that heparin likely has its principal contribution at the very early stages of the Tau fibrillization process. The binding of negatively-charged heparin to Tau neutralizes the positive charge on the Tau monomer and, importantly, on the aggregation-driving regions within the microtubule-binding region (MTBR), which contributes to the high solvability of Tau under normal conditions. This leads to misfolding of Tau through the loss of the long-range contacts between the N-terminus and central regions, as well as local restructuring of the MTBR to aggregation-prone configuration. After the heparin-dependent priming of the Tau monomers and assembly of the seeding-competent Tau nucleus, the self-assembly and further polymerization are thought to be Tau seed template-dependent and may not be reliant on the binding of the exogenous molecules such as heparin to the growing fibrils (for a recent review see [751]).

Therefore, we hypothesized that surface covalent immobilization of heparin would allow us to leverage the first and crucial step of the heparin action on Tau monomers, at the same time completely preventing its incorporation into the growing Tau fibrils as the heparin molecules are bound to the vessel surface, whereas Tau molecules are free-floating in the large volume of the aqueous buffer (Figure 1c). To test this hypothesis, we assessed the efficiency of fibrillization of all six Tau isoforms in Eppendorf tubes coated with covalently-immobilized heparin, i.e., in the absence of FFH. Our results show that this new method allows for the efficient production of a large amount of homogeneously-aggregated heparin-free fibrils that are morphologically distinct from those produced in the presence of FFH. The ClearTau fibrils retain the ability to bind RNA, share some structural/morphological features with brain-derived pathological fibrils, and induce efficient seeding of Tau aggregation *in vitro*, in biosensor cells, and human neurons. Our novel method for in vitro ClearTau fibril production represents a crucial milestone for developing accessible, cheap, and high-fidelity tools for studying the Tau fibrillization processes relevant to NDs. As a proof of concept, we demonstrate that the ClearTau assay can be used as a platform to screen small molecule-based modulators of Tau aggregation and to identify, for the first time, stabilizers of heparin-free Tau oligomers. The

ease of implementation, availability of the heparin-coating methods [752], and minimal buffer composition requirements (high efficiency in the phosphate-buffered saline, PBS) allow for the production of high yields of clean heparin-free fibrils for in vitro and in vivo mechanistic studies and for future screenings aimed at developing novel diagnostic tools and therapies to treat AD and other Tauopathies. Finally, the generation of ClearTau fibrils also paves the way for a more systematic analysis of Tau post-fibrillization PTMs and fibril interactome without interference from heparin or heparin-induced polymorphisms.

Results

A new method for generating heparin-free ClearTau fibrils

To determine if the surface-immobilized heparin retains the ability to induce Tau fibrillization, we assessed and compared the extent of Tau 4R2N monomers (10 μM) fibril formation in 1.5 ml Eppendorf tubes that are covalently coated with heparin molecules and in standard 1.5 ml Eppendorf tubes containing no FFH. The kinetics of aggregation was followed by the thioflavin S fluorescence (ThS) assay over the course of 48 h. As shown in Figure 2a, a rapid increase in ThS fluorescence was only observed in the heparin-coated tubes, whereas no change in ThS signal was detected in the standard Eppendorf tube without immobilized or FFH at this concentration. Circular dichroism (CD) measurement of the samples during the reaction revealed a significant drop in the CD signal, suggesting that the majority of the Tau monomer have converted to insoluble Tau fibrils that precipitate out of solution as early as 1 day into the reaction progression (Figure 2b). Electron microscopy (EM) imaging revealed the formation of short fibrillar aggregates at 6 and 18 h into the reaction time course, with the dominant appearance of long curvy fibrils at 24 h and later (Figure 2c, Supplementary Figure 1). These results demonstrate that our ClearTau protocol is efficient for the fibrillization of Tau, is easy to implement, and is highly versatile.

ClearTau fibrils are different from FFH-induced Tau fibrils

Next, we compared the kinetics of aggregation of Tau 4R2N using our ClearTau method to the conventional FFH at a high concentration of 100 μM, which favors the formation of fibrils. As shown in Figure 3a, a rapid increase in ThS fluorescence as early as 8 h was observed using both the ClearTau and FFH systems, illustrating the comparable kinetic profiles of Tau fibrillization at this concentration. EM imagining of the fibrils revealed the formation of the fibrils under both conditions. However, the fibril morphologies substantially differed (Figure 3b and

c). ClearTau fibrils preparations were long, wavy, and of consistent morphology, with no accumulation of intermediate oligomers or amorphous aggregates. In contrast, FFH-induced Tau fibril preparations were fragmented and lacked consistent twisting. These results suggest that ClearTau fibrils could differ in their ultrastructure properties. Therefore, we measured and quantified the fibril widths of the ClearTau and FFH-induced Tau fibrils (Figure 3b). The mean width of the ClearTau fibrils was greater than the FFH-induced fibrils (15.2 ± 2.24 nm and 13 ± 2.5 nm, respectively, p<<0.001).

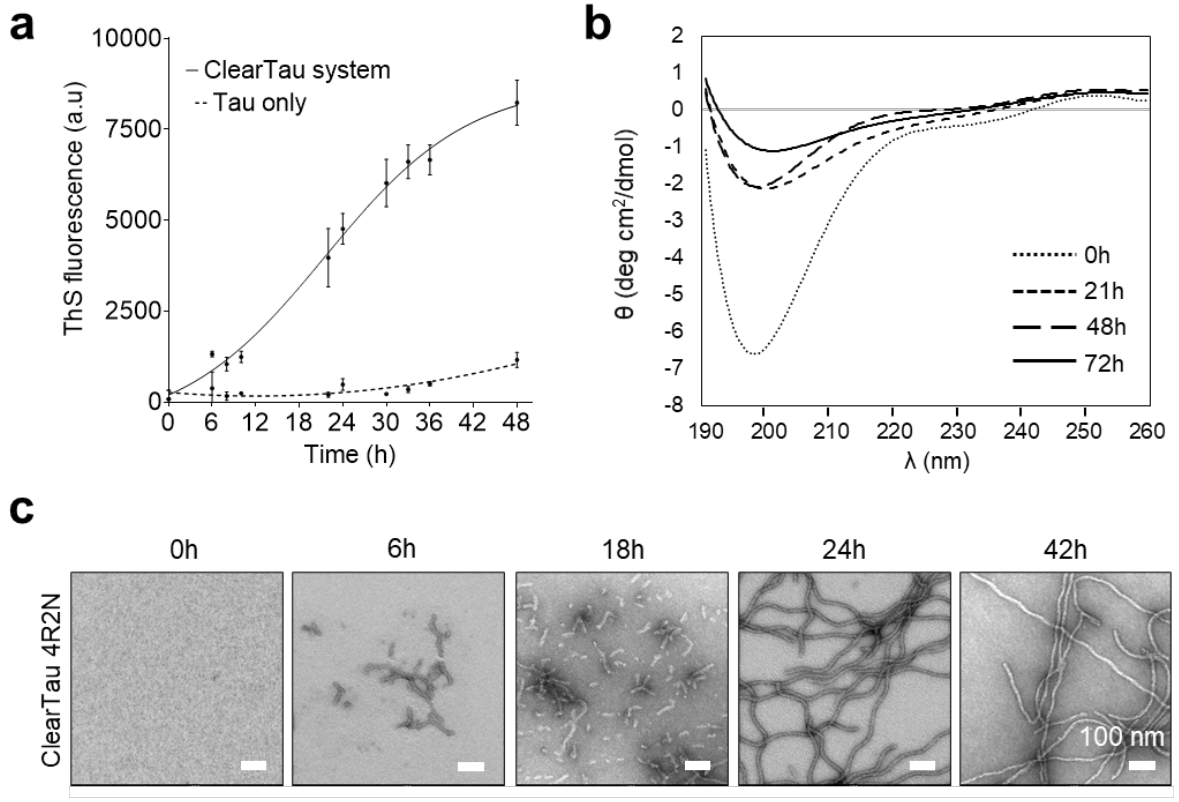

Figure 2. Characterization of ClearTau 4R2N Tau fibrils. a ThS aggregation assay followed two independent ClearTau aggregation reactions, compared to the normal Eppendorf tube without additional co-factors. The ThS fluorescence signal is rapidly generated only for ClearTau fibrils over the course of 48 h and follows a sigmoidal curve reaching the plateau phase. All reactions comprised 10 μM of Tau monomer at the inception. Measurements were performed in triplicates. **b** Circular dichroism (CD) spectra of ClearTau fibrils **c** Electron microscopy imaging reveals the formation of the fibrils by 4R2N Tau in ClearTau aggregation reaction, with shorter fibrils appearing at 6 and 18 h, to long fibrils at day 1 and 2 of aggregation. Scale bars = 100 nm. For a wider profile of fibril morphologies, see Supplementary Fig1.

We also assessed and compared aggregation of 4R2N, 4R0N, 3R2N, 3R0N, mutant 4R2N P301L, and fragments K18 and K19 using ClearTau or FFH systems. The EM imaging

revealed consistently longer and more homogeneous fibrils in the ClearTau system (Supplementary Figure 2) and illustrated the versatility of the ClearTau system for a variety of Tau proteins and fragments.

These results show that our novel ClearTau method for Tau fibrillization 1) works on experimentally-relevant time scales; 2) is devoid of Tau oligomers or amorphous aggregates; and 3) produces long fibrils with consistent morphology, rather than variably twisted or straight fibrils within a sample.

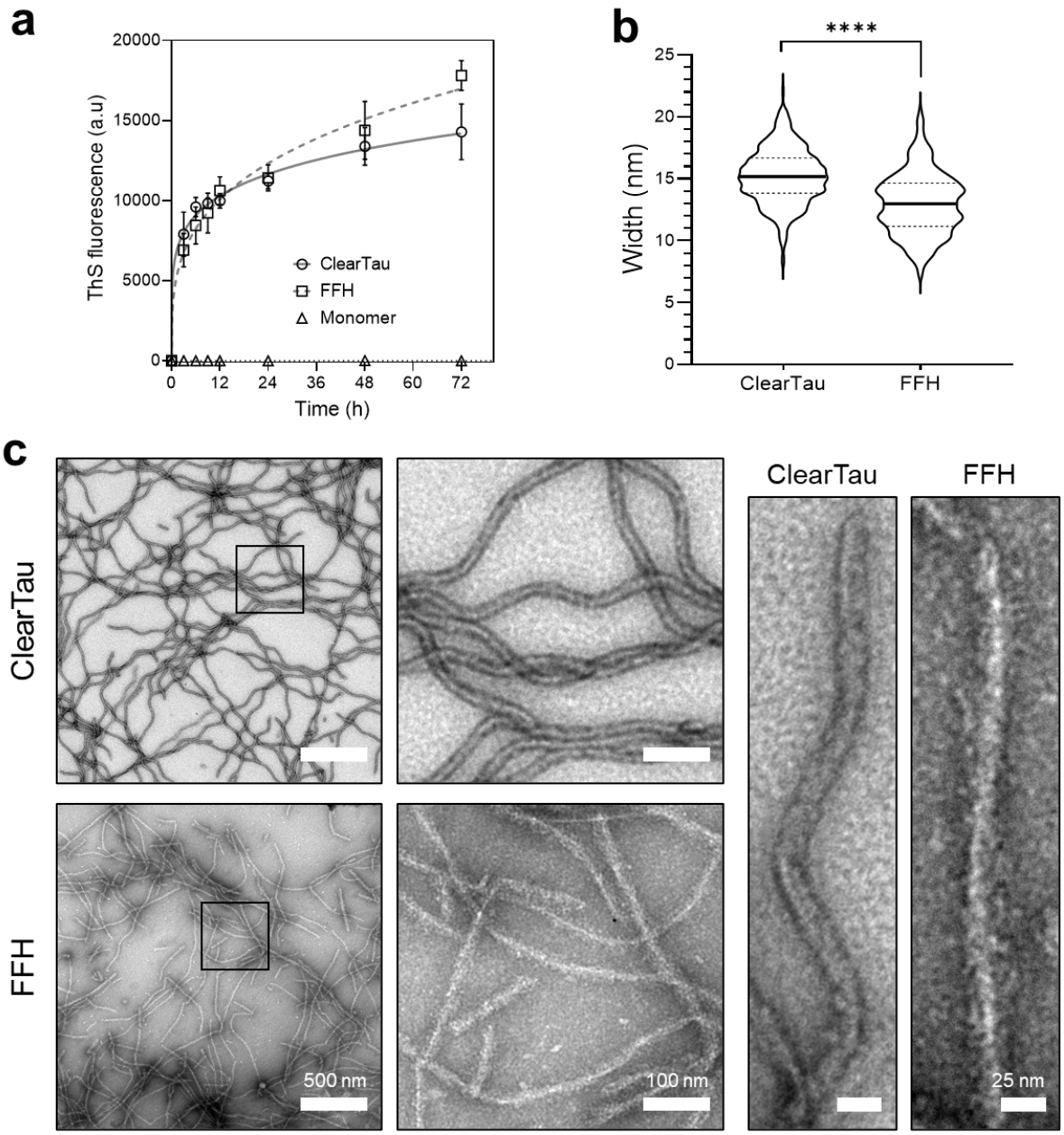

Figure 3. Comparison of 4R2N Tau fibrils generated by ClearTau versus FFH methods. **a** ThS aggregation kinetics comparison of ClearTau and FFH-induced Tau fibrils. FFH was

added to the 4R2N Tau monomer at 1:4 molar concentration both reactions comprised 100 µM of Tau monomers. Reactions were set up as four independent replicates, and measurements were performed in triplicates. b Width quantification of fibrils shows significantly narrower FFH fibrils. N of ClearTau = 618, N of FFH = 292 fibrils quantified, p **** <<0.001. **c** Electron microscopy imaging reveals the formation of the fibrillar structures in both reactions over 72h of differing morphologies. Scale bars = 500 and 100 nm. Scale bars = 25 nm.

ClearTau fibrils' seeding potency in vitro and in cells

To assess whether 4R2N ClearTau fibrils were competent to seed aggregation of the Tau monomer in the absence of any co-factors in vitro, the aggregation assay was performed using a microplate setup (Figure 4a). Tau 4R2N monomers were seeded with either sonicated 4R2N ClearTau or FFH fibrils. There was a rapid increase in the ThS fluorescence in the ClearTau fibril-seeded reaction right after the addition of the seed. The aggregation kinetics profiles did not differ from FFH. However, the magnitude of the ThS signal was higher in the ClearTau-seeded samples.

The formation of fluorescent foci in the HEK293T TauRD P301S biosensor (BS) cell line is commonly used to assess Tau seeding activity [753] (reviewed in [754]). These BS cells stably express the repeat domain of Tau with the P301S mutation (TauRD P301S) fused with a yellow fluorescent protein (YFP) or cyan fluorescent protein (CFP). The FRET signal is generated upon the reporter foci formation in these cells, where the two fluorophores, YFP and CFP, come in close proximity for the wavelength energy transfer, the signal from which is then detected and quantified using flow cytometry set up as initially described [755].

The results in Figure 4b demonstrate the FRET signal's detection contingent on the amount of the fibrillar seeds added, demonstrating the dose-dependency of the seeding with ClearTau fibrils in this cellular model. In addition, confocal imaging verified the presence of both cytoplasmic (Figure 4c, red arrows) and nuclear reporter foci (Figure 4c, yellow arrowheads), whereas none were present in the non-transduced cultures.

To investigate the ability of Clear Tau fibrils to seed the aggregation of endogenous Tau in neurons, ClearTau fibrils were applied to the human induced pluripotent stem cell-derived neurons and aggregation of endogenous Tau was examined by immunofluorescence and biochemical analyses. The triple mutant Tau MAPT-P301S/E10 + 16 (TM) and knockout (KO) Tau hiPSC-derived cortical neurons were exposed to different amounts of ClearTau fibrils generated from recombinant P301L 2N4R Tau, as previously described [756].

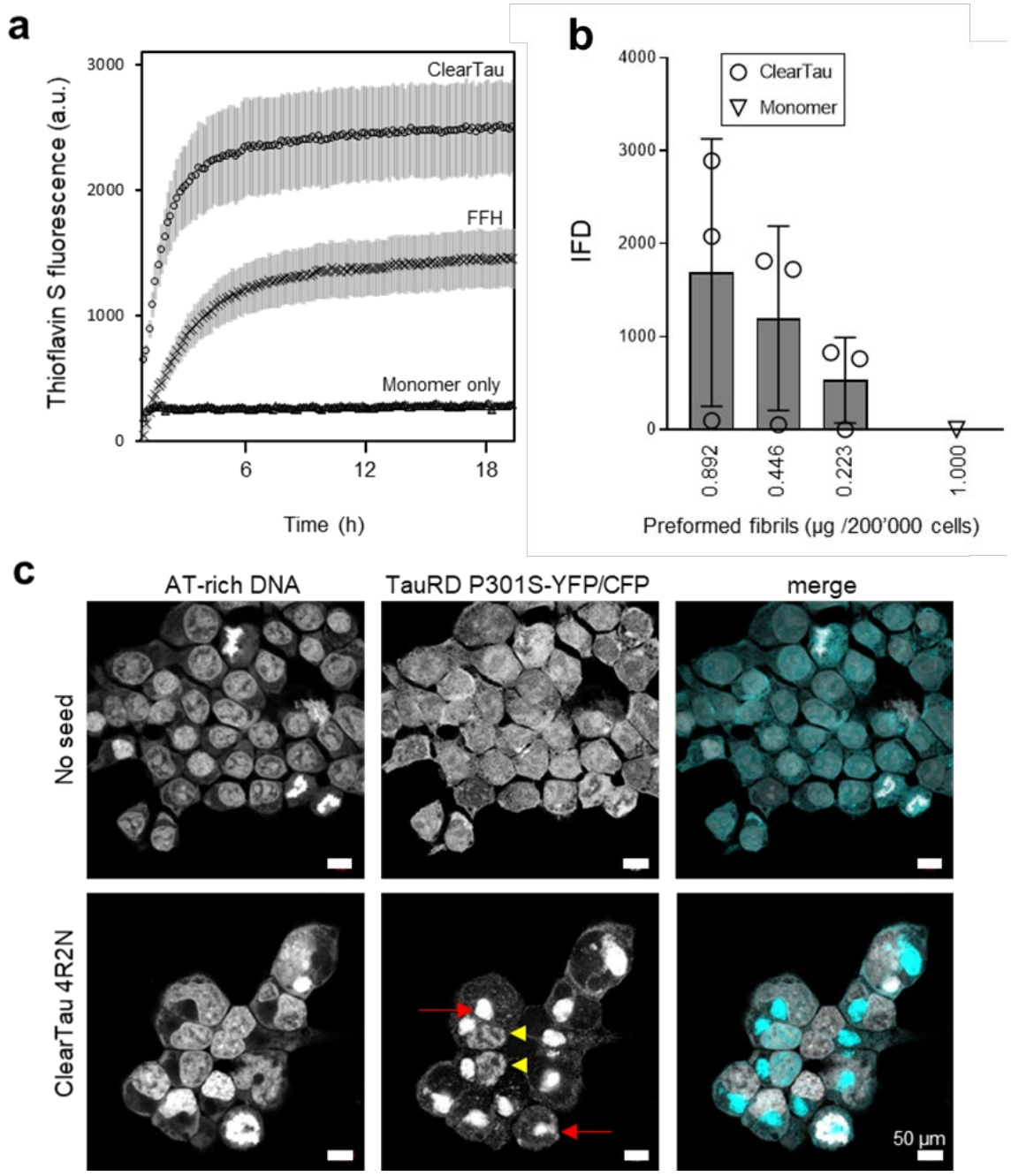

Figure 4. ClearTau Tau preformed fibril seeding potency. a In vitro seeding of Tau 4R2N monomer with the ClearTau preformed fibrillar seed at 1:4 molar ratio (identical to heparin-to-Tau ratio). The ClearTau seeds show high efficiency in generating the ThS-positive Tau species, with a fluorescence signal magnitude higher than FFH. Data were collected in five independent experiments in triplicates, each for ClearTau seed and FFH, and four independent experiments in triplicates for monomer-only conditions. **b** FRET flow cytometry assessment of the HEK293T TauRDP301S biosensor cell line with added ClearTau 4R2N preformed fibrillar seed. IFD = integrated FRET density. Experiments were performed in triplicates, a minimum of 100,000 cells per run were sorted. **c** Confocal imaging ClearTau 4R2N fibrillar seed assessment of cytoplasmic (red arrows) and nuclear reporter foci (yellow arrowheads) formation in HEK293T TauRD P301S biosensor cell line. Nuclei are demarcated by AT-rich DNA stain DRAQ5. Scale bars = 50 µm.

3 weeks later, the neurons were stained with the MC1 Tau antibody to detect endogenous Tau aggregates (Figure 5a, green) and MAP2 to stain the neurites (Figure 5a red). ClearTau fibrils induced the formation of Tau aggregates in TM Tau hiPSC-derived neurons in a concentration-dependent manner as demonstrated by the quantification of MC1 signal (Figure 5b) and symmetric ELISA using Tau12 antibody for both capture and detection (Figure 5c). No Tau aggregates were detected when ClearTau fibrils were applied to KO Tau hiPSC-neurons, indicating that endogenous Tau expression is required for aggregates formation (Figure 5). FFH Tau fibrils also induced aggregation of endogenous Tau in TM Tau iPSC-derived neurons (Supplementary Figure 3) as previously described [756]. These results demonstrate that ClearTau fibrils efficiently seed the aggregation of Tau monomer in vitro, induce reporter foci formation in the HEK293T TauRD P301S biosensor cell line, and trigger endogenous Tau aggregation in TM Tau hiPSC-derived neurons.

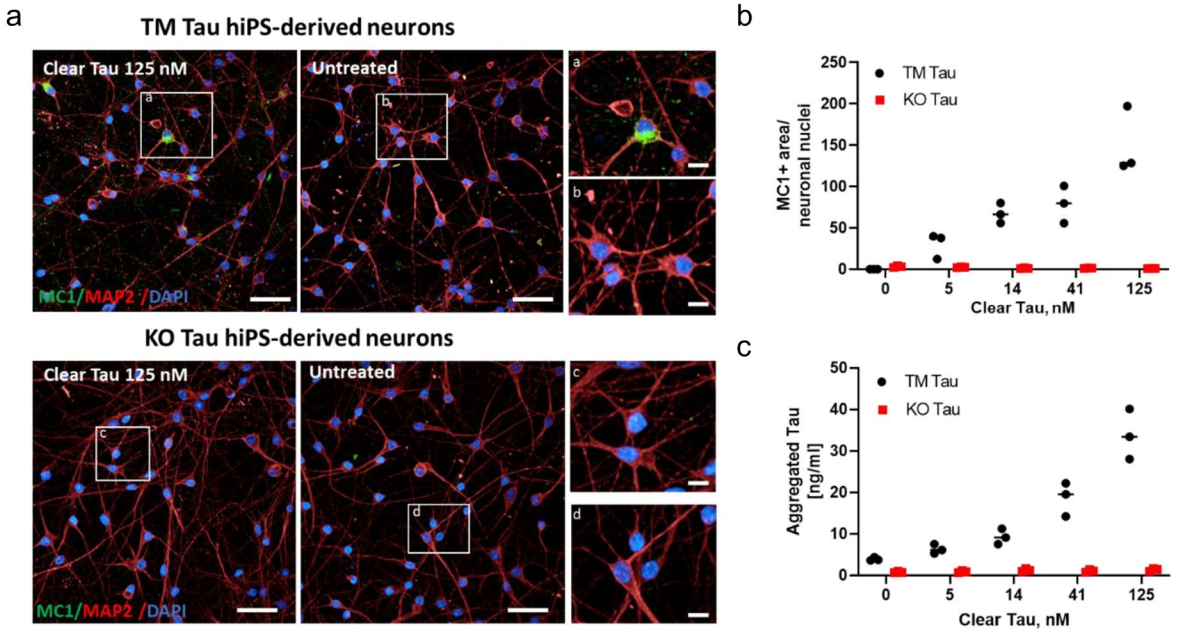

Figure 5. Clear Tau fibrils induced dose-dependent aggregation of endogenous Tau in TM Tau, but not KO Tau, hiPSC-derived cortical neurons. TM Tau and KO Tau hiPS-derived cortical neurons were exposed to different amounts of ClearTau fibrils generated from recombinant P301L 2N4R Tau. 3 weeks later, the neurons were stained with the MC1 Tau antibody to detect endogenous tau aggregates (green) and MAP2 to stain the neurites (red). Nuclei were stained by DAPI. **a** Representative stack images. Scale bar 50 µm in main panels; 10 µm in insets a-d. **b** Quantification of MC1 positive (MC1+) area over neuronal nuclei. Two-way ANOVA: seed concentration $p < 0.0001$, genotype $p < 0.0001$). **c** Aggregation of endogenous Tau was evaluated by symmetric ELISA using Tau12 antibody for both capture and detection. The graphs show results from one experiment with 3 replicates/condition. Two-way ANOVA: Tau concentration $p < 0.0001$, genotype $p < 0.0001$). Images and graphs

represent data from one experiment. 2 independent experiments with 3 replicates/condition were performed for immunofluorescence analysis. In one experiment, biochemical analysis was also performed.

ClearTau method induces efficient fibrillization of all six isoforms, mutant, and fragments of Tau

In human CNS, Tau is expressed as six isoforms differing in the number of incorporated N-terminal repeats, and differential inclusion of the R2 domain in the MTBR. As different isoforms contribute to Tau aggregation in the specific Tauopathies, it is important to develop high-fidelity methods for in vitro production of Tau fibrils of all six Tau isoforms or mixtures of the specific isoforms. Therefore, we first evaluated the applicability of our novel ClearTau method to the fibrillization of Tau 4R2N, 4R1N, 4R0N, 3R2N, 3R1N, and 3R0N proteins. Three independent ClearTau reactions were conducted for each of the six Tau isoforms, and resulting aggregates were evaluated using ThS assay, CD, and EM.

Each Tau isoform was fibrillized as described previously. The extent of fibrillization was assessed on the whole sample aliquots by ThS fluorescence assay before ultracentrifugation separating monomers and pellets (Figure 6a), showing the signal for all Tau isoforms and repeats. However, we observed inter-isoform variability with 3R2N showing the highest ThS fluorescence. Then the fibrils were separated by ultracentrifugation to yield pure fibril fraction for further analyses. The quantification of the ClearTau fibril widths, at the widest part with respect to the twists (if present) of all Tau isoforms, showed the shortest isoform 3R0N having the narrowest fibrils at 12.49 ± 2.59 nm (Figure 6b, Supplementary Table 1), followed by 3R1N at 14.49 ± 3.19 nm, 3R2N at 14.73 ± 2.55 nm, 4R2N at 15.20 ± 2.24 nm, 4R0N at 15.70 ± 3.04 nm, with widest fibrils shown by 4R1N isoform at 15.83 ± 3.49 nm.

The extent of monomer incorporation into fibrils showed high efficiency for 4R0N and all 3R, as evident by the shift of Tau from soluble (S) to insoluble pellet (P) fractions isoforms (Figure 6c and g, Supplementary Figure 3). Examination of the fibrils by EM reveals morphological differences between the fibrils derived from the various Tau isoforms (Figure 6d and f). The 4R2N, 4R1N, and 4R0N samples formed long, flexible curved fibrils. 3R2N formed straight, more rigid fibrils. 3R1N and 3R0N showed curved, twisted fibrils. The 3R2N stood out with non-twisted straight fibrils, whereas all other isoforms' twists differed in their periodicity and higher-order coiling, resulting in fibrils of differing conformations (Figure 6e).

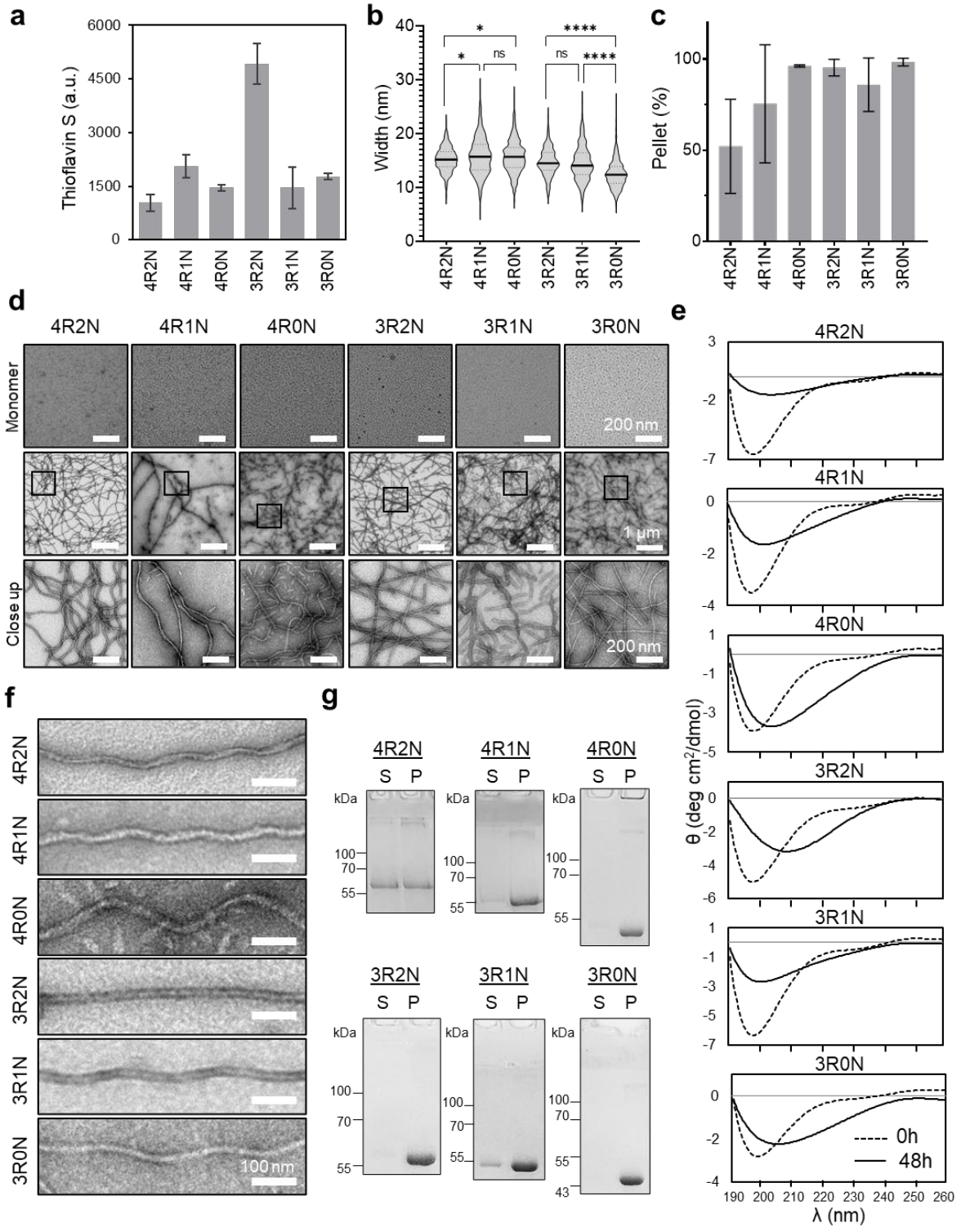

Figure 6. Characterization of ClearTau Tau fibrils generated from all six Tau isoforms. **a** Reaction endpoint at ThS fluorescence shows the signal for all isoforms, with the highest ThS signal found for ClearTau 3R2N isoforms, likely due to the unique straight fibril morphology. Three independent ClearTau aggregation reactions for each Tau isoform were set up at 100 µM for 48 h at 37 °C under shaking conditions. **b** Quantification of ClearTau isoforms' fibrillar widths. Tukey's test with multiple comparisons shows significance levels at

p * <0.05, **** <<0.001. **c** Tau isoform incorporation into the pellet fraction. Average and st. dev of three independent reactions. **d** Transmission electron microscopy assessment of ClearTau fibrils composed of different Tau isoforms. Close-ups of the boxed areas are in black squares. **e** CD spectra of the endpoint of the ClearTau fibrillization of all six Tau isoforms reveal the adoption of higher-order molecular structures compared to the starting isoforms' monomers. **f** High magnification of the different isoform fibril morphologies. **g** SDS-PAGE gel visualization of Tau protein retainment in the supernatant (S) and incorporation into insoluble pellet (P).

The CD spectra of the aggregated solutions of the isoforms 4R2N and 3R1N demonstrated a signal loss, indicating the formation of structured insoluble material, whereas isoforms 4R1N, 4R0N, 3R2N, and 3R0N demonstrated the shift towards the higher-order secondary structure-containing species (Figure 6e). Interestingly, the 3R2N showed the most prominent shift of the minimum towards 210 nm.

Next, we used cryo-EM to gain more insight into the ultrastructural properties of ClearTau fibrils composed of 4R2N and 3R2N Tau isoforms. Raw cryo-EM micrographs demonstrated that both fibrils from ClearTau 4R2N (Figure 7a, Supplementary Figure 5a) and 3R2N (Supplementary Figure 5b) proteins were straight and fragmented.

Furthermore, an inspection of raw micrographs and 2D class averages revealed the presence of two polymorphs with different widths. The singlet polymorphs comprised long and 160 Å wide filaments with major and minor grooves and visible crossover representing 64% and 73% in all of the extracted segments for samples 3R2N and 4R2N, respectively. The doublet polymorphs (36% for 3R2N and 27% for 4R2N) are short and 380 Å wide filaments that appeared to be composed of two copies of 180 Å wide polymorphs zipped together with minor grooves. The data allowed a partial reconstruction of the 3D structure of the ClearTau 4R2N fibrils at a final resolution of 3.1 Å (Figure 7b). The results show that ClearTau 4R2N fibrils comprise two filaments crossing-over, with the gap between the filaments measuring approximately 0.7 nm in width.

These observations suggest that the absence of heparin at the protofibril interface allowed for the formation of fibrils composed of two intertwined filaments - the doublets. Interestingly, the edges of the protofibrils exhibited different lengths and lacked a uniform flat edge (Figure SI5). It is possible that the formation of doublets is preceded by the formation of singlet fibrils, which then come together, and, depending on isoforms, either twist around each other or remain flat. It was possible to reconstruct the 3D structure of the ClearTau 4R2N isoform fibrils, however, the resolution must be improved.

a

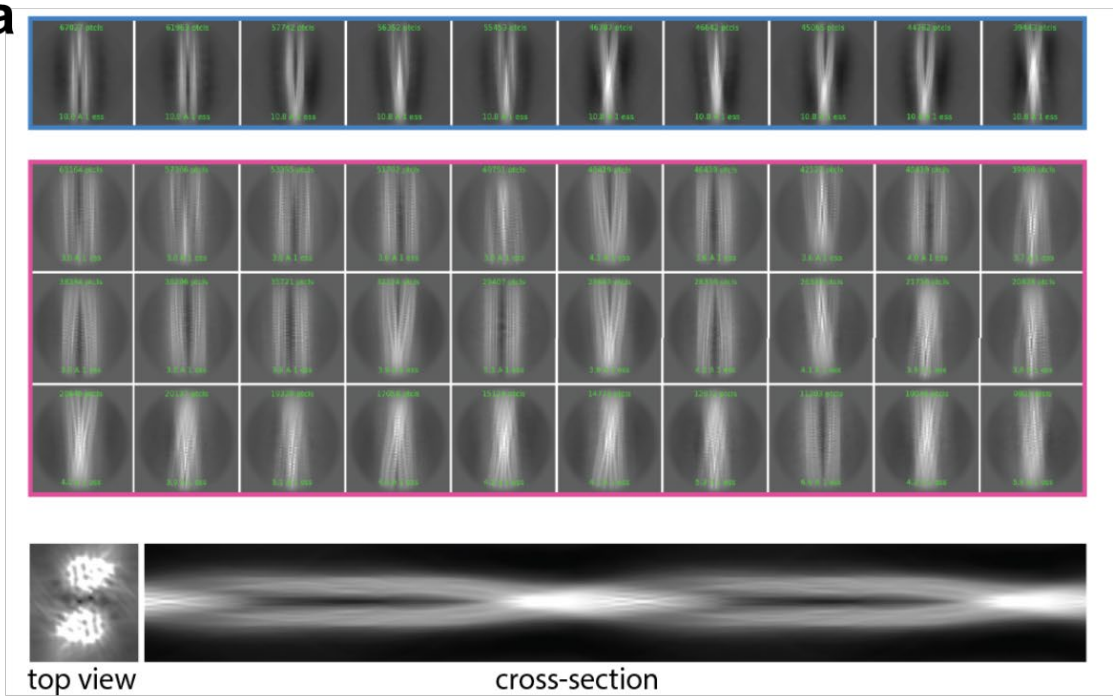

b

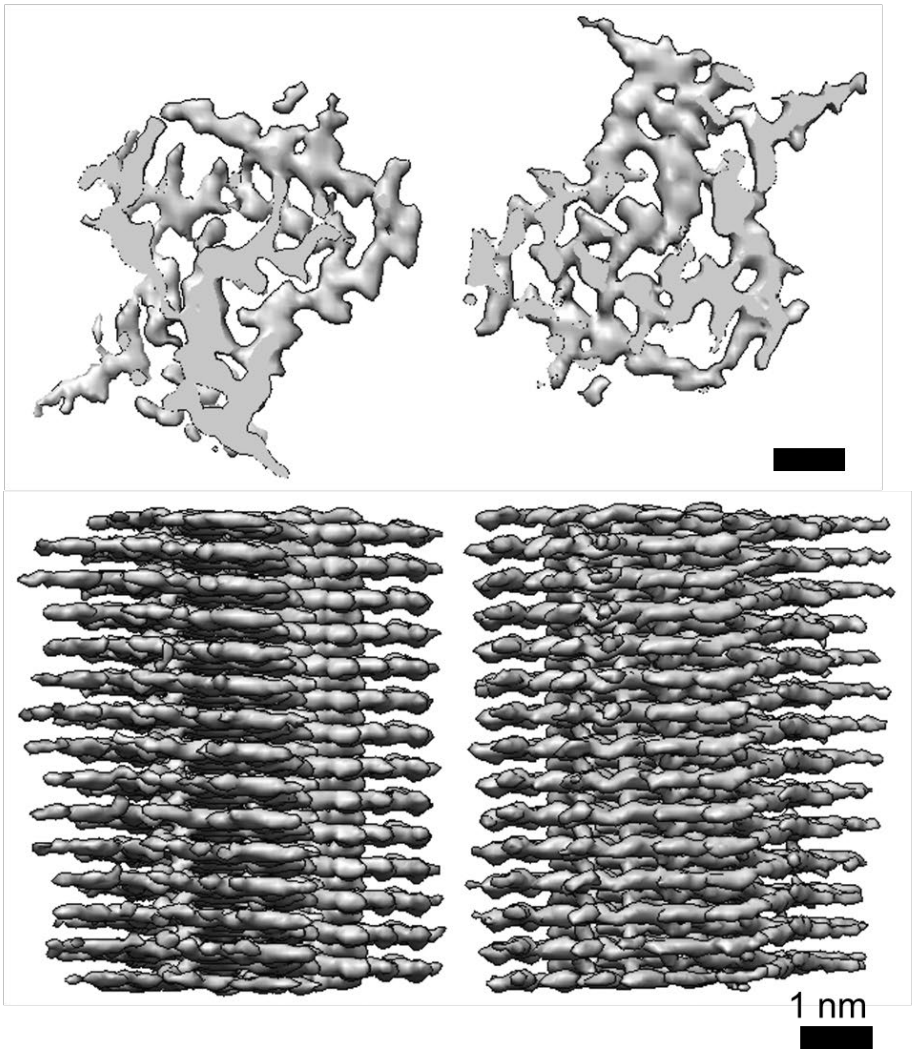

Figure 7. Cryoelectron microscopy image processing and 3D model generation for ClearTau 4R2N fibrils. a 2D classes were performed with a 612 Å box size (blue) depicting 4R2N fibrils formed by two protofilaments crossing each other. Pink outlines small 2D classes, a 3D reference created by Inimodel2D, top view, and 2D cross-section images are shown. **b** 3D cross-sections and side view of the 3D reconstruction. The ClearTau 4R2N fibrils comprise two filaments, with a gap at approximately 0.7 nm width. Scale bar = 1 nm.

These results demonstrate that our ClearTau fibrillization method is highly efficient for all Tau isoforms and is conducive to forming double-filament Tau fibrils. This thus far has not been demonstrated for conventional FFH-fibrillized 4R2N isoform using cryo-EM [164], whereas 3R2N doublets detected previously [164] appeared asymmetrical.

ClearTau fibrillization of Tau isoform mixtures

The isoform composition of patient-derived pathological Tau fibrils is non-homogeneous and contains all six Tau isoforms, with ratios differing between Tauopathies. Therefore, to determine if our method is suitable for modeling the complexity of Tau aggregation in the brain, we assessed the aggregation of four mixtures of Tau isoforms in varying compositions in the ClearTau system under the same conditions described above.

The mixtures comprised equimolar amounts of all six Tau isoforms [(All isoforms; 4R2N, 4R1N, 4R0N, 3R2N, 3R1N, 3R0N), isoforms containing 2N and 1N repeats (2N + 1N; 4R2N, 4R1N, 3R2N, 3R1N), isoforms containing 2N repeats (2N; 4R2N, 3R2N) and isoforms containing 1N repeats (1N; 4R1N, 3R1N) in three individual reactions, (Reaction 1, 2 or 3) (Figure 8a)]. All samples showed efficient fibrillization, where Tau was enriched in the pellet fractions (Figure 8b). Interestingly, the relative incorporation of 4R-containing isoforms into the fibril-containing pellet fractions was consistently higher than 3R-containing isoforms (Figure 8c, Figure SI6). Notably, the All isoforms (Reaction 2) showed a complete incorporation of all six Tau isoforms into the fibrils.

Next, we assessed the binding of the fibrils generated in the different mixtures to ThS (Figure 8d). All samples showed a ThS signal indicating a formation of the amyloid motif-containing fibrils. Notably, the All isoforms (Reaction 2) demonstrated the highest ThS signal, indicating potential morphological or ultrastructural differences from all other isoform mixtures' fibrils. To further assess the morphology of the fibrils, EM imaging was performed (Figure 8e). All isoforms (Reaction 1) contained flexible fibrils of 15.15 ± 3.03 nm in width, and 3 contained similarly bendy fibrils of 15.08 ± 3.00 nm in width. The All isoforms (Reaction 2), however, showed a homogeneous population of the thin, rigid fibrils 11.02 ± 1.83 nm in width,

significantly narrower than the All isoforms (Reaction 1) and the All isoforms (Reaction 3) (Figure 8f, Supplementary Table 2).

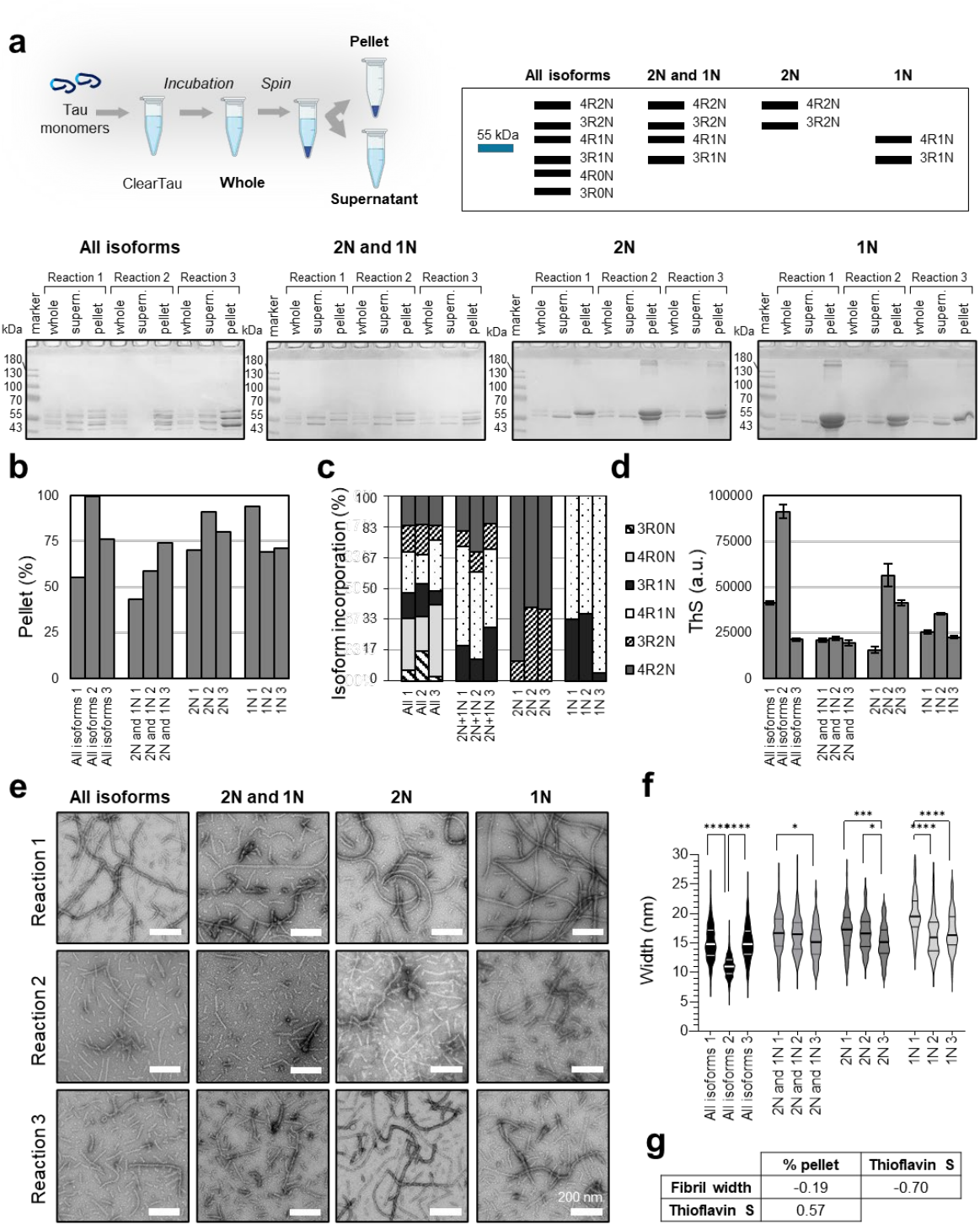

Figure 8. Characterization of ClearTau fibrils generated from Tau isoform mixtures. a Three independent ClearTau reactions were set up to include equal amounts of indicated Tau isoforms for 48 h for each condition. The fibrils (*pellet* fraction) were isolated from the remaining monomers (supernatant fraction) by ultracentrifugation. On the right: expected banding patterns of SDS-PAGE gel Tau isoform under four reaction conditions. (See

Supplementary Figure 6). **b** Quantification of the percentage of the monomer incorporation into the fibrils for all reactions shows high efficiency as early as 48 h of the aggregation. **c** Representation of the quantification of the relative isoform incorporation into the fibrils for all repeats of the four mixtures. **d** ThS fluorescence of the endpoint fibrils for all reactions. **e** Electron microscopy assessment of ClearTau fibrils prepared from the mixtures of Tau isoforms. All samples contain well-defined doublet fibrils, except the All isoforms (Sample 2), which appear to comprise straight, rigid singlet filaments. Scale bars= 200 nm. **f** Quantifications of the fibril widths for each repeat of the four mixtures. Tukey's test with multiple comparisons shows significance levels at * <0.05, ***<0.01, **** <0.001. **g** Correlation analysis of fibril with ThS, monomer incorporation into the pellet, and ThS fluorescence.

2N + 1N (Reactions 1, 2 and 3) contained thick, flexible fibrils; similar to the 2N (Reactions 1, 2 and 3). 1N (Reactions 1, 2 and 3), however, formed flat, right-hand twisting ribbon-like fibrils. The fibril width showed a strong negative correlation with the ThS signal, signifying those thinner, likely singlet fibrils have higher surface availability for the ThS dye binding (Figure 8g) and thus a high ThS binding/fluorescence.

Together, these data show that the ClearTau fibrilization method is suitable for investigating the aggregation of Tau isoform mixtures and allows for the efficient production of Tau fibril preparations composed of mixtures of Tau isoforms, providing further opportunities to investigate variable ratios of non-modified and modified Tau isoforms that more closely represent isoform profiles in the human pathologies.

ClearTau fibrillization in the presence of co-factor molecules

Previous polyanion-based Tau aggregation methods did not allow for investigation into the effects of co-factors or other Tau ligands at different stages of Tau oligomerization and fibril formation because of competition with the polyanions or drugs in solution or their tight binding to Tau aggregates [161,243]. Our protocol addresses this limitation because the heparin is immobilized, and other co-factors or ligands could be added at different time points during the aggregation of Tau proteins without interference. Polynucleotide molecules, such as RNA [94], and mononucleotide molecules, such as ATP [757], contain a negative charge and have been used to induce aggregation of Tau in vitro. RNA has been detected associated with Tau-positive aggregates in human pathologies [568,569]. Furthermore, Tau-RNA interactions are important in liquid-liquid phase separation and the formation of condensates [758]. As shown previously, heparin could compete with the binding of RNA, displacing it from the growing Tau fibril [114], likely due to partially-overlapping binding sites on Tau. Therefore, we investigated the

interactions of these molecules, RNA and ATP, with Tau upon fibrillization, but in the absence of the free-floating polysaccharide heparin.

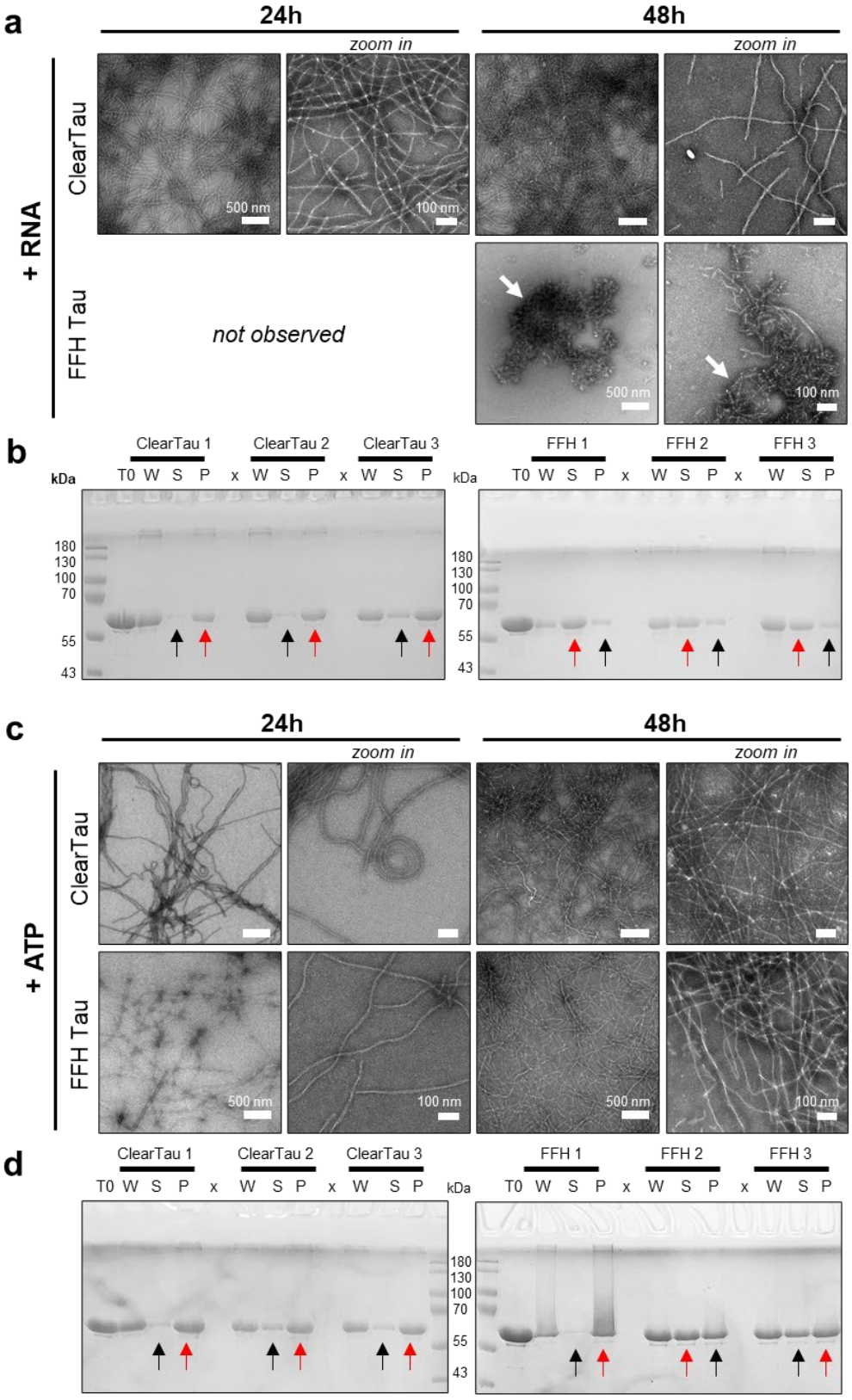

Figure 9. ClearTau fibrillization in the presence of co-factors. **a** Electron microscopy imaging and **b** SDS-PAGE gel of Tau fibrils in the presence of polyU RNA. **c** Electron microscopy imaging and **d** SDS-PAGE gel of Tau fibrils in the presence of adenosine triphosphate (ATP). T0 – time 0, W – whole sample, S – soluble fraction, P – pellet fraction. Both reactions were performed in triplicate independent aggregation reactions. Red arrows indicate thicker bands, and black arrows indicate narrower bands.

We assessed the aggregation of 4R2N Tau in the presence of other co-factors, polyuridylic acid (polyU, single-stranded RNA), or ATP by the ClearTau method or in the presence of FFH (1:4 ratio). The whole samples were imaged using EM midway through the reaction at 24 h and at the endpoint at 48 h (Figures 9a and c). Endpoint samples were fractionated to yield soluble supernatant (S) fractions containing monomeric Tau that was not incorporated into the fibrils, and pellet (P) fractions, containing fibrillized Tau. The samples were visualized using SDS-PAGE (Figures 9b and d).

In the presence of RNA, the EM imaging demonstrated the fibrillization of Tau by the ClearTau method, with numerous fibrils present at 24 h of the reaction (Figure 9a). FFH samples failed to aggregate at 24 h and showed indiscriminate amorphous aggregates and short fibrils at the later time point at 48 h (Figure 9a, white arrows).

In addition, the sedimentation assay showed efficient incorporation of Tau monomers into the pellet fraction (Figure 9b, ClearTau, red arrows) in the presence of RNA, with a small amount of monomer present in the supernatant (Figure 9b, ClearTau, black arrows) for ClearTau samples. In contrast, the FFH samples showed low levels of incorporation of Tau into the pellet fraction (Figure 9b, FFH, red arrows), with most protein detected in the supernatant (Figure 9b, FFH, black arrows). These observations illustrate the unique advantage of using our ClearTau method to investigate the interaction between Tau and other ligands or aggregation co-factors and highlight the limitations of the standard FFH method.

In the presence of ATP, both ClearTau and FFH samples showed the presence of the fibrils both at 24 h and 48 h of aggregation reactions (Figure 9c). The ClearTau fibrils appear long, curly, flexible, and fuzzy. FFH samples show long, more flat fibrils. Again, the sedimentation assay demonstrated high levels of Tau incorporation into the pellet in ClearTau samples (Figure 9d, ClearTau, red arrows) with a small amount of Tau remaining in the supernatant (Figure 9d, ClearTau, black arrows). The FFH samples showed high intersample variability, with the reaction FFH 1 demonstrating good incorporation of Tau into the pellet, whereas samples FFH 2 and FFH 3 showed lower incorporation of the protein into the fibril-containing

fractions (Figure 9d, FFH, red arrows). FFH 3 demonstrated a lower amount of protein in the pellet fraction (Figure 9d, FFH, black arrows).

These results demonstrate the higher reproducibility and efficient fibrillization of Tau in the presence of co-factors by the ClearTau method. EM imaging showed extremely long fibrils (upwards of 5 μm) bundled into flexible cable-like structures and a fuzzy appearance. Interestingly, biochemically the ClearTau samples appear to be more stable upon both RNA and ATP addition and show a higher amount of fibrillar Tau compared to co-factor-free reactions (see Figure 9b and d, ClearTau; Supplementary Figure 3c and c, 4R2N). FFH samples demonstrated poor fibrillization in the presence of RNA and highly variable fibrillization in the presence of ATP. These results suggest potential interference of FFH with the co-factor or ligand molecules and their interactions impacting the Tau fibrillization propensity, as opposed to the ClearTau method.

ClearTau 4R2N P301L fibrils are twisted and bind RNA

Next, we extended our in vitro ClearTau system to aggregation of pathologically-relevant 4R2N Tau containing mutation P301L. P301L is associated with familial frontotemporal dementia linked to chromosome 17 [759], and P301L Tau readily forms fibrils in vitro in the presence of heparin, and in our ClearTau system (see Supplementary Figure 2). Therefore, we investigated its fibrillization and biochemical, RNA-binding, and ultrastructural properties in ClearTau and FFH systems.

From the EM imaging, we noted that the ClearTau P301L fibrils indistinctly showed periodical twisting, whereas the FFH P301L samples showed flatter fibrils (Figure 10b and c, -PK). This led us to hypothesize that the Tau N- and C-termini that remain disordered may obstruct the visualization of the ultrastructure of the ordered amyloid core of the fibrils. Thus, we have employed the limited proteolysis approach (Figure 10a) using 10 μM proteinase K digestion of the fibrils for 1 min to cleave off the disordered “brush” residues. After digestion, the ClearTau fibrils demonstrated the sharp outline of the periodically-twisted fibrillar core (Figure 10b and c, +PK), whereas the FFH fibrils were straighter. Further, the quantifications of the fibril widths pre- and post-proteolysis showed ClearTau fibrils consistently wider than FFH fibrils, suggesting differing fibrillar core morphologies (Figure 10d and Supplementary Table 3). Biochemical fractionation by ultracentrifugation of the fibrils into soluble and pellet fractions revealed a consistently higher amount of monomer incorporation into the fibrils for the ClearTau samples than for FFH samples (Figure 10e and Supplementary Figure 7a).

Finally, we assessed the RNA-binding properties of the fibrils prepared by both methods by incubating fibrils with RNA and assessing the presence of RNA in the soluble and fibril-bound fractions. The results showed significantly higher binding of the polyU RNA to the ClearTau fibrils in both buffer conditions, with the higher ionic buffer strength resulting in a substantial increase in RNA binding to the fibrils (Figure 10g). polyA RNA binding was not significantly different between the ClearTau and FFH samples, with low binding levels in the aggregation buffer and high binding in the presence of 100 mM $MgCl_2$.

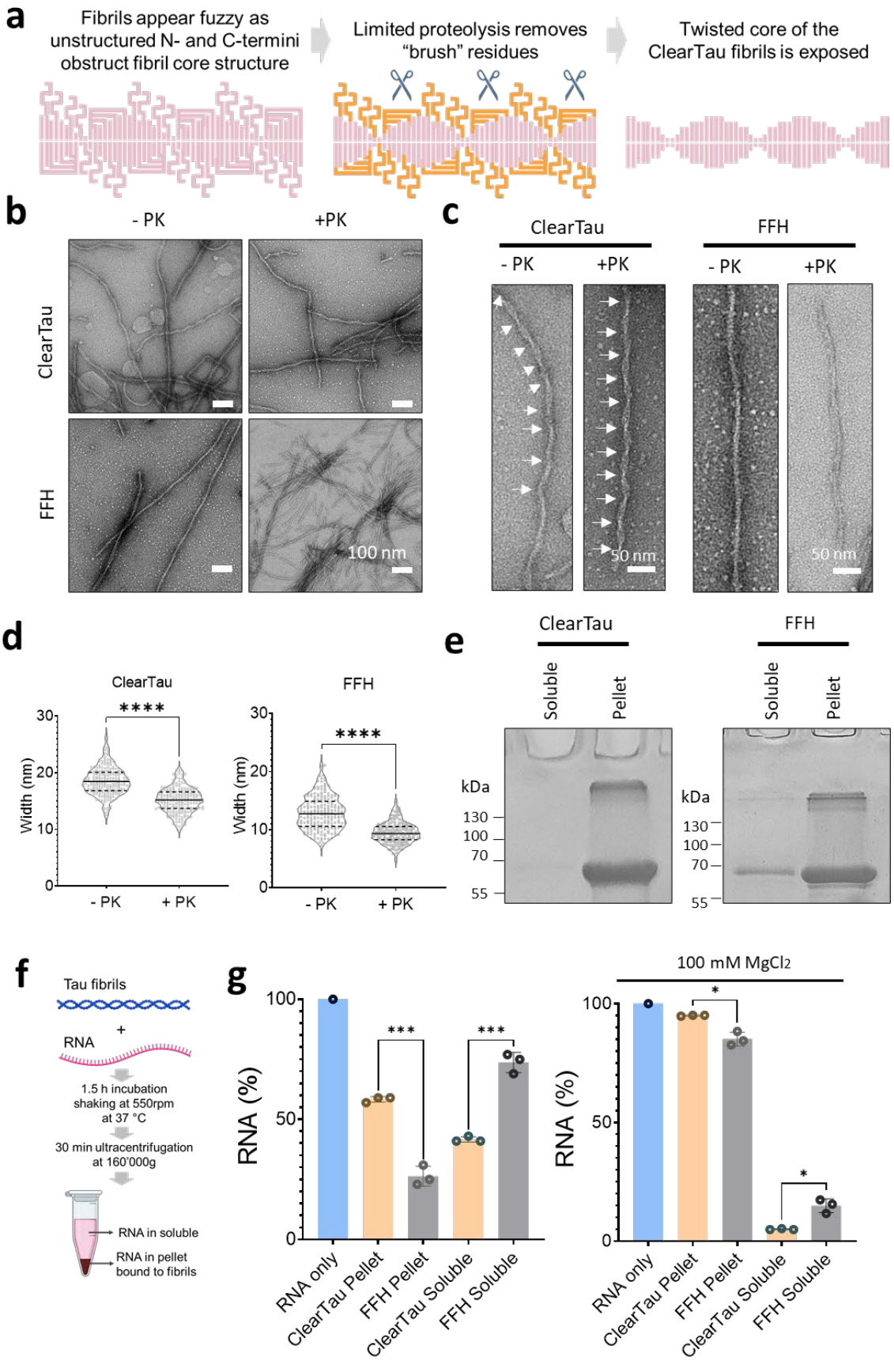
a
Fibrils appear fuzzy as unstructured N- and C-termini obstruct fibril core structure
Limited proteolysis removes "brush" residues
Twisted core of the ClearTau fibrils is exposed
b
- PK
+PK
ClearTau
FFH
100 nm
c
ClearTau
FFH
- PK
+PK
50 nm
d
ClearTau
FFH
****
Width (nm)
- PK
+ PK
e
ClearTau
FFH
Soluble
Pellet
kDa
130
100
70
55
f
Tau fibrils
RNA
1.5 h incubation shaking at 550rpm at 37 °C
30 min ultracentrifugation at 160'000g
RNA in soluble
RNA in pellet bound to fibrils
g
RNA (%)
***
RNA only
ClearTau Pellet
FFH Pellet
ClearTau Soluble
FFH Soluble
100 mM MgCl2
*

Figure 10. The ClearTau method application for fibrillization of full-length Tau 4R2N with mutation P301L. **a** Schematic of proteinase K limited proteolysis to remove the "brush" residues to reveal the fibril core structure. **b** EM of ClearTau and FFH-fibrillized Tau 4R2N P301L. Scale bars = 100 nm. **c** Proteolytic digestion of the fibrils by protease K (PK). Arrows point out the twists on the ClearTau fibrils, absent in the FFH samples. Scale bars = 50 nm. **d** Quantification of the widths of fibrils pre- and post-PK digestion, p **** <<0.001. **e** Representative gels demonstrating the monomer incorporation at 24h aggregation reaction for Tau 4R2N P301L ClearTau and FFH systems. For complete gels and individual replicates see Supplementary Figure 5a. **f** Schematic of RNA-binding assay workflow. **g** PolyU RNA-binding capacity of the 4R2N P301L fibrils prepared using ClearTau or FFH methods was assessed in the aggregation buffer, or in the higher ionic strength aggregation buffer (+100 mM $MgCl_2$).

The yeast transfer RNA failed to bind either type of fibrils in aggregation buffer or the presence of 100 mM $MgCl_2$ (Supplementary Figure 7b). These results further strengthen the versatility of the ClearTau system for use with different Tau proteoforms and in combination with downstream investigational methods.

The ClearTau method enables the identification of small-molecule stabilizers of Tau oligomers and modulators of Tau fibrillization

Next, we sought to determine if the ClearTau assay could be used to screen and identify inhibitors of Tau oligomerization and fibril formation (Figure 11a). Given that we can induce the misfolding and oligomerization of co-factor-free monomers and oligomers, we hypothesized that this assay could provide unique opportunities to identify compounds or drug-like molecules that can either stabilize Tau monomers or oligomers and inhibit their fibrillization. Such compounds could serve as powerful tools to test the role of Tau oligomerization and fibrillization in the pathogenesis of Tauopathies.

As a proof of concept, we tested a panel of known modulators and/or inhibitors of Tau aggregation (Figure 11b-d; ATPZ, pyrocatechol violet, BSc3094, LMTX, myricetin, L-DOPA, 4-HNE and DMSO), in addition to other compounds that have been shown to inhibit the aggregation of other amyloid proteins. The aldehyde 4-HNE and catechin EGCG compounds emerged as the most effective at preventing Tau fibril formation (Figure 11b) and induced the formation of predominantly oligomeric Tau species as detected by EM (Figure 11c). These results suggest that 4-HNE and EGCG inhibit Tau fibrillization by stabilizing oligomeric forms of the protein, consistent with their mode of action on other amyloid-forming proteins, including α-synuclein [760-765].

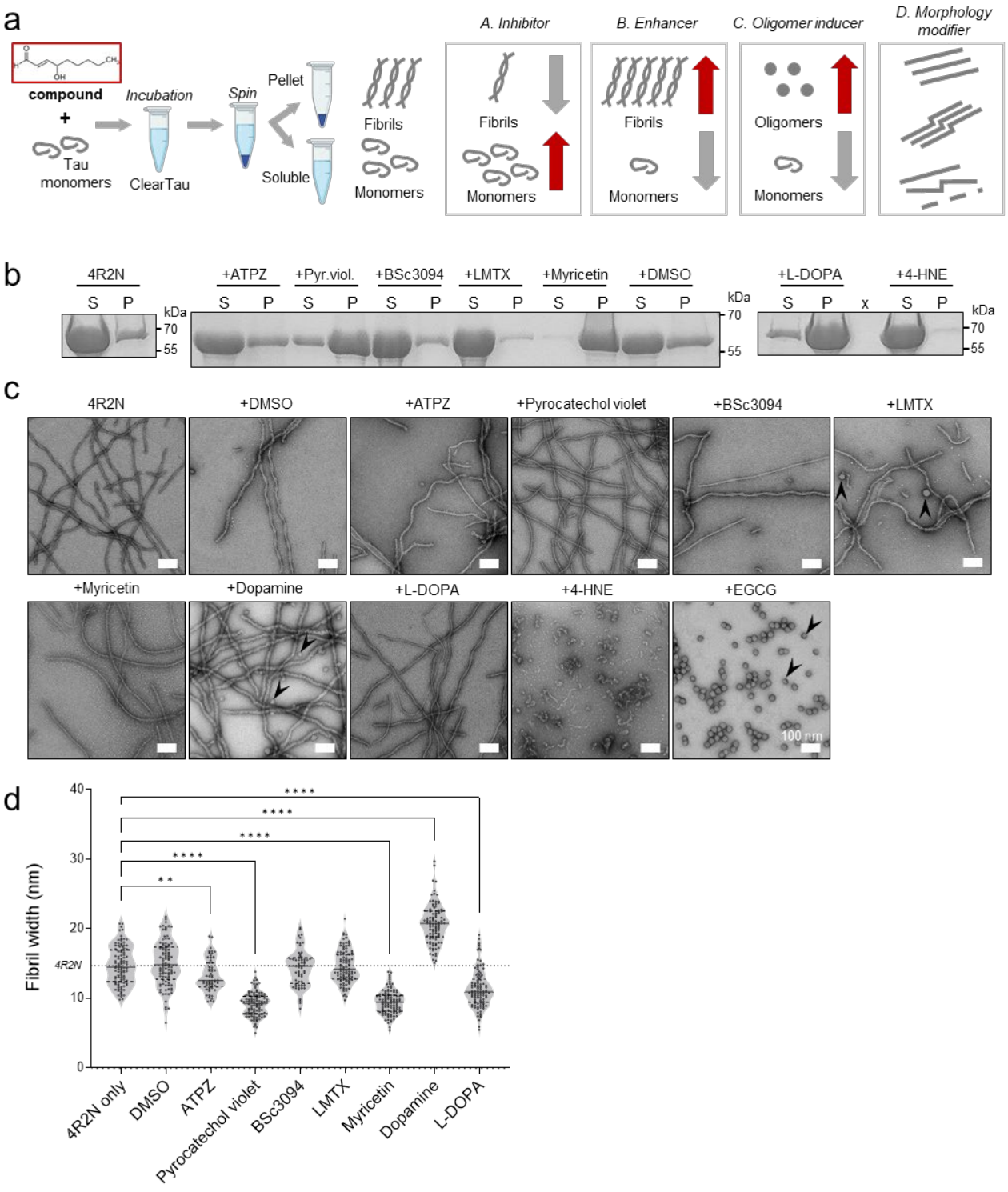

Figure 11. ClearTau assay implementation for small molecule screening of the aggregation-modifying properties. a Schematic illustration of ClearTau assay workflow implementation for screening of Tau aggregation inhibitors, enhancers, or oligomerization-inducing compounds and drugs. **b** SDS-PAGE illustrating the distribution of the Tau in the soluble (S) and pellet (P) fractions after incubation in the presence of small molecules. **c** Electron microscopy assessment of ClearTau fibrils and oligomers (arrowheads) formed in the presence of the compounds. **d** Quantifications of the fibril widths for each repeat of the four

mixtures. ANOVA tests with multiple comparisons show significance levels at * <0.05, ***<0.01, **** <0.001.

LMTX compound is a reduced form of methylene blue, a well-studied Tau aggregation inhibitor [766]. Although LMTX did not fully prevent fibril formation, most of the Tau protein remained in the Soluble fraction (Figure 11b), indicating that it works by stabilizing soluble forms of the protein. Interestingly, the fibrils formed in the presence of LMTX were fragmented and had an aberrant morphology with regular bends or twisting, but only a few oligomers were present (Figure 11c). The absence of visible oligomeric structures by TEM indicates that it either stabilized monomeric or low molecular weight oligomers of Tau. The compounds ATPZ, pyrocatechol violet, BSc3094, and myricetin did not prevent Tau fibril formation. In fact, all but BSc3094 increased the aggregation of Tau to varying levels, with myricetin being the most potent enhancer. All compounds had pronounced effects on the fibril morphologies, giving rise to fibrils with widths significantly smaller than observed for Tau fibrils formed in the absence of compounds (Figure 11c, d, Table SI4). Morphologically, ATPZ and BSc3094 induced the formation of fibrils of varied morphologies and a high amount of fragmentation. On the other hand, pyrocatechol violet and myricetin induced the formation of uniform populations of thin fibrils, with wavy morphology in pyrocatechol violet, and sharply defined thin fibrils in myricetin reactions (Figure 11c, d). As expected, fibrils formed in the presence of DMSO were similar to those formed by Tau alone. Interestingly, L-DOPA, a precursor to dopamine, was shown to enhance the shift of Tau into the *Pellet* fraction, with only a minority of protein remaining in the soluble state (Figure 11b).

The fibrils formed in the presence of L-DOPA were of uniform morphology, however, they were thinner, at 11.3 ± 2.72 nm, and visually straighter than control fibrils (14.7 ± 2.72 nm, Figure 11c, d). In contrast to L-DOPA fibrils, the fibrils formed in the presence of dopamine showed wide cable-like bendy fibrils without a clear definition of the fibril surface. Some oligomeric species were also present. Here, we demonstrate that the Clear Tau methods can be used to screen and identify small molecule modifiers of the kinetics and morphology of Tau oligomerization and fibril formation. These findings suggest that it could also be used to screen putative natural co-factors to identify conditions that enable the conversion of wild-type of post-translationally modified forms of monomeric Tau into stable oligomeric forms or fibrillar structures that resemble those found in the brain of patients with Tauopathies (Figure 12).

Discussion

Attempts to develop methods for efficient production of clean co-factor-free fibrils from full-length Tau isoforms have thus far failed. One attempt to produce the co-factor-free Tau fibrils involved repeated cycles of Tau self-seeding reactions. However, the experimental timescales were limiting, for example, six cycles of self-repeated seeding at 5 - 7 days incubation per cycle equated to more than a month to produce the co-factor-free Tau fibrils [160]. Likewise, another recent attempt to produce the co-factor-free fibrils from a single Tau isoform using polytetrafluoroethylene beads suffered from long production timescales [161]. Furthermore, the co-factor-free nature of the fibrils could not be ascertained due to the use of uncharacterized free-floating co-factor components in the aggregation buffer (protease inhibitor tablet containing aprotinin, bestatin, calpain I, calpain II, chymostatin, E-64, leupeptin, alpha-macroglobulin, pefabloc SC, pepstatin, TLCK-HCL, and trypsin inhibitors in undisclosed proportions) that could contribute to Tau fibrillization and intercalate into the growing fibrils [161]. In addition, a recent study attempted to generate Tau fibrils resembling patient-derived fibrils in vitro without the use of co-factors, but success in achieving this goal was limited to the truncated Tau constructs. Under all conditions tested, the unmodified full-length isoform 4R0N [767] did not form fibrils. Therefore, novel, efficient, and cheap methods for producing co-factor-free, clean, unmodified full-length Tau fibrils are needed.

In this work, we present a novel ClearTau method for the production of large amounts of polysaccharide/co-factor-free Tau aggregates in vitro. This method provides a platform for Tau aggregate production in the presence of additional cofactors, that can be used for in vitro and in vivo applications to study the aggregation of Tau under various conditions associated with the different types of Tauopathies, and to screen and identify compounds that modulate this process. Covalent immobilization of polysaccharides, heparin, onto the surfaces of the vessels used to induce Tau aggregation results in the formation of high yields of pure, polysaccharide-free Tau protein fibrils. We demonstrate that fibrils produced using our method are morphologically-homomorphic within single isoforms and retain their structures upon association into the doublets; are amyloid reporter-dye positive; have high RNA-binding propensity; and are seeding-competent in vitro, in Tau biosensor cells and human iPSC-derived neurons. All six Tau isoforms, mixtures thereof, as well as truncated and mutant Tau, can be efficiently fibrillized using our method, including in the presence of other co-factor molecules, such as RNA and ATP. Further, we provided the proof of concept experiments illustrating the potential for extending this approach to screening applications aimed at identifying Tau aggregation inhibitors and modifiers. For example, we identified small molecules that inhibit or enhance Tau fibrillization, induce the formation of stable Tau

oligomers, or produce fibrils with distinct morphologies, all in the absence of heparin or other co-factors. These compounds and conditions present unique opportunities to dissect the role of different aggregated forms of Tau and different Tau fibril strains in regulating its neurotoxicity, seeding, and spreading in the brain.

Our ClearTau aggregation assay has multiple advantages over Tau aggregation assays containing free-floating polysaccharides as Tau aggregation co-factors. The lyophilized heparin has varying qualities from a vendor to vendor, and batch-to-batch, such as a wide range of polysaccharide lengths, which impact the efficiency of Tau aggregation. Furthermore, the free-floating co-factors can tightly bind and integrate into Tau aggregation intermediates or the growing fibrils, thus impacting their structural features. The presence of polysaccharides in the mixture may have unfavorable interactions with the screened Tau-binding compounds. For example, Tau anti-aggregation compound leuco-methylthioninium molecule (TauRx Therapeutics) [243] was found to bind to the heparin, therefore introducing artifacts into the experimental system potentially resulting in significant economic and resource losses. In the cellular Tauopathy models, heparin has the potential to activate differential signaling pathways within cells that are not related to Tau fibril treatment [236-241], and stimulate the aberrant modifications of Tau monomers [242] or fibrils in cells. In animal models of Tau spreading, heparin can potentially interact with extracellular matrix constituents that influence Tau fibril spread and its cellular uptake [158,235]; elicit immune cell responses [233] that are Tau-independent and impact the cardiovascular system cells and its components, resulting in polysaccharide-induced vasodilation [234].

In our ClearTau aggregation assay, we solve these issues by removing the catalyst of the aggregation reaction to yield clean Tau fibrils at short time scales. In our method, the consistent Tau-to-polysaccharide ratio allows for optimizing the stoichiometry for best Tau aggregation at desired Tau concentrations. The high levels of interconversion of Tau monomer to fibril (up to 100%) are compatible with use with the high-cost, ultrapure, post-translationally modified, chemically modified, synthetic or semisynthetic, in combination with other co-factors, and precious protein material only accessible at low amounts to prevent the waste and loss of the material. Lack of the polysaccharide association with Tau protein fibrils allows for the downstream use in the ultrasensitive biochemical and biophysical assays, as well as in cell and in vivo studies in cell lines, primary cultures, and non-mammalian and mammalian animal models using direct treatment with fibrils by intracranial or systemic fibril delivery. Finally, our results demonstrate that free-floating co-factor heparin can interact with other molecules, such as RNA, and impede Tau aggregation (Figure 9). The clean Tau aggregation assay utilizes

minimal buffer conditions – up to containing PBS or dH_2O (data not shown) only – thus enabling the identification and characterization of Tau interacting molecules without interference from other co-factors that may alter Tau fibril structures or interactome.

Recent advances in cryo-EM have provided us with remarkable insights into the structural diversity and landscape of Tau fibrils isolated from the brain of patients with different Tauopathies, thus enabling the shift towards the structure-based classification of these diseases [768]. Despite a wealth of information about the structure of Tau regions directly contributing to the core, the impact of the sequences in N- and C-termini, and mutations and PTMs in these regions on Tau fibrillization and final morphology of the fibrils remains largely unknown. These regions could also influence the binding of antibodies and other molecules, including PET tracers, which target the Tau sequences folded within the fibril core. Therefore, it is paramount to develop methods for generating fibrils composed of full-length Tau isoforms that resemble the morphological and structural properties of fibrils found in pathological Tau aggregates. Our preliminary cryo-EM results show that the fibrils generated using our ClearTau method exhibit structural features that are different from the known heparin-induced Tau fibrils. Further, ClearTau core structures appear reminiscent of pathology-derived Tau fibrils in an isoform-specific manner, but further studies are needed to determine the complete 3D structures of the pure monoisoform Clear Tau fibrils. Irrespective of whether the fibrils formed under the conditions used here are identical to those found in AD brain or not, we believe that the methods and data we present here pave the way for unprecedented opportunities to dissect the molecular and sequence determinants of Tau aggregation and pathology formation and bring us closer to reproducing the structural diversity of Tau fibrils isolated from different Tauopathies.

Accumulating evidence from mass spectrometry and Cryo-EM studies of brain-derived Tau aggregates demonstrate the brain-derived Tau fibrils contain several post-translational modifications and non-proteinaceous compounds, which are thought to play a role in the initiation of Tau aggregation or influencing the final structure of the fibrils. Therefore, it could prove challenging to reproduce both the biochemical and structural diversity of brain-derived fibrils starting with unmodified Tau proteins and/or in the absence of specific cofactors. Previous methods used to induce Tau aggregation, precluded in vitro screening and identification of putative cofactors, because of interference by the polyanions used to induce Tau misfolding and aggregation.

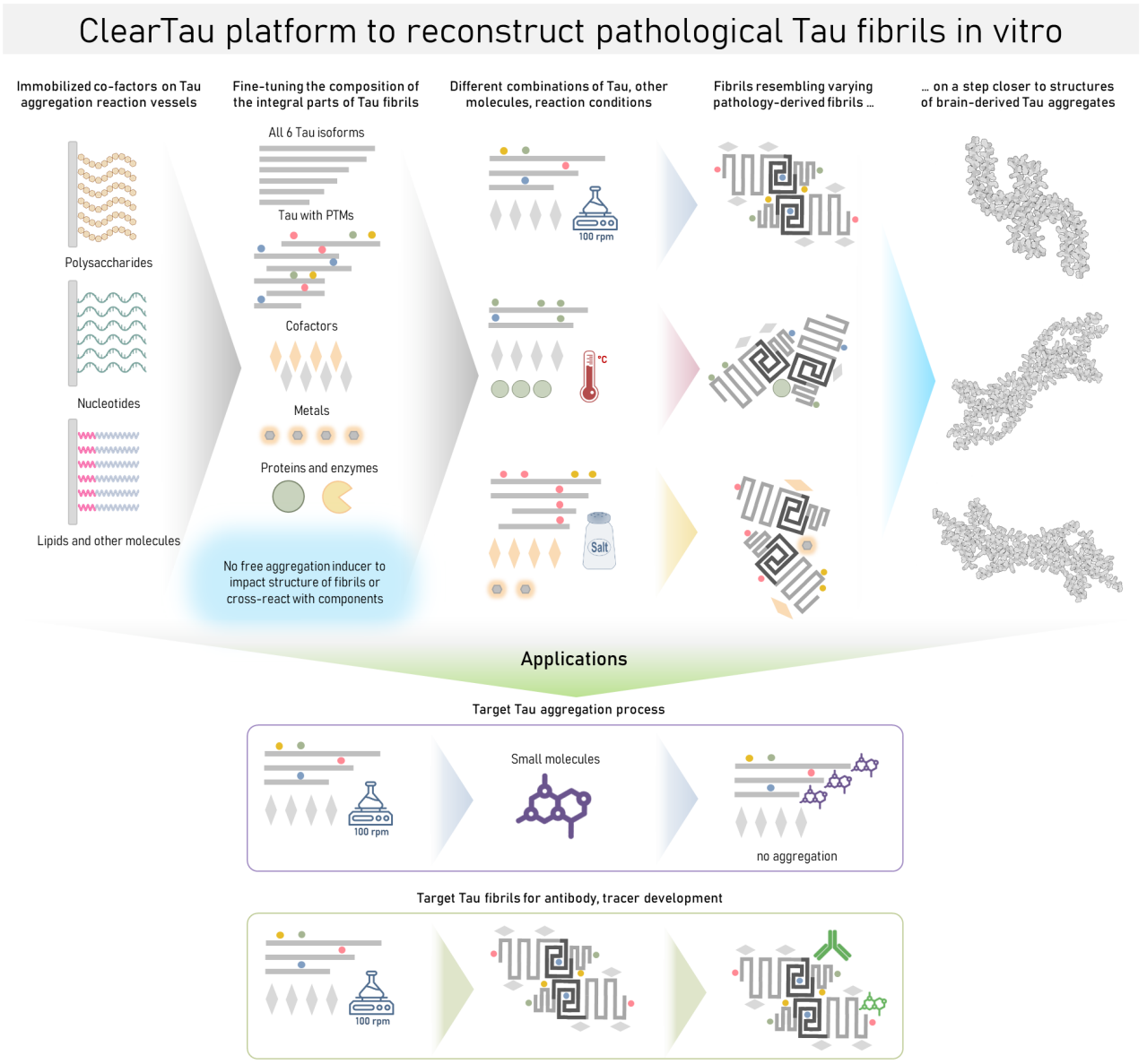

Figure 12. ClearTau platform to reconstruct pathology-resembling Tau fibrils in vitro for research into Tau aggregation processes and development of Tau fibril-targeting therapies. Different types of co-factor molecules, such as polysaccharides, nucleotides, lipids, and others could be immobilized on the reaction vessel surface, allowing them to induce and/or catalyze Tau polymerization, but preventing them from integration into the growing Tau fibrils. The composition of Tau fibrillar aggregates can be tailored to contain specific Tau isoforms, PTMs, and other molecules, to more faithfully represent the pathological aggregates. The lack of free-floating co-factors prevents undesirable reactivity with the components in the aggregation reaction. Fine-tuning reaction conditions, such as temperature, agitation, or buffer, helps our ability to produce in vitro Tau fibrils more closely resembling the pathology-derived Tau aggregates. ClearTau methods can be applied to target the early stages of Tau aggregation for screening of aggregation-modifying compounds. ClearTau co-factor-free aggregates could be used to develop Tau fibril-targeting antibodies or PET tracer molecules.

Our Clear Tau aggregation method makes such screening assays possible today. Furthermore, we and others have recently reported on the development of protein semisynthetic strategies that enable the generation of site-specifically modified forms of Tau bearing single or multiple PTMS in pure form [171,207,405]. We believe that combining these advances with new insights into putative natural co-factors and PTMs that regulate Tau aggregation and pathology formation will provide a powerful platform to systematically evaluate and screen different combinations of Tau proteins and biochemical conditions and identify conditions that enable reproducing the structure of pathological Tau aggregates from different Tauopathies (Figure 12, Applications). This would enable the generation of disease-relevant Tau targets to support drug discovery and development and to develop disease-specific Tau imaging agents. This is paramount to bridge the gap between the efficiency of Tau-targeting compounds in the laboratory, and the compounds' effectiveness in patients suffering from AD and other Tauopathies, and we hope that the ClearTau approach is the stepping stone to this goal.

Materials and methods

Protein expression and purification

All proteins were expressed and purified as described previously [380].

Human 4R2N: Briefly, for the 4R2N isoform, the competent *E. coli* cells BL21 were transformed with plasmid pT7-7 SUMO-Tau human full-length 4R2N and incubated for 30 min on ice, heat-shocked for 45 sec at 42 °C water bath, incubated on ice for 2 min. 300 µl of SOC outgrowth media (Thermo Fisher Scientific) were added, and the tube was incubated for 30 min @ 37 °C with shaking. Cells were plated on Luria-Bertani (LB) solid agar broth with kanamycin plates and incubated overnight in a 37 °C incubator for single colony growth. 20 ml of LB (Thermo Fisher Scientific) with 50 mg/L kanamycin were inoculated with a single bacterial colony and grown in the shaking incubator at 18 °C overnight. To 8 L of autoclaved and filtered LB antibiotic kanamycin was added to the final concentration of 50 mg/L, media was split into 4 x 2 L flasks, inoculated with an overnight starter culture of SUMO-Tau 4R2N transformed bacteria and grown at 37 °C at 180 rpm in the shaking incubator to the confluence of 0.6-0.9 density. The culture was induced for the protein production by adding isopropyl β-d-1-thiogalactopyranoside (IPTG, Thermo Fisher Scientific) to the final concentration of 0.4 mM and grown at 18 °C overnight in the shaking incubator. The culture was decanted into 1 L

centrifuge tubes and centrifuged at 3'000 rpm for 30 min. 150 ml of lysis buffer (50 mM Tris pH7.5, 30 mM imidazole, 500 mM NaCl) with 1 mM phenylmethylsulfonyl fluoride (PMSF) and protease inhibitor cocktail (SigmaAldrich) were added, bacterial pellet was solubilized fully, then sonicated on ice using probe sonicator using the following protocol: 70% amplitude, 30 s on, 30 s off for 5 minutes. Sonicated lysate was centrifuged for 30 min at 10 °C at 13'000 rpm. The supernatant was filtered and loaded on a HisTrap HP 5ml column (GE Healthcare). The purification was then performed using a linear elution gradient of His Trap Buffer A (50 mM Tris pH7.5, 30 mM imidazole, 500 mM NaCl) 100% to His Trap Buffer B (50 mM Tris pH7.5, 500 mM imidazole, 500 mM NaCl) 100%. The fractions were analyzed by SDS-PAGE, pooled accordingly, and cleaved by ULP1 enzyme (Thermo Fisher Scientific) for 1 hour at room temperature (RT). The pooled fractions were then loaded on a reverse-phase HPLC C4 column (PROTO 300 C4 10 µm, Higgins Analytical; buffer A: 0.1% TFA in water, buffer B: 0.1% TFA in acetonitrile), and the protein was eluted using a gradient from 20 to 40% buffer B over 90 min (15 ml/min). Fractions were analyzed by mass spectrometry and ultra-performance liquid chromatography for purity and pooled accordingly. Protein samples were flash-frozen in liquid nitrogen and placed into a vacuum lyophilizer for 48 h to produce lyophilized protein powder. All other Tau isoforms and variants were produced following a similar protocol.

ClearTau aggregation reaction

The aggregation reactions were carried out in accordance with the procedures described in patent application No. 22204800.1 (priority founding). Briefly, monomeric human full-length 4R2N Tau was diluted to 100 µM (or other specified concentration) in phosphate buffer (10 mM Phosphate, 50 mM NaF, 0.5 mM fresh DTT) and added to a heparin-coated reaction tube (ThermoFisherScientific). The reaction mixture was incubated for 24 h with orbital shaking at 1'000 rpm (Peqlab, Thriller) at 37 °C. The reaction was ultracentrifuged using Beckman-Coulter ultracentrifuge at 100'000 g for 1 h at 4 °C, the supernatant was removed and discarded, and the pellet was washed twice with dH_2O. The pellet containing fibrils was resuspended in dH_2O to 100 mM, aliquoted to single-use aliquots, and stored at -80 °C. Analogous measurement procedures were followed for other Tau isoforms and mixtures thereof.

ClearTau seed preparation

The ClearTau fibrils were diluted to 10 µM in dH_2O and sonicated at 70 % amplitude for 50 s with 1 sec ON 1 sec OFF cycle in-tube using UP200St with VialTweeter (Hielscher, USA). Seeds were characterized by electron microscopy.

ThS fluorescence measurement

The ClearTau fibrils were diluted to 2.5 µM in dH_2O and sonicated at 70 % amplitude for 50 s with 1s ON 1 sec OFF cycle in-tube using UP200St with VialTweeter (Hielscher, USA). 2.5 µM full-length Tau 4R2N monomer was used as a control. To the 100 µl reaction, 100 µl of ThS (10 µM) were added, yielding final protein concentrations of 1.25 µM. Single-timepoint ThS fluorescence was measured using 96 well clear bottom plates (Corning) set up in FLUOstar Omega microplate reader (BMG LABTECH, Germany) with excitation at 445 nm and emission at 485 nm was recorded. Four independent measurements were conducted in triplicates using ClearTau fibrils from two independent aggregation preparations. Raw fluorescence values were standardized to the blank reaction samples containing ThS. The plot represents the average of four experiments in triplicates, and the bars show the standard deviation. Analogous measurement procedures were followed for other Tau isoforms and mixtures thereof, the details for each indicated in the legends.

ThS ClearTau seeding aggregation assay

The ClearTau seeds were prepared from Tau fibrils produced using the ClearTau aggregation protocol as described above. Reactions were set up in the clear bottom 96 well plates (Corning) as follows: Tau 4R2N monomer was diluted in the phosphate aggregation buffer (10 mM Phosphate, 50 mM NaF, 0.5 mM fresh DTT) to 10 µM. The ClearTau seed or free heparin sodium salt (Applichem GmbH) was added at a final concentration of 2.5 µM. The monomers without seeds were incubated with the buffer. A fresh ThS solution was added at 10 µM and the plate was sealed with clear film. Reactions were conducted in the FLUOstar Omega microplate reader (BMG LABTECH, Germany). The reading was taken from time 0 (corresponding to the maximum 20 min after the seed addition) every 10 min (1 cycle) for 19 h with shaking at 600 rpm for 10 min followed by the idle 10 min at 37 °C. 4 independent experiments were performed in triplicates for each condition. The ClearTau seeding values were standardized to the values derived from a reaction containing only seeds, but no monomer, heparin seeding values were standardized to the reaction containing heparin only

and no monomer, monomer only reaction values were standardized to the reaction containing buffer, and ThS only. The plot represents average values for 4 experiments, and the bars represent the standard deviation.

Negative stain transmission electron microscopy (EM)

2 µl of protein in solution were deposited on the glow-discharged Formvar/carbon-coated 200-mesh copper grids (Electron Microscopy Sciences) for electron microscopy, incubated for 5 min, washed three times in dH_2O, and stained using 2% uranyl formate solution. Images were acquired using a Tecnai Spirit BioTWIN transmission electron microscope operated at 80 kV and equipped with a LaB6 filament and a 4K x 4K FEI Eagle CCD camera.

Width quantification of ClearTau fibrils

The ClearTau and FFH fibrils widths were quantified using EM images from at least 3 independent fibril preparations and independent EM grid preparations. Fibril widths were measured using ImageJ [769] Measurement Tool (ImageJ, RRID: SCR_003070).

Monomer – Fibril fractionation

The ClearTau reaction was ultracentrifuged using Beckman-Coulter ultracentrifuge at 100’000 g for 1 h at 4 °C. The supernatant was removed, and the remaining pellet was washed in dH_2O twice and then resuspended in dH_2O.

SDS-PAGE protein assay

Twenty-five µg of total protein per well was loaded on fixed polyacrylamide concentration of 15 % SDS-PAGE gels (Invitrogen, Thermo Fisher Scientific) and run in MES buffer (Invitrogen, Thermo Fisher Scientific). The total protein content was visualized using the Coomassie protein stain.

Biosensor (BS) cellular flow cytometry assay

Cell line Tau RD P301S FRET Biosensor (CRL-3275™) was acquired from ATCC® and maintained in DMEM medium with 0.5 % L-Glutamine, 0.5 % penicillin-streptomycin antibiotic cocktail and 10 % fetal bovine serum supplementation (Gibco, Thermo Fisher Scientific). BS

cells were plated in poly-L-lysine treated 6 well plates at a density of 100’000 cells/well. Cells were allowed to grow and divide in an incubator at 37 °C. BS cultures were allowed to reach a confluency of 50-60%. The ClearTau sonicated fibril seeds were incubated with Lipofectamine2000 at a 1:2 ratio weight to volume in OptiMEM (Gibco, Thermo Fisher Scientific). The cultures were transduced with ClearTau sonicated fibril seeds at amounts of 0.892 µg, 0.446 µg, and 0.223 µg of fibrils per 200’000 cells. Cells were exposed to the fibrils for 4 h, cultures were washed twice in phosphate-buffered saline (PBS, Gibco, Thermo Fisher Scientific) to remove all residual seeds, and further incubated for 96 h in standard medium to allow to have two cell division cycles. Cultures were washed once in PBS and dissociated using 200 µl Trypsin-EDTA 0.05% for 5 min at 37 °C. 150 µl of DMEM medium was added to each well to neutralize Trypsin action, cells were gently dissociated into single cells by pipetting, and they were transferred into Eppendorf tubes and centrifuged at 1000g at room temperature for 5 min. The supernatant was removed, and cells were re-suspended in the 900 µl of 2% paraformaldehyde (Thermo Fisher Scientific) and incubated for 10 min, then pelleted by centrifugation at 1000 g 4 °C for 5 min. The supernatant was removed, and the pellet was re-suspended in HBSS.

FRET Flow cytometry protocol was adjusted from [755]. FRET detection was performed using BD LSR Fortessa with excitation-emission laser filters: 405 – 465/30, and 488 – 530/30, with the FRET signal detectable at 405 – 530/30 couple. Parental HEK293T cells were used to define the cell population on the SC-A vs FCS-A bivariate plot (Supplementary Figure SI8). Doublet events were excluded on FSC-H vs. FSC-A bivariate plot. Voltages were adjusted to exclude any signal on CFP, YFP, or FRET filters. Double-positive CFP-YFP BS cell population was defined by the negative Lipofectamine-only BS cell line control sample. Compensation was adjusted to remove any bleed-through of CFP and YFP signal to the FRET channel.

For data analysis, cell populations were gated to exclude the debris events and doublets. Negative control (BS-Lipofectamine) was used to define a double-positive cell population, and spill-over to the FRET channel was excluded on CFP-FRET and YFP-FRET bivariate plots (See Figure SI7). For each sample, the percent of FRET-positive events and the Median of fluorescence intensity was recorded, and the product was plotted to represent Integrated FRET Density (IFD). Three independent experiments were performed for each condition with a minimum of 100’000 events per sample recorded. The plot represents average measurements; bars represent standard deviation.

Confocal imaging

For confocal imaging, Tau RD P301S FRET Biosensor cells were plated at a low density (>5'000/well) in the 24 well plates on the poly-l-lysine-coated (3438-100-01, R&D Systems) glass coverslips and allowed to attach overnight. Cells were incubated in the HBSS (Gibco) overnight, and then the medium was changed to normal, and cells were allowed to double. Media was aspirated, cells were washed in 1X PBS, 10 µM ClearTau preformed seeds were added in OptiMEM (Gibco) for 4 h, then the media was aspirated and replaced by the standard media. Cells were allowed to have two cell divisions, after which they were washed in 1X PBS, and were fixed using a 4% formaldehyde solution for 20 min. Cells were washed twice in 1X PBS, and coverslips were mounted onto microscopy slides using a Molwiol mounting medium (Sigma-Aldrich). Confocal images were acquired using Zeiss LSM 700 microscope.

Seeding experiments in hiPSC-derived cortical neurons

The human induced pluripotent stem cell lines used in this study were derived from the line iPSC0028, which was obtained from Sigma. The following biallelic genetic modifications were introduced as described [756]: microtubule-associated protein Tau (MAPT) knockout (KO Tau) and triple mutant MAPT IVS10+14, IVS10+16, P301S (TM Tau).

hiPSCs were differentiated using a guided protocol based on various published protocols [756] with slight modifications. Briefly, cultures were cultured in E8 Flex (ThermoFisher) on Matrigel (Corning)-coated cell culture ware. For differentiation, cells were harvested as single cells using Accutase (ThermoFisher) and seeded at 500,000 cells per cm2 onto 77.5 µg/mL Matrigel-coated 6-well plates in E8 Flex medium supplemented with the 10µM ROCK inhibitor Y-27632 (Millipore). Protocols for differentiation into cortical neurons have been previously described [756].14 days after plating TM Tau and KO Tau hiPS-derived cortical neurons were exposed to different amounts of recombinant Tau (P301L 2N4R) aggregates generated in the absence (ClearTau) or presence (Free Heparin) of heparin in solution. Three weeks later, the neurons were fixed and stained to detect endogenous tau aggregates as described below.

Immunocytochemistry: Three weeks after incubation with Tau fibrils, the hiPSC-derived cortical neurons were washed twice with PBS and fixed in ice-cold methanol for 15 mins at 20°C, followed by rinsing in PBS and blocking in 5% fetal calf serum (FCS), 5% BSA and 5% goat serum (Sigma) for 1h at RT and overnight incubation with primary antibodies at 4°C. After rinsing, secondary Alexa fluor 488-conjugated goat anti-mouse and Alexa fluor 647-conjugated rabbit anti-chicken antibodies (Jackson Laboratory) were applied for 2h at RT. The

following primary antibodies were used: MC1 antibody (kindly provided by Peter Davies to AbbVie through a Material Transfer Agreement with Feinstein Institute; 2µg/mL dilution) to detect the insoluble tau aggregates and anti-MAP2 antibody (chicken, Abcam, #5392; 1:5000 dilution) to counterstain the neurites, Nuclei were counterstained by DAPI. Immunoreactivity was imaged in the Operetta CLS High-Content Analysis System (Perkin Elmer) using the 40X water immersion objective (25 fields of view per well, z-stack with 6 images with 0.5 µm step). Image analysis was carried out on the maximum intensity projection images using the Harmony Software (Perkin Elmer, version 4.9). The neuronal nuclei were detected based on a threshold of > 0.4 and an area of 40 µm2. MAP2 area was determined by a common threshold of 0.5 (as calculated by the Harmony software). The endogenous tau aggregates were detected using the spot detection method B with a detection sensitivity of 0.2 and a split sensitivity of 0.5 (as calculated by the Harmony software). Thereafter, the selected tau aggregates are further filtered by a relative, as well as corrected and uncorrected spot intensity. Based on these features, the MC1+ area (> 2µm2) was calculated and normalized to the number of neuronal nuclei.

Symmetric ELISA: hiPSC-derived neurons were cultured in 96well plate format and seeded with recombinant P301L 2N4R Tau aggregates as described above. Cells were lysed in 50 µl/well Triton buffer (150mM NaCl; 20mM Tris, pH 7.5; 1mM EDTA; 1mM EGTA; 1% Triton-X-100; 1× cOmplete Protease inhibitors; 1× PhosStop Phosphatase inhibitors (Roche) and diluted 50-150-fold in assay buffer (20 mM NaH2PO4 pH 7.4, 140 mM NaCl, 0.05% Tween 20, 0.1 % BSA) to fall within the experimentally validated linear range of the assay. ELISA plates (Maxi Sorp, Thermo Scientific) were coated over night at 4°C with 100 µl Tau-12 capture antibody per well (2 µg/ml; Biolegend, cat. no 806502) in 20 mM NaH2PO4 pH 7.4, 140 mM NaCl, 20% glycerol. Plates were rinsed with 250 µl/well wash buffer (20 mM NaH2PO4 pH 7.4, 140 mM NaCl, 0.05% Tween 20) and blocked for 1.5 h at RT with 250 µl/well-blocking buffer (20 mM NaH2PO4 pH 7.4, 140 mM NaCl, 0.05% Tween 20, 20% glycerol, 2% BSA). After rinsing, 100 µl/well samples were added and incubated for 2 h at RT. After rinsing, 0.1 mg/ml Biotin-Tau 12 (100 µl/well; BioLegend) was added for detection and incubated for 1 h at RT followed by Pierce Streptavidin poly-HRP conjugate was used (Thermo Scientific, diluted 1:10 000 in assay buffer) for 1 h at RT. TMB ELISA substrate (100 µl/well; KEM EN TEC Diagnostics) was incubated for 10 min in the dark for signal detection. The reaction was stopped by 100 µl/well 0.18 M H2SO4, and the absorbance was read at 450 nm on an Anthos LEDetect microplate reader (Anthos Mikrosysteme GmbH, Frisoythe, Germany).

Circular dichroism (CD) spectroscopy

CD spectra were recorded on a Jasco J-815 CD spectrometer operated at 20°C. To minimize buffer absorption, the samples were diluted with 1:50 deionized H_2O. CD spectra were acquired from 190 nm to 260 nm at a scan rate of 50 nm/min and in increments of 0.2 nm. For each sample, three to four spectra were averaged and smoothed using binomial approximation.

Cryoelectron microscopy

The fibrils from ClearTau 3R2N and 4R2N proteins were screened with negative staining (NS) TEM for fibril concentration and morphology. Aliquots of optimized fibril samples were applied onto gold Ultrafoil 1.2/1.3 grids, and plunge frozen in liquid ethane. Frozen cryo-EM grids were imaged on a ThermoScientific 200kV Glacios on a K3 electron counting direct detection camera (Gatan Inc.) in counted (non-CDS) mode (50 fractions) using the SerialEM [770] at a physical pixel size 1.113 Å for 3R2N fibrils and 0.878 Å for 4R2N fibrils, and a total dose of 50 electrons per square angstrom (e-/Å2) for each exposure. After inspection, the best 6021 (3R2N) and 3331 (4R2N) aligned, CTF-estimated, and dose-weighted movies were selected from FOCUS [771] for further processing. Fibrils were selected manually from aligned micrographs, and 1,842,783 3R2N and 570,876 4R2N segments were extracted with a box size of 300 pixels and subjected to reference-free 2D classification in cryoSPARCv3.2 [772]. Several rounds of 2D classifications allowed to select only particles with clear 4.77 Å beta-strand separation along the fibril axis, measured from Fourier amplitudes of the 2D class average. To separate singlet and doublet fibrils, helical segments were re-extracted with a larger box size of 900 pixels, re-scaled to 360 pixels and subjected for reference-free 2D classification in cryoSPARC and RELION. 2D class averages corresponding to singlets and doublets were separated and further classified. 4R2N data further refined, both cylinder and initial model by IniModel2d converged to the same structure. After a couple of rounds of 3D classification and refinement, pseudo-2_1 screw symmetry was applied. Bayesian polishing and CTF refinement were applied, and the final reconstruction was post-processed with a soft-edge mask and a sharpening *B*-factor of -70 $Å^2$. The resolution was estimated as 3.1 Å from the Fourier shell correlation (FSC) at 0.143.

Co-factor aggregation

To aggregate 4R2N Tau in the presence of co-factor polyuridylic acid single-stranded RNA (P9528, Sigma-Aldrich), or adenosine triphosphate (987-65-5, SERVA/Cayman chemical) by ClearTau method or in the Eppendorfs in the presence of free-floating heparin (FFH), Tau 4R2N was added at 10 µg/ml to 1 mM of co-factor molecules. FFH was added at a 1:4 ratio. The reactions were set up in triplicates and incubated at 37 °C with orbital shaking at 1000 rpm for 48 h. 100 µl of endpoint reactions (W) were ultracentrifuged using Beckman-Coulter ultracentrifuge at 100'000 g for 30 min at 4 °C. The supernatant (SN) was removed, remaining pellet (P) was washed in PBS twice, then resuspended in 100 µl PBS to yield a fraction containing fibrils. 10 µl of the fractions were mixed with 10 µl 2X Laemmli buffer, and 2 µl per well was loaded on the SDS-PAGE as described above.

Proteinase K digestion of 4R2N P301L fibrils

10 µM of Tau 4R2N P301L was fibrillized in the ClearTau system and the presence of FFH for 24 h. 300 µl of samples were ultracentrifuged, the supernatant removed and the pellet resuspended in 300 ul of PBS. 50 µl of samples were digested by proteinase K (39450-01-6, Invitrogen) at 10 µg/ml for 1 min. The reactions were quenched by the PMSF at 0.3 mM. The samples were imaged using electron microscopy as described above.

RNA-binding assay

Tau 4R2N P301L was fibrillized in the ClearTau system and the presence of FFH for 24 h. 300 µl of samples were ultracentrifuged, the supernatant removed, and the pellet resuspended in 300 µl of PBS. A total of 10 µg/mL of polyU RNA (P9528, Sigma-Aldrich), polyA RNA (P9403, Sigma-Aldrich), or yeast tRNA (R1753, Sigma-Aldrich) were added to 100 µL of 5 µM fibrils in the aggregation assay buffer (Phosphate buffer, pH 7.4). The fibril/RNA mixture was incubated at 37 °C with 550 rpm shaking for 1.5 h. After the incubation, the 80 µL of fibril/RNA-mixtures was centrifuged at 160'000 g at 37 °C for 30 min in an ultracentrifuge. The supernatant was removed, and the pellet was resuspended in 80 µL of aggregation assay buffer with 2% SDS. The concentration of RNA in the supernatant and the pellet (resuspended) was calculated using a Nanodrop One spectrophotometer (Thermo Fischer Scientific) [161]. Spectra were baseline corrected using the buffer as a reference. The concentrations of RNA were calculated from a sample of 10 µg/mL RNA in 100 µL of

aggregation buffer. Measurements were performed with three independently prepared samples in each case.

ClearTau system for screening of Tau aggregation inhibitors, enhancers, and structure modifiers

Monomeric human full-length 4R2N Tau was obtained as described previously and was diluted to 10 µM in phosphate buffer (10 mM Phosphate, 50 mM NaF, 0.5 mM fresh DTT) to obtain a suspension of the monomers in aqueous solution in an Eppendorf tube. 10 µM of the small molecules ATPZ (580222, Sigma), pyrocatechol violet (P7884, Sigma), BSc3094 (B7937, Sigma), LMTX (S7762, Selleckchem), myricetin (M6760, Sigma), DMSO (D841, Sigma), dopamine (H8502, Sigma), L-DOPA (D9628, Sigma), 4-HNE (32100, Cayman), EGCG (E4143, Sigma) were added to monomer, resulting in at 1:1 ratio. The reactions were then transferred to the ClearTau tubes at 200 µl and were placed on an orbital shaker at 1000rpm at 37 °C for 48h aggregation. The reaction mixtures were then ultracentrifuged using Beckman-Coulter ultracentrifuge at 100'000 g for 1 h at 4°C, the supernatant was removed and saved as a Soluble fraction, and the pellet was washed twice with dH2O. The pellet containing fibrils was resuspended in dH2O to 200 µl and labeled Pellet fraction. For EM, 5 µl of the Pellet was loaded as described below. For SDS-PAGE, 10 µl of samples and 10 µl of Laemmli buffer were added, and 5 or 10 µl of each sample was loaded on 15/5% PAA gel. Total protein was visualized by Coomassie stain. The quantification of the soluble and pellet fraction ratios was performed using ImageJ [769] Gel Tool (ImageJ, RRID: SCR_003070).

Statistical analyses and data visualizations

All statistical analyses and data visualizations were performed using GraphPad Prism 9 software (San Diego, USA) and Microsoft Office Suite tools (USA). Atomic visualizations were performed using PyMOL software [773].

Acknowledgments

This work was supported by funding from the EPFL. We thank Pedro Santana Magalhães and Anne-Laure Mahul-Mellier for providing valuable discussions throughout this work and for their critical feedback. We also thank all members of the Lashuel laboratory as well as core facilities for flow cytometry and electron microscopy at EPFL for their support during the preparation of the manuscript. Special thanks to Peter Davies of the Feinstein Institute for providing the MC1

antibody, which has been invaluable to AbbVie Tau research. The antibody was received by AbbVie through a Material Transfer Agreement. We would also like to thank Washington University in St. Louis Genome Engineering and iPSC Center for performing gene editing (funded by Abbvie). We thank EPFL and AbbVie for partial funding of this work.

Author contributions:

HL and GL conceived the project and designed all the experiments. GL performed protein expression and purifications, all the in vitro biophysical and aggregation studies, confocal and transmission electron microscopy imaging, and cell line seeding experiments. RK aided with the biochemical experiment replications and provided technical support. M.-T.W, D.C.S., D.E.E., and L.G performed, analyzed, and supervised the hiPSC experiments. SN, MT, and HS performed, analyzed, and supervised the cryo-electron microscopy experiments included in the supplementary information or the peer review report. HL designed and supervised the study, and provided funding and resources. GL and HL wrote the manuscript with editing comments from all authors.

Competing interests:

HL has received funding from the industry to support research on neurodegenerative diseases, including from Merck Serono, UCB, Idorsia, and Abbvie. These companies had no specific role in the conceptualization and preparation of and decision to publish this work. Hilal Lashuel is also the Founder and Chief Scientific Officer of ND BioSciences SA, a company that develops diagnostics and treatments for neurodegenerative diseases based on platforms that reproduce the complexity and diversity of proteins implicated in neurodegenerative diseases and their pathologies. D.C.S., D.G., P.R., D.E.E., and L.G. are employees of AbbVie. M.-T.W. is a former AbbVie employee. GL, RK, and SN have no conflicts of interest to declare.

..

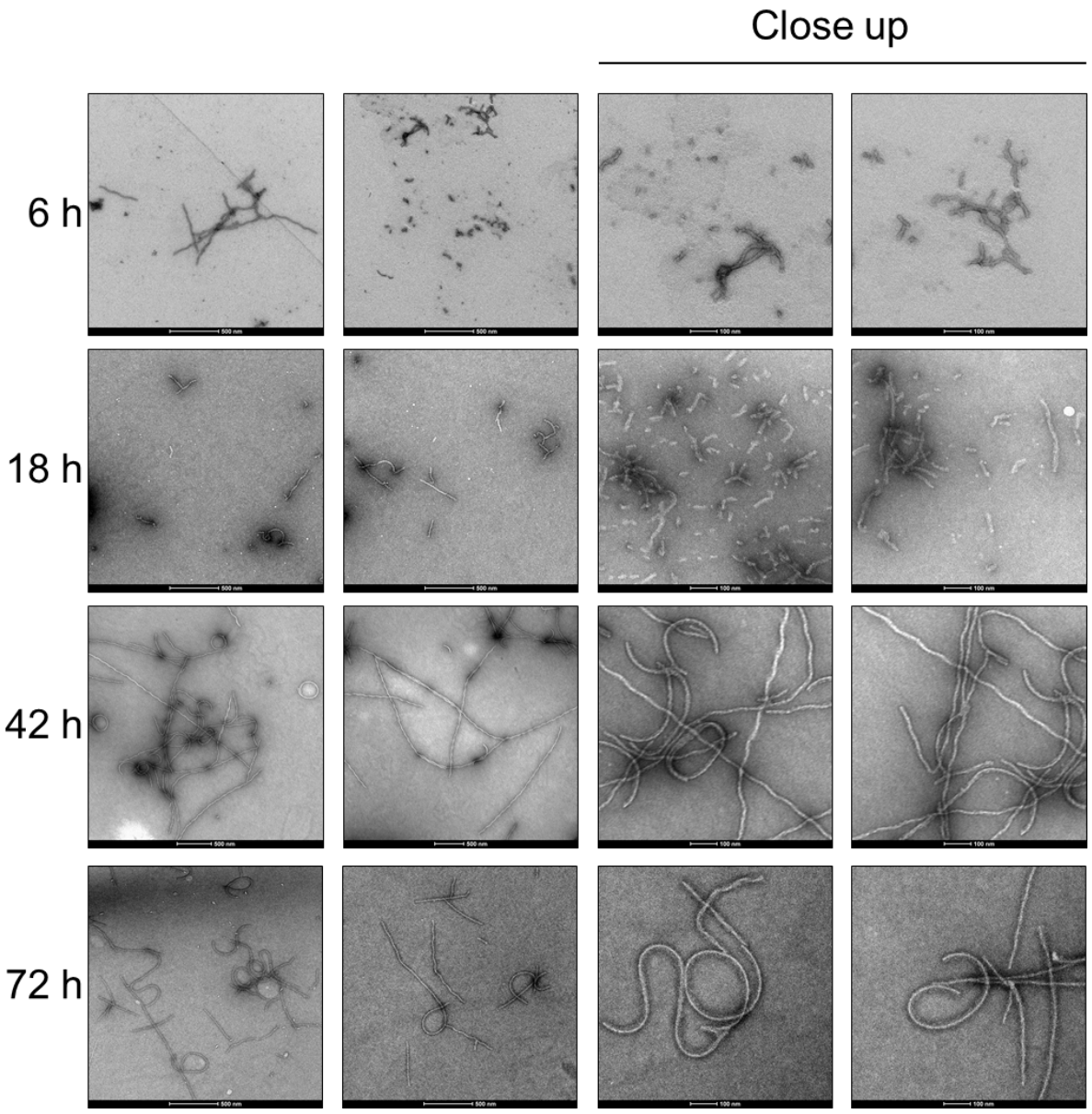

Figure SI1. Electron micrograph gallery of 4R2N ClearTau fibril aggregation overtime.

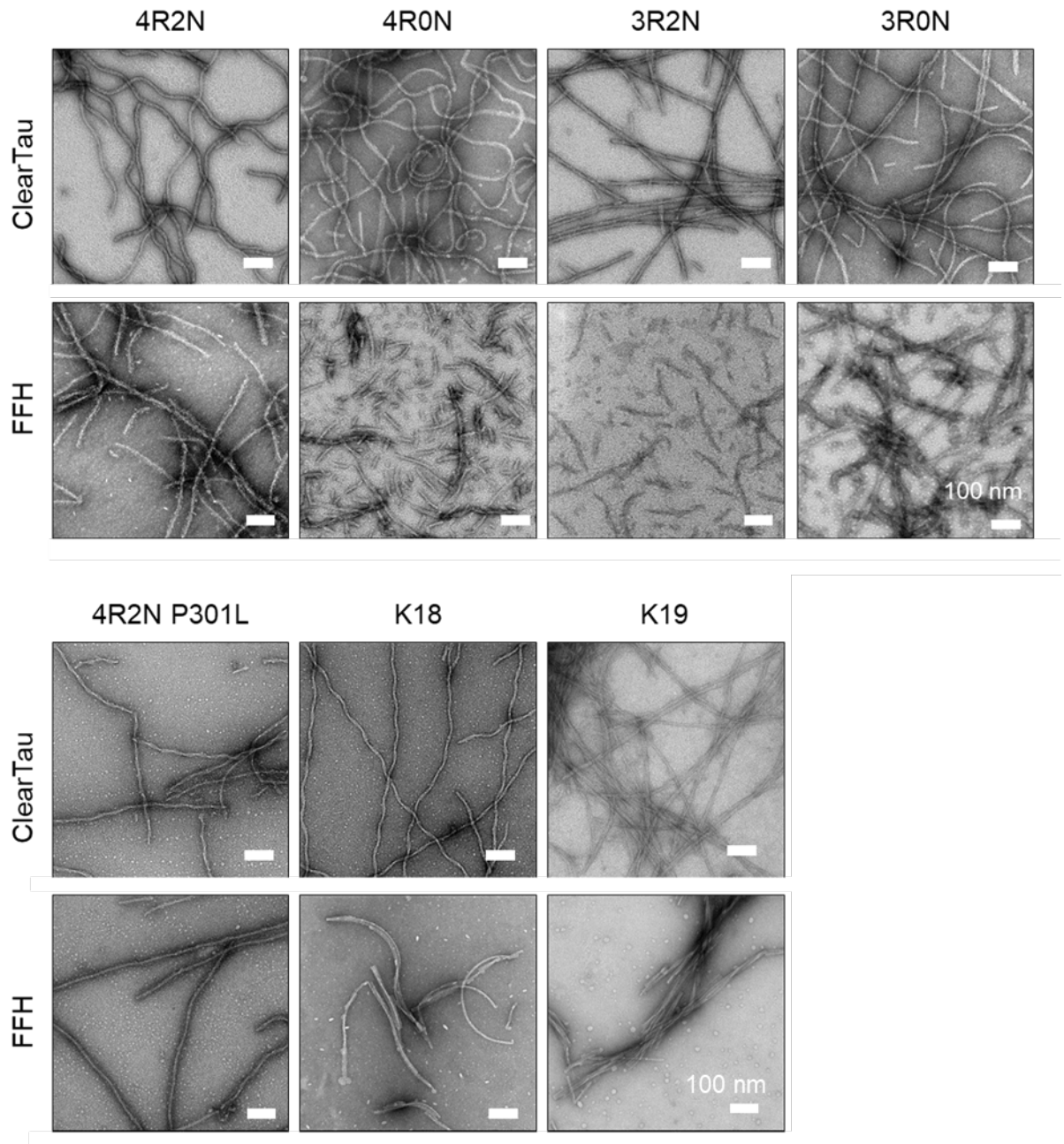

Figure SI2. Relating to Figure 3. A gallery of electron micrographs illustrating Tau variants' fibrillization in the ClearTau system and in the presence of FFH. The size bar = 100 nm

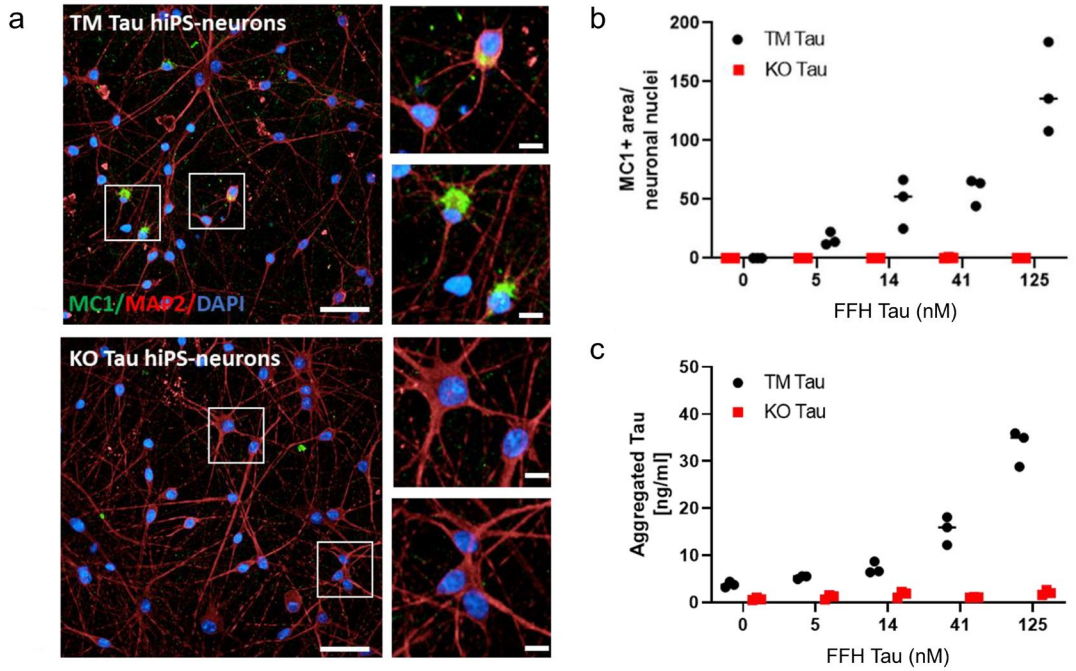

Figure SI3. Free Heparin Tau fibrils induced dose-dependent aggregation of endogenous Tau in TM Tau, but not KO Tau, hiPSC-derived cortical neurons. TM Tau and TauKO hiPS-derived cortical neurons were exposed to different amounts of Free Heparin Tau fibrils generated from recombinant P301L 2N4R Tau. 3 weeks later, the neurons were stained with the MC1 Tau antibody to detect endogenous tau aggregates (green) and MAP2 to stain the neurites (red). Nuclei were stained by DAPI. **a** Representative stack images of TM Tau and KO Tau hiPS-derived neurons treated with 125 nM Free Heparin Tau. **b** Quantification of MC1+ area over neuronal nuclei. Scale bar 50 µm in main panels; 10 µm in insets. Two-way ANOVA: seed concentration $p < 0.0001$, genotype. **c** Aggregation of endogenous Tau was evaluated by symmetric ELISA (Tau12/Tau12, N = 2 independent cultures, n = 3 replicates each). Two-way ANOVA: Tau concentration $p < 0.0001$, genotype $p < 0.0001$. Images and graphs represent data from one experiment. 2 independent experiments with 3 replicates/condition were performed for immunofluorescence analysis. In one experiment, biochemical analysis was also performed.

Table SI1. Quantification of ClearTau isoform fibril widths

	4R2N	**4R1N**	**4R0N**	**3R2N**	**3R1N**	**3R0N**
Number of fibrils	618	470	621	225	521	516
Median	15.17	15.69	15.67	14.49	14.05	12.35
Mean	15.20	15.83	15.70	14.73	14.49	12.49
Std. Deviation	2.24	3.49	3.04	2.55	3.19	2.59

Table SI2. Quantification of ClearTau isoform mixtures' fibril widths

	All			**2N +1N**			**2N**			**1N**		
ClearTau reaction	**1**	**2**	**3**	**1**	**2**	**3**	**1**	**2**	**3**	**1**	**2**	**3**
Number of fibrils	307	313	337	230	210	89	145	89	89	116	108	124
Mean	15.15	11.02	15.08	16.71	16.52	15.3	17.08	16.66	15.11	19.84	16.46	17.01
Std. Deviation	3.03	1.83	3.00	3.25	3.23	3.08	3.39	2.96	2.99	3.44	3.43	3.40

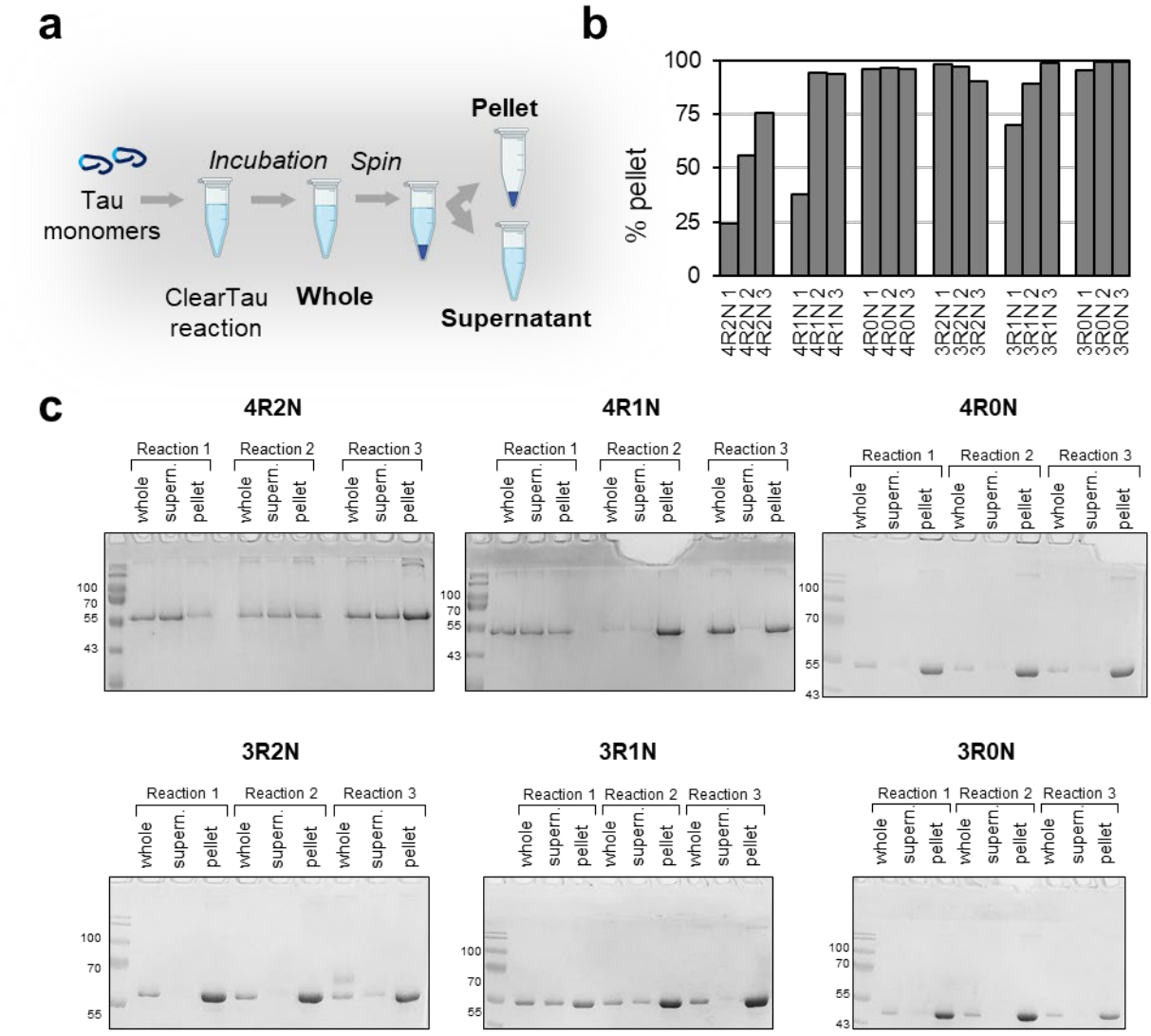

Figure SI4. Characterisation of monomer incorporation into the fibril-containing Tau pellet fraction across three independent ClearTau repeats for each Tau isoform. Three independent ClearTau aggregation reactions for each Tau isoform (18 in total) were set up at 100 µM for 48 h at 37 °C under shaking conditions. The ~500 ul mixtures were ultracentrifuged at 100'000g for 1 h, supernatant was removed, pellets washed in dH2O twice and resuspended in 500 ul of dH2O. PAAG gels were run by loading 10 µl of supernatant or pellet + 10 µl 2X Laemmli buffer, or 5 µl Whole + 15 µl Laemmli buffer. Whole samples were loaded at half the amount to prevent the oversaturation. Whole sample signals were not included in the quantification. **a** Workflow of the fractionation protocol to separate the Tau fibrils (*pellet*) and monomers (*supernatant*). **b** Quantification of the monomer-to-fibril proportion of all 18 reactions shows efficient incorporation of monomers into the fibrillar fraction as early as at 48 h of the reaction in the current set up. **c** The whole, supernatant and pellet fractions were loaded on the SDS-PAGE gel and stained with the Coomassie total protein stain to assess fibrillization efficiency and monomer incorporation. All isoforms across all three independent repeats show efficient formation of the fibrils separated into the pellet fractions.

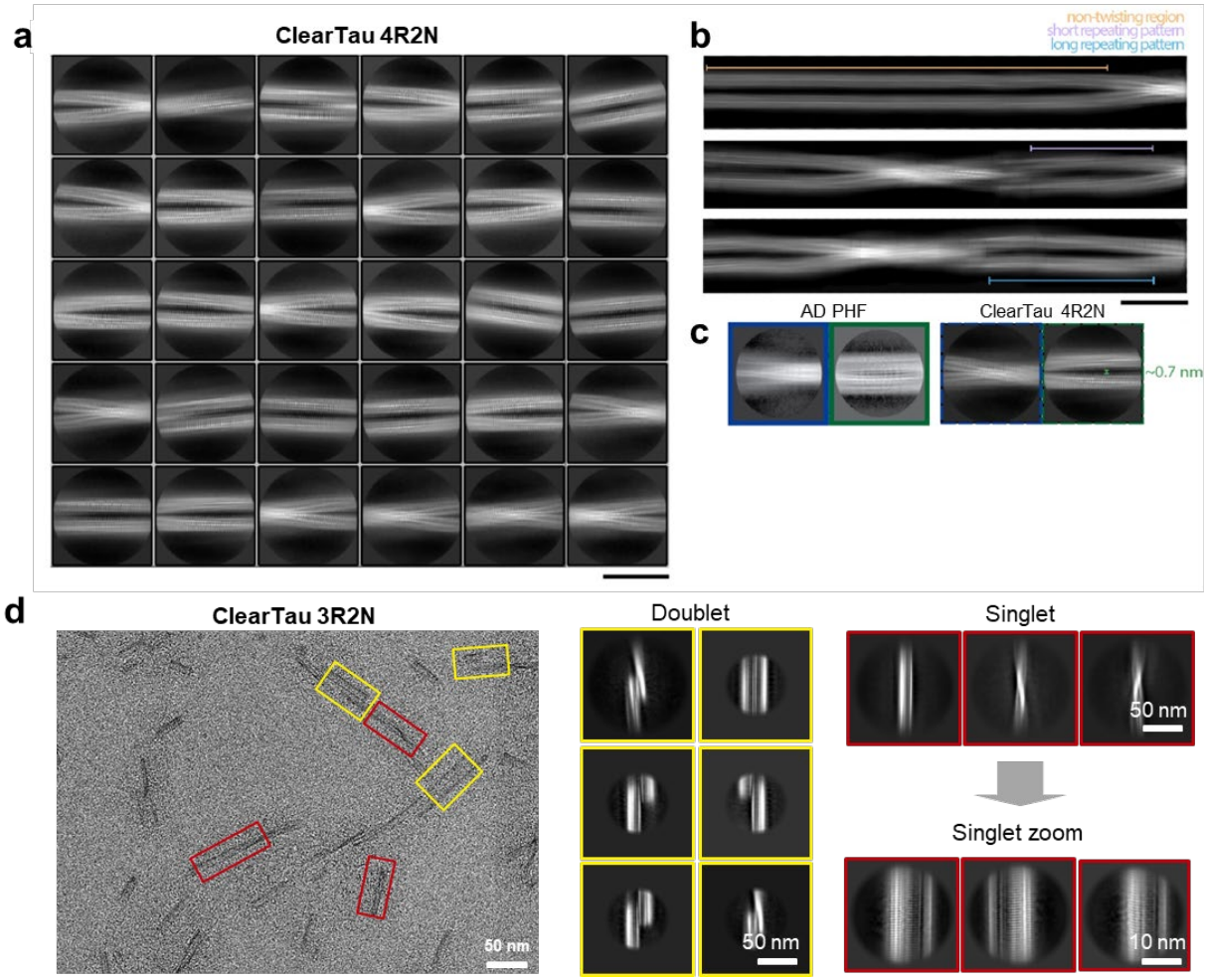

Figure SI5. Cryo-EM micrograph of fibrils from ClearTau 4R2N a-c and ClearTau 3R2N d proteins. a 2D classes of ClearTau 4R2N isoform depicts different views of the fibril; two protofilaments assemble to form the fibril. **b** 2D classes were mapped back to their original positions to reveal long fibrils. Three types of fibrils have been observed; the fibrils with non-twisting regions (orange) are the lowest in number. Twisting filaments vary in cross-over distance; two (purple and blue) are shown here. The filaments with the short repeating pattern (purple) are the most abundant. **c** Compared to patient-derived AD PHF on the left [189], there is a bigger gap between the protofilaments in this study (on the right). Scale bars 20 nm. **d** ClearTau 3R2N. Selected singlets and doublets are outlined with red or yellow boxes. Representative 2D class averages of singlets and doublets from large 900-pixel segments downscaled to 300 pixels with a visible twist of the amyloid core. Representative 2D class averages of singlets from 300 pixel non-scaled segments with clear amyloid core and 4.77 Å separation of beta-strands. Scale bars = 10 and 50 nm.

Table SI3. Quantification of ClearTau and FFH 4R2N P301L fibril widths pre- and post-proteolysis with proteinase K.

	ClearTau 4R2N P301L		**FFH 4R2N P301L**	
Reaction	**-PK**	**+PK**	**-PK**	**+PK**
Number of fibrils	200	200	200	200
Mean	18.50	15.10	12.90	9.50
Std. Deviation	2.50	2.23	2.84	1.85

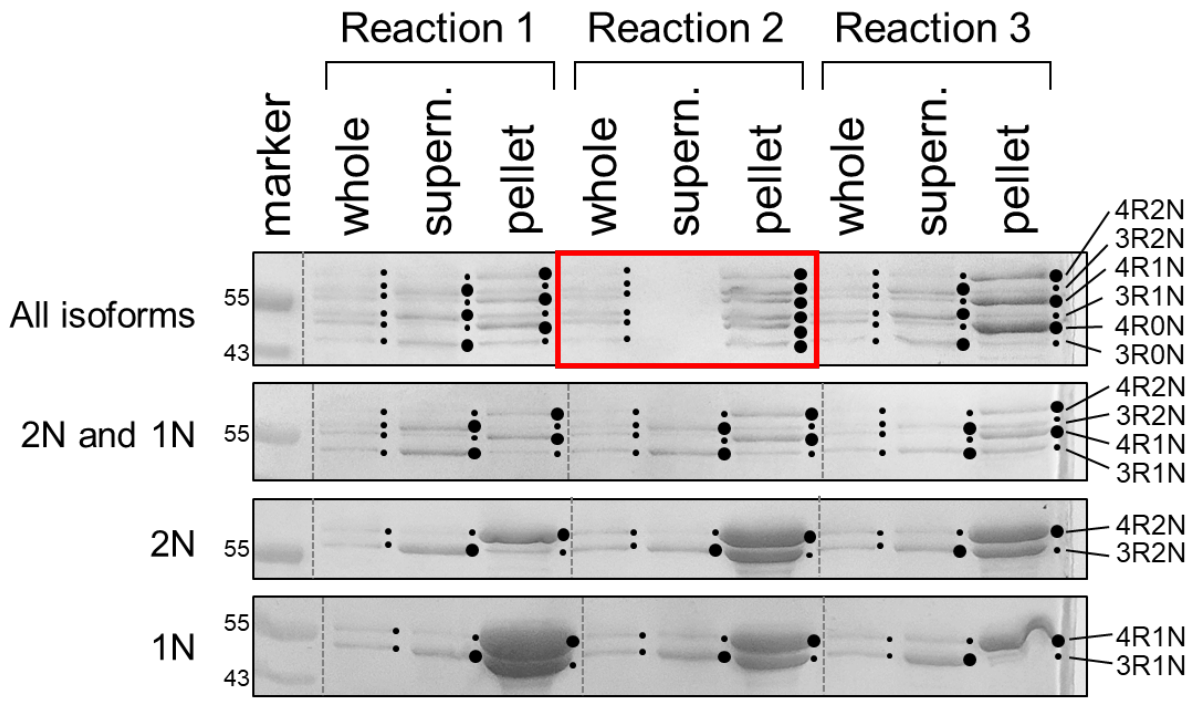

Figure SI6. Annotated SDS-PAGE gel of the Tau isoform mixtures shows relative incorporation of the Tau isoform monomers into the ClearTau fibrils. The circle size besides each band indicates the relative amount for better perception. The *whole* samples contain equal amounts of all isoforms as expected. Across the triplicate repeats for all mixtures, the 4R-containing Tau isoforms were more efficiently incorporated into the fibrils. The notable exception was All isoforms Sample 2 (red box), that demonstrated the complete incorporation of all the Tau monomers into the fibrils, at the same time showing the highest thioflavin S fluorescence and singlet Tau filaments (see main text). The ClearTau reactions were performed at 100 μM initial Tau concentration for 48 h with orbital shaking at 1000 rpm at 37 °C. The ~500 ul mixtures were ultracentrifuged at 100'000g for 1 h, supernatant was removed, pellets washed in dH_2O twice and resuspended in 500 ul of dH_2O. Polyacrylamide gels were run by loading 10 μl of supernatant or pellet + 10 μl 2X Laemmli buffer, or 5 μl Whole + 15 μl Laemmli buffer. Whole samples were loaded at half the amount to prevent the oversaturation.

Table SI4. Quantification of widths of Tau fibrils in the presence of compounds.

	DMSO	**ATPZ**	**Pyrocatechol violet**	**BSc3094**	**LMTX**	**Myricetin**	**Dopamine**	**L-DOPA**
Fibrils number	100	58	103	60	101	104	102	101
Mean (nm)	15.0	13.3	9.15	14.4	14.6	9.45	20.7	11.3
Std. Deviation	3.23	2.34	1.72	2.65	2.38	1.70	2.79	2.72

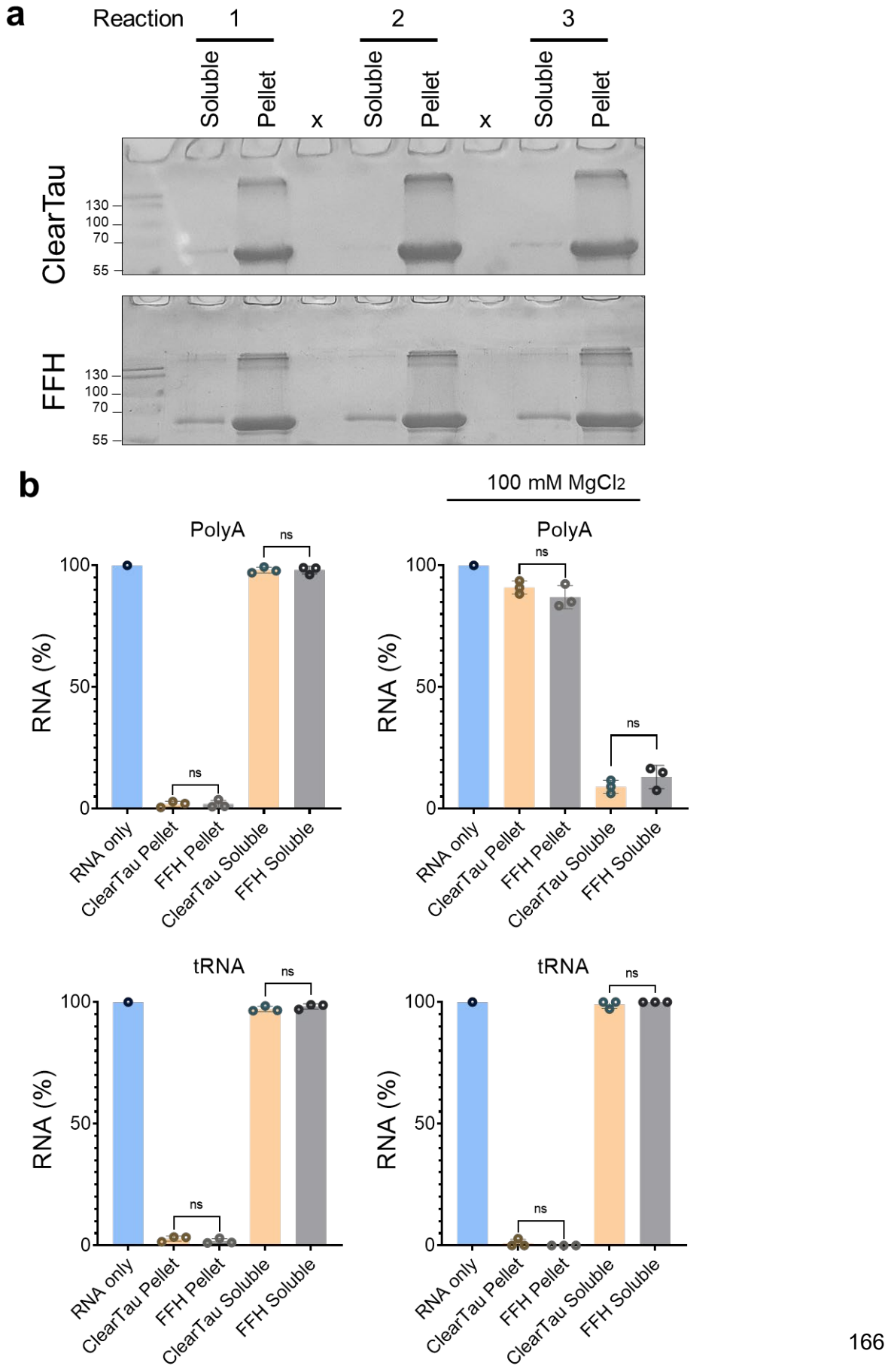
a
Reaction
1
2
3
Soluble
Pellet
x
Soluble
Pellet
x
Soluble
Pellet
ClearTau
FFH
130
100
70
55
b
100 mM MgCl2
PolyA
tRNA
RNA (%)
100
50
0
ns
RNA only
ClearTau Pellet
FFH Pellet
ClearTau Soluble
FFH Soluble

Figure SI7. Monomer incorporation into the fibrils and RNA-binding capacity of Tau 4R2N P301L in the ClearTau system and in the presence of FFH. a Three independent samples were fibrillized at 100 µM for 24h, the ~500 µl mixtures were ultracentrifuged at 100'000g for 1 h, supernatant was removed, pellets washed in dH_2O twice and resuspended in 500 µl of dH2O. Polyacrylamide gels were run by loading 10 µl of supernatant or pellet + 10 µl 2X Laemmli buffer. **b** PolyA and tRNA binding capacity of 4R2N P301L fibrils in the aggregation buffer and in the higher ionic strength buffer (+ 100 mM $MgCl_2$).

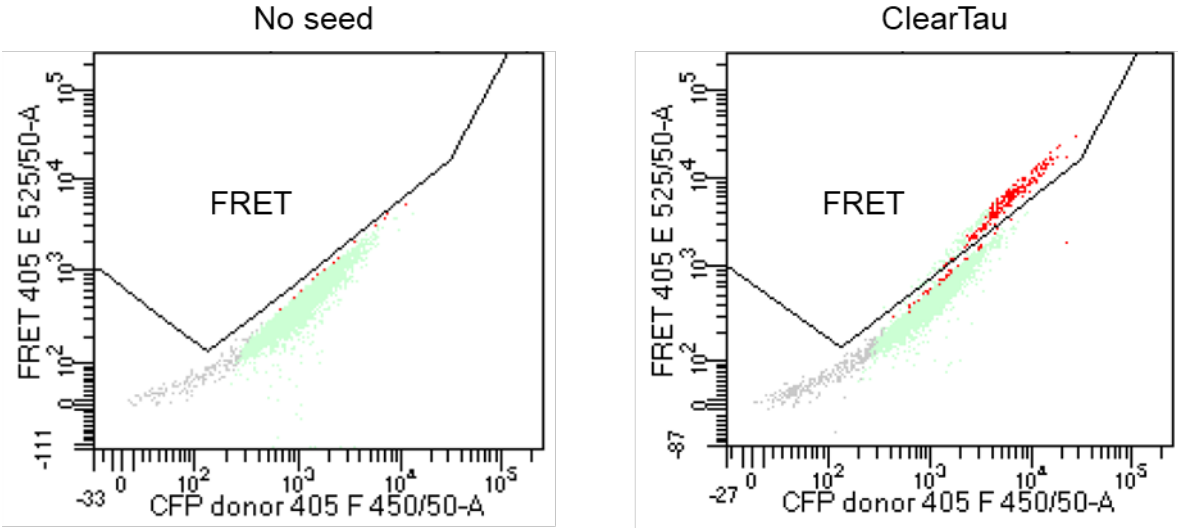

Figure SI8. FRET flow cytometry bivariate plots. FRET vs. CFP donor bivariate plots depict the FRET-negative HEK293T TauRDP301S biosensor cells used to configure the gating strategy to detect FRET-positive ClearTau-seeded HEK293T TauRDP301S biosensor cells**.**

xx

CHAPTER 4

What exactly are Tau biosensor assays sensing? In-depth characterization of the commonly used cellular model thought to report on the Tau seeding propensity

Galina Limorenko and Hilal Lashuel

Laboratory of Molecular and Chemical Biology of Neurodegeneration, Brain Mind Institute, School of Life Sciences, Ecole Polytechnique Fédérale de Lausanne, CH-1015 Lausanne, Switzerland.

Abstract

One of the dominant topics in the research into pathological Tau aggregation is the assessment of the propensity of Tau species', detected in Tauopathy patient brains, tissues, and fluids, to convert the normal Tau proteins into pathological forms upon contact, and these species are referred to as "seeds". This process is thought to play an important role in Tau pathology formation and spreading in the brain. Therefore, to investigate the molecular and cellular determinants of seeding and pathology spreading, investigators have sought to develop easy-to-use approaches to detect the pathological Tau seeds and seeding-mediated Tau fibrillization. One such cellular model that is most commonly used by the research community today is the Tau Biosensor cells, based on the use of HEK293T overexpressing the K18 mutant P301S Tau fragments tagged with CFP or YFP (TauRD). Despite the large number of papers using these Tau Biosensor cells and their increasing use in drug discovery and validation assays, very little is known about the structural and biochemical properties of the Tau aggregates that form in these cells. Therefore, there is an urgent need for an in-depth understanding of what exactly is the relationship between the seed, expressed tagged Tau constructs, and other cellular components and processes and how these interactions give rise to the signals measured in these cells. In this chapter, we asked three key questions: a) does TauRD cellular assay truly report the aggregation-triggering propensity of the transduced Tau seeds; b) can it determine the differences between the various types of Tau seeds; and c) what cell physiological processes are implicated in the output generation of the TauRD system? Ultimately, we seek to answer the question of whether this and similar systems can be reliably used as a characterization technique for Tau seeding propensity, and give recommendations on what is needed to improve it. We extensively characterized and assessed the TauRD system using observational, functional, and interventional assays, including imaging, correlative light and electron microscopy (CLEM), and biochemistry. Our findings suggest that a) the TauRD system does not explicitly report on the human pathology-relevant seeding propensity of the Tau seeds; b) the TauRD system does not faithfully distinguish between different types of seeds, and c) the formation of the expected output signal is heavily dependent on the cellular proteostasis functioning. Our results show how cells are responding to the Tau fibrillar seeds, and how it impacts their physiology. Our findings underscore the critical importance of characterizing cellular models at the molecular, biochemical, and ultrastructural levels to verify that they report on the desired aggregation processes. This is crucial to prevent us from embarking on a "wild goose chase", and focus our efforts on molecular targets that are implicated in human disease, and not just found in the cell culture dish.

Introduction

Tau protein aggregation is a hallmark of a family of neurodegenerative disorders termed Tauopathies. Alzheimer's disease (AD) is by far the most well-known disorder and underlies the largest proportion of dementia diagnoses[774]. Thus far, no definitive diagnostic tests, effective treatments, or disease-modifying therapies for Tauopathies have been developed. To reach these goals, easily accessible cellular and animal models that faithfully reproduce different features of the disease processes are needed. Increasing evidence point to major differences in the biochemical and structural properties of Tau pathological aggregates in the brain of patients with tauopathies and Tau aggregates produced in cell-free systems or used in drug discovery and to develop PET tracers and diagnostic assays. These observations underscore the critical importance of bridging this divide and investigating Tau aggregation and pathology formation in the complex cellular environment. Therefore, cellular models of Tau aggregation have emerged as the ideal tools to bridge this gap, because they allow not only direct monitoring of protein aggregation in the physiological milieu of the cell but also allow for assessing cellular responses to this process. This usually requires modification of the protein sequence and/or the addition of fluorescent proteins.

One of the major challenges in using these systems is to be able to directly monitor the aggregation process and to know whether they indeed recapitulate the relevant processes in the diseases they are meant to model. Among the most commonly used approaches to study Tau conversion from soluble disordered monomers into structured oligomers and higher-order fibrillar assemblies is the use of fluorescent proteins to tag the protein of interest and monitor their aggregation. Several assays have been developed to monitor early oligomerization events of Tau and other amyloid proteins, including assays utilizing FRET, bi-molecular fluorescence complementation (BiFC), and split luciferase complementation (SLC) technologies, among many others. These approaches rely on the close proximity of the fluorophores tagging the protein of interest to generate the output signal. FRET involves the transfer of energy between two fluorophores [775] at a close proximity of 10 nm or less [776,777], designated as donor-acceptor pair [778]. The homo-FRET approach utilizes a singular fluorophore selected to display a small Stokes shift and a large excitation-emission wavelength overlap, such as enhanced GFP. Hetero-FRET employs two fluorophores and is a popular approach for the measurement of oligomerization of amyloidogenic proteins such as Tau and α-synuclein (reviewed in [755] and [779] respectively). The commonly used hetero-FRET combinations include cyan and yellow (CFP-YFP) and green and red (GFP-RFP) fluorescent protein pairs, among many others (reviewed in [778]).

The most likely mechanism of the signal generation is the association of the two, or a small number of molecules of the tagged Tau, however, the assay does not determine the nature of this association, such as transient interactions of disordered soluble monomers, formation of non-amyloidogenic amorphous oligomers (OFF-pathway) or β-sheet containing amyloidogenic precursor oligomers (ON-pathway). The only prerequisite for the FRET between the fluorophore pair is their proximity of 10 nm or less irrespective of the interactions of the protein tagged with them. The addition of a large fluorescent tag onto an often-small protein molecule of interest may hinder and obstruct its normal activity, and interfere with the tag with the protein oligomerization and assembly due to steric hindrance. These issues could lead to erroneous and misleading measurements of the protein-protein interactions. Thus, determining the nature of these interactions and the biochemical characterization of the resultant Tau assemblies that give rise to the FRET signal is essential to ascertain the relevance to the Tau aggregation mechanisms in these cellular models to those occurring in the brain of patients with Tauopathies.

Tau seeding investigations

One of the dominant topics in the research into pathological Tau aggregation is the assessment of the propensity of Tau species' detected in Tauopathy patient brain, tissues, and fluids to convert the normal Tau proteins into pathological forms upon contact, and these species are referred to as "seeds". This has been preliminarily designated as a prion-like propagation of Tau pathology [780], and it is facilitated by the cell-to-cell transfer of Tau through direct secretion and uptake through extracellular vesicles, tunnelling nanotubes, receptor-mediated endocytosis, or other pathways (reviewed in [751]). Prion-like Tau propagation paradigm is compatible with the observations of Tau pathology formation along the anatomically-connected brain regions in different Tauopathies, as well as in the animal models [619]. Therefore, investigating this specific aspect of the pathogenicity of Tau seed – the seeding potential – has garnered much attention from investigators. The general concept of this experimental approach is the induction of the aggregation of native Tau in its physiological state in vitro, in cell cultures, or in animal models via the addition of preformed Tau aggregates/seeds prepared from recombinant proteins, isolated from animal models of Tauopathies, or isolated from the brain of patients with AD or other Tauopathies. Changes in the physiological state of the naïve Tau or its aggregation are measured by assessing increased accumulation of in insoluble Tau species in vitro or in vivo, increased Tau

phosphorylation, or the signals generated by specific designed probes that selectively binds to Tau aggregates (i.e. Thioflavin S/T, Congo Red, Amytracker and others).

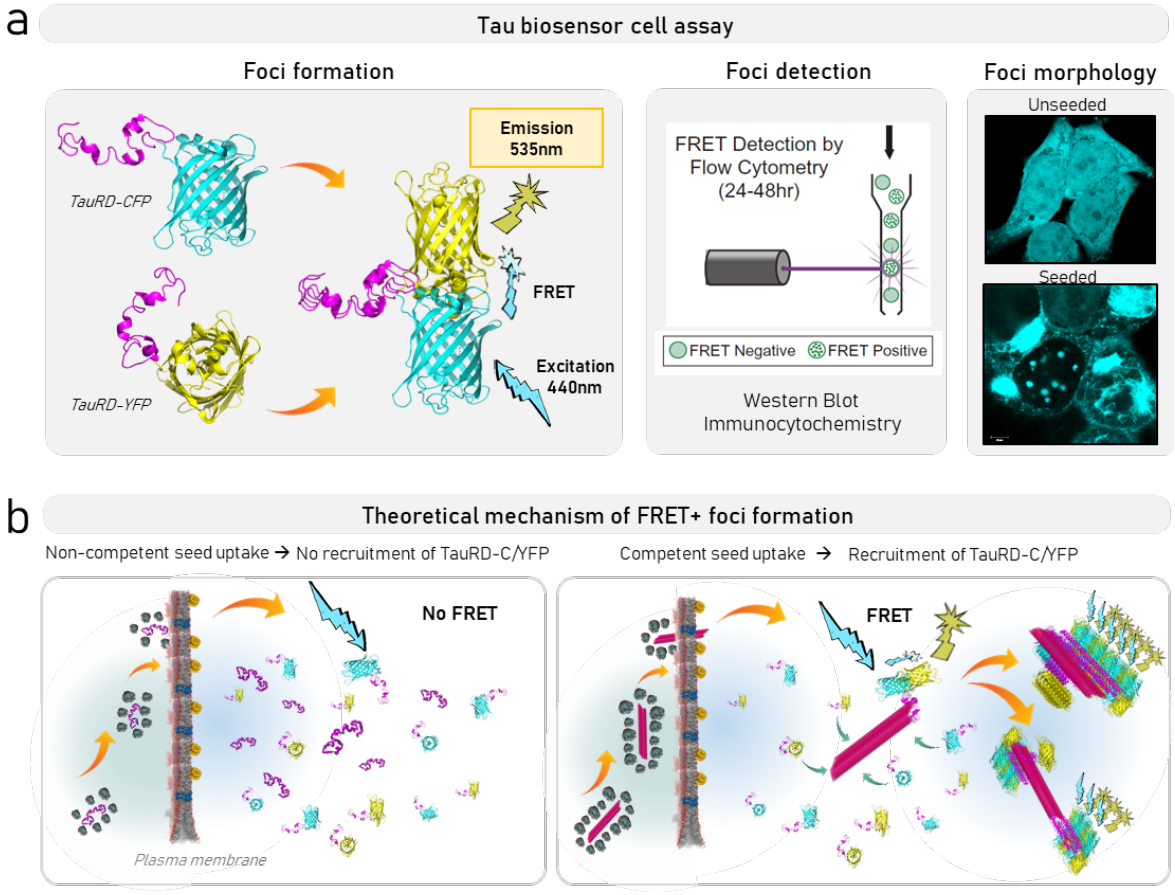

Figure 1. Stylized theoretical mechanism of TauRD cell biosensor assay. a. HEK293T cells stably express the tagged K18 mutant P301S Tau fragments or other Tau forms tagged with CFP or YFP. When the fluorophores come together in close proximity, the FRET signal is generated and can be detected by flow cytometry or confocal imaging. b. Seeding-competent Tau species generate the FRET signal when added to cells.

FRET TauRD biosensor cells

To allow for direct detection and monitoring of Tau seeded-mediated aggregation processes, Holmes et al. developed FRET biosensor cells that become fluorescent upon the addition of preformed Tau aggregates of seeding competent species[781] (Figure 1). Briefly, the HEK293T cells stably express the tagged K18 mutant P301S Tau fragments or other Tau forms tagged with CFP or YFP. At the baseline, in the naïve state, the cells morphologically show diffuse fluorescence throughout cell cytoplasm and in the nucleus, and no FRET signal is generated. The exogenous seed is then added to the cell culture and is internalized into the cells. The lack of the seeding propensity is defined by no deviation from the baseline, i.e. the

fluorescence of the cells remains diffuse, no FRET or sarcosyl-insoluble Tau species are detected, presumably due to the failure of the seed to induce the recruitment, and the association of the tagged endogenous constructs. On the contrary, the indication of seeding propensity by the added Tau seed is defined by the presence of the FRET signal, and the level of seeding is reflected by the localized accumulation of different amounts of tagged Tau constructs in the form of foci of different sizes. The biochemical and ultrastructural properties of Tau in these foci structures remain poorly characterized.

When the seeding-potent Tau species are added to cells, after 24 or 48 h the bright structures are observed in the cell cytoplasm and nuclei, concomitant with the disappearance of the diffuse fluorescent signals. The variable morphologies of these structures in the cytoplasm range from small, thin, long, and short hair-like, to rods and puncta, to large extended web-like assemblies, and the morphologies change and evolve when observed over time. Nuclear foci differ from cytoplasmic foci in their shapes and sizes, predominantly forming fluid gel-like round globules, that are regularly interspersed throughout the nucleus, and over time mature from small round to large round, to large filamentous assemblies. Furthermore, co-staining experiments indicate that these assemblies differ in their molecular contents, such as cytoskeletal components present in the cytoplasmic structures, and nuclear structures being enriched with RNA.

Another study by the same team [781] used the flow cytometry-based FRET biosensor detection assay (FRET BS). Here, the K18 mutant P301S Tau fragments tagged with CFP or YFP were stably expressed under the human ubiquitin C promotor in the HEK293 cell line. A similar seeding paradigm with preformed exogeneous K18 fibrils and lysates from the brains of P301S transgenic mice or Alzheimer's disease patients' brains was employed. The seeded HEK293 cultures were sorted based on the FRET signal presence or absence, and the resultant cell population sizes were quantified and compared. In this work, no biochemical characterization of the resultant Tau species was performed, and the negative control samples included α-synuclein and huntingtin (Q50) fibrils. Despite the relative ease of the classification of the HEK293 cells based on the FRET presence/absence, the nature of the Tau proteoforms formed by the tagged P301S K18 constructs was uncertain, and it has not been possible to rule out the possibility that it could also arise due transient associations of between soluble Tau molecules, a non-specific association of the Tau constructs with the added seeds but no oligomerization, or other physiological processes occurring in cells as a result of the seed addition. In subsequent studies, the three strains of Tau seed isolated from HEK293 YFP-tagged P301L/V337M K18 Tau [782], designated DS1 (non-seeding), DS9, and DS10 (seeding)

were tested in the FRET BS assay for the FRET signal, in parallel with the sedimentation to assay the presence of insoluble species [783]. Clones DS9, DS10, and their derivatives showed both FRET and the presence of insoluble pellets in the sedimentation assays. However, despite the near absence of the insoluble pellet of the non-seeding clone DS1, the FRET fluorescence showed a signal indistinguishable from the seeding clones. This discrepancy between FRET assay output and biochemical analyses, and several other observations, underscore the importance of a more thorough characterization of this model.

In this chapter, we ask three key questions: a) does Tau FRET BS cellular assay truly report the aggregation-triggering propensity of the transduced Tau seeds; b) can it determine the differences between the various types of Tau seeds; and c) what cell physiological processes are implicated in the output generation of the FRET BS system? We extensively characterized the FRET BS system using imaging approaches, such as co-localization confocal, live, correlative light and electron microscopy; and biochemistry, such as by the cellular fractionation assays. We assessed the FRET BS using interventional functional assays, such as seeding assays with different recombinant Tau seeds, manipulation of the cell cycle using protein synthesis inhibition by nutrient deprivation or inhibitors, seeding of the FRET BS cultures with sequential extracts from the initially-seeded or non-seeded FRET BS cultures, and overexpression of different Tau isoforms in the BS cells from the transfected plasmids. Ultimately, we seek to answer the question of whether this and similar systems can be reliably used as a characterization technique for Tau seeding propensity, and what could we do to improve it.

Results

Fibrillar Tau seeds induce the formation of FRET+ foci

FRET flow cytometry assay is used to assess the appearance of FRET-positive foci in HEK293T TauRDP301S biosensor (TauRD) cell line [755] induced by the Tau fibrils. Therefore, we generated fibrils of Tau 4R2N, 4R0N, 3R2N, 3R1N, 3R0N, tetramethylrhodamine (TAMRA)-labeled K18, K18 and microtubule-binding fragment (MBF) by incubating the monomeric proteins in 10 mM phosphate pH 7.4, 50 mM NaF and 0.5 mM DTT with heparin sodium salt (Applichem GmbH) at molar heparin: protein ratio of 1:4 under constant orbital agitation (1000 rpm, Peqlab, Thriller) at 37°C for up to 72 hours. Heparin-induced fibrils are designated by the prefix h-. We also used fibrils generated under conditions that lead to the

formation of PHF-like filaments, designated by rPHFs from isoforms 4R2N, 4R1N, and 4R0N were prepared as described in[784].

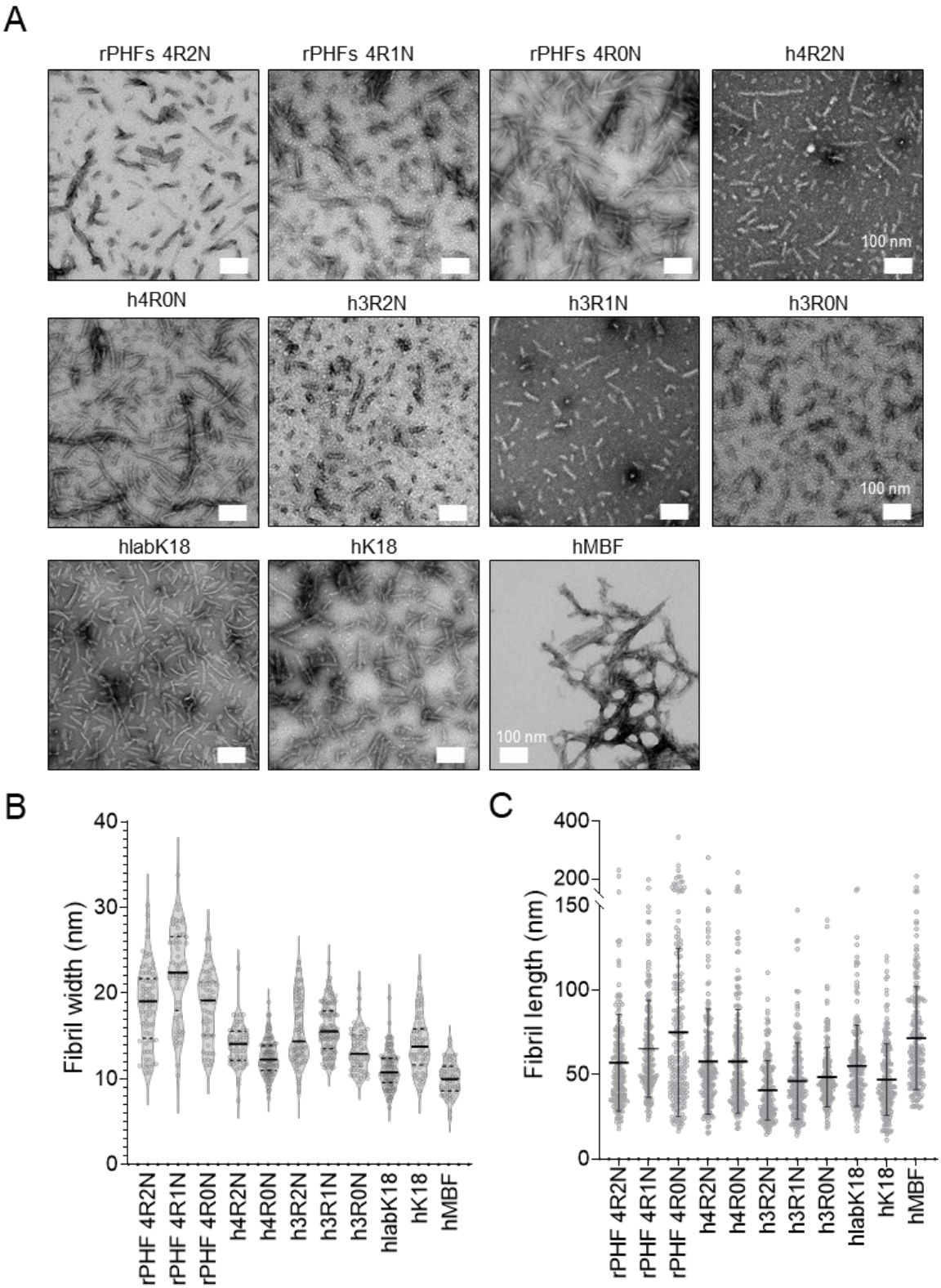

Figure 2. Characterization of Tau seeds from different isoforms by EM. A. EM imaging of the fibrillar seeds. B. Width and C. Length quantifications of the fibrillar seeds. hlabK18= labelled Tau K18; MBF= microtubule-binding fragment.

Fibrils were diluted to 10 μM in dH_2O and sonicated at 70% amplitude for 50 s with 1 sec ON 1 sec OFF cycle in-tube using UP200St with VialTweeter (Hielscher, USA). Seeds were characterized by electron microscopy (Figure 2) and their diameters were measured (Table 1).

TauRD cells were seeded with monomeric or fibrillar forms of Tau at 500 ng/ml for 48h to assess the potential of the seeds to trigger the formation of the bright foci. The foci formation was assessed using live cell imaging, confocal imaging, and FRET flow cytometry. Live cell imaging shows no formation of the bright foci in the cultures seeded with the monomeric Tau 4R2N, K18, MBF, and no seed control. The cultures seeded with fibrillar rPHF 4R2N, h4R2N, hK18, and hMBF fibrillar seeds induced the formation of the foci (orange arrows).

Confocal microscopy confirmed the presence of cytoplasmic and nuclear foci in the rPHF 4R2N, h4R2N, hK18, and hMBF fibril-seeded cultures (Figure 3A), but not in cells treated with their monomeric forms. FRET flow cytometry showed the highest proportion of the TauRD cell population with the foci was in hK18 seeded culture at 35.9%, followed by the h4R2N at 10.3%, with both rPHF 4R2N and hMBF at less than 1% (Figure 3B). When other isoform fibrils were tested, however, only a small fraction of the population, under 1%, were detected by FRET flow cytometry for fibrils h4R0N and h3R1N, as well as by confocal imaging (Figure 3C and D). Interestingly, however, this was in discrepancy to the confocal imaging detection of the foci for fibrils rPHF 4R1N, rPHF 4R0N, h4R1N, and h3R2N but not by flow cytometry. No foci or flow cytometry detection was observed for cultures seeded by fibrils h3R0N, Tau isoform corresponding to human fetal Tau.

Table 1. Characterization of Tau seeds

	rPHF 4R2N	rPHF 4R1N	rPHF 4R0N	h4R2N	h4R0N	h3R2N	h3R1N	h3R0N	hlabK18	hK18	hMBF
N of fibrils	72	58	53	54	104	65	100	54	101	52	51
Median (nm)	19.0	22.4	19.1	14.1	12.3	14.4	15.5	12.9	10.8	13.8	9.97
Mean (nm)	18.7	22.4	18.5	14.0	12.5	15.6	15.9	13.4	11.1	14.0	10.0
Std. Dev. (nm)	4.60	5.27	3.96	2.48	2.04	3.74	2.80	2.42	2.14	3.13	1.95

These results suggest that the fibrillar, but not monomeric forms of Tau trigger foci formation in TauRD cells, in line with the previous reports. The highest extent of the population was seen

in the hK18-seeded cultures, whereas most fibrillized Tau. The discrepancy between FRET flow cytometry and confocal imaging was found for fibrils rPHF 4R1N, rPHF 4R0N, and h4R1N in the detection of the foci.

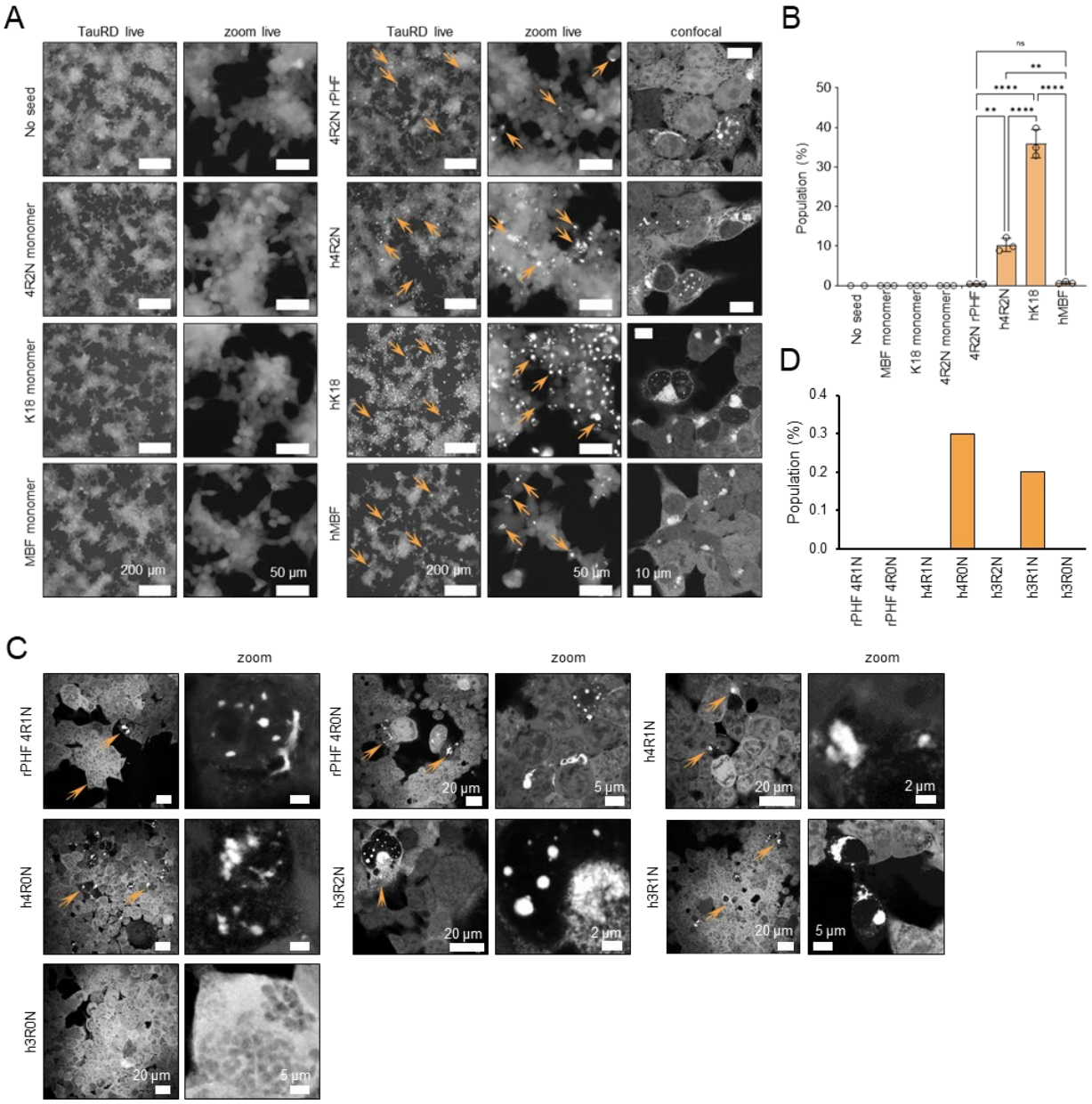

Figure 3. TauRD cells seeded with preformed Tau seeds. A. Live cell and fixed cell confocal microscopy imaging. Orange arrows indicate the formed fluorescent foci. B. Quantification of the percentage of the cell population with foci by FRET flow cytometry. C. FRET flow cytometric detection in the cells seeded with multiple Tau isoform fibrils. D. Flow cytometry quantification of the cell population proportions with FRET-positive signal.

The fate of the seeds inside the TauRD cells

Next, to discern the fate of the fibrils added to cells, very early time points or the internalization were captured using live-cell imaging over up to 1 h and 15 min. Cells were treated with the labelled fibrillar K18 (hlabK18) and immediately imaged for 75 min. DRAQ5 was used as a nuclear marker. The imaging shows that the distinguishable diffuse fluorescence of the hlabK18 within the cells started around 18 min after treatment (Figure 4, white arrows), whereas the larger punctated agglomerations of hlabK18 started appearing at around 27 min (Figure 4, yellow arrows). This shows that fibrillar seed is initially taken into the cell cytoplasm, and after about half an hour is sequestered into the puncta. As time progressed, the punctate fluorescence of the engulfed seed was apparent in the cells at 75 min (Figure 4, yellow arrows).

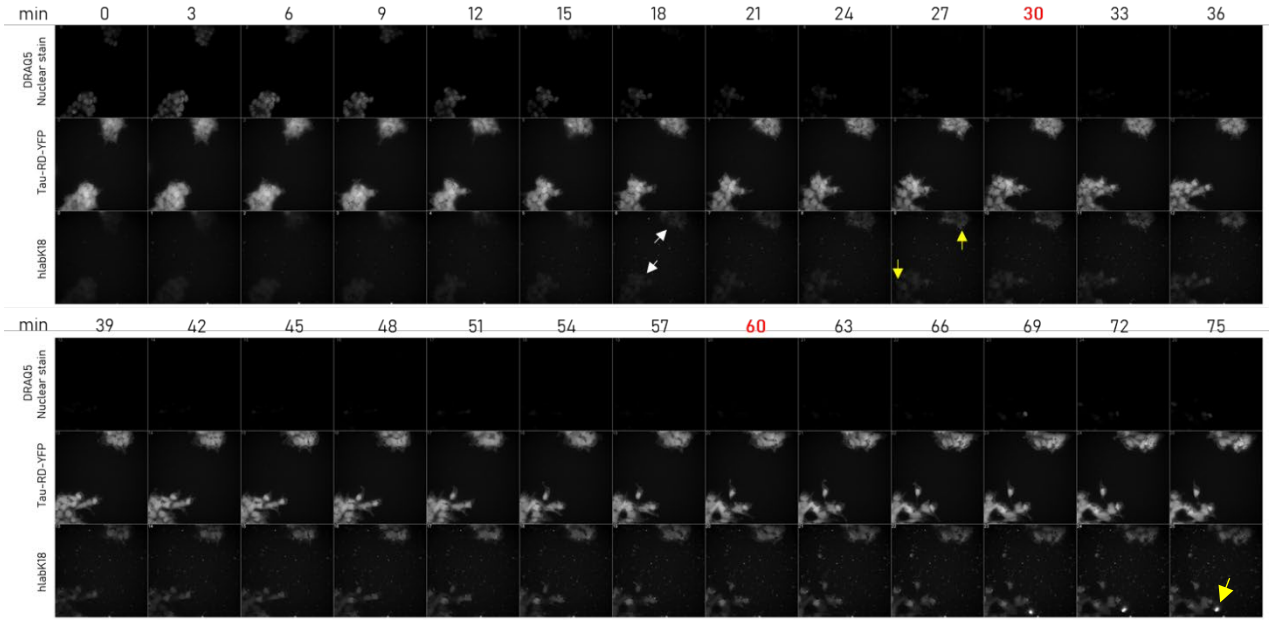

Figure 4. The uptake of Tau seed into the cells was assessed by live cell imaging. Cells were seeded in the clear bottom 96-well plates and imaged using Operetta live imaging system using three channels for 75 min.

Following the findings of live cell imaging of TauRD over time, the fibrils were internalized into the cell cytoplasm within a quarter of an hour, and at around half an hour sequestered into the dynamic puncta predominantly localized in the cell processes. The confocal imaging showed the distinguishable fluorescence within the cell body at the early time point after seeding (Figure 5, ~20 min), but diminished as the incubation time progressed (Figure 5, ~40 min, orange arrows) whereas the punctate structures started to appear (Figure 5, ~40 min, white

arrows), culminating in the sequestration of the fluorescently-labeled hlabK18 fibrils into the punctate structures that appear hollow based on the imaging of the C/YFP tagged endogenous Tau constructs (Figure 5, ~5h, white arrows). Not all hollow structures contained the hlabK18 (Figure 5, ~5h, green arrows).

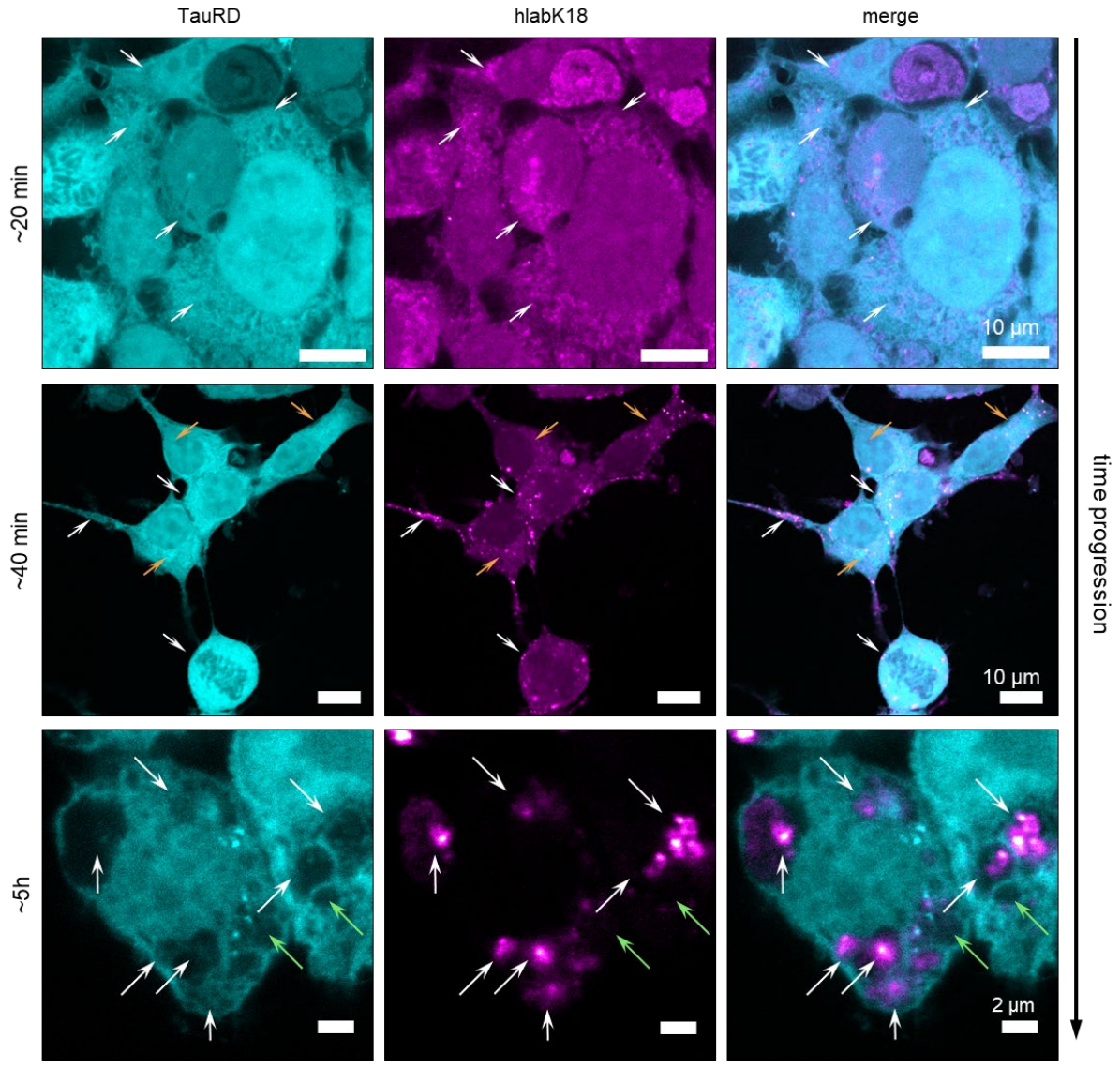

Figure 5. The uptake of Tau seed into the cells was assessed by confocal microscopy imaging.

Fibril fate inside the HEK293T cells

To better understand the fate of the Tau fibrils internalized into the cells, we used correlative light and electron microscopy (CLEM), where the HEK293T cells were treated with labelled K18 fibrils (hlabK18). HEK293T is the parental cell line to TauRD without the overexpression

of Tau constructs. It does not form any Tau-positive aggregates upon seeding with Tau fibrils, which would allow us to track the fate of the engulfed Tau seeds.

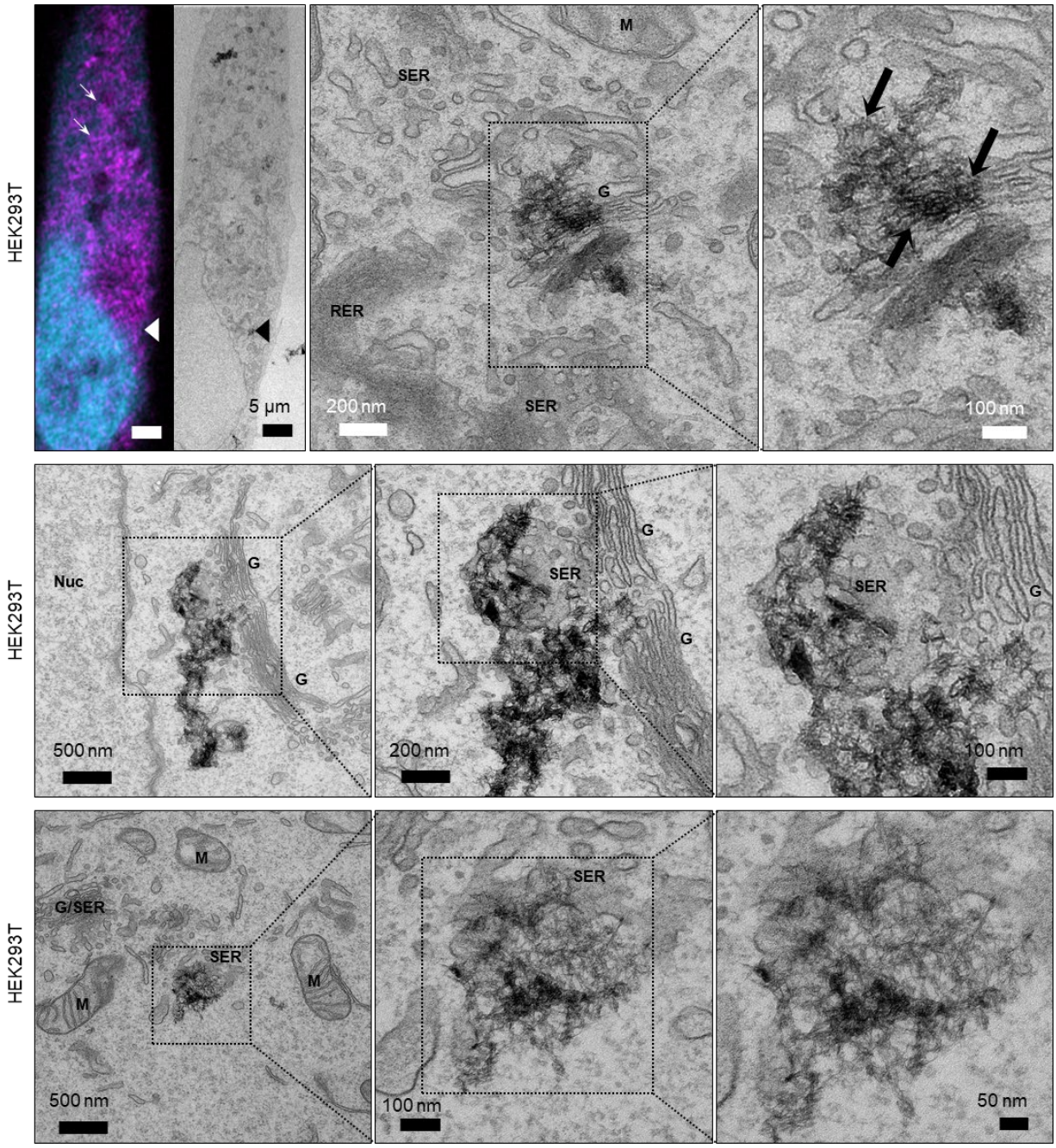

Figure 6. CLEM of Tau seed internalization parental HEK293T cells (B) at the early stages. The confocal fluorescence was aligned with the EM images. We observed a slight shrinkage and distortion of the cell components due to cryopreservation in relation to the fluorescence, which we accounted for during the analysis of the data. Further, the angle of confocal imaging and cryosectioning of the cell could have slight deviation, therefore the images may not be perfectly aligned, but to the best ability possible. SER= smooth endoplasmic reticulum; RER= rough endoplasmic reticulum; G= Golgi apparatus; Nuc= nucleus; M= mitochondrion.

The early stages of hlabK18 uptake were assessed in HEK293T by CLEM. The cell preparation protocol has purposefully been adjusted to preserve as much of the internal cell structures as possible, no detergents or harsh treatments were used that could disrupt the lipid-rich organelles, and no antibody staining was used, that would require cell fixation and multiple washes. The cells were imaged live by confocal microscopy. Next, the same cells were cryopreserved and sliced into thin sections for EM imaging.

The hlabK18 fibrils were located in the confocal images, and at the early stages of the internalization appear diffuse, but some puncta were also seen in the cell cytoplasm (Figure 6, white arrows). Interestingly, despite the detection of punctate structures of the hlabK18 fibrils throughout cell cytoplasm in the confocal images, no fibrils were detectable in the EM images besides the distinct clumps associated with the lipid-rich structures. EM images showed a high extent of fibril association with membranous organelles, such as vesicles, Golgi complexes, and endoplasmic reticulum. The fibrils were clearly interspersed within the organelles (Figure 6B, black arrows).

These results prompted us to look closer at the organelle association of the internalized hlabK18 fibrils in the absence of the TauRD overexpression constructs in HEK293T cells.

The hlabK18 fibril clumps were associated with lipid-rich cellular structures.

At the later stage of fibril uptake by HEK293T parental cells (~40 min), more punctate hlabK18 fluorescence started to form (Figure 6A, white arrow), however, the diffuse hlabK18 was also still present (Figure 7A, yellow arrow). EM images showed that the fibrillar clumps were still discernible and aligned with the fluorescence (white box). Fibrils were associated with mitochondria (Figure 7, M) to a high extent, spanning both inner and outer membranes. The cristae appeared irregular and very sparse. At this stage, the membranes surrounding the fibril-laden mitochondria started to appear (Figure 7B, mem). These membranes were morphologically consistent with autophagic vesicle formation. Thin long filaments (Figure 7A, arrowheads) were present in the cell cytoplasm, which were likely the intermediate filaments and other cytoskeletal elements, consistent with the scaffolding processes required for autophagy. Fibrils were also found spanning the cytoplasmic membrane from the outside of the cell (Figure 7C and D, O, arrows). Further, fibrils were detected inside the nucleus, as well as associated with the nuclear membranes (Figure 7D, Nuc). In addition to mitochondria, various vesicular structures were observed.

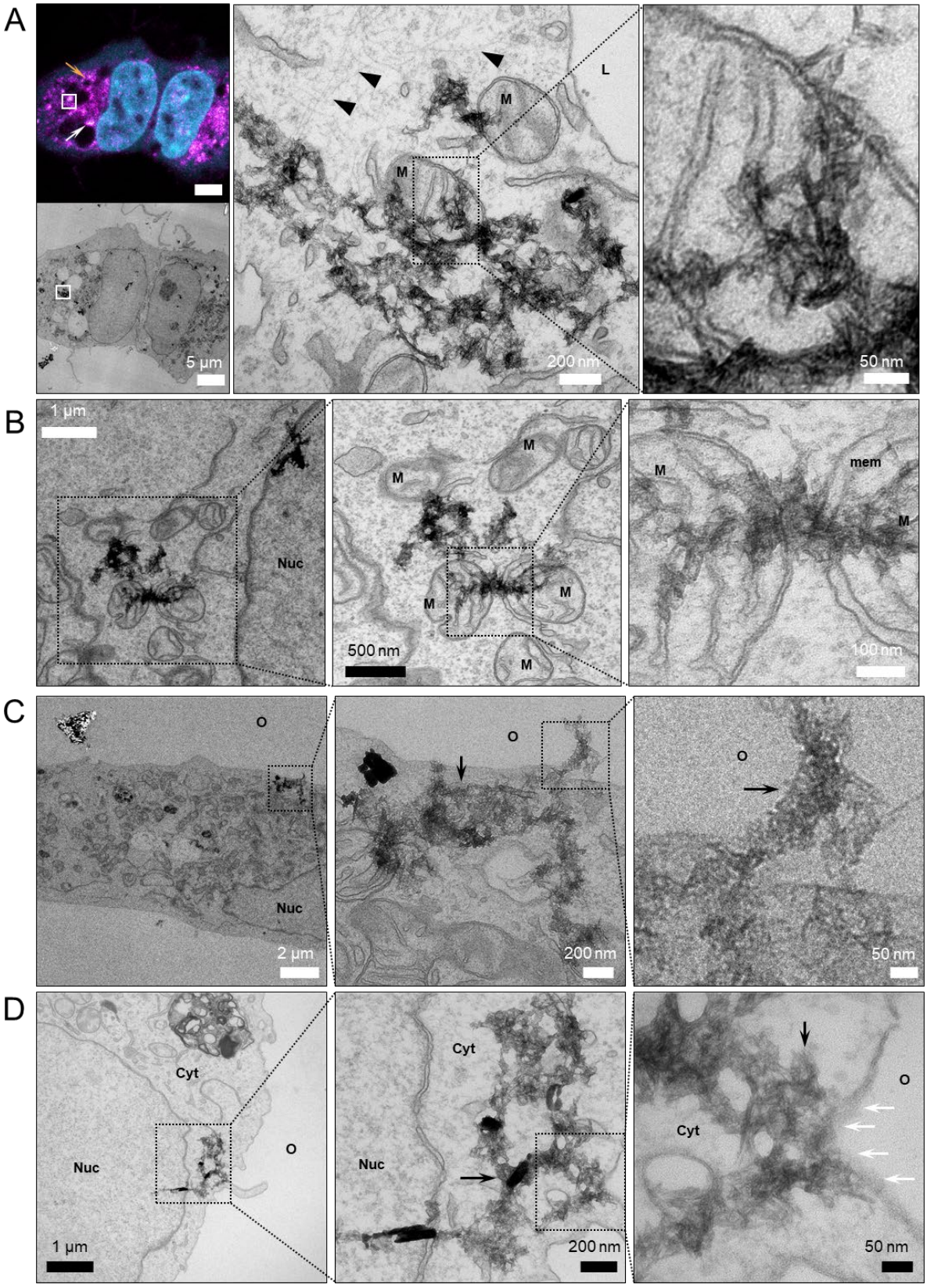

Figure 7. CLEM of Tau seed internalization in parental HEK293T cells at the later stages.
L= lysosome; Nuc= nucleus; M= mitochondrion; mem= membrane.

Specifically, multilamellar and multivesicular structures are associated with endolysosomal protein degradation pathways and autophagy. Amphisomes are membranous organelles formed by the fusion of the endosomal vesicles with autophagic vesicles and multivesicular bodies (MVB) in cells, after which they are fused with the lysosomes for the degradation of the contents in the amphisomes. Amphisomes are the intermediate organelles and sit at the cross-section between the lysosomal and autophagic pathways. The proteins involved in the amphisome formation and maturation include endosomal sorting complexes required for transport (ESCRT), soluble N-ethylmaleimide-sensitive factor activating protein receptors (SNAREs), Rab GTPases, and tethering protein complexes [785]. ESCRT complexes are also involved in the abscission processes of the midbody (Flemming body), the organelle localized to the site of cytokinetic scission upon cell division. The polymerized ESCRT-III complexes are involved at the late stage of the midbody abscission, and also are involved in the biogenesis of the MVBs [786]. Rab5 is the GTPase associated with early endosomes (EEs), whereas Rab7 is predominantly found on late endosomes (LE) and MVBs [787,788].

Therefore, we used CLEM to determine what internal structures colocalize with the hlabK18 fluorescence in the HEK293T cells. The alignment of the confocal and EM images revealed that the agglomerations of the fluorescence into ordered round puncta coincided with the structures rich in vesicles, MVBs, multilamellar bodies, and lysosomal vesicles with loosely or densely packed multi-layered membranes (Figure 8, arrows). These agglomerations were morphologically similar to amphisomes. The fibrils were clearly distinguishable only when they were associated with the membranes outside the amphisome core. In the multilamellar lysosomes, however, only remnants of fibrillar species could be observed (Figure 8, white arrowheads) associated with the innermost layer of the lysosomal membrane (Figure 8, golden arrowheads), morphing into the dense granular material (Figure 8, asterisk). Within the vesicles, no clear fibrillar appearances were observed, despite the fluorescence coinciding with these structures. It is possible that the low pH quenched the fluorophores, which made them appearing as dark vacuoles on the confocal, and empty vacuoles on the EM images. The disrupted mitochondrion was fully enamoured in the fibrillar material and was closely associated with the lysosomal multilamellar vesicle, where the outside membrane partially encircled the fibrils.

These results demonstrate that the fibril-treated cells are employing the protein degradation pathway components to sequester the fibrils into the vesicular structures.

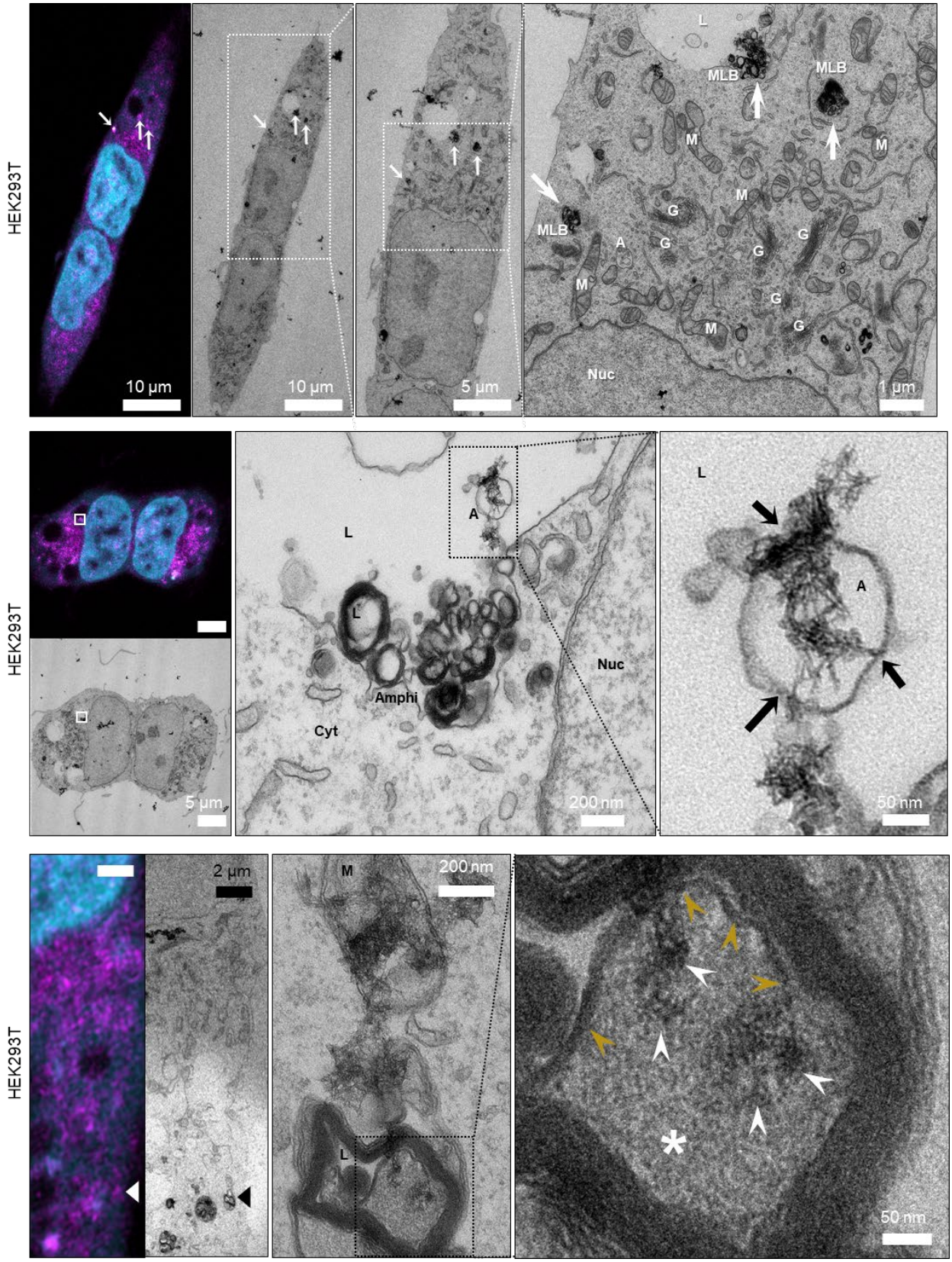

Figure 8. CLEM of Tau seed processing in parental HEK293T cells. L= lysosome; Nuc= nucleus; M= mitochondrion; mem= membrane. A= amphisome; Amphi= amphisome; Cyt= cytoplasm

Next, we sought to determine whether the fibrils are further sequestered through the endolysosomal pathway. CLEM was used to interrogate the latest stage (~5 h) of fibril internalization and processing in the parental HEK293T cells. Similar to the TauRD cells, the cytoplasmic diffuse fluorescence of hlabK18 in HEK293T cells was absent under the confocal microscope imaging. The punctate fluorescence of hlabK18 was aligned to the structures observed by EM. The alignments demarcated the localization of fibrils into the multilamellar structures and vesicles (Figure 9, white arrows confocal = black arrows EM)).

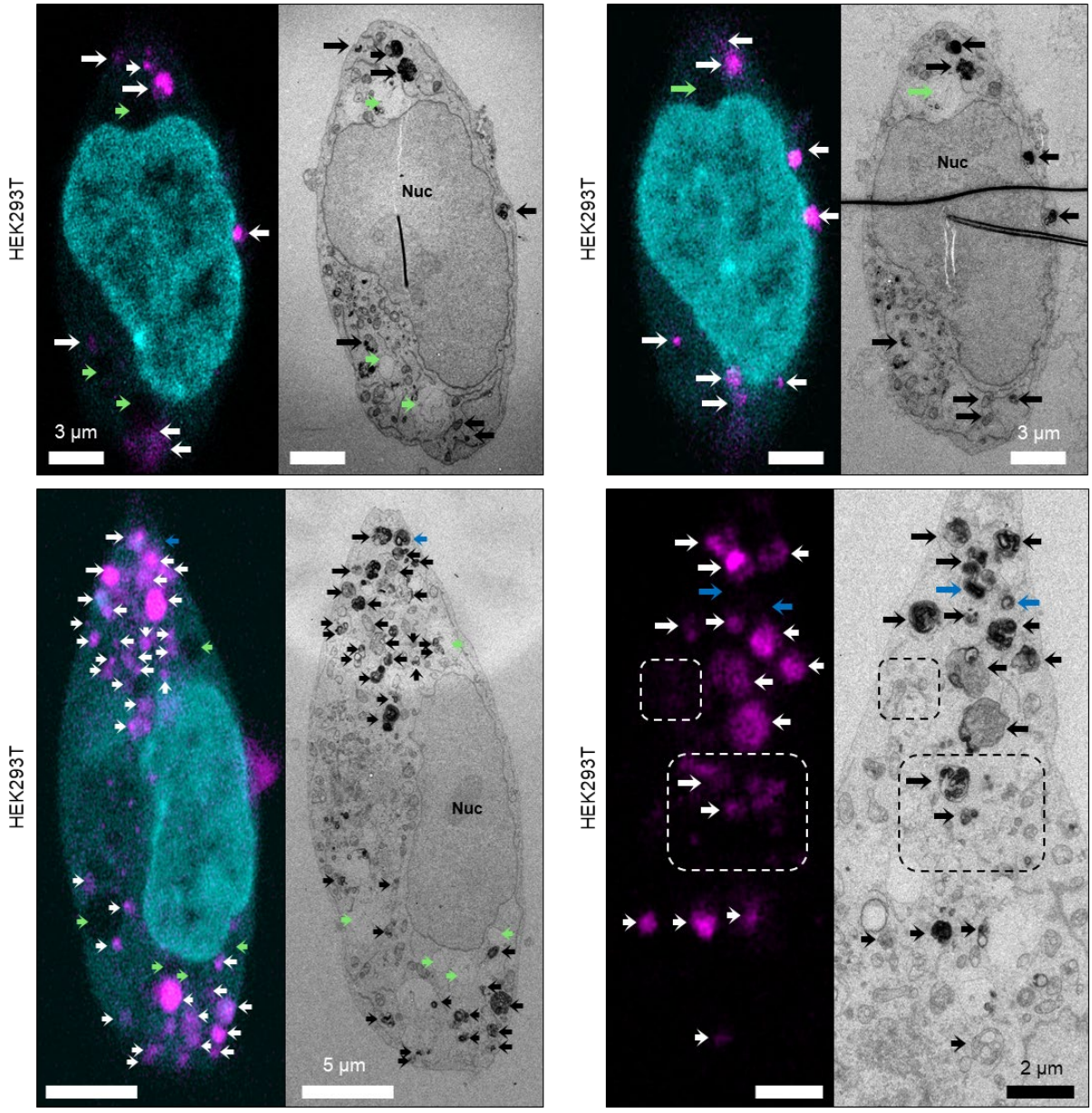

Figure 9. CLEM of Tau seed processing and sequestration into vesicles in the parental HEK293T cells. Nuc= nucleus.

The empty vesicles were aligned with the empty vacuolar structures (Figure 9, green arrows). Not all multilamellar bodies, however, were hlabK18-positive (Figure 9, blue arrows). Some hlabK18 fluorescence was associated with the plethora of membranous structures and vesicles, rather than encased by the membranes (Figure 9, box).

Next, the amphisomes and lysosomes were aligned with hlabK18 fluorescence for a closer examination at high resolution (Figure 10).

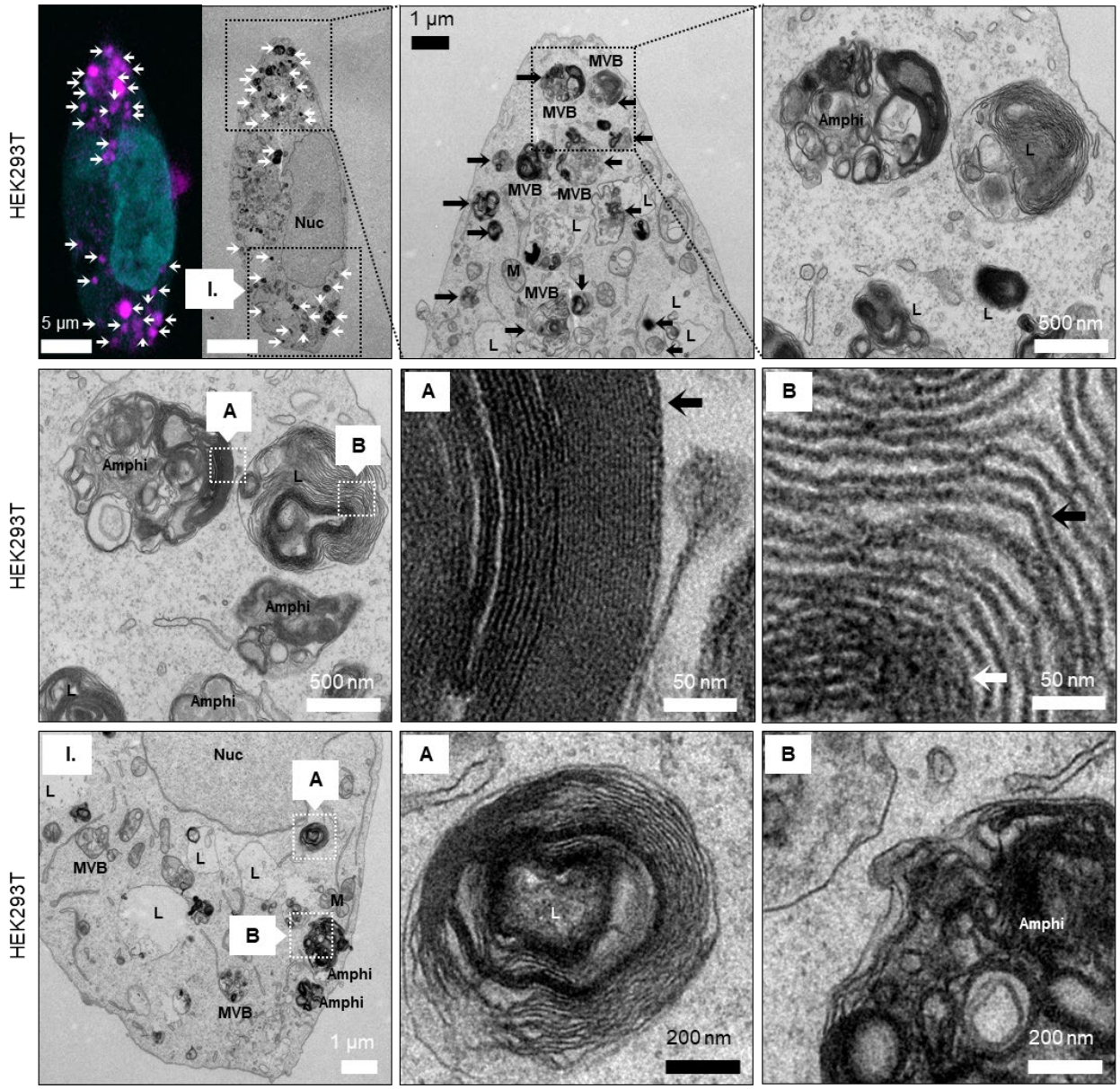

Figure 10. CLEM of Tau seed localization in the lysosomes and amphisomes in the parental HEK293T cells. Amphi= amphisome; L= lysosome; MVB= multivesicular body; Nuc= nucleus.

Amphisomes contained ultrafine densely packed lamellar structures (2.26±0.31 nm, Figure 10, A arrow), whereas the lysosomal vesicles were composed of the loosely associated, membrane layers were twice as thick as the fine lamellas (5.73±0.72, p<<0.001; Figure 10, B arrow). The lysosomal membranes are known to be composed of a single phospholipid layer, which measures ~5 nm [789], and lysosomal membranes measure ~7-10 nm in thickness [790], depending on the membrane modifications, such as the addition of glycocalyx. Further, the granular material was observed in the interior of the lysosomes, but no distinct fibrils were found.

In conclusion, in the HEK293T cells, without TauRD overexpression, upon the ~40 min and onwards of the seed internalization and processing, fibrils are sequestered into the vesicles on the autophagosomal and lysosomal pathway, such as amphisomes. No distinct internalized fibrils are present at this stage anymore, however, fluorescence was still observed in these vesicular structures. Multilamellar vesicles consist of finely packed thin membranes or loosely associated thick membranes. Both illustrate the necessity of the cell to invest a lot of energy expenditure for the processing and degradation of the engulfed seeds. In TauRD cells, no FRET signals or apparent foci were detected at this time point. In the HEK293T cells, no de-novo fibrillar aggregate formation is present. Interestingly, the subcellular morphology and organelles appear distraught compared to the early stages of seed internalization. More and much larger empty vacuoles are present, misshapen mitochondria, Golgi and ER, a plethora of membranes and vesicles throughout the cell, amphisomes, and lysosomes.

Interestingly, the subcellular morphology and organelles appear distraught compared to the early stages of seed internalization. More and much larger empty vacuoles are present, misshapen mitochondria, Golgi and ER, a plethora of membranes and vesicles throughout the cell, amphisomes, and lysosomes. The nucleus shows the presence of chromatin condensation and likely the presence of the nucleolar aggresomes. This suggests that cells are under stress conditions and upregulate the autophagic/lysosomal pathways to process and clear the internalized fibrils. Multilamellar bodies encasing the fibrillar material suggest the high level of insulation required for the fibril clearance, likely to prevent their association with lipid-rich organelles, leading to disruption and autophagy.

Foci formation in the TauRD cells after the addition of the exogenous fibrils'

As we discovered earlier, the fibrils are internalized into the TauRD cells at around 20 min post-addition, and distinct puncta, predominantly at the cell extremities, start to appear after

40 min. Therefore, we next wanted to see the process of the foci formation as it proceeded in the live cells.

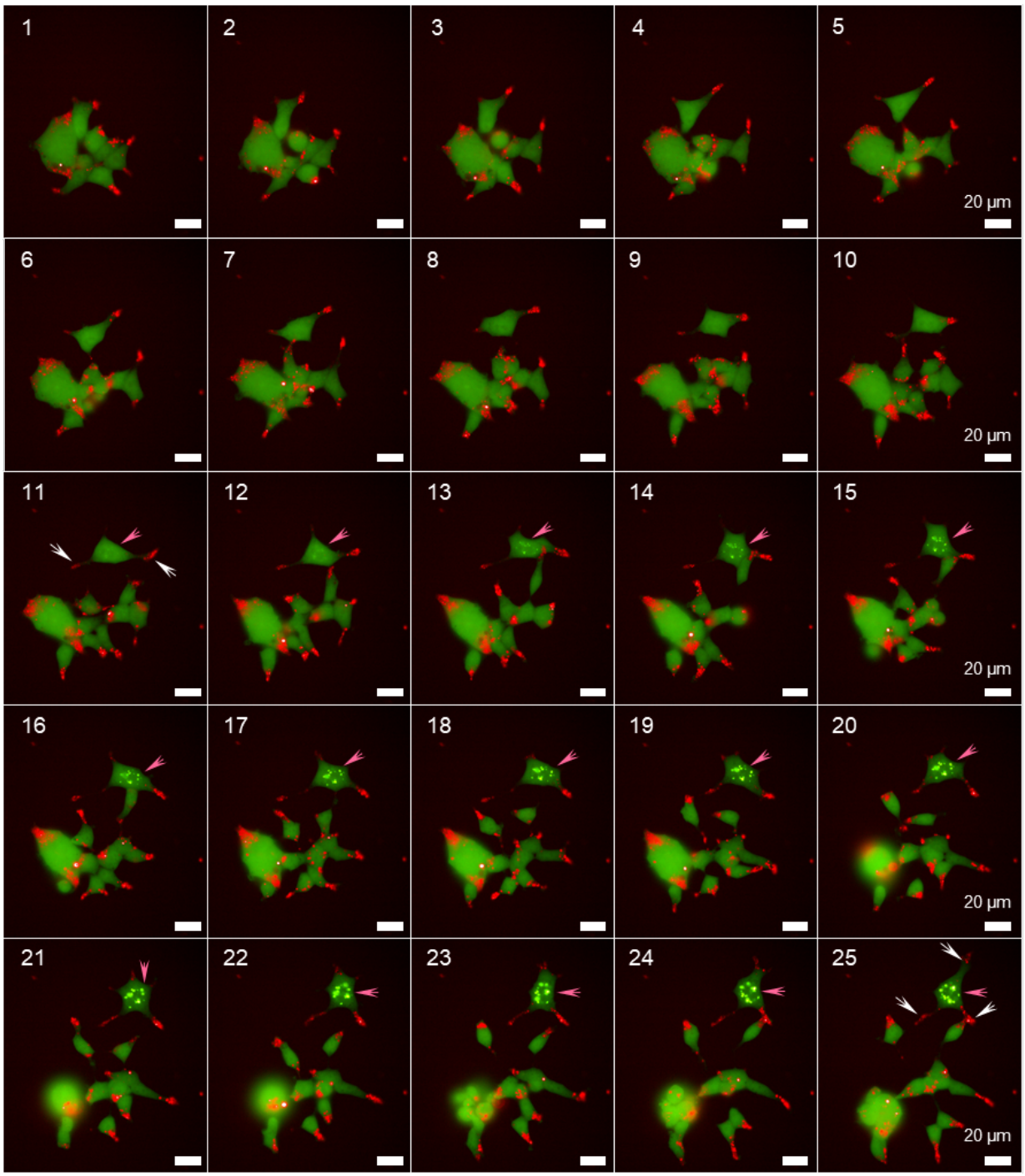

Figure 11. Live cell imaging of TauRD cells forming the nuclear foci after seeding with hlabK18 fibrils. Fibrils hlabK18 (100 ng/50'000 cells) were added to cells for 4h, washed 3xPBS, and imaged using Operetta Live imaging system with an image taken every 30 min throughout 12 h (end frame 25 = 16h after fibril addition).

We used live cell imaging to capture the initiation of the formation of foci. Cells were incubated with hlabK18 fibrils for 4h at which time the imaging commenced (Figure 11, frame 1) and proceeded with the image taken every 30 min. The first appearance of small distinct foci was observed at 9 hours post-addition (Figure 11, frame 11, magenta arrow). The red fluorescence showing the hlabK18 seeds was localized in puncta at the cell extremities (Figure 11, frame 11, white arrows). The cells were highly mobile, and the fibrils within these puncta were also dynamic as the cells moved around. As time progressed, the bright foci grew in their size (Figure 11, magenta arrows). Notably, the majority of the cells did not form the foci despite the presence of the fibrils within the cells.

Next, we wanted to capture the whole fate of the cells forming the nuclear foci. Cells were treated with the hlabK18 fibrils are were immediately placed into the live imaging system, where the pictures were taken every 20 min (Figure 12, Frame 1 = 20 min post-addition of the seed).

Three channels captured hlabK18 seed localization, TauRD-C/YFP construct to observe the formation of the foci, and nuclear stain (DRAQ5, an anthraquinone compound, binding DNA A-T minor groove, mimicking histone 2b distribution) to visualize the nuclear dynamics. As shown previously, the hlabK18 puncta start appearing at around 40 min post-addition of the seeds (Figure 12, Frame 2), with clear puncta within cell body extremities apparent starting from 2h (Figure 12, Frame 6, arrow). From around 5 h 40 min (Figure 12, Frame 17, arrow) the nuclear staining of A/T-rich DNA start appearing within the cell body, and not just in the nucleus. This proceeds for a further 12 h, after which the DNA staining is again localized predominantly in the nucleus (Figure 12, Frame 55). This process likely indicated the initiation of the mitosis of the cell. At this stage, no foci were present, and their first appearance could be identified 11 hours post-addition of the seed (Figure 12, Frame 33, yellow box, arrow), at which timepoint the cell formed two nuclei, but not yet divided into two cell bodies. Interestingly, the hlabK18 fluorescence was still predominantly observed in puncta in the vicinity of the foci, but not associated with it (Figure 12, Frame 32, arrow). The foci formed could be identified in only one of the sister nuclei (Figure 12, Frame 42, arrow). The hlabK18 seeds were localized on the division plane between two sister nuclei, however, the cell was incapable of telokinesis to successfully complete its division (Figure 12, Frame 40, arrow). At around 15 h (Figure 12, Frame 45) we could observe the hlabK18 signal coinciding with the TauRD-C/YFP foci, and at 23 h hlabK18 signal is present both outside and overlapping with the foci (Figure 12, Frame 70, arrows).

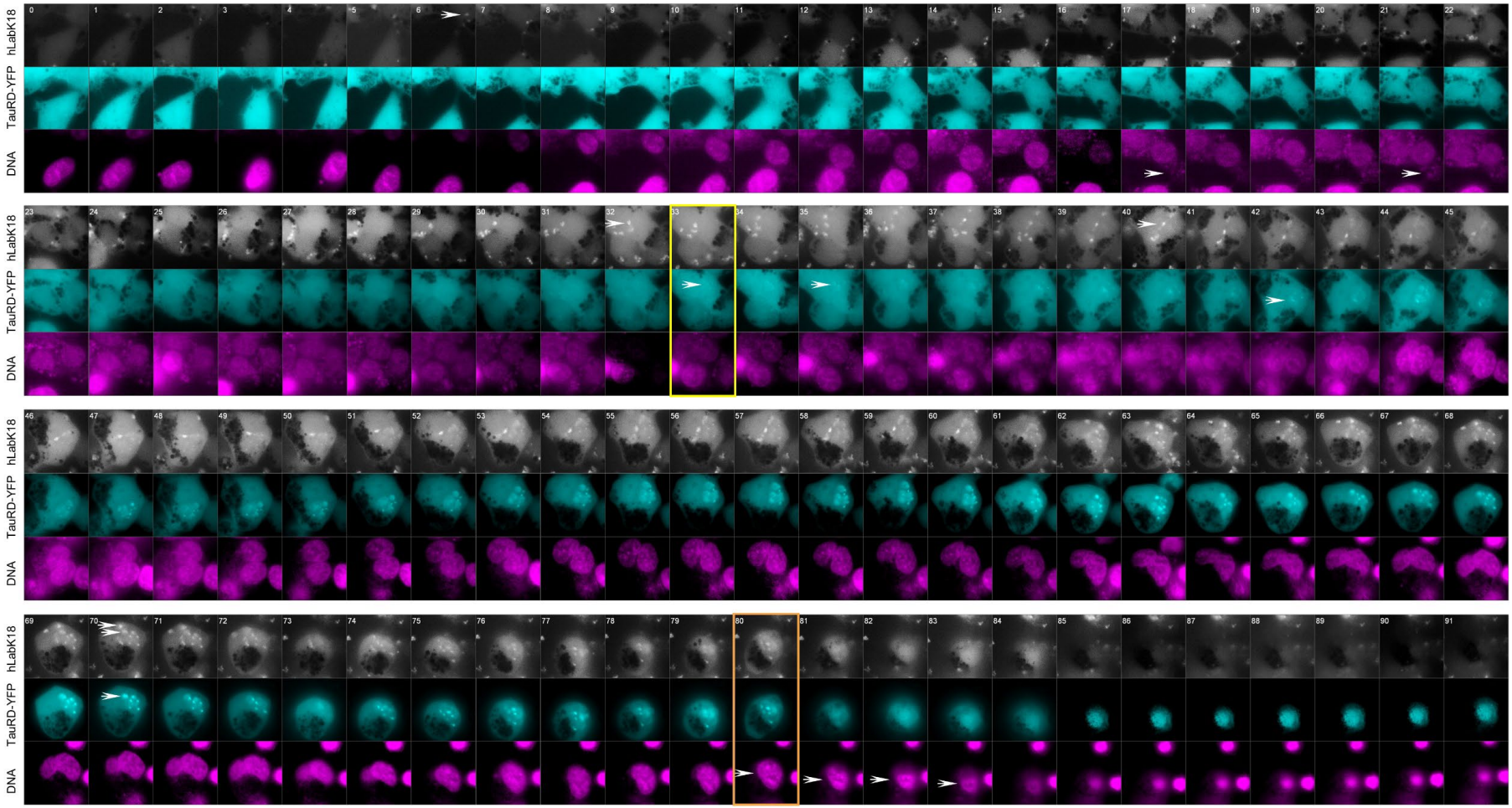

Figure 12. Live cell imaging of TauRD cells forming the nuclear foci after seeding with hlabK18 fibrils and apoptosis. Fibrils hlabK18 (100 ng/50'000 cells) were added to cells and imaged using Operetta Live imaging system with an image taken every 20 min throughout 30 h (end frame 91 = 30 h 20 min after fibril addition).

The cell would not complete its division cycle and at around 26 h and 40 min post-seed addition, and 15 h and 40 min post-foci appearance, it initiated the nuclear material condensation, rounded up and detached from the plate, signifying the apoptotic death (Figure 12, Frame 80, orange box arrow).

These results show us the process of formation of the bright nuclear foci only in some of the seeded TauRD cells despite the uptake of the fibrils. Cells developing the foci appeared distressed and unable to complete normal processes, such as cell division leading to cell death.

Next, we sought to capture the formation of the cytoplasmic foci in TauRD cells. The cells were treated with hlabK18 fibrils for 4h, after which the media was changed to normal and cells were further incubated for over 36 hours to allow for two cell division cycles to occur, after which images were taken every 45 min. The cell containing no nuclear foci were identified and followed to observe initiation of the cytoplasmic focus formation through the loss of TauRD-C/YFP diffuse signal from its nucleus (Figure 13, Frame 11, arrow).

As the signal loss proceeded, after the 6 hours the condensation of the TauRD-C/YFP commenced (Figure 13, Frame 18, arrow), and after 9 h 45 min, clear cytoplasmic inclusion was formed (Figure 13, Frame 21, arrow). The cell then detached from the well bottom, migrated over the cell cluster, and landed in the middle of other cells as two not fully divided sister cells (Figure 13, Frame 31, arrow), both containing large cytoplasmic and orderly spaced nuclear inclusions. The two foci-containing cells remained within the cluster fairly immobile. These observations support the timing of foci formation co-occurring with the cell division.

Previously, work on α-synuclein from our lab has shown that the process of Lewy body formation, and not just the α-synuclein fibrillization contributes to the toxicity and cellular dysfunction [231]. Therefore, our next goal was to see the cell dynamics and behavior in the processes of forming and managing the condensation of TauRD-C/YFP constructs, and nuclear and cytoplasmic inclusions. We located the two incompletely divided sister cells containing a cytoplasmic inclusion of the division plane between the two (Figure 14). The hlabK18 fibrils were in distinct puncta locations at the cell peripheries (Figure 14, red). As time progressed the sister cells were mobile and appeared to try and resolve the incomplete division. The TauRD-C/YFP started condensing from diffuse to granular and was localized out of the nuclei (Figure 14, Frame 4, arrow), to the nuclear membranes, and into the cytoplasma. The small round nuclear inclusions, spaced out evenly, appeared in both sister nuclei (Figure 14, Frame 5, Frame 11, arrows). Over time the two large cytoplasmic inclusions could be resolved associated with each sister cell, and both cells started to lose their motility.

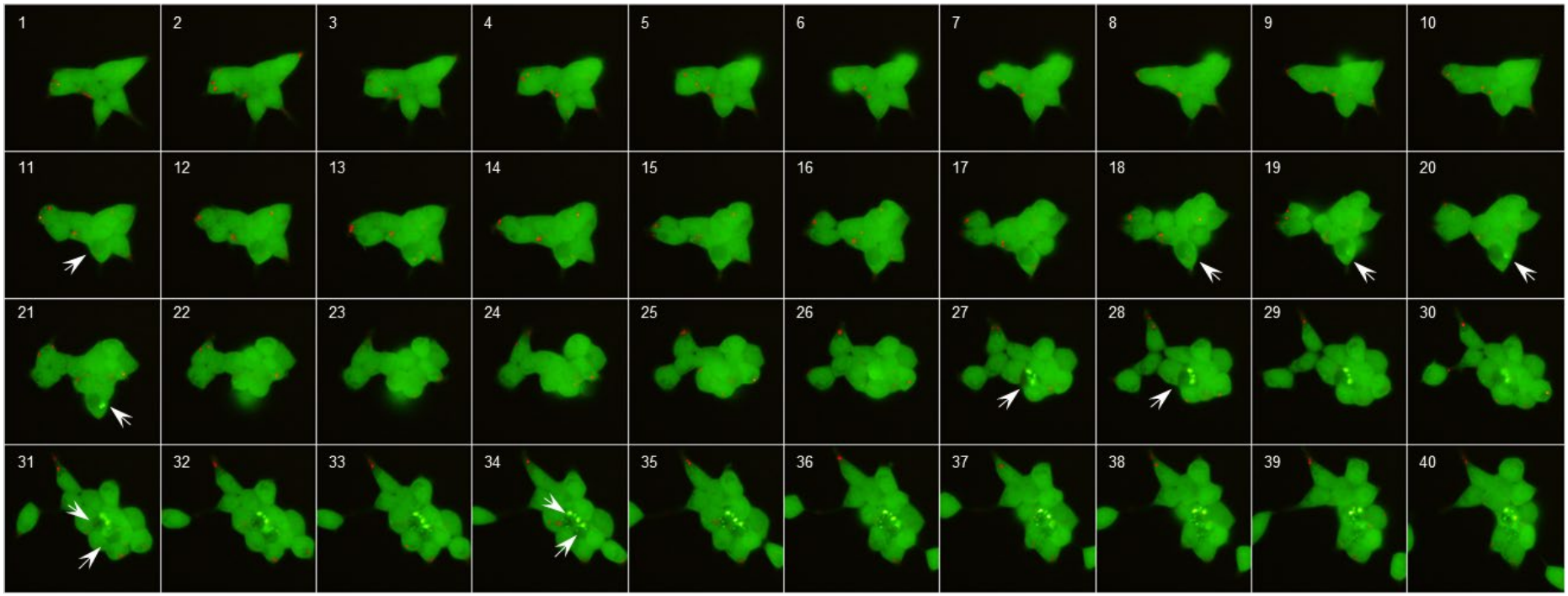

Figure 13. Formation of the cytoplasmic foci followed by the nuclear in the TauRD cells. The cells were incubated with hlabK18 fibrils for 4h, washed 3xPBS, and incubated for 40h to allow one cell division to occur. Starting at 40 h (Frame 1), the cells were imaged every 45 min. Green= TauRD-C/YFP; red= hlabK18

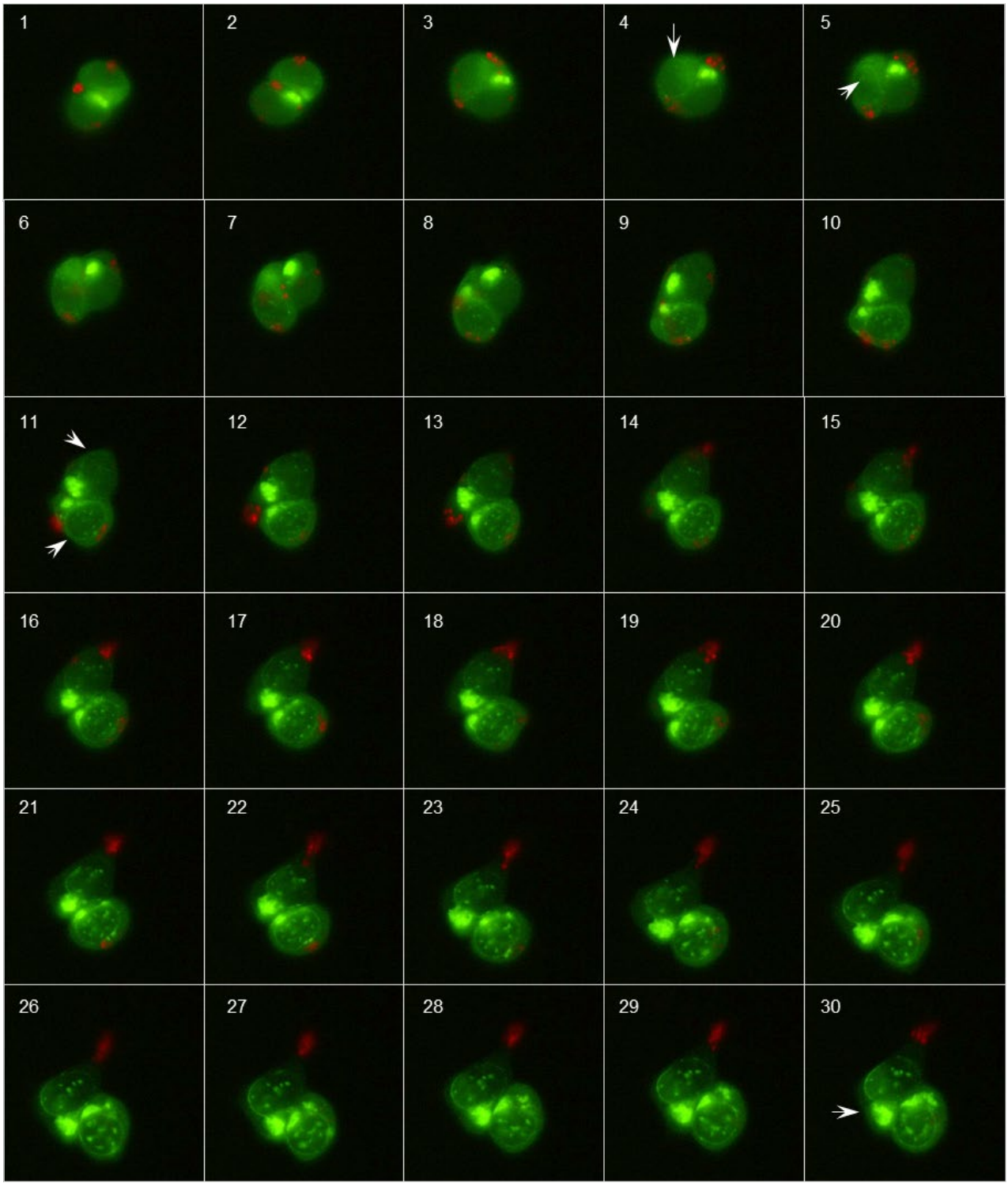

Figure 14. Cytoplasmic and nuclear foci dynamics in the TauRD cells. The cells were incubated with hlabK18 fibrils for 4h, washed 3xPBS, and incubated for 40h to allow one cell division to occur. Starting at 40 h (Frame 1), the cells were imaged every 45 min. Green= TauRD-C/YFP; red= hlabK18.

Both nuclear and cytoplasmic foci became fibrillar and thread-like in appearance (Figure 14, Frame 30), and the two cells seemed to succumb to apoptosis before the successful resolution of the division.

Live imaging is a powerful technique for cellular work. It allows us to directly witness the processes of the formation of the subcellular structures, and the cell behavior during this time. Our observations indicate that the TauRD cells form foci through at least two distinct pathways, nuclear, resulting in evenly-spaced round foci, and cytoplasmic, resulting in predominantly singular, perinuclear inclusion. The foci formation is closely associated with the cell division and the processes such as the doubling of the genetic material and protein content at the S phase of the cell cycle. Notably, the appearance of both nuclear and cytoplasmic inclusions leads to incomplete resolution of the cell cycle, at the various stages, such as telokinesis and abscission, leading to the apoptotic death of multinucleated TauRD cells. Further, the live cell imaging revealed that the foci formations tend to proceed through only a few distinct mechanisms.

We were intrigued by the invariable morphologies of both nuclear and cytoplasmic foci and noticed the resemblance to the nuclear and cytoplasmic aggresomal structures. These findings prompted us to look closer at the ultrastructural composition of these formations in TauRD cells.

Ultrastructural investigation of the fluorescent foci in TauRD cells

The HEK293T cells do not form any aggregate structures upon the addition of fibrils over time, and as we found in the previous section, the internalized hIabK18 seeds are processed by the endolysosomal pathway at the early stages of internalization. Next, we asked what are the ultrastructural properties of the bright fluorescent and FRET-positive foci in the HEK293T cells overexpressing TauRD constructs?

To determine the ultrastructural features of the foci in the TauRD cells, correlative light and electron microscopy was performed. In TauRD cells, the foci form at around 24 h post-seeding with the fibrils. Electron microscopy imaging of the TauRD cells transduced with hMBF or h4R2N showed the formations of the large cytoplasmic fibrillar inclusions and round nuclear foci (Figure 15). In hMBF-seeded TauRD cells (Figure 15A) the cytoplasmic focus demonstrated the appearance of the aggresomal features and collapsed microtubule-organizing center (MTOC) at the periphery of the nucleus.

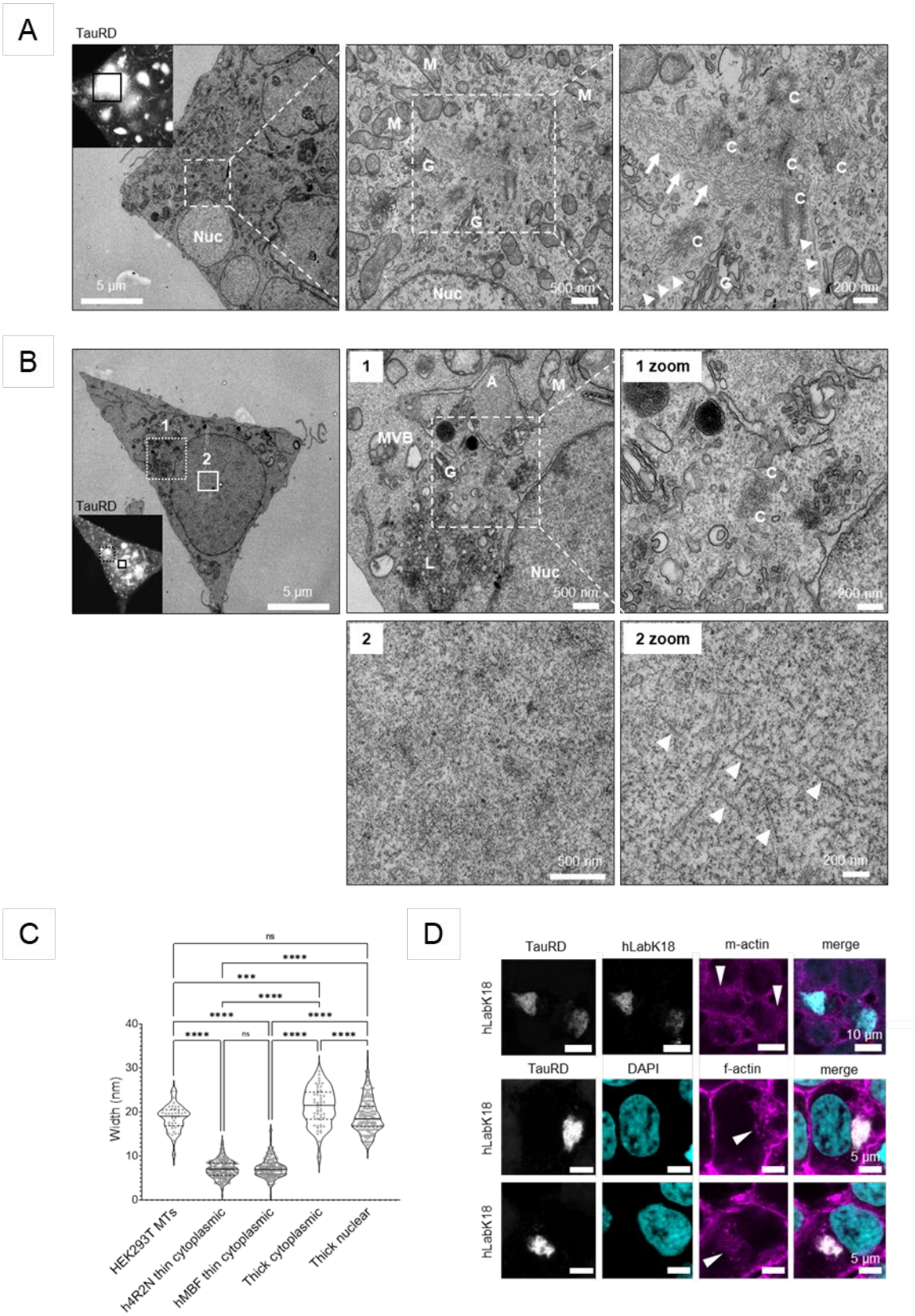

Figure 15. CLEM of fluorescent cytoplasmic and nuclear inclusions in HEK293T TauRD cells. A= amphisome; L= lysosome; MVB= multivesicular body; Nuc= nucleus; C= centriole.

Multiple centrioles were present in different orientations, the radial organization included a fibrillar core of thin actin-like filaments arranged in parallel (arrows), and thick microtubule-like filaments (arrowheads) pointing towards the core. Further, at the periphery of cytoplasmic inclusion, the membranous organelles were arranged, including Golgi complexes, mitochondria, smooth ER, and other membranous and vesicular structures. In h4R2N-seeded TauRD cells (Figure 15B), similar to the hMBF-seeded cell, the cytoplasmic inclusion (zoom 1) resembled a collapsed MTOC, few thin actin-like filaments were found but were not arranged in a parallel fashion. The structure was very vesicle-rich showing autophagosomes, smooth ER, mitochondria, and Golgi at the periphery. The nuclear focus (zoom 2) showed the presence of thick fibrils.

Therefore, to discern whether the fibrils (Figure 15, arrows) in the core of the cytoplasmic inclusion (thin cytoplasmic), at the periphery (thick cytoplasmic), or thick nuclear were consistent with the Tau fibrils of dimensions of ~14 nm, or likely represented the actin filaments and MTs, quantifications of the widths of these fibrillar species was performed (Figure 15C, Table 2). The quantification shows that thick nuclear fibrils at 19.1±3.87 nm were not significantly different from the expected MT widths at 18.7±2.94 nm. The thick cytoplasmic, though, were thicker than expected for MTs at 21.2±4.22 nm. The thin cytoplasmic filaments were at 7±2.04 nm in h4R2N-seeded and 7.3±2.22 nm in hMBF-seeded cells, which were consistent with reported actin filament widths [791].

Table 2. Quantification of the fibril widths in the cells.

	HEK293T MTs	**h4R2N thin cytoplasmic**	**hMBF thin cytoplasmic**	**Thick cytoplasmic**	**Thick nuclear**
Number of fibrils	40	192	170	53	157
Median (nm)	19.0	6.99	6.98	21.5	18.5
Mean (nm)	18.7	7.00	7.30	21.2	19.1
Std. Deviation (nm)	2.94	2.04	2.22	4.22	3.87

Further, confocal microscopy was used to visualize the distribution of the actin monomers or filaments within the cytoplasmic inclusion (Figure 15D). Cells were seeded with the hlabK18 fibrillar seeds, and upon the late stage of the foci formation, the cells were fixed and stained with the antibody detecting monomeric actin (m-actin), or small molecule phalloidin, staining the fibrillar actin (f-actin). Images show that monomeric actin was not highly detected within the cytoplasmic inclusions, whereas the f-actin was integrated and interspersed within the inclusions (arrowheads).

The cytoplasmic inclusions in TauRD cells resemble the canonical ultrastructural morphological profile of an aggresome. Cytoplasmic inclusions presented as a radially organized structure at the perinuclear localization resembling the localization of MTOC, with a multiplicity of centrioles and microtubules oriented towards the core of the inclusion. A plethora of lipid-rich organelles was clustered around the cytoplasmic inclusions, including mitochondria, Golgi, endoplasmic reticulum, lysosomes, as well as many vesicles.

In the core, thin filaments are observed, the nature of which is yet to be determined. Aggresomes tend to contain intermediate filaments and actin bundles, and indeed confocal imaging of filamentous actin staining showed its presence within the cytoplasmic inclusion structure. The perinuclear inclusions were morphologically similar to the aggresomes and were possibly formed as a consequence of the proteasomal impairment and defects in protein clearance mechanisms.

The nuclear foci are drastically different from the cytoplasmic inclusions. They did not display any clear structures, and few fibrils detected within several foci were very rare. Indeed, only in a single cell, the fibrils were observed. The morphology of the nuclear foci was unclear on EM images despite the obvious fluorescence seen on the confocal images (Figure 15).

The quantifications of the width of the filaments within the cell cytoplasm and nucleus showed that thicker cytoplasmic filaments were slightly wider that MTs, whereas the thin filaments were approximately 7 nm wide. Thick nuclear filament widths were indistinguishable from the MTs, suggesting these filaments were possibly the remnants of the MTs involved in the chromosomal segregation. Curiously, when the bright confocal fluorescence was aligned with the EM images, the structures on EM were visibly smaller than the extent of the fluorescence. No clear fibrils were distinguishable that could indicate the de novo formation of Tau fibrils from TauRD constructs. The major observation was the presence of many vesicles and lysosomes within the area of the fluorescence, indicating the active process of protein clearance within the cell.

Protein markers reveal an aggresome-like composition of cytoplasmic inclusions

Next, we wanted to substantiate the ultrastructural similarities of the cytoplasmic inclusions to the aggresome-like morphology by immunocytochemistry of the known aggresomal protein markers. The confocal imaging revealed an association of multiple aggresomal, proteostatic, organellar, and cytoskeletal markers with cytoplasmic inclusions, including HDAC6, vimentin, fibrillar actin (phalloidin), β-actin, β-tubulin, lysosomal markers p62, ubiquitin and LAMP1,

nuclear pore complex (NPC), mitochondrial (TOM20), endoplasmic reticulum (BiP) markers. Phospholipid, sphingolipid, and neutral lipid-rich vesicles were embedded within the cytoplasmic inclusions (Figure 16 A-M).

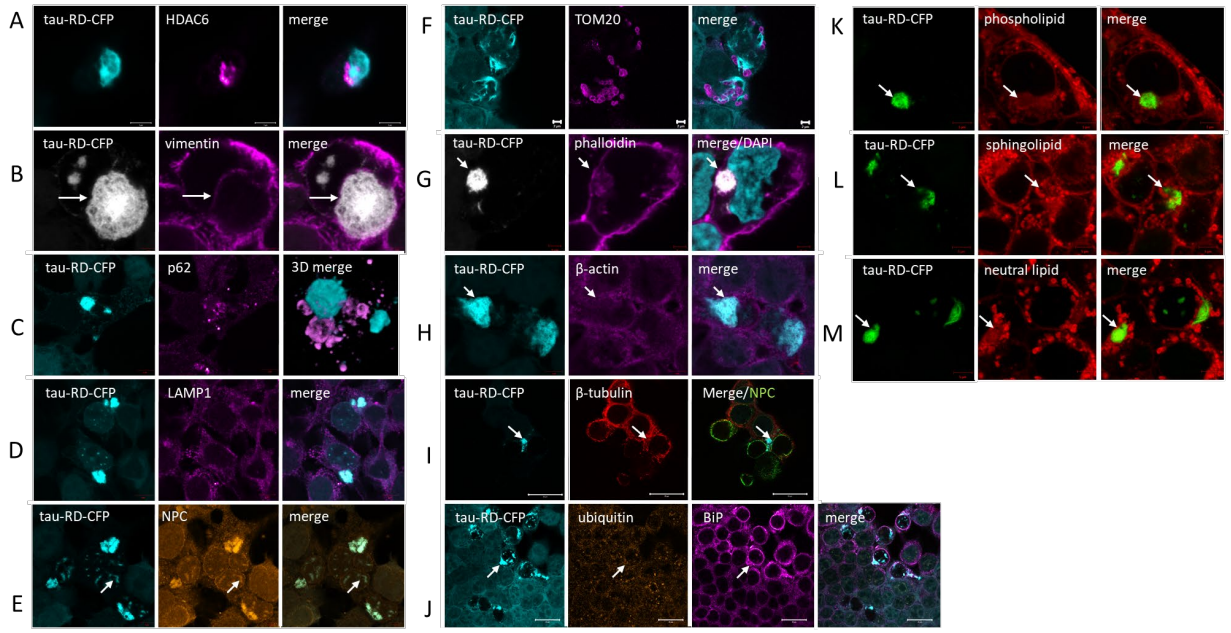

Figure 16. Confocal imaging of co-staining of known aggresomal protein markers in the seeded TauRD cells.

The immunostaining further confirmed the compositional similarities of the cytoplasmic inclusions to the aggresome-like structures, indicating that the foci formed in the TauRD cells are likely manifestations of impaired proteostasis.

Formation of cytoplasmic inclusion can be manipulated by nutrient deprivation and cell division arrest

Next, we wanted to interrogate the specific cellular processes that mediated the formation of the foci leading to cell death. We asked whether the formation of foci was Tau dose-dependent. And was the formation of foci coupled to the specific physiological process or cell cycle stage, and not contingent on the presence of the internalized seed? HEK293T cells have 3 copies of complete and 1 partial copy of chromosome 17 where gene *MAPT* is located, increasing to 6 complete + 2 partial Chr17 copies during chromosome duplication at the DNA duplication phase, prophase, and metaphase. The transcription and protein synthesis are active during mitosis, and this may influence the levels of endogenously expressed Tau. In

addition, the biosensor cells have stably integrated tau fragment overexpression constructs, however, the genomic integration position is unknown, which will also oscillate the construct levels in the cells. Upon fibril uptake by the cells, the internal amount of Tau is increased, and depending on the sensitivity threshold to the levels of available tau, the onset of the appearance of foci/aggregates may be mediated by the increase in the total intracellular levels of the tau. The apparent lag in the onset of foci appearance after the observed fibril internalization appears to be alleviated coinciding with the first, and progress through second cell division cycles. At the DNA replication phase, the chromosome complement increases two times, possibly overcoming the manageable expression/degradation tau levels threshold in a subpopulation of cells. Higher levels of tau (if not recycled efficiently) may result in exaggerated functions of Tau, for example, stabilization and bundling of microtubules, both cytoplasmic and spindle components, impairing resolution of the structures, that depend upon MT depolymerization, such as spindle and intercellular bridge resolution during cytokinesis. Further, the proteasomal pathways may be overwhelmed by the abundance of the same protein for the processing, for example by sequestration of the chaperones and co-chaperones. Impairment of the physiological processes may induce the aggresome-like proteostatic stress pathway, resulting in further cytoplasmic foci accumulation and cell death.

Therefore, we investigated whether cell division arrest by nutrient deprivation or inhibition of protein synthesis affected the formation of the foci. Cycloheximide is a eukaryote protein synthesis inhibitor, produced by the bacterium Streptomyces griseus. Cycloheximide exerts its effect by interfering with the translocation step in protein synthesis (movement of two tRNA molecules and mRNA in relation to the ribosome), thus blocking translational elongation.

Cells were treated for 4h with the following conditions: cycloheximide [50 ug/ml] (protein synthesis inhibition), hlabK18 fibrils [0.1ug/ul] + DMSO (foci inducer), hlabK18 fibrils [0.1ug/ul] + cycloheximide [50 ug/ml] (foci induction in the presence of protein synthesis inhibitor) and hlabK18 fibrils [0.1ug/ul] + HBSS media (foci induction under starvation). Cells were washed and normal media was added, after which the cells were imaged live for 74h post-treatment (Figure 17). The live imaging revealed that all *hlabK18 fibril*-treated cells took up and engulfed the fibrils (Figure 17, red arrows), with fluorescence observed in the cells in a form of puncta throughout the experiment. However, despite the presence of the fibrils inside the cells, the ones treated with protein synthesis inhibitors and nutritionally deficient cells failed to form an extensive amount of foci.

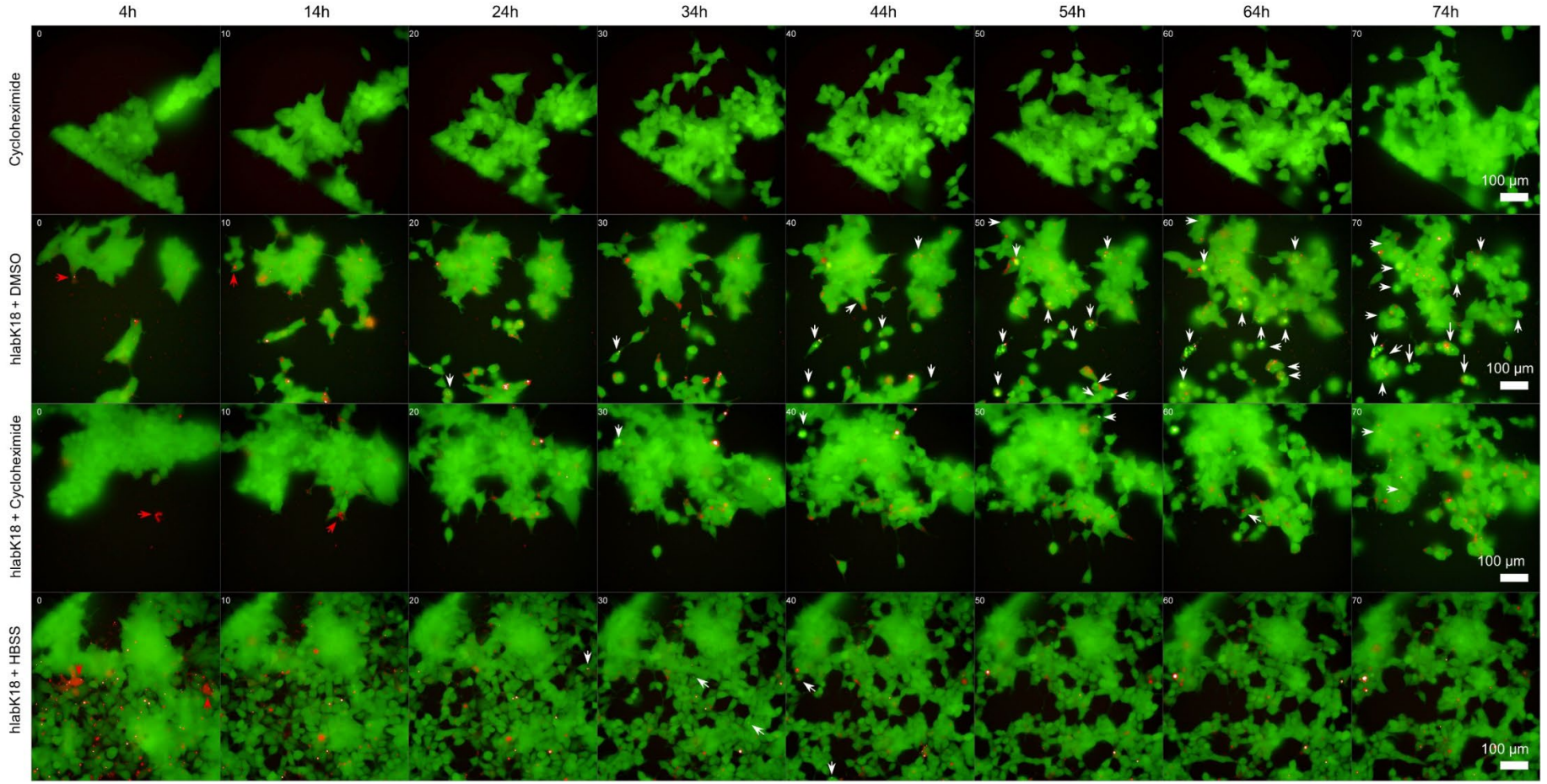

Figure 17. Live cell imaging of foci formation in TauRD cells in the presence of cycloheximide or HBSS treatment. Cells were incubated with the fibril and inhibitor complexes for 4h, washed 2x with media, replenished with 200 µl of media per well and imaged live using Operetta system for ~71h (~74h post-seeding) with images taken every 1h in Green channel (TauRD-YFP, 75ms exposure) and Red channel (labhK18, 75ms exposure). Image was taken every hour for 72

Reduction in the numbers of foci-containing cells was observed in *hlabK18 fibrils + cycloheximide* treated, as well as *hlabK18 fibrils + HBSS-starved* cells compared to *hlabK18 fibrils*-treated only. *hlabK18 fibril*-treated cells developed the nuclear foci followed by the cytoplasmic and died by rounding up and membrane blebbing, indicating autophagic death. As expected, *cycloheximide-only* treated cells did not develop foci, however, the cells were less prolific, highly mobile, and not autophagic. Similarly, the *hlabK18 fibrils + HBSS*-starved cells were less dividing and highly mobile. The cell division arrest and protein synthesis inhibition shift the cell state towards survival, and away from proliferation.

Together with the live imaging showing cell division impairment, confocal imaging showing the chromosome segregation impairment, and stalled metaphase (See Article 3, Figure 4C), these results suggest the potential link between prophase/metaphase-specific events and the onset of the formation of foci. These may include an increase in the levels of endogenous tau proteins exacerbated by the exogenous uptake of tau fibrils. Regulation of the oscillation in the tau levels by protein expression-degradation cycle during cell-cycle progression in mitotic cells may be overwhelmed by the exogenous transduction of Tau fibrils, that upon reaching a certain threshold may prevent the successful resolution of the Tau-mediated reversible cellular processes (i.e. dynamic association-dissociation of tau with microtubules), leading to the induction of proteostatic stress by aggresome-like pathway and autophagic cell death.

Biochemical fractionation showed no insoluble Tau aggregates

To determine the presence of high-molecular and insoluble Tau species within the seeded TauRD cells, sequential cell fractionation was performed (Figure 18A). Cells were seeded with the h4R2N or hlabK18 fibrils, and after 48h harvested using trypsinization and centrifugation. Cells were then lysed using RIPA buffer, and after centrifugation, the supernatant was removed and designated as Soluble (A). The pellet was resuspended in 1% Triton X-100 non-ionic detergent, sonicated, and centrifuged. The supernatant was removed and designated as Triton-soluble (B). The pellet was washed with 1% Triton X-100, resuspended in 1% SDS ionic detergent, sonicated, and centrifuged. This yielded an SDS-soluble fraction (C). The insoluble pellet (D) was washed in 1% SDS, resuspended in PBS and sonicated. The fractions were run on the SDS-PAGE gel and stained with three anti-Tau, as well as anti-GFP antibodies (Figure 18B). The signals from

antibodies were standardized to the total protein loaded per lane. The tagged TauRD constructs were expected to run at around 46 kDa.

Figure 18. Biochemical profiling of the differential solubility of the cellular fractions. A. Fractionation workflow schematic. B. Western blotting of the cell fractions seeded with h4R2N or hlabK18 seeds, and detection by the antibodies against GFP and Tau (77G7, 4R Tau Biolegend, BT2). The antibody signals were standardized to the total protein signal for each fraction.

The results revealed no presence of high molecular weight Tau aggregates, nor the enrichment of the signal in any insoluble fractions of cells seeded with either h4R2N or hlabK18 Tau fibrils (Figure 18B). 77G7 anti-Tau antibody, recognizing epitope at 316-355, showed enrichment of TauRD constructs in the soluble fraction for both types of fibrils, whereas 4R Tau (Biolegend) antibody showed enrichment in the soluble fraction in the cells seeded with h4R2N. Interestingly,

the BT2 antibody, which recognized epitope at 194-198, absent in the TauRD constructs, showed some, albeit very low-level signal for both cells seeded with h4R2N and hLabK18.

The cell fractionation into soluble, non-ionic, and ionic detergent-soluble and insoluble fractions revealed no enrichment of the insoluble fractions or high-molecular-weight Tau species. This suggests that the biochemical profile of the inclusions formed within the TauRD cells is drastically different from the inclusions found in the brains of patients with Tauopathies.

Sequential seeding does not require fibrillar seed to induce the formation of the reporter foci

Finally, we asked, can the foci formation be induced without the addition of the Tau fibrillar seed? To address this, we performed sequential seeding experiments. Here, the two initial cell cultures were either seeded with preformed h4R0N Tau seeds or not treated. After incubation for 24h, the insoluble fractions were extracted from the cultures and used as a seed for the following naïve TauRD cell cultures (Figure 19A). This process has been repeated for up to 4^{th}-order seed generation and cell culture treatments.

As expected, the h4R0N seed induced the formation of foci in the seeded cultures, and the non-treated cultures showed no foci formation (Figure 19B). However, after the treatment of the naïve cell cultures with the seeds derived from the initially non-treated cultures, the foci formations were observed. The foci were also formed in the naïve cultures seeded by the extracts from the h4R0N-treated.

Next, we characterized the biochemical composition of the 1^{st} order seed from non-seeded and h4R0N-seeded cultures by size-exclusion chromatography (SEC; Figure 19C) and Western blotting. The 25 fractions were collected, and the selected fractions corresponding to the peaks observed by SEC were run on SDS-PAGE, transferred onto the nitrocellulose membranes, and probed by anti-GFP and anti-Tau 4R Biolegend antibodies. The results showed that in the 1^{st} order seed from non-treated initial cultures, the strongest signals for 46kDa TauRD-C/YFP were detected with anti-GFP antibodies in fractions A15, B5, B4, B1, and C1, whereas the anti-Tau antibody detected 46kDa construct in B5 and B4. In the 1^{st} order extract prepared from h4R0N-treated cultures, the strongest anti-GFP signal was detected in fractions A15, B15, B5, B4, and B1, whereas the strongest anti-Tau signals were found in B5 and B4 (Figure 19C).

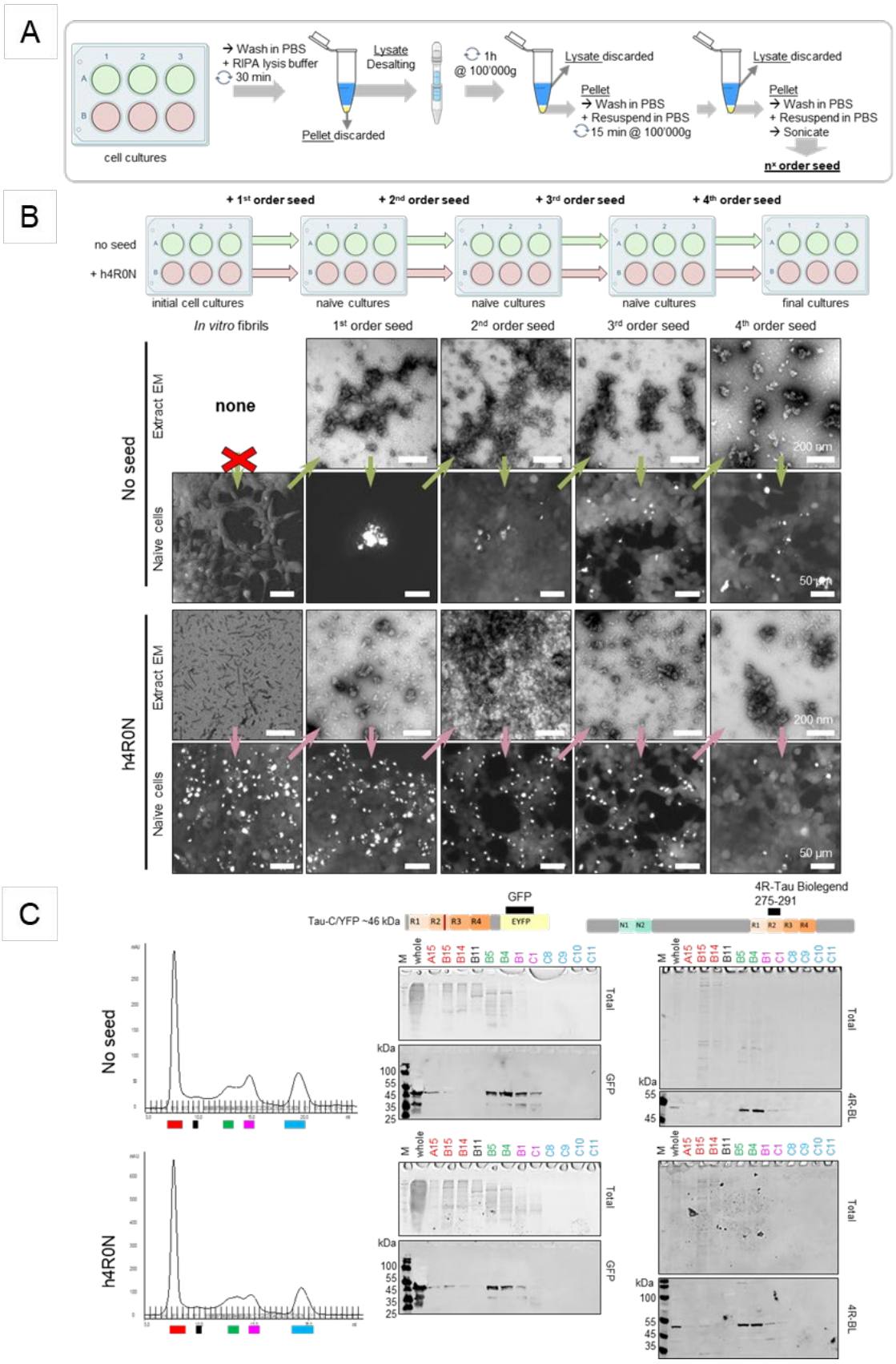
A
cell cultures
→ Wash in PBS
+ RIPA lysis buffer
30 min
Lysate
Desalting
Pellet discarded
1h
@ 100'000g
Lysate discarded
Pellet
→ Wash in PBS
+ Resuspend in PBS
15 min @ 100'000g
Lysate discarded
Pellet
→ Wash in PBS
+ Resuspend in PBS
→ Sonicate
nx order seed
B
+ 1st order seed
+ 2nd order seed
+ 3rd order seed
+ 4th order seed
no seed
+ h4R0N
initial cell cultures
naive cultures
naive cultures
naive cultures
final cultures
In vitro fibrils
1st order seed
2nd order seed
3rd order seed
4th order seed
No seed
Extract EM
Naive cells
none
h4R0N
Extract EM
Naive cells
200 nm
50 µm
C
Tau-C/YFP ~46 kDa
R1 R2 R3 R4
EYFP
GFP
4R-Tau Biolegend
275-291
N1 N2
R1 R2 R3 R4
No seed
h4R0N
M whole A15 B15 B14 B11 B5 B4 B1 C1 C8 C9 C10 C11
Total
GFP
4R-BL
kDa
100
55
45
35
25

Figure 19. Sequential seeding of TauRD cultures by the seeds prepared from the previous seeded or non-seeded cultures. A. The workflow of the seed preparation. B. EM imaging of the prepared seed and foci formation in the naïve TauRD cell cultures after seed transduction. C. Size exclusion chromatography of the 1st order seeds and western blotting and probing with anti-GFP and anti-Tau antibodies.

Next, we wanted to understand the biological activity of the extract fractions in the naïve TauRD cells, and how the foci-inducing potency of the fractions corresponded to the antibody detection of 46kDa species. The selected SEC-derived seed fractions were imaged using EM and then transduced into the naïve TauRD cell cultures.

The foci formation was visualized in the live cells using the EVOS imaging system (Figure 20A). The EM imaging showed the presence of abundant large clumps of material in fractions A15, B15, and B14 for both non-treated and h4R0N-treated culture seed extracts. These fractions correspond to the large peak detected by SEC (Figure 19C, red bar peak), and the strongest anti-GFP signal was found in fraction A15 for non-treated culture-derived seed, and A15 and B15 fractions of h4R0N-treated culture-derived seed. However, the very weak anti-Tau signal was detected in the A15 and B15 fractions of h4R0N-treated culture-derived seed. The foci formation was observed in all three red peak fractions A15, B15, and B14 for both 1st-order seeds, however, the abundance of the cells with the presence of the foci was much higher for the h4R0N-derived seed (Figure 20A).

The fractions of the SEC green and magenta peaks (Figure 19C, green and magenta bar peaks) corresponded to the strongest detection by both anti-GFP and anti-Tau antibodies for both seed preparations, with fractions B5 and B4 showing major signals.

Despite this, the EM imaging detected only sparse material in these fractions, and the extent of naïve cell foci formation was diminished for both seed preparations as compared to the fractions of the SEC red peak. The SEC cyan peak fractions showed no either antibody reactivity (Figure 159, cyan bar peak) and sparse material by EM in both seed preparations.

However, despite this, the foci formation was detected in the naïve TauRD cell cultures seeded by the fractions C9 and C10 of both seed extracts, albeit its extent was heavily diminished compared to the previous fractions. These findings suggest that components other than fibrillar Tau within the seed preparations may be contributing to the foci induction in the naïve TauRD cells. Therefore, we stained fraction A15 of h4R0N-treated culture seed, the highest foci-inducing

fraction, with the phospholipid and methylester probes and imaged the dynamics of the components using a confocal microscope (Figure 20B). The imaging showed staining of the clumped material with both lipid probes, with the vesicular structures appearing and morphing upon the movement of the material (Figure 19B, arrows).

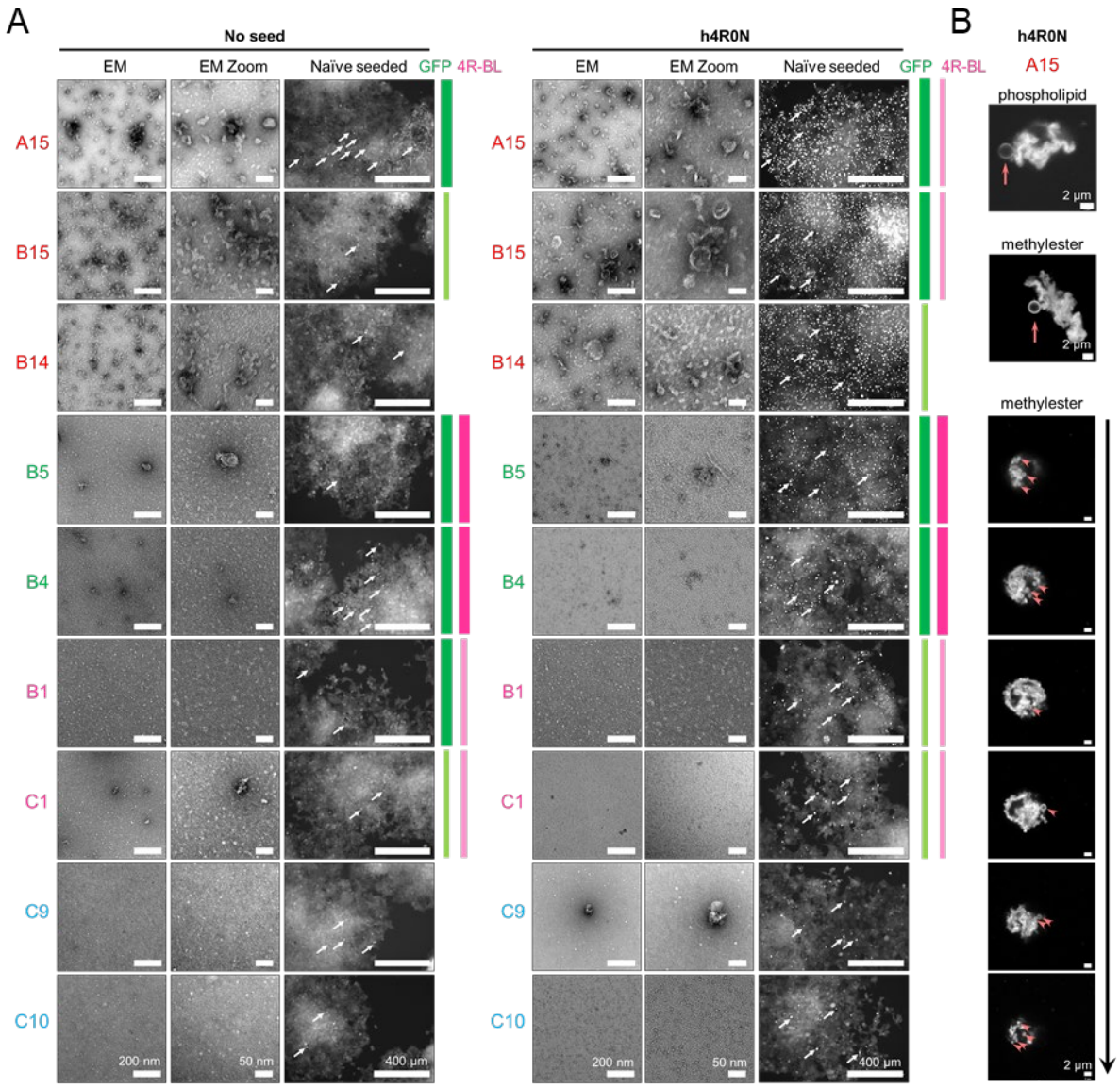

Figure 20. Characterization of 1st order seed SEC fractions by EM and seeding in the naïve TauRD cell cultures. A. Selected SEC fraction EM and seeding in TauRD cells corresponding to the peaks shown in Figure 19C. The antibody bars show the relative intensity of the probing bands in the Western blot in Figure 19C. B. Lipid probe staining of the A15 fraction of the seed prepared from the h4R0N-seeded cultures.

Discussion

The TauRD cells stably express the repeat domain of Tau with the P301S mutation (TauRD P301S) fused with a yellow fluorescent protein (YFP) or cyan fluorescent protein (CFP). The FRET signal is captured in the bright foci formation in these cells using a flow cytometry setup. Formation of aggresomes is directly dependent on the TauRD cell cycle stage, where the cell division arrest using either pharmacological or metabolic modulation leads to complete abrogation of foci formation independent of the transduced Tau seed nature, characterized in exhaustive detail in this paper. This signifies that TauRD cells report not on transduced Tau seed's fibril-seeding capacity, but rather on the proteasomal stress response upon overwhelming of the proteostatic system due to elevated levels of Tau within cells, possibly through sequestration of co-chaperones, as well as cell division impairment. This is underlined by the high expression of endogenous Tau due to multiploidy of chromosome 17, containing MAPT gene (triplication and partial quadruplication) in the HEK293T cells, and overexpression of the tagged TauRD constructs, expressions of which are upregulated during cell division, exacerbated by the internalized Tau seed.

Our work has revealed

a) what percent of cell populations show foci formation;
b) foci formation does not always co-localize with the exogenous seeds;
c) Tau seeds are sequestered within membranous structures;
d) the foci formation in TauRD cells proceeds through two distinct pathways, nuclear and cytoplasmic;
e) the cytoplasmic aggresome-like inclusions in TauRD cells show the canonical morphological and compositional proteomic profile of an aggresome, likely formed as a consequence of the proteasomal impairment and defects in protein clearance mechanisms;
f) the Tau seed internalization and processing proceeds through the endolysosomal pathway;
g) Tau seeds from various Tau fibrils induce the formation of the foci of similar morphologies and ultrastructures when enough cells are surveyed, therefore it is impossible to differentiate between the properties of the seeds only by the foci morphologies;
h) the formation of the foci can be manipulated and abrogated by cell division cycle arrest or nutrient deprivation, and is not dependent on the presence of the internalized seed,

implicating the proteostatic clearance mechanisms leading to the formation of the reporter foci signal;

i) biochemical profiles of the inclusions formed within the TauRD cells show no enrichment in the insoluble fractions, and
j) the presence of the exogenous seed is unnecessary to induce the formation of the foci through sequential seeding of the cell cultures by the material derived from the previously-harvested culture.

Collectively, our findings suggest that the TauRD system does not explicitly report on the human pathology-relevant seeding propensity of the Tau seeds, and the foci formation is not dependent on the fibrillar seed under certain circumstances. The output generated by these assays must be interpreted with caution before extrapolation to human-pathology-relevant conclusions. Furthermore, the ultrastructure properties of the foci structure do not show the formation of PHF-like Tau aggregates. It is a good sensor of Tau aggregates but does not replicate these aggregates or form pathologically relevant forms of Tau.

Model drawbacks

If assessed as a snapshot in time in the limited number of cells, the morphologies observed in different Tau-seeded cultures could appear drastically different. This morphological and biochemical variability has quickly been attributed to the possible differences not only in the extent of the seeding propensity of the added Tau seed (binary presence/absence of FRET plus levels of FRET intensity) but in the seed potency to induce the *varying morphologies* of the bright structures. Further, it has been suggested that the same types of Tau seed induced consistent types of bright structures, and this had somehow been linked to the intrinsic properties of the seed, such as molecular conformations. The seeds could include Tau monomers, in vitro prepared fibrils, brain-derived Tau aggregates, Tau, and/or other molecules present in the whole brain homogenate or cerebrospinal fluid from Tauopathy patients.

Implications

Unfortunately, since the introduction of the FRET BS flow cytometry system in 2014 [781], many papers [792-811], have used this and similar models to conclude about the seeding potency of the

examined Tau species from various human sources without verifying the system by biochemical methods and relied solely on the FRET or fluorescence instead.

FRET BS has been extensively used to differentiate, characterize and assess the seeding potency of the human brain or fluid-derived Tau seeds by FRET flow cytometry, often without cross-validation using other biochemical approaches. The foci morphologies have also been used as sentinels for differentiating between Tau seed strains, however, our data demonstrate that both nuclear and cytoplasmic foci are dynamic and evolving structures, with multiple morphologies present throughout their formation. The lack of in-depth understanding of the processes occurring in this model has the potential to contribute to misleading interpretations of the presence or absence of the seeding potency of specific Tau species. The false positives may result in the wrongful selection of Tau targets for therapeutic development, whereas false negatives will result in missing the potentially pathogenic Tau protein species.

What is needed

For the Tau FRET BS model to reliably inform on the true characteristics of the Tau seed an in-depth understanding is necessary of exactly the relationship between the seed, expressed tagged Tau constructs, and other cellular components and processes. Despite some apparent similarities, the mechanisms, such as FRET, characterized by in vitro experiments may not directly translate to the cellular models due to the huge complexity of living organisms. Especially in the systems such as FRET BS, where the singular type of output, such as the presence/absence of FRET, is progressively employed in the advantage of simplicity and cost-efficiency, it is crucial to understand the underlying mechanisms leading to the baseline deviation. This will help ensure that the interpretation of the results is reliable and could be used to build a body of knowledge based on solid foundations, pertinent to the development of therapies based on these models.

xx

REFERENCES

1 Arendt, T., Stieler, J. T. & Holzer, M. Tau and tauopathies. *Brain Res Bull* **126**, 238-292, doi:https://doi.org/10.1016/j.brainresbull.2016.08.018 (2016).

2 Delacourte, A. & Defossez, A. Alzheimer's disease: Tau proteins, the promoting factors of microtubule assembly, are major components of paired helical filaments. *J. Neurol. Sci.* **76**, 173 (1986).

3 Grundke-Iqbal, I. *et al.* Microtubule-associated protein tau. A component of Alzheimer paired helical filaments. *J. Biol. Chem.* **261**, 6084 (1986).

4 Goedert, M., Spillantini, M. G., Potier, M. C., Ulrich, J. & Crowther, R. A. Cloning and sequencing of the cDNA encoding an isoform of microtubule-associated protein tau containing four tandem repeats: differential expression of tau protein mRNAs in human brain. *EMBO J* **8**, 393-399, doi:10.1002/j.1460-2075.1989.tb03390.x (1989).

5 Jebarupa, B., Muralidharan, M., Arun, A., Mandal, A. K. & Mitra, G. Conformational heterogeneity of tau: Implication on intrinsic disorder, acid stability and fibrillation in Alzheimer's disease. *Biophysical chemistry* **241**, 27-37, doi:10.1016/j.bpc.2018.07.005 (2018).

6 Hefti, M. M. *et al.* High-resolution temporal and regional mapping of MAPT expression and splicing in human brain development. *PloS one* **13**, e0195771, doi:10.1371/journal.pone.0195771 (2018).

7 Jovanov-Milosevic, N. *et al.* Human fetal tau protein isoform: possibilities for Alzheimer's disease treatment. *The international journal of biochemistry & cell biology* **44**, 1290-1294, doi:10.1016/j.biocel.2012.05.001 (2012).

8 Kent, S. A., Spires-Jones, T. L. & Durrant, C. S. The physiological roles of tau and Aβ: implications for Alzheimer's disease pathology and therapeutics. *Acta neuropathologica* **140**, 417-447, doi:10.1007/s00401-020-02196-w (2020).

9 Kosik, K. S. & Finch, E. A. MAP2 and tau segregate into dendritic and axonal domains after the elaboration of morphologically distinct neurites: an immunocytochemical study of cultured rat cerebrum. *Journal of Neuroscience* **7**, 3142-3153 (1987).

10 Zempel, H. & Mandelkow, E. Mechanisms of Axonal Sorting of Tau and Influence of the Axon Initial Segment on Tau Cell Polarity. *Adv Exp Med Biol* **1184**, 69-77, doi:10.1007/978-981-32-9358-8_6 (2019).

11 Hoover, B. R. *et al.* Tau mislocalization to dendritic spines mediates synaptic dysfunction independently of neurodegeneration. *Neuron* **68**, 1067-1081 (2010).

12 Decker, J. M. & Mandelkow, E.-M. in *Tau Biology* 97-103 (Springer, 2019).

13 Park, L. *et al.* Tau induces PSD95–neuronal NOS uncoupling and neurovascular dysfunction independent of neurodegeneration. *Nature Neuroscience* **23**, 1079-1089, doi:10.1038/s41593-020-0686-7 (2020).

14 Mandell, J. & Banker, G. The microtubule cytoskeleton and the development of neuronal polarity. *Neurobiology of aging* **16**, 229-237 (1995).

15 Shahpasand, K. *et al.* Regulation of mitochondrial transport and inter-microtubule spacing by tau phosphorylation at the sites hyperphosphorylated in Alzheimer's disease. *Journal of Neuroscience* **32**, 2430-2441 (2012).

16 Chaudhary, A. R., Berger, F., Berger, C. L. & Hendricks, A. G. Tau directs intracellular trafficking by regulating the forces exerted by kinesin and dynein teams. *Traffic* **19**, 111-121 (2018).

17 Li, H. *et al.* FTO is involved in Alzheimer's disease by targeting TSC1-mTOR-Tau signaling. *Biochemical and biophysical research communications* **498**, 234-239 (2018).

18 Villasante, A., Corces, V. G., Manso-Martinez, R. & Avila, J. Binding of microtubule protein to DNA and chromatin: possibility of simultaneous linkage of microtubule to nucleic acid and assembly of the microtubule structure. *Nucleic Acids Res* **9**, 895-908 (1981).

19 Galas, M. C., Bonnefoy, E., Buee, L. & Lefebvre, B. Emerging Connections Between Tau and Nucleic Acids. *Adv Exp Med Biol* **1184**, 135-143, doi:10.1007/978-981-32-9358-8_12 (2019).

20 Maina, M. B. *et al.* The involvement of tau in nucleolar transcription and the stress response. *Acta Neuropathol Commun* **6**, 70 (2018).

21 Yi, S. *et al.* Tau modulates Schwann cell proliferation, migration and differentiation following peripheral nerve injury. *J Cell Sci* **132** (2019).

22 Chen, J., Kanai, Y., Cowan, N. & Hirokawa, N. Projection domains of MAP2 and tau determine spacings between microtubules in dendrites and axons. *Nature* **360**, 674-677 (1992).
23 Brandt, R., Léger, J. & Lee, G. Interaction of tau with the neural plasma membrane mediated by tau's amino-terminal projection domain. *Journal of Cell Biology* **131**, 1327-1340, doi:10.1083/jcb.131.5.1327 (1995).
24 Arikan, M. C. *et al.* Modulation of the membrane-binding projection domain of tau protein: splicing regulation of exon 3. *Mol Brain Res* **101**, 109-121 (2002).
25 Stancu, I. C., Ferraiolo, M., Terwel, D. & Dewachter, I. Tau Interacting Proteins: Gaining Insight into the Roles of Tau in Health and Disease. *Adv Exp Med Biol* **1184**, 145-166, doi:10.1007/978-981-32-9358-8_13 (2019).
26 Goedert, M. & Spillantini, M. G. Ordered Assembly of Tau Protein and Neurodegeneration. *Adv Exp Med Biol* **1184**, 3-21, doi:10.1007/978-981-32-9358-8_1 (2019).
27 Battisti, A., Ciasca, G., Grottesi, A., Bianconi, A. & Tenenbaum, A. Temporary secondary structures in tau, an intrinsically disordered protein. *Molecular Simulation* **38**, 525-533, doi:10.1080/08927022.2011.633347 (2012).
28 Schweers, O., Schonbrunn-Hanebeck, E., Marx, A. & Mandelkow, E. Structural studies of tau protein and Alzheimer paired helical filaments show no evidence for beta-structure. *J. Biol. Chem.* **269**, 24290 (1994).
29 Mylonas, E. *et al. Biochemistry* **47**, 10345 (2008).
30 Mukrasch, M. D. *et al.* Structural polymorphism of 441-residue tau at single residue resolution. *PLoS biology* **7**, e34, doi:10.1371/journal.pbio.1000034 (2009).
31 Friedhoff, P., von Bergen, M., Mandelkow, E. M. & Mandelkow, E. *Biochim. Biophys. Acta* **1502**, 122 (2000).
32 Trabzuni, D. *et al.* MAPT expression and splicing is differentially regulated by brain region: relation to genotype and implication for tauopathies. *Human molecular genetics* **21**, 4094-4103 (2012).
33 Spillantini, M. G. & Goedert, M. Tau protein pathology in neurodegenerative diseases. *Trends Neurosci* **21**, 428-433, doi:10.1016/s0166-2236(98)01337-x (1998).
34 Goedert, M. & Jakes, R. Expression of separate isoforms of human tau protein: correlation with the tau pattern in brain and effects on tubulin polymerization. *EMBO J* **9**, 4225-4230 (1990).
35 Hong, M. *et al.* Mutation-specific functional impairments in distinct Tau isoforms of hereditary FTDP-17. *Science* **282**, 1914-1917, doi:DOI 10.1126/science.282.5395.1914 (1998).
36 Wang, Y. & Mandelkow, E. Tau in physiology and pathology. *Nature Reviews Neuroscience* **17**, 22-35, doi:10.1038/nrn.2015.1 (2015).
37 Gao, Y.-L. *et al.* Tau in neurodegenerative disease. *Annals of Translational Medicine* **6**, 7 (2018).
38 Dujardin, S. *et al.* Tau molecular diversity contributes to clinical heterogeneity in Alzheimer's disease. *Nat Med* **26**, 1256-1263, doi:10.1038/s41591-020-0938-9 (2020).
39 Hameed, S. *et al.* Role of Fluid Biomarkers and PET Imaging in Early Diagnosis and its Clinical Implication in the Management of Alzheimer's Disease. *J Alzheimers Dis Rep* **4**, 21-37, doi:10.3233/adr-190143 (2020).
40 Betthauser, T. J. *et al.* Amyloid and tau imaging biomarkers explain cognitive decline from late middle-age. *Brain* **143**, 320-335, doi:10.1093/brain/awz378 (2019).
41 Mehta, D., Jackson, R., Paul, G., Shi, J. & Sabbagh, M. Why do trials for Alzheimer's disease drugs keep failing? A discontinued drug perspective for 2010-2015. *Expert opinion on investigational drugs* **26**, 735-739, doi:10.1080/13543784.2017.1323868 (2017).
42 Yiannopoulou, K. G., Anastasiou, A. I., Zachariou, V. & Pelidou, S.-H. Reasons for Failed Trials of Disease-Modifying Treatments for Alzheimer Disease and Their Contribution in Recent Research. *Biomedicines* **7**, 97, doi:10.3390/biomedicines7040097 (2019).
43 Falcon, B. *et al.* Structures of filaments from Pick's disease reveal a novel tau protein fold. *Nature* **561**, 137-140, doi:10.1038/s41586-018-0454-y (2018).
44 Zhang, W. *et al.* Novel tau filament fold in corticobasal degeneration. *Nature* **580**, 283-287, doi:10.1038/s41586-020-2043-0 (2020).
45 Buee, L. & Delacourte, A. Comparative biochemistry of tau in progressive supranuclear palsy, corticobasal degeneration, FTDP-17 and Pick's disease. *Brain pathology (Zurich, Switzerland)* **9**, 681-693, doi:10.1111/j.1750-3639.1999.tb00550.x (1999).
46 Orr, M. E., Sullivan, A. C. & Frost, B. A Brief Overview of Tauopathy: Causes, Consequences, and Therapeutic Strategies. *Trends in pharmacological sciences* **38**, 637-648, doi:10.1016/j.tips.2017.03.011 (2017).

47 Kovacs, G. G. Tauopathies. *Handb Clin Neurol* **145**, 355-368, doi:10.1016/b978-0-12-802395-2.00025-0 (2017).

48 Lee, V. M. Y., Goedert, M. & Trojanowski, J. Q. Neurodegenerative Tauopathies. *Annu Rev Neurosci* **24**, 1121-1159, doi:10.1146/annurev.neuro.24.1.1121 (2001).

49 Goedert, M., Eisenberg, D. S. & Crowther, R. A. Propagation of Tau Aggregates and Neurodegeneration. *Annu Rev Neurosci* **40**, 189-210, doi:10.1146/annurev-neuro-072116-031153 (2017).

50 Schaffert, L.-N. & Carter, W. G. Do Post-Translational Modifications Influence Protein Aggregation in Neurodegenerative Diseases: A Systematic Review. *Brain Sci* **10**, 232, doi:10.3390/brainsci10040232 (2020).

51 Ercan, E. *et al.* A validated antibody panel for the characterization of tau post-translational modifications. *Mol Neurodegener* **12**, 87, doi:10.1186/s13024-017-0229-1 (2017).

52 Park, S., Lee, J. H., Jeon, J. H. & Lee, M. J. Degradation or aggregation: the ramifications of post-translational modifications on tau. *BMB Rep* **51**, 265-273, doi:10.5483/bmbrep.2018.51.6.077 (2018).

53 Serena, M. *et al.* The Involvement of Post-Translational Modifications in Alzheimer's Disease. *Curr Alzheimer Res* **15**, 313-335, doi:http://dx.doi.org/10.2174/1567205014666170505095109 (2018).

54 Martin, L., Latypova, X. & Terro, F. Post-translational modifications of tau protein: Implications for Alzheimer's disease. *Neurochem Int* **58**, 458-471, doi:10.1016/j.neuint.2010.12.023 (2011).

55 Mietelska-Porowska, A., Wasik, U., Goras, M., Filipek, A. & Niewiadomska, G. Tau protein modifications and interactions: their role in function and dysfunction. *International journal of molecular sciences* **15**, 4671-4713 (2014).

56 Alquezar, C., Arya, S. & Kao, A. W. Tau Post-translational Modifications: Dynamic Transformers of Tau Function, Degradation, and Aggregation. *Front Neurol* **11**, 595532, doi:10.3389/fneur.2020.595532 (2020).

57 Wesseling, H. *et al.* Tau PTM Profiles Identify Patient Heterogeneity and Stages of Alzheimer's Disease. *Cell*, doi:https://doi.org/10.1016/j.cell.2020.10.029 (2020).

58 Lashuel, H. A. & Limorenko, G. *Commentary on "Mounting Modifications Move Tau Toward Aggregation in Alzheimer's Brain"*, <https://www.alzforum.org/news/research-news/mounting-modifications-move-tau-toward-aggregation-alzheimers-brain> (2020).

59 Park, S.-Y. & Ferreira, A. The generation of a 17 kDa neurotoxic fragment: an alternative mechanism by which tau mediates β-amyloid-induced neurodegeneration. *Journal of Neuroscience* **25**, 5365-5375 (2005).

60 Canu, N. *et al.* Tau cleavage and dephosphorylation in cerebellar granule neurons undergoing apoptosis. *Journal of Neuroscience* **18**, 7061-7074 (1998).

61 Rametti, A., Esclaire, F., Yardin, C. & Terro, F. Linking alterations in tau phosphorylation and cleavage during neuronal apoptosis. *Journal of Biological Chemistry* **279**, 54518-54528 (2004).

62 Guillozet-Bongaarts, A. L. *et al.* Pseudophosphorylation of tau at serine 422 inhibits caspase cleavage: in vitro evidence and implications for tangle formation in vivo. *Journal of neurochemistry* **97**, 1005-1014 (2006).

63 Gu, J. *et al.* Truncation of tau selectively facilitates its pathological activities. *Journal of Biological Chemistry*, jbc. RA120. 012587 (2020).

64 Cook, C. *et al.* Acetylation of the KXGS motifs in tau is a critical determinant in modulation of tau aggregation and clearance. *Human molecular genetics* **23**, 104-116 (2014).

65 Kontaxi, C., Piccardo, P. & Gill, A. C. Lysine-Directed Post-translational Modifications of Tau Protein in Alzheimer's Disease and Related Tauopathies. *Front Mol Biosci* **4**, doi:10.3389/fmolb.2017.00056 (2017).

66 Liu, F., Iqbal, K., Grundke-Iqbal, I., Hart, G. W. & Gong, C. X. O-GlcNAcylation regulates phosphorylation of tau: a mechanism involved in Alzheimer's disease. *Proceedings of the National Academy of Sciences of the United States of America* **101**, 10804-10809, doi:10.1073/pnas.0400348101 (2004).

67 Lefebvre, T. *et al.* Evidence of a balance between phosphorylation and O-GlcNAc glycosylation of Tau proteins—a role in nuclear localization. *Biochimica et Biophysica Acta (BBA)-General Subjects* **1619**, 167-176 (2003).

68 Bourré, G. *et al.* Direct Crosstalk Between O-GlcNAcylation and Phosphorylation of Tau Protein Investigated by NMR Spectroscopy. *Front Endocrinol (Lausanne)* **9**, 595 (2018). <http://europepmc.org/abstract/MED/30386294

https://doi.org/10.3389/fendo.2018.00595

https://europepmc.org/articles/PMC6198643

https://europepmc.org/articles/PMC6198643?pdf=render>.

69 Lhara, Y. & Kondo, J. Polypeptide Composition of Paired Helical Filaments. *Annals of Medicine* **21**, 121-125, doi:10.3109/07853898909149198 (1989).

70 Mori, H., Kondo, J. & Ihara, Y. Ubiquitin is a component of paired helical filaments in Alzheimer's disease. *Science* **235**, 1641-1644 (1987).

71 Perry, G., Friedman, R., Shaw, G. & Chau, V. Ubiquitin is detected in neurofibrillary tangles and senile plaque neurites of Alzheimer disease brains. *Proceedings of the National Academy of Sciences* **84**, 3033-3036 (1987).

72 Mann, D. M. *et al.* Immunocytochemical profile of neurofibrillary tangles in Down's syndrome patients of different ages. *Journal of the neurological sciences* **92**, 247-260, doi:10.1016/0022-510x(89)90140-8 (1989).

73 Morishima-Kawashima, M. *et al.* Ubiquitin is conjugated with amino-terminally processed tau in paired helical filaments. *Neuron* **10**, 1151-1160 (1993).

74 Cripps, D. *et al.* Alzheimer disease-specific conformation of hyperphosphorylated paired helical filament-Tau is polyubiquitinated through Lys-48, Lys-11, and Lys-6 ubiquitin conjugation. *Journal of Biological Chemistry* **281**, 10825-10838 (2006).

75 Petrucelli, L. *et al.* CHIP and Hsp70 regulate tau ubiquitination, degradation and aggregation. *Human molecular genetics* **13**, 703-714, doi:10.1093/hmg/ddh083 (2004).

76 Bancher, C. *et al.* Abnormal phosphorylation of tau precedes ubiquitination in neurofibrillary pathology of Alzheimer disease. *Brain Res* **539**, 11-18 (1991).

77 García-Sierra, F. *et al.* Ubiquitin is associated with early truncation of tau protein at aspartic acid421 during the maturation of neurofibrillary tangles in Alzheimer's disease. *Brain Pathology* **22**, 240-250 (2012).

78 Iwatsubo, T., Hasegawa, M., Esaki, Y. & Ihara, Y. Lack of ubiquitin immunoreactivities at both ends of neuropil threads. Possible bidirectional growth of neuropil threads. *The American journal of pathology* **140**, 277 (1992).

79 Riederer, I. M., Schiffrin, M., Kövari, E., Bouras, C. & Riederer, B. M. Ubiquitination and cysteine nitrosylation during aging and Alzheimer's disease. *Brain Res Bull* **80**, 233-241 (2009).

80 Tan, J. M. *et al.* Lysine 63-linked ubiquitination promotes the formation and autophagic clearance of protein inclusions associated with neurodegenerative diseases. *Human molecular genetics* **17**, 431-439 (2008).

81 Dickey, C. A. *et al.* Deletion of the ubiquitin ligase CHIP leads to the accumulation, but not the aggregation, of both endogenous phospho-and caspase-3-cleaved tau species. *Journal of Neuroscience* **26**, 6985-6996 (2006).

82 Iqbal, K. *et al.* in *Ageing and Dementia* 169-180 (Springer, 1998).

83 Abreha, M. H. *et al.* Quantitative Analysis of the Brain Ubiquitylome in Alzheimer's Disease. *Proteomics* **18**, e1800108, doi:10.1002/pmic.201800108 (2018).

84 Kametani, F. *et al.* Comparison of Common and Disease-Specific Post-translational Modifications of Pathological Tau Associated With a Wide Range of Tauopathies. *Frontiers in neuroscience* **14**, 581936, doi:10.3389/fnins.2020.581936 (2020).

85 Arakhamia, T. *et al.* Posttranslational Modifications Mediate the Structural Diversity of Tauopathy Strains. *Cell* **180**, 633-644.e612, doi:https://doi.org/10.1016/j.cell.2020.01.027 (2020).

86 Luo, H. B. *et al.* SUMOylation at K340 inhibits tau degradation through deregulating its phosphorylation and ubiquitination. *Proceedings of the National Academy of Sciences of the United States of America* **111**, 16586-16591, doi:10.1073/pnas.1417548111 (2014).

87 Avila, J. Tau aggregation into fibrillar polymers: taupathies. *FEBS letters* **476**, 89-92 (2000).

88 Wille, H., Drewes, G., Biernat, J., Mandelkow, E.-M. & Mandelkow, E. Alzheimer-like paired helical filaments and antiparallel dimers formed from microtubule-associated protein tau in vitro. *J Cell Biol* **118**, 573-584 (1992).

89 Crowther, R. A., Olesen, O. F., Jakes, R. & Goedert, M. The microtubule binding repeats of tau protein assemble into filaments like those found in Alzheimer's disease. *FEBS Lett.* **309**, 199 (1992).

90 Al-Hilaly, Y. K. *et al.* Tau (297-391) forms filaments that structurally mimic the core of paired helical filaments in Alzheimer's disease brain. *FEBS letters* **594**, 944-950, doi:10.1002/1873-3468.13675 (2020).

91 Despres, C. *et al.* Identification of the Tau phosphorylation pattern that drives its aggregation. *Proceedings of the National Academy of Sciences of the United States of America* **114**, 9080-9085, doi:10.1073/pnas.1708448114 (2017).

92 Despres, C. *et al.* Major Differences between the Self-Assembly and Seeding Behavior of Heparin-Induced and in Vitro Phosphorylated Tau and Their Modulation by Potential Inhibitors. *ACS chemical biology* **14**, 1363-1379, doi:10.1021/acschembio.9b00325 (2019).

93 Goedert, M. *et al.* Assembly of microtubule-associated protein tau into Alzheimer-like filaments induced by sulphated glycosaminoglycans. *Nature* **383**, 550-553, doi:10.1038/383550a0 (1996).

94 Kampers, T., Friedhoff, P., Biernat, J., Mandelkow, E.-M. & Mandelkow, E. RNA stimulates aggregation of microtubule-associated protein tau into Alzheimer-like paired helical filaments. *FEBS letters* **399**, 344-349 (1996).

95 Wilson, D. M. & Binder, L. I. Free fatty acids stimulate the polymerization of tau and amyloid beta peptides. In vitro evidence for a common effector of pathogenesis in Alzheimer's disease. *The American journal of pathology* **150**, 2181 (1997).

96 Friedhoff, P., Schneider, A., Mandelkow, E. M. & Mandelkow, E. Rapid assembly of Alzheimer-like paired helical filaments from microtubule-associated protein tau monitored by fluorescence in solution. *Biochemistry* **37**, 10223-10230, doi:10.1021/bi980537d (1998).

97 Perez, M., Valpuesta, J. M., Medina, M., Montejo de Garcini, E. & Avila, J. Polymerization of tau into filaments in the presence of heparin: the minimal sequence required for tau-tau interaction. *Journal of neurochemistry* **67**, 1183-1190, doi:10.1046/j.1471-4159.1996.67031183.x (1996).

98 Luo, J. Y. & He, R.-Q. Effect of acetaldehyde on aggregation of neuronal tau. *Protein and peptide letters* **6**, 105-110 (1999).

99 Kim, A. C., Lim, S. & Kim, Y. K. Metal Ion Effects on Aβ and Tau Aggregation. *International journal of molecular sciences* **19**, doi:10.3390/ijms19010128 (2018).

100 Jeganathan, S., von Bergen, M., Brutlach, H., Steinhoff, H. J. & Mandelkow, E. Global hairpin folding of tau in solution. *Biochemistry* **45**, 2283-2293, doi:10.1021/bi0521543 (2006).

101 Barghorn, S. & Mandelkow, E. Toward a unified scheme for the aggregation of tau into Alzheimer paired helical filaments. *Biochemistry* **41**, 14885-14896, doi:10.1021/bi026469j (2002).

102 Giamblanco, N. *et al.* Mechanisms of heparin-induced tau aggregation revealed by single nanopore. *ACS sensors*, doi:10.1021/acssensors.0c00193 (2020).

103 Ferrone, F. in *Methods in enzymology* Vol. 309 256-274 (Elsevier, 1999).

104 Chirita, C. N., Congdon, E. E., Yin, H. & Kuret, J. Triggers of full-length tau aggregation: a role for partially folded intermediates. *Biochemistry* **44**, 5862-5872 (2005).

105 King, M. E., Ahuja, V., Binder, L. I. & Kuret, J. Ligand-dependent tau filament formation: implications for Alzheimer's disease progression. *Biochemistry* **38**, 14851-14859 (1999).

106 Kyte, J. & Doolittle, R. F. A simple method for displaying the hydropathic character of a protein. *Journal of molecular biology* **157**, 105-132 (1982).

107 Berman, H. M. *et al.* The protein data bank. *Nucleic acids research* **28**, 235-242 (2000).

108 Kim, S. *et al.* PubChem substance and compound databases. *Nucleic acids research* **44**, D1202-D1213 (2016).

109 Breydo, L., Wu, J. W. & Uversky, V. N. α-Synuclein misfolding and Parkinson's disease. *Biochimica et Biophysica Acta (BBA) - Molecular Basis of Disease* **1822**, 261-285, doi:https://doi.org/10.1016/j.bbadis.2011.10.002 (2012).

110 Elbaum-Garfinkle, S. & Rhoades, E. Identification of an aggregation-prone structure of tau. *Journal of the American Chemical Society* **134**, 16607-16613, doi:10.1021/ja305206m (2012).

111 von Bergen, M. *et al.* Assembly of tau protein into Alzheimer paired helical filaments depends on a local sequence motif ((306)VQIVYK(311)) forming beta structure. *Proceedings of the National Academy of Sciences of the United States of America* **97**, 5129-5134, doi:10.1073/pnas.97.10.5129 (2000).

112 Chen, D. *et al.* Tau local structure shields an amyloid-forming motif and controls aggregation propensity. *Nat Commun* **10**, 2493 (2019). <http://europepmc.org/abstract/MED/31175300

https://doi.org/10.1038/s41467-019-10355-1

https://europepmc.org/articles/PMC6555816

https://europepmc.org/articles/PMC6555816?pdf=render>.

113 Mirbaha, H. *et al.* Inert and seed-competent tau monomers suggest structural origins of aggregation. *eLife* **7** (2018). <http://europepmc.org/abstract/MED/29988016

https://doi.org/10.7554/eLife.36584

https://europepmc.org/articles/PMC6039173

https://europepmc.org/articles/PMC6039173?pdf=render>.

114 Fichou, Y. *et al.* Cofactors are essential constituents of stable and seeding-active tau fibrils. *Proceedings of the National Academy of Sciences of the United States of America* **115**, 13234-13239, doi:10.1073/pnas.1810058115 (2018).

115 Pettegrew, J. W., Moossy, J., Withers, G., McKeag, D. & Panchalingam, K. 31P nuclear magnetic resonance study of the brain in Alzheimer's disease. *J Neuropathol Exp Neurol* **47**, 235-248, doi:10.1097/00005072-198805000-00004 (1988).

116 Lee, V. M., Balin, B. J., Otvos, L. & Trojanowski, J. Q. A68: a major subunit of paired helical filaments and derivatized forms of normal Tau. *Science* **251**, 675-678 (1991).

117 Hasegawa, M. in *Tau Biology* (eds Akihiko Takashima, Benjamin Wolozin, & Luc Buee) 23-34 (Springer Singapore, 2019).

118 Baum, L. *et al.* Overexpressed tau protein in cultured cells is phosphorylated without formation of PHF: implication of phosphoprotein phosphatase involvement.

119 Kimura, T. *et al.* Sequential changes of tau-site-specific phosphorylation during development of paired helical filaments. *Dementia (Basel, Switzerland)* **7**, 177-181, doi:10.1159/000106875 (1996).

120 Virchow, R. Zur Cellulose-Frage. *Archiv für pathologische Anatomie und Physiologie und für klinische Medicin* **8**, 140-144, doi:10.1007/BF01935322 (1855).

121 Hass, G. Studies of amyloid. II. The isolation of a polysaccharide from amyloid-bearing tissues. *Arch. Path* **34**, 92-105 (1942).

122 Ancsin, J. B. Amyloidogenesis: historical and modern observations point to heparan sulfate proteoglycans as a major culprit. *Amyloid* **10**, 67-79 (2003).

123 Kato, T. *et al.* The binding of basic fibroblast growth factor to Alzheimer's neurofibrillary tangles and senile plaques. *Neurosci Lett* **122**, 33-36 (1991).

124 Su, J., Cummings, B. & Cotman, C. Localization of heparan sulfate glycosaminoglycan and proteoglycan core protein in aged brain and Alzheimer's disease. *Neuroscience* **51**, 801-813 (1992).

125 Dewitt, D. A., Silver, J., Canning, D. R. & Perry, G. Chondroitin sulfate proteoglycans are associated with the lesions of Alzheimer's disease. (1993).

126 Dewitt, D. A., Richey, P., Praprotnik, D., Silver, J. & Perry, G. Chondroitin sulfate proteoglycans are a common component of neuronal inclusions and astrocytic reaction in neurodegenerative diseases. *Brain Res* **656**, 205-209 (1994).

127 Ma, J. *et al.* Extracellular matrix proteins involved in Alzheimer's disease. *Chemistry (Weinheim an der Bergstrasse, Germany)*, doi:10.1002/chem.202000782 (2020).

128 Maiza, A. *et al.* The role of heparan sulfates in protein aggregation and their potential impact on neurodegeneration. *FEBS letters* **592**, 3806-3818, doi:10.1002/1873-3468.13082 (2018).

129 Fukuchi, K., Hart, M. & Li, L. Alzheimer's disease and heparan sulfate proteoglycan. *Frontiers in bioscience : a journal and virtual library* **3**, d327-337, doi:10.2741/a277 (1998).

130 Lorente-Gea, L. *et al.* Heparan Sulfate Proteoglycans Undergo Differential Expression Alterations in Alzheimer Disease Brains. *J Neuropathol Exp Neurol* **79**, 474-483, doi:10.1093/jnen/nlaa016 (2020).

131 Snow, A. D. *et al.* Early accumulation of heparan sulfate in neurons and in the beta-amyloid protein-containing lesions of Alzheimer's disease and Down's syndrome. *The American journal of pathology* **137**, 1253-1270 (1990).

132 Perlmutter, L., Barron, E., Saperia, D. & Chui, H. Association between vascular basement membrane components and the lesions of Alzheimer's disease. *J Neurosci Res* **30**, 673-681 (1991).
133 Perry, G. *et al.* Association of heparan sulfate proteoglycan with the neurofibrillary tangles of Alzheimer's disease. *Journal of Neuroscience* **11**, 3679-3683 (1991).
134 Snow, A. D. *et al.* The presence of heparan sulfate proteoglycans in the neuritic plaques and congophilic angiopathy in Alzheimer's disease. *The American journal of pathology* **133**, 456 (1988).
135 Horssen, J. *et al.* Heparan sulfate proteoglycan expression in cerebrovascular amyloid β deposits in Alzheimer's disease and hereditary cerebral hemorrhage with amyloidosis (Dutch) brains. *Acta neuropathologica* **102**, 604-614 (2001).
136 Bruinsma, I. B. *et al.* Sulfation of heparan sulfate associated with amyloid-beta plaques in patients with Alzheimer's disease. *Acta neuropathologica* **119**, 211-220, doi:10.1007/s00401-009-0577-1 (2010).
137 Verbeek, M. M. *et al.* Agrin is a major heparan sulfate proteoglycan accumulating in Alzheimer's disease brain. *The American journal of pathology* **155**, 2115-2125, doi:10.1016/s0002-9440(10)65529-0 (1999).
138 Cotman, S. L., Halfter, W. & Cole, G. J. Agrin binds to beta-amyloid (Abeta), accelerates abeta fibril formation, and is localized to Abeta deposits in Alzheimer's disease brain. *Mol Cell Neurosci* **15**, 183-198, doi:10.1006/mcne.1999.0816 (2000).
139 Spillantini, M. G., Tolnay, M., Love, S. & Goedert, M. Microtubule-associated protein tau, heparan sulphate and alpha-synuclein in several neurodegenerative diseases with dementia. *Acta neuropathologica* **97**, 585-594, doi:10.1007/s004010051034 (1999).
140 Fraser, P. E., Nguyen, J. T., Chin, D. T. & Kirschner, D. A. Effects of sulfate ions on Alzheimer β/A4 peptide assemblies: implications for amyloid fibril-proteoglycan interactions. *Journal of neurochemistry* **59**, 1531-1540 (1992).
141 Brunden, K. R., Richter-Cook, N. J., Chaturvedi, N. & Frederickson, R. C. pH-dependent binding of synthetic β-amyloid peptides to glycosaminoglycans. *Journal of neurochemistry* **61**, 2147-2154 (1993).
142 Hasegawa, M., Crowther, R. A., Jakes, R. & Goedert, M. Alzheimer-like changes in microtubule-associated protein Tau induced by sulfated glycosaminoglycans. Inhibition of microtubule binding, stimulation of phosphorylation, and filament assembly depend on the degree of sulfation. *The Journal of biological chemistry* **272**, 33118-33124, doi:10.1074/jbc.272.52.33118 (1997).
143 Narindrasorasak, S. *et al.* High affinity interactions between the Alzheimer's beta-amyloid precursor proteins and the basement membrane form of heparan sulfate proteoglycan. *Journal of Biological Chemistry* **266**, 12878-12883 (1991).
144 Buee, L. *et al.* Binding of vascular heparan sulfate proteoglycan to Alzheimer's amyloid precursor protein is mediated in part by the N-terminal region of A4 peptide. *Brain Res* **627**, 199-204, doi:10.1016/0006-8993(93)90321-d (1993).
145 Clarris, H. J. *et al.* Identification of heparin-binding domains in the amyloid precursor protein of Alzheimer's disease by deletion mutagenesis and peptide mapping. *Journal of neurochemistry* **68**, 1164-1172, doi:10.1046/j.1471-4159.1997.68031164.x (1997).
146 Mok, S. S. *et al.* Expression and analysis of heparin-binding regions of the amyloid precursor protein of Alzheimer's disease. *FEBS letters* **415**, 303-307, doi:10.1016/s0014-5793(97)01146-0 (1997).
147 Multhaup, G., Mechler, H. & Masters, C. L. Characterization of the high affinity heparin binding site of the Alzheimer's disease beta A4 amyloid precursor protein (APP) and its enhancement by zinc(II). *Journal of molecular recognition : JMR* **8**, 247-257, doi:10.1002/jmr.300080403 (1995).
148 Williamson, T. G., Nurcombe, V., Beyreuther, K., Masters, C. L. & Small, D. H. Affinity purification of proteoglycans that bind to the amyloid protein precursor of Alzheimer's disease. *Journal of neurochemistry* **65**, 2201-2208, doi:10.1046/j.1471-4159.1995.65052201.x (1995).
149 Huynh, M. B. *et al.* Glycosaminoglycans from Alzheimer's disease hippocampus have altered capacities to bind and regulate growth factors activities and to bind tau. *PloS one* **14**, e0209573 (2019). <http://europepmc.org/abstract/MED/30608949

https://doi.org/10.1371/journal.pone.0209573

https://europepmc.org/articles/PMC6319808

https://europepmc.org/articles/PMC6319808?pdf=render>.

150 Shimizu, H., Ghazizadeh, M., Sato, S., Oguro, T. & Kawanami, O. Interaction between beta-amyloid protein and heparan sulfate proteoglycans from the cerebral capillary basement membrane in Alzheimer's disease. *Journal of clinical neuroscience : official journal of the Neurosurgical Society of Australasia* **16**, 277-282, doi:10.1016/j.jocn.2008.04.009 (2009).

151 Castillo, G. M., Lukito, W., Wight, T. N. & Snow, A. D. The sulfate moieties of glycosaminoglycans are critical for the enhancement of beta-amyloid protein fibril formation. *Journal of neurochemistry* **72**, 1681-1687, doi:10.1046/j.1471-4159.1999.721681.x (1999).

152 Zhong, Q., Congdon, E. E., Nagaraja, H. N. & Kuret, J. Tau isoform composition influences rate and extent of filament formation. *The Journal of biological chemistry* **287**, 20711-20719, doi:10.1074/jbc.M112.364067 (2012).

153 Liu, K. *et al.* Glycation alter the process of Tau phosphorylation to change Tau isoforms aggregation property. *Biochimica et Biophysica Acta (BBA) - Molecular Basis of Disease* **1862**, 192-201, doi:https://doi.org/10.1016/j.bbadis.2015.12.002 (2016).

154 Arrasate, M., Perez, M., Valpuesta, J. M. & Avila, J. Role of glycosaminoglycans in determining the helicity of paired helical filaments. *The American journal of pathology* **151**, 1115-1122 (1997).

155 Falcon, B. *et al.* Novel tau filament fold in chronic traumatic encephalopathy encloses hydrophobic molecules. *Nature* **568**, 420-423, doi:10.1038/s41586-019-1026-5 (2019).

156 Shi, Y. *et al.* Structure-based Classification of Tauopathies. *bioRxiv*, 2021.2005.2028.446130, doi:10.1101/2021.05.28.446130 (2021).

157 Dinkel, P. D., Holden, M. R., Matin, N. & Margittai, M. RNA Binds to Tau Fibrils and Sustains Template-Assisted Growth. *Biochemistry* **54**, 4731-4740, doi:10.1021/acs.biochem.5b00453 (2015).

158 Stopschinski, B. E. *et al.* Specific glycosaminoglycan chain length and sulfation patterns are required for cell uptake of tau versus alpha-synuclein and beta-amyloid aggregates. *The Journal of biological chemistry* **293**, 10826-10840, doi:10.1074/jbc.RA117.000378 (2018).

159 Townsend, D., Fullwood, N. J., Yates, E. A. & Middleton, D. A. Aggregation Kinetics and Filament Structure of a Tau Fragment Are Influenced by the Sulfation Pattern of the Cofactor Heparin. *Biochemistry* **59**, 4003-4014, doi:10.1021/acs.biochem.0c00443 (2020).

160 Guo, J. L. *et al.* Unique pathological tau conformers from Alzheimer's brains transmit tau pathology in nontransgenic mice. *J Exp Med* **213**, 2635-2654, doi:10.1084/jem.20160833 (2016).

161 Chakraborty, P. *et al.* Co-factor-free aggregation of tau into seeding-competent RNA-sequestering amyloid fibrils. *Nat Commun* **12**, 4231, doi:10.1038/s41467-021-24362-8 (2021).

162 Rauch, J. N., Olson, S. H. & Gestwicki, J. E. Interactions between Microtubule-Associated Protein Tau (MAPT) and Small Molecules. *Cold Spring Harb Perspect Med* **7** (2017). <http://europepmc.org/abstract/MED/27940599

https://doi.org/10.1101/cshperspect.a024034

https://europepmc.org/articles/PMC5495054

https://europepmc.org/articles/PMC5495054?pdf=render>.

163 Scheres, S. H., Zhang, W., Falcon, B. & Goedert, M. Cryo-EM structures of tau filaments. *Curr Opin Struct Biol* **64**, 17-25, doi:10.1016/j.sbi.2020.05.011 (2020).

164 Zhang, W. *et al.* Heparin-induced tau filaments are polymorphic and differ from those in Alzheimer's and Pick's diseases. *eLife* **8**, doi:10.7554/eLife.43584 (2019).

165 Xu, S., Brunden, K. R., Trojanowski, J. Q. & Lee, V. M.-Y. Characterization of tau fibrillization in vitro. *Alzheimer's & Dementia* **6**, 110-117, doi:https://doi.org/10.1016/j.jalz.2009.06.002 (2010).

166 Wegmann, S. *et al.* Human Tau isoforms assemble into ribbon-like fibrils that display polymorphic structure and stability. *The Journal of biological chemistry* **285**, 27302-27313, doi:10.1074/jbc.M110.145318 (2010).

167 von Bergen, M. *et al.* The core of tau-paired helical filaments studied by scanning transmission electron microscopy and limited proteolysis. *Biochemistry* **45**, 6446-6457, doi:10.1021/bi052530j (2006).

168 Taniguchi-Watanabe, S. *et al.* Biochemical classification of tauopathies by immunoblot, protein sequence and mass spectrometric analyses of sarkosyl-insoluble and trypsin-resistant tau. *Acta neuropathologica* **131**, 267-280 (2016).
169 Dickson, D. W., Kouri, N., Murray, M. E. & Josephs, K. A. Neuropathology of frontotemporal lobar degeneration-tau (FTLD-tau). *J Mol Neurosci* **45**, 384-389, doi:10.1007/s12031-011-9589-0 (2011).
170 Forman, M. S. *et al.* Signature Tau Neuropathology in Gray and White Matter of Corticobasal Degeneration. *The American journal of pathology* **160**, 2045-2053, doi:https://doi.org/10.1016/S0002-9440(10)61154-6 (2002).
171 Haj-Yahya, M. & Lashuel, H. A. Protein semisynthesis provides access to tau disease-associated post-translational modifications (PTMs) and paves the way to deciphering the tau PTM code in health and diseased states. *Journal of the American Chemical Society* **140**, 6611-6621 (2018).
172 Berriman, J. *et al.* Tau filaments from human brain and from in vitro assembly of recombinant protein show cross-beta structure. *Proceedings of the National Academy of Sciences of the United States of America* **100**, 9034-9038, doi:10.1073/pnas.1530287100 (2003).
173 Arima, K. Ultrastructural characteristics of tau filaments in tauopathies: immuno-electron microscopic demonstration of tau filaments in tauopathies. *Neuropathology* **26**, 475-483 (2006).
174 Yamada, K. In Vivo Microdialysis Method to Collect Large Extracellular Proteins from Brain Interstitial Fluid with High-molecular Weight Cut-off Probes. *Journal of visualized experiments : JoVE*, doi:10.3791/57869 (2018).
175 Yamada, K. In Vivo Microdialysis of Brain Interstitial Fluid for the Determination of Extracellular Tau Levels. *Methods in molecular biology (Clifton, N.J.)* **1523**, 285-296, doi:10.1007/978-1-4939-6598-4_17 (2017).
176 Yamada, K. *et al.* Neuronal activity regulates extracellular tau in vivo. *J Exp Med* **211**, 387-393, doi:10.1084/jem.20131685 (2014).
177 Yamada, K. *et al.* In vivo microdialysis reveals age-dependent decrease of brain interstitial fluid tau levels in P301S human tau transgenic mice. *The Journal of neuroscience : the official journal of the Society for Neuroscience* **31**, 13110-13117, doi:10.1523/JNEUROSCI.2569-11.2011 (2011).
178 Melrose, H. L. *et al.* Impaired dopaminergic neurotransmission and microtubule-associated protein tau alterations in human LRRK2 transgenic mice. *Neurobiol Dis* **40**, 503-517, doi:10.1016/j.nbd.2010.07.010 (2010).
179 Frasca, D. *et al.* Metronidazole and hydroxymetronidazole central nervous system distribution: 1. microdialysis assessment of brain extracellular fluid concentrations in patients with acute brain injury. *Antimicrob Agents Chemother* **58**, 1019-1023, doi:10.1128/aac.01760-13 (2014).
180 Eberlin, L. S. *et al.* Ambient mass spectrometry for the intraoperative molecular diagnosis of human brain tumors. *Proceedings of the National Academy of Sciences* **110**, 1611, doi:10.1073/pnas.1215687110 (2013).
181 Hänel, L., Kwiatkowski, M., Heikaus, L. & Schlüter, H. Mass spectrometry-based intraoperative tumor diagnostics. *Future Sci OA* **5**, FSO373, doi:10.4155/fsoa-2018-0087 (2019).
182 Zhang, J. *et al.* Nondestructive tissue analysis for ex vivo and in vivo cancer diagnosis using a handheld mass spectrometry system. *Sci Transl Med* **9**, eaan3968, doi:10.1126/scitranslmed.aan3968 (2017).
183 Mirza, K. B., Golden, C. T., Nikolic, K. & Toumazou, C. Closed-Loop Implantable Therapeutic Neuromodulation Systems Based on Neurochemical Monitoring. *Frontiers in neuroscience* **13**, 808, doi:10.3389/fnins.2019.00808 (2019).
184 Chatard, C., Sabac, A., Moreno-Velasquez, L., Meiller, A. & Marinesco, S. Minimally Invasive Microelectrode Biosensors Based on Platinized Carbon Fibers for in Vivo Brain Monitoring. *ACS central science* **4**, 1751-1760 (2018).
185 Kirschner, D. A., Abraham, C. & Selkoe, D. J. X-ray diffraction from intraneuronal paired helical filaments and extraneuronal amyloid fibers in Alzheimer disease indicates cross-beta conformation. *Proceedings of the National Academy of Sciences of the United States of America* **83**, 503-507, doi:10.1073/pnas.83.2.503 (1986).
186 von Bergen, M. *et al.* Mutations of tau protein in frontotemporal dementia promote aggregation of paired helical filaments by enhancing local β-structure. *Journal of Biological Chemistry* **276**, 48165-48174 (2001).

187 Giannetti, A. M. *et al.* Fibers of tau fragments, but not full length tau, exhibit a cross beta-structure: implications for the formation of paired helical filaments. *Protein Sci* **9**, 2427-2435, doi:10.1110/ps.9.12.2427 (2000).
188 Barghorn, S., Davies, P. & Mandelkow, E. Tau paired helical filaments from Alzheimer's disease brain and assembled in vitro are based on beta-structure in the core domain. *Biochemistry* **43**, 1694 (2004).
189 Fitzpatrick, A. W. P. *et al.* Cryo-EM structures of tau filaments from Alzheimer's disease. *Nature* **547**, 185-190, doi:10.1038/nature23002 (2017).
190 Margittai, M. & Langen, R. Template-assisted filament growth by parallel stacking of tau. *Proceedings of the National Academy of Sciences of the United States of America* **101**, 10278-10283, doi:10.1073/pnas.0401911101 (2004).
191 Daebel, V. *et al. Journal of the American Chemical Society* **134**, 13982 (2012).
192 Lippens, G. & Gigant, B. Elucidating Tau function and dysfunction in the era of cryo-EM. *The Journal of biological chemistry* **294**, 9316-9325, doi:10.1074/jbc.REV119.008031 (2019).
193 Xiang, X. *et al.* Role of molecular polymorphism in defining tau filament structures in neurodegenerative diseases. *bioRxiv*, 2021.2005.2024.445353, doi:10.1101/2021.05.24.445353 (2021).
194 Hallinan, G. I. *et al.* Structure of Tau filaments in Prion protein amyloidoses. *Acta neuropathologica*, doi:10.1007/s00401-021-02336-w (2021).
195 Fichou, Y., Vigers, M., Goring, A. K., Eschmann, N. A. & Han, S. Heparin-induced tau filaments are structurally heterogeneous and differ from Alzheimer's disease filaments. *Chemical communications (Cambridge, England)* **54**, 4573-4576, doi:10.1039/c8cc01355a (2018).
196 Siddiqua, A. & Margittai, M. Three- and four-repeat Tau coassemble into heterogeneous filaments: an implication for Alzheimer disease. *The Journal of biological chemistry* **285**, 37920-37926, doi:10.1074/jbc.M110.185728 (2010).
197 Xu, S., Brunden, K. R., Trojanowski, J. Q. & Lee, V. M. Y. Characterization of tau fibrillization in vitro. *Alzheimers Dement* **6**, 110-117, doi:10.1016/j.jalz.2009.06.002 (2010).
198 Crowther, R. A. Straight and paired helical filaments in Alzheimer disease have a common structural unit. *Proceedings of the National Academy of Sciences of the United States of America* **88**, 2288-2292, doi:10.1073/pnas.88.6.2288 (1991).
199 Weismiller, H. A. *et al.* Structural disorder in four-repeat Tau fibrils reveals a new mechanism for barriers to cross-seeding of Tau isoforms. *The Journal of biological chemistry* **293**, 17336-17348, doi:10.1074/jbc.RA118.005316 (2018).
200 Sibille, N. *et al.* Structural impact of heparin binding to full-length Tau as studied by NMR spectroscopy. *Biochemistry* **45**, 12560-12572, doi:10.1021/bi060964o (2006).
201 Paudel, H. K. & Li, W. Heparin-induced conformational change in microtubule-associated protein Tau as detected by chemical cross-linking and phosphopeptide mapping. *The Journal of biological chemistry* **274**, 8029-8038, doi:10.1074/jbc.274.12.8029 (1999).
202 Basurto-Islas, G. *et al.* Accumulation of aspartic acid421-and glutamic acid391-cleaved tau in neurofibrillary tangles correlates with progression in Alzheimer disease. *Journal of Neuropathology & Experimental Neurology* **67**, 470-483 (2008).
203 Guillozet-Bongaarts, A. L. *et al.* Tau truncation during neurofibrillary tangle evolution in Alzheimer's disease. *Neurobiology of aging* **26**, 1015-1022, doi:https://doi.org/10.1016/j.neurobiolaging.2004.09.019 (2005).
204 Ganguly, P. *et al.* Tau assembly: the dominant role of PHF6 (VQIVYK) in microtubule binding region repeat R3. *J Phys Chem B* **119**, 4582-4593, doi:10.1021/acs.jpcb.5b00175 (2015).
205 Wang, J. Z., Grundke-Iqbal, I. & Iqbal, K. Kinases and phosphatases and tau sites involved in Alzheimer neurofibrillary degeneration. *European Journal of Neuroscience* **25**, 59-68, doi:10.1111/j.1460-9568.2006.05226.x (2007).
206 Ellmer, D., Brehs, M., Haj-Yahya, M., Lashuel, H. A. & Becker, C. F. Single posttranslational modifications in the central repeat domains of Tau4 impact its aggregation and tubulin binding. *Angewandte Chemie* **131**, 1630-1634 (2019).

207 Haj-Yahya, M. *et al.* Site-Specific Hyperphosphorylation Inhibits, Rather than Promotes, Tau Fibrillization, Seeding Capacity, and Its Microtubule Binding. *Angewandte Chemie (International ed. in English)* **59**, 4059-4067, doi:10.1002/anie.201913001 (2020).

208 Schwagerus, S., Reimann, O., Despres, C., Smet-Nocca, C. & Hackenberger, C. P. Semi-synthesis of a tag-free O-GlcNAcylated tau protein by sequential chemoselective ligation. *Journal of Peptide Science* **22**, 327-333 (2016).

209 Munari, F. *et al.* Semisynthetic modification of tau protein with di-ubiquitin chains for aggregation studies. *International journal of molecular sciences* **21**, 4400 (2020).

210 Reimann, O., Glanz, M. & Hackenberger, C. P. Native chemical ligation between asparagine and valine: application and limitations for the synthesis of tri-phosphorylated C-terminal tau. *Bioorg Med Chem* **23**, 2890-2894 (2015).

211 Dujardin, S. *et al.* Tau molecular diversity contributes to clinical heterogeneity in Alzheimer's disease. *Nat Med*, doi:10.1038/s41591-020-0938-9 (2020).

212 Zetterberg, H. Review: Tau in biofluids - relation to pathology, imaging and clinical features. *Neuropathology and applied neurobiology* **43**, 194-199, doi:10.1111/nan.12378 (2017).

213 Russell, C. L. *et al.* Comprehensive Quantitative Profiling of Tau and Phosphorylated Tau Peptides in Cerebrospinal Fluid by Mass Spectrometry Provides New Biomarker Candidates. *Journal of Alzheimer's Disease* **55**, 303-313, doi:10.3233/jad-160633 (2016).

214 Vos, S. J. B. *et al.* Variability of CSF Alzheimer's Disease Biomarkers: Implications for Clinical Practice. *PloS one* **9**, e100784, doi:10.1371/journal.pone.0100784 (2014).

215 Zemlan, F. P. *et al.* C-tau biomarker of neuronal damage in severe brain injured patients: association with elevated intracranial pressure and clinical outcome. *Brain Res* **947**, 131-139, doi:10.1016/s0006-8993(02)02920-7 (2002).

216 Blennow, K. & Hampel, H. CSF markers for incipient Alzheimer's disease. *The Lancet Neurology* **2**, 605-613 (2003).

217 Borroni, B. *et al.* Pattern of Tau forms in CSF is altered in progressive supranuclear palsy. *Neurobiology of aging* **30**, 34-40, doi:https://doi.org/10.1016/j.neurobiolaging.2007.05.009 (2009).

218 Ramcharitar, J. *et al.* Cerebrospinal Fluid Tau Cleaved by Caspase-6 Reflects Brain Levels and Cognition in Aging and Alzheimer Disease. *Journal of Neuropathology & Experimental Neurology* **72**, 824-832, doi:10.1097/nen.0b013e3182a0a39f (2013).

219 Vigo-Pelfrey, C. *et al.* Elevation of microtubule-associated protein tau in the cerebrospinal fluid of patients with Alzheimer's disease. *Neurology* **45**, 788-793, doi:10.1212/wnl.45.4.788 (1995).

220 Johnson, G. V. W. *et al.* The τ Protein in Human Cerebrospinal Fluid in Alzheimer's Disease Consists of Proteolytically Derived Fragments. *Journal of neurochemistry* **68**, 430-433, doi:10.1046/j.1471-4159.1997.68010430.x (2002).

221 Arai, T. *et al.* Identification of amino-terminally cleaved tau fragments that distinguish progressive supranuclear palsy from corticobasal degeneration. *Annals of neurology* **55**, 72-79, doi:10.1002/ana.10793 (2003).

222 Sato, C. *et al.* Tau Kinetics in Neurons and the Human Central Nervous System. *Neuron* **97**, 1284-1298.e1287, doi:https://doi.org/10.1016/j.neuron.2018.02.015 (2018).

223 Slats, D. *et al.* Hourly variability of cerebrospinal fluid biomarkers in Alzheimer's disease subjects and healthy older volunteers. *Neurobiology of aging* **33**, 831.e831-831.e839, doi:https://doi.org/10.1016/j.neurobiolaging.2011.07.008 (2012).

224 Lashuel, H. A. Rethinking protein aggregation and drug discovery in neurodegenerative diseases: Why we need to embrace complexity? *Curr Opin Chem Biol* **64**, 67-75, doi:https://doi.org/10.1016/j.cbpa.2021.05.006 (2021).

225 Chung, D.-e. C., Roemer, S., Petrucelli, L. & Dickson, D. W. Cellular and pathological heterogeneity of primary tauopathies. *Mol Neurodegener* **16**, 57, doi:10.1186/s13024-021-00476-x (2021).

226 Singleton, E. *et al.* Heterogeneous distribution of tau pathology in the behavioural variant of Alzheimer's disease. *J Neurol Neurosurg Psychiatry* **92**, 872-880, doi:10.1136/jnnp-2020-325497 (2021).

227 Kovacs, G. G. *et al.* A peculiar constellation of tau pathology defines a subset of dementia in the elderly. *Acta neuropathologica* **122**, 205-222, doi:10.1007/s00401-011-0819-x (2011).
228 Kovacs, G. G. & Budka, H. in *Prions and diseases* 103-119 (Springer, 2013).
229 Peng, C. *et al.* Cellular milieu imparts distinct pathological α-synuclein strains in α-synucleinopathies. *Nature* **557**, 558-563, doi:10.1038/s41586-018-0104-4 (2018).
230 Riguet, N. *et al.* Nuclear and cytoplasmic huntingtin inclusions exhibit distinct biochemical composition, interactome and ultrastructural properties. *bioRxiv*, 2020.2007.2029.226977, doi:10.1101/2020.07.29.226977 (2021).
231 Mahul-Mellier, A.-L. *et al.* The process of Lewy body formation, rather than simply α-synuclein fibrillization, is one of the major drivers of neurodegeneration. *Proceedings of the National Academy of Sciences* **117**, 4971-4982, doi:10.1073/pnas.1913904117 (2020).
232 Fichou, Y. *et al.* Tau-Cofactor Complexes as Building Blocks of Tau Fibrils. *Frontiers in neuroscience* **13**, 1339, doi:10.3389/fnins.2019.01339 (2019).
233 Khandelwal, S. & Arepally, G. M. Immune pathogenesis of heparin-induced thrombocytopenia. *Thromb Haemost* **116**, 792-798, doi:10.1160/TH16-01-0074 (2016).
234 Putranto, T. A., Yusuf, I., Murtala, B. & Wijaya, A. Intra Arterial Heparin Flushing Increases Cereberal Blood Flow in Chronic Ischemic Stroke Patients. *The Indonesian Biomedical Journal* **8**, 119-126 (2016).
235 Stopschinski, B. E. *et al.* A synthetic heparinoid blocks Tau aggregate cell uptake and amplification. *The Journal of biological chemistry* **295**, 2974-2983, doi:10.1074/jbc.RA119.010353 (2020).
236 Tanaka, M., Xiao, H. & Kiuchi, K. Heparin facilitates glial cell line-derived neurotrophic factor signal transduction. *Neuroreport* **13**, 1913-1916 (2002).
237 Daum, G. n., Hedin, U., Wang, Y., Wang, T. & Clowes, A. W. Diverse effects of heparin on mitogen-activated protein kinase–dependent signal transduction in vascular smooth muscle cells. *Circulation research* **81**, 17-23 (1997).
238 Hills, F. A. *et al.* Heparin prevents programmed cell death in human trophoblast. *MHR: Basic science of reproductive medicine* **12**, 237-243 (2006).
239 Chatzinikolaou, G. *et al.* Heparin regulates colon cancer cell growth through p38 mitogen-activated protein kinase signalling. *Cell proliferation* **43**, 9-18 (2010).
240 Chen, Y. *et al.* Perturbation of the heparin/heparin-sulfate interactome of human breast cancer cells modulates pro-tumourigenic effects associated with PI3K/Akt and MAPK/ERK signalling. *Thromb Haemost* **109**, 1148-1157 (2013).
241 Rider, C. (Portland Press Ltd., 2006).
242 Moreno, F. J., Medina, M., Perez, M., Montejo de Garcini, E. & Avila, J. Glycogen synthase kinase 3 phosphorylates recombinant human tau protein at serine-262 in the presence of heparin (or tubulin). *FEBS letters* **372**, 65-68, doi:10.1016/0014-5793(95)00934-2 (1995).
243 Al-Hilaly, Y. K. *et al.* Cysteine-Independent Inhibition of Alzheimer's Disease-like Paired Helical Filament Assembly by Leuco-Methylthioninium (LMT). *Journal of molecular biology* **430**, 4119-4131, doi:10.1016/j.jmb.2018.08.010 (2018).
244 Drubin, D. G. & Kirschner, M. W. Tau protein function in living cells. *J Cell Biol* **103**, 2739, doi:10.1083/jcb.103.6.2739 (1986).
245 Sotiropoulos, I. *et al.* Atypical, non-standard functions of the microtubule associated Tau protein. *Acta Neuropathol Commun* **5**, doi:10.1186/s40478-017-0489-6 (2017).
246 Dixit, R., Ross, J. L., Goldman, Y. E. & Holzbaur, E. L. Differential regulation of dynein and kinesin motor proteins by tau. *Science* **319**, 1086-1089 (2008).
247 Barghorn, S. *et al.* Structure, microtubule interactions, and paired helical filament aggregation by tau mutants of frontotemporal dementias. *Biochemistry* **39**, 11714-11721 (2000).
248 Ding, H., Matthews, T. A. & Johnson, G. V. Site-specific phosphorylation and caspase cleavage differentially impact tau-microtubule interactions and tau aggregation. *Journal of Biological Chemistry* **281**, 19107-19114 (2006).

249 Baudier, J. & Cole, R. D. Interactions between the microtubule-associated tau proteins and S100b regulate tau phosphorylation by the Ca2+/calmodulin-dependent protein kinase II. *Journal of Biological Chemistry* **263**, 5876-5883 (1988).

250 Carlier, M.-F., Simon, C., Cassoly, R. & Pradel, L.-A. Interaction between microtubule-associated protein tau and spectrin. *Biochimie* **66**, 305-311 (1984).

251 Samsonov, A., Yu, J.-Z., Rasenick, M. & Popov, S. V. Tau interaction with microtubules in vivo. *J Cell Sci* **117**, 6129-6141, doi:10.1242/jcs.01531 (2004).

252 Venkatramani, A. & Panda, D. Regulation of neuronal microtubule dynamics by tau: Implications for tauopathies. *International journal of biological macromolecules* **133**, 473-483, doi:https://doi.org/10.1016/j.ijbiomac.2019.04.120 (2019).

253 Masters, C. L. *et al.* Alzheimer's disease. *Nature Reviews Disease Primers* **1**, doi:10.1038/nrdp.2015.59 (2015).

254 Glenner, G. G. & Wong, C. W. Alzheimer's disease: Initial report of the purification and characterization of a novel cerebrovascular amyloid protein. *Biochemical and biophysical research communications* **120**, 885-890, doi:https://doi.org/10.1016/S0006-291X(84)80190-4 (1984).

255 Lee, V. M., Goedert, M. & Trojanowski, J. Q. Neurodegenerative tauopathies. *Annu Rev Neurosci* **24**, 1121-1159 (2001).

256 Goedert, M. *et al.* Assembly of microtubule-associated protein tau into Alzheimer-like filaments induced by sulphated glycosaminoglycans. *Nature* **383**, 550-553 (1996).

257 Kidd, M. Paired Helical Filaments in Electron Microscopy of Alzheimer's Disease. *Nature* **197**, 192-193, doi:10.1038/197192b0 (1963).

258 Tomlinson, B. E., Blessed, G. & Roth, M. Observations on the brains of demented old people. *Journal of the neurological sciences* **11**, 205-242, doi:https://doi.org/10.1016/0022-510X(70)90063-8 (1970).

259 BrionJP, P. H., Nunez, J. & Flament-Durand, J. Mise en evidence immunologique de la proteine tau au niveau des lesions de degenerescence neurofibril-laire de la maladie d'Alzheimer. *Arch Biol (Bruxelles)* **95**, 229-235 (1985).

260 Murray, M. E. *et al.* Clinicopathologic assessment and imaging of tauopathies in neurodegenerative dementias. *Alzheimers Res Ther* **6**, 1 (2014).

261 Shi, Y. *et al.* Structure-based classification of tauopathies. *Nature* **598**, 359-363, doi:10.1038/s41586-021-03911-7 (2021).

262 Lippens, G. & Gigant, B. Elucidating Tau function and dysfunction in the era of cryo-EM. *Journal of Biological Chemistry* **294**, 9316-9325 (2019).

263 Vignon, A., Salvador-Prince, L., Lehmann, S., Perrier, V. & Torrent, J. Deconstructing Alzheimer's Disease: How to Bridge the Gap between Experimental Models and the Human Pathology? *International journal of molecular sciences* **22**, doi:10.3390/ijms22168769 (2021).

264 Candelise, N. *et al.* Protein Aggregation Landscape in Neurodegenerative Diseases: Clinical Relevance and Future Applications. *International journal of molecular sciences* **22**, doi:10.3390/ijms22116016 (2021).

265 Lashuel, H. A. Rethinking protein aggregation and drug discovery in neurodegenerative diseases: Why we need to embrace complexity? *Curr Opin Chem Biol* **64**, 67-75, doi:10.1016/j.cbpa.2021.05.006 (2021).

266 Goedert, M., Spillantini, M. G., Jakes, R., Rutherford, D. & Crowther, R. A. Multiple isoforms of human microtubule-associated protein tau: sequences and localization in neurofibrillary tangles of Alzheimer's disease. *Neuron* **3**, 519-526, doi:https://doi.org/10.1016/0896-6273(89)90210-9 (1989).

267 Boutajangout, A., Boom, A., Leroy, K. & Brion, J. P. Expression of tau mRNA and soluble tau isoforms in affected and non-affected brain areas in Alzheimer's disease. *FEBS letters* **576**, 183-189 (2004).

268 Chambers, C. B., Lee, J. M., Troncoso, J. C., Reich, S. & Muma, N. A. Overexpression of four-repeat tau mRNA isoforms in progressive supranuclear palsy but not in Alzheimer's disease. *Annals of Neurology: Official Journal of the American Neurological Association and the Child Neurology Society* **46**, 325-332 (1999).

269 De Silva, R. *et al.* Pathological inclusion bodies in tauopathies contain distinct complements of tau with three or four microtubule-binding repeat domains as demonstrated by new specific monoclonal antibodies. *Neuropathology and applied neurobiology* **29**, 288-302 (2003).

270 Delacourte, A., Sergeant, N., Wattez, A., Gauvreau, D. & Robitaille, Y. Vulnerable neuronal subsets in Alzheimer's and Pick's disease are distinguished by their τ isoform distribution and phosphorylation. *Annals of Neurology: Official Journal of the American Neurological Association and the Child Neurology Society* **43**, 193-204 (1998).
271 Sergeant, N., Wattez, A. & Delacourte, A. Neurofibrillary degeneration in progressive supranuclear palsy and corticobasal degeneration: tau pathologies with exclusively "exon 10" isoforms. *Journal of neurochemistry* **72**, 1243-1249 (1999).
272 D'Souza, I. & Schellenberg, G. D. Regulation of tau isoform expression and dementia. *Biochimica et Biophysica Acta - Molecular Basis of Disease* **1739**, 104-115, doi:10.1016/j.bbadis.2004.08.009 (2005).
273 Qiang, L. *et al.* Tau does not stabilize axonal microtubules but rather enables them to have long labile domains. *Current Biology* **28**, 2181-2189. e2184 (2018).
274 Chang, C. W., Shao, E. & Mucke, L. Tau: Enabler of diverse brain disorders and target of rapidly evolving therapeutic strategies. *Science* **371**, doi:10.1126/science.abb8255 (2021).
275 Marciniak, E. *et al.* Tau deletion promotes brain insulin resistance. *J Exp Med* **214**, 2257-2269, doi:10.1084/jem.20161731 (2017).
276 Kimura, T. *et al.* Microtubule-associated protein tau is essential for long-term depression in the hippocampus. *Philos Trans R Soc Lond B Biol Sci* **369**, 20130144-20130144, doi:10.1098/rstb.2013.0144 (2013).
277 Ondrejcak, T. *et al.* Soluble tau aggregates inhibit synaptic long-term depression and amyloid β-facilitated LTD in vivo. *Neurobiol Dis* **127**, 582-590, doi:10.1016/j.nbd.2019.03.022 (2019).
278 Lasagna-Reeves, C. A. *et al.* Tau oligomers impair memory and induce synaptic and mitochondrial dysfunction in wild-type mice. *Mol Neurodegener* **6**, 39 (2011). <http://europepmc.org/abstract/MED/21645391

https://www.ncbi.nlm.nih.gov/pmc/articles/pmid/21645391/?tool=EBI

https://www.ncbi.nlm.nih.gov/pmc/articles/pmid/21645391/pdf/?tool=EBI

https://doi.org/10.1186/1750-1326-6-39

https://europepmc.org/articles/PMC3224595

https://europepmc.org/articles/PMC3224595?pdf=render>.
279 Robbins, M., Clayton, E. & Kaminski Schierle, G. S. Synaptic tau: A pathological or physiological phenomenon? *Acta Neuropathol Commun* **9**, 149, doi:10.1186/s40478-021-01246-y (2021).
280 Dupret, D. *et al.* Spatial relational memory requires hippocampal adult neurogenesis. *PloS one* **3**, e1959 (2008).
281 Pino, A., Fumagalli, G., Bifari, F. & Decimo, I. New neurons in adult brain: distribution, molecular mechanisms and therapies. *Biochem Pharmacol* **141**, 4-22, doi:10.1016/j.bcp.2017.07.003 (2017).
282 Houben, S. *et al.* Tau Pathology and Adult Hippocampal Neurogenesis: What Tau Mouse Models Tell us? *Front Neurol* **12**, 610330, doi:10.3389/fneur.2021.610330 (2021).
283 Li Puma, D. D., Piacentini, R. & Grassi, C. Does Impairment of Adult Neurogenesis Contribute to Pathophysiology of Alzheimer's Disease? A Still Open Question. *Frontiers in molecular neuroscience* **13**, 578211, doi:10.3389/fnmol.2020.578211 (2020).
284 Goldman, S. Glia as neural progenitor cells. *Trends Neurosci* **26**, 590-596 (2003).
285 Morrens, J., Van Den Broeck, W. & Kempermann, G. Glial cells in adult neurogenesis. *Glia* **60**, 159-174 (2012).
286 Andorfer, C. *et al.* Cell-Cycle Reentry and Cell Death in Transgenic Mice Expressing Nonmutant Human Tau Isoforms. *The Journal of Neuroscience* **25**, 5446-5454, doi:10.1523/jneurosci.4637-04.2005 (2005).
287 Arendt, T., Brückner, M. K., Mosch, B. & Lösche, A. Selective cell death of hyperploid neurons in Alzheimer's disease. *The American journal of pathology* **177**, 15-20 (2010).
288 Lee, H.-g. *et al.* Cell cycle re-entry mediated neurodegeneration and its treatment role in the pathogenesis of Alzheimer's disease. *Neurochem Int* **54**, 84-88 (2009).

289 Lei, P. *et al.* Motor and cognitive deficits in aged tau knockout mice in two background strains. *Mol Neurodegener* **9**, 29-29, doi:10.1186/1750-1326-9-29 (2014).
290 Andorfer, C. *et al.* Hyperphosphorylation and aggregation of tau in mice expressing normal human tau isoforms. *Journal of neurochemistry* **86**, 582-590 (2003).
291 Wijesekara, N., Gonçalves, R. A., Ahrens, R., De Felice, F. G. & Fraser, P. E. Tau ablation in mice leads to pancreatic β cell dysfunction and glucose intolerance. *Faseb j* **32**, 3166-3173, doi:10.1096/fj.201701352 (2018).
292 Gonçalves, R. A., Wijesekara, N., Fraser, P. E. & De Felice, F. G. Behavioral abnormalities in knockout and humanized tau mice. *Front Endocrinol (Lausanne)* **11**, 124 (2020).
293 Hradek, A. C. *et al.* Distinct chronology of neuronal cell cycle re-entry and tau pathology in the 3xTg-AD mouse model and Alzheimer's disease patients. *Journal of Alzheimer's disease : JAD* **43**, 57-65, doi:10.3233/JAD-141083 (2015).
294 Li, L., Cheung, T., Chen, J. & Herrup, K. A comparative study of five mouse models of Alzheimer's disease: cell cycle events reveal new insights into neurons at risk for death. *International Journal of Alzheimer's Disease* **2011** (2011).
295 Seward, M. E. *et al.* Amyloid-β signals through tau to drive ectopic neuronal cell cycle re-entry in Alzheimer's disease. *J Cell Sci* **126**, 1278-1286, doi:10.1242/jcs.1125880 (2013).
296 Kerrien, S. *et al.* The IntAct molecular interaction database in 2012. *Nucleic acids research* **40**, D841-D846 (2012).
297 Oughtred, R. *et al.* The BioGRID interaction database: 2019 update. *Nucleic acids research* **47**, D529-D541 (2019).
298 Lang, B., Armaos, A. & Tartaglia, G. G. RNAct: Protein–RNA interaction predictions for model organisms with supporting experimental data. *Nucleic acids research* **47**, D601-D606 (2019).
299 Ashburner, M. *et al.* Gene ontology: tool for the unification of biology. *Nature genetics* **25**, 25-29 (2000).
300 Trinczek, B., Biernat, J., Baumann, K., Mandelkow, E.-M. & Mandelkow, E. Domains of tau protein, differential phosphorylation, and dynamic instability of microtubules. *Molecular biology of the cell* **6**, 1887-1902 (1995).
301 Barbier, P. *et al.* Role of Tau as a Microtubule-Associated Protein: Structural and Functional Aspects. *Front Aging Neurosci* **11**, doi:10.3389/fnagi.2019.00204 (2019).
302 Trushina, N. I., Bakota, L., Mulkidjanian, A. Y. & Brandt, R. The Evolution of Tau Phosphorylation and Interactions. *Front Aging Neurosci* **11**, 256 (2019). <http://europepmc.org/abstract/MED/31619983

https://doi.org/10.3389/fnagi.2019.00256

https://europepmc.org/articles/PMC6759874

https://europepmc.org/articles/PMC6759874?pdf=render>.
303 Drummond, E. *et al.* Phosphorylated tau interactome in the human Alzheimer's disease brain. *Brain* **143**, 2803-2817, doi:10.1093/brain/awaa223 (2020).
304 Kovacech, B., Zilka, N. & Novak, M. New age of neuroproteomics in Alzheimer's disease research. *Cell Mol Neurobiol* **29**, 799-805, doi:10.1007/s10571-009-9358-6 (2009).
305 Drummond, E. & Wisniewski, T. in *Alzheimer's Disease* (ed T. Wisniewski) (Codon Publications

306 Sinsky, J. *et al.* Physiological Tau Interactome in Brain and Its Link to Tauopathies. *J Proteome Res* **19**, 2429-2442, doi:10.1021/acs.jproteome.0c00137 (2020).
307 Gunawardana, C. G. *et al.* The Human Tau Interactome: Binding to the Ribonucleoproteome, and Impaired Binding of the Proline-to-Leucine Mutant at Position 301 (P301L) to Chaperones and the Proteasome. *Mol Cell Proteomics* **14**, 3000-3014, doi:10.1074/mcp.M115.050724 (2015).
308 Choi, H. *et al.* Acetylation changes tau interactome to degrade tau in Alzheimer's disease animal and organoid models. *Aging Cell* **19**, e13081 (2020).

309 Wang, P. *et al.* Tau interactome mapping based identification of Otub1 as Tau deubiquitinase involved in accumulation of pathological Tau forms in vitro and in vivo. *Acta neuropathologica* **133**, 731-749, doi:10.1007/s00401-016-1663-9 (2017).
310 Sultan, A. *et al.* Nuclear tau, a key player in neuronal DNA protection. *Journal of Biological Chemistry* **286**, 4566-4575 (2011).
311 Violet, M. *et al.* A major role for Tau in neuronal DNA and RNA protection in vivo under physiological and hyperthermic conditions. *Frontiers in cellular neuroscience* **8**, 84 (2014).
312 Gil, L., Niño, S. A., Capdeville, G. & Jiménez-Capdeville, M. E. Aging and Alzheimer's disease connection: Nuclear Tau and lamin A. *Neurosci Lett* **749**, 135741, doi:https://doi.org/10.1016/j.neulet.2021.135741 (2021).
313 Klein, H.-U. *et al.* Epigenome-wide study uncovers large-scale changes in histone acetylation driven by tau pathology in aging and Alzheimer's human brains. *Nat Neurosci* **22**, 37-46, doi:10.1038/s41593-018-0291-1 (2019).
314 Hanger, D. P., Anderton, B. H. & Noble, W. Tau phosphorylation: the therapeutic challenge for neurodegenerative disease. *Trends in Molecular Medicine* **15**, 112-119, doi:10.1016/j.molmed.2009.01.003 (2009).
315 Crary, J. F. *et al.* Primary age-related tauopathy (PART): a common pathology associated with human aging. *Acta neuropathologica* **128**, 755-766 (2014).
316 Braak, H. & Del Tredici, K. The preclinical phase of the pathological process underlying sporadic Alzheimer's disease. *Brain* **138**, 2814-2833 (2015).
317 Harrison, T. M. *et al.* Longitudinal tau accumulation and atrophy in aging and alzheimer disease. *Annals of neurology* **85**, 229-240, doi:10.1002/ana.25406 (2019).
318 Lowe, V. J. *et al.* Elevated medial temporal lobe and pervasive brain tau-PET signal in normal participants. *Alzheimer's & Dementia: Diagnosis, Assessment & Disease Monitoring* **10**, 210-216, doi:https://doi.org/10.1016/j.dadm.2018.01.005 (2018).
319 Maass, A. *et al.* Entorhinal tau pathology, episodic memory decline, and neurodegeneration in aging. *Journal of Neuroscience* **38**, 530-543 (2018).
320 Lowe, V. J. *et al.* Cross-sectional associations of tau-PET signal with cognition in cognitively unimpaired adults. *Neurology* **93**, e29-e39 (2019).
321 Braak, H. & Braak, E. Neuropathological stageing of Alzheimer-related changes. *Acta neuropathologica* **82**, 239-259 (1991).
322 Williams, D. R. *et al.* Pathological tau burden and distribution distinguishes progressive supranuclear palsy-parkinsonism from Richardson's syndrome. *Brain* **130**, 1566-1576 (2007).
323 Iovino, M. *et al.* Early maturation and distinct tau pathology in induced pluripotent stem cell-derived neurons from patients with MAPT mutations. *Brain* **138**, 3345-3359, doi:10.1093/brain/awv222 (2015).
324 Dickson, D. W., Kouri, N., Murray, M. E. & Josephs, K. A. Neuropathology of frontotemporal lobar degeneration-tau (FTLD-tau). *Journal of Molecular Neuroscience* **45**, 384-389 (2011).
325 Schöll, M. *et al.* PET imaging of tau deposition in the aging human brain. *Neuron* **89**, 971-982 (2016).
326 Schwarz, A. J. *et al.* Regional profiles of the candidate tau PET ligand 18 F-AV-1451 recapitulate key features of Braak histopathological stages. *Brain* **139**, 1539-1550 (2016).
327 Tsuboi, Y., Wszolek, Z. K., Graff-Radford, N., Cookson, N. & Dickson, D. W. Tau pathology in the olfactory bulb correlates with Braak stage, Lewy body pathology and apolipoprotein ε4. *Neuropathology and applied neurobiology* **29**, 503-510 (2003).
328 Lowe, V. J. *et al.* Widespread brain tau and its association with ageing, Braak stage and Alzheimer's dementia. *Brain* **141**, 271-287 (2017).
329 Spillantini, M. G. & Goedert, M. Tau protein pathology in neurodegenerative diseases. *Trends in neurosciences* **21**, 428-433 (1998).
330 Yang, W., Ang, L. C. & Strong, M. J. Tau protein aggregation in the frontal and entorhinal cortices as a function of aging. *Developmental brain research* **156**, 127-138 (2005).

331 Sander, K. *et al.* Characterization of tau positron emission tomography tracer [18F] AV-1451 binding to postmortem tissue in Alzheimer's disease, primary tauopathies, and other dementias. *Alzheimer's & Dementia* **12**, 1116-1124 (2016).

332 Braak, F., Braak, H. & Mandelkow, E.-M. A sequence of cytoskeleton changes related to the formation of neurofibrillary tangles and neuropil threads. *Acta neuropathologica* **87**, 554-567 (1994).

333 Duyckaerts, C., Uchihara, T., Seilhean, D., He, Y. & Hauw, J. J. Dissociation of Alzheimer type pathology in a disconnected piece of cortex. *Acta neuropathologica* **93**, 501-507, doi:10.1007/s004010050645 (1997).

334 Olajide, O. J., Suvanto, M. E. & Chapman, C. A. Molecular mechanisms of neurodegeneration in the entorhinal cortex that underlie its selective vulnerability during the pathogenesis of Alzheimer's disease. *Biol Open* **10**, doi:10.1242/bio.056796 (2021).

335 Bischof, G. N., Endepols, H., van Eimeren, T. & Drzezga, A. Tau-imaging in neurodegeneration. *Methods* **130**, 114-123 (2017).

336 Johnson, K. A. *et al.* Tau positron emission tomographic imaging in aging and early A lzheimer disease. *Annals of neurology* **79**, 110-119 (2016).

337 Leyns, C. E. G. *et al.* TREM2 deficiency attenuates neuroinflammation and protects against neurodegeneration in a mouse model of tauopathy. *Proceedings of the National Academy of Sciences of the United States of America* **114**, 11524-11529, doi:10.1073/pnas.1710311114 (2017).

338 Gratuze, M. *et al.* Impact of TREM2R47H variant on tau pathology–induced gliosis and neurodegeneration. *J Clin Invest* **130**, 4954-4968, doi:10.1172/JCI138179 (2020).

339 Zhang, Z.-G., Li, Y., Ng, C. T. & Song, Y.-Q. Inflammation in Alzheimer's disease and molecular genetics: recent update. *Archivum immunologiae et therapiae experimentalis* **63**, 333-344 (2015).

340 Narasimhan, S. *et al.* Human tau pathology transmits glial tau aggregates in the absence of neuronal tau. *J Exp Med* **217**, doi:10.1084/jem.20190783 (2020).

341 Kovacs, G. G. Astroglia and Tau: New Perspectives. *Front Aging Neurosci* **12**, 96-96, doi:10.3389/fnagi.2020.00096 (2020).

342 Maphis, N. *et al.* Reactive microglia drive tau pathology and contribute to the spreading of pathological tau in the brain. *Brain* **138**, 1738-1755, doi:10.1093/brain/awv081 (2015).

343 Leng, F. & Edison, P. Neuroinflammation and microglial activation in Alzheimer disease: where do we go from here? *Nature Reviews Neurology* **17**, 157-172, doi:10.1038/s41582-020-00435-y (2021).

344 Asai, H. *et al.* Depletion of microglia and inhibition of exosome synthesis halt tau propagation. *Nat Neurosci* **18**, 1584-1593, doi:10.1038/nn.4132 (2015).

345 Fu, H. *et al.* A tau homeostasis signature is linked with the cellular and regional vulnerability of excitatory neurons to tau pathology. *Nat Neurosci* **22**, 47-56, doi:10.1038/s41593-018-0298-7 (2019).

346 Vogel, J. W. *et al.* Spread of pathological tau proteins through communicating neurons in human Alzheimer's disease. *Nat Commun* **11**, 2612, doi:10.1038/s41467-020-15701-2 (2020).

347 Decker, Y. *et al.* Decreased pH in the aging brain and Alzheimer's disease. *Neurobiology of aging* **101**, 40-49, doi:https://doi.org/10.1016/j.neurobiolaging.2020.12.007 (2021).

348 Ponto, L. *et al.* Brain pH and Alzheimer's pathology. *Journal of Nuclear Medicine* **55**, 192-192 (2014).

349 Yin, X. *et al.* Dendritic/Post-synaptic Tau and Early Pathology of Alzheimer's Disease. *Frontiers in molecular neuroscience* **14**, 671779, doi:10.3389/fnmol.2021.671779 (2021).

350 Charafeddine, R. A. *et al.* Tau repeat regions contain conserved histidine residues that modulate microtubule-binding in response to changes in pH. *Journal of Biological Chemistry* **294**, 8779-8790 (2019).

351 Silva, M. & Haggarty, S. J. Tauopathies: Deciphering Disease Mechanisms to Develop Effective Therapies. *International journal of molecular sciences* **21**, 8948 (2020).

352 Fernández-Nogales, M. *et al.* Huntington's disease is a four-repeat tauopathy with tau nuclear rods. *Nat Med* **20**, 881-885 (2014).

353 Galpern, W. R. & Lang, A. E. Interface between tauopathies and synucleinopathies: a tale of two proteins. *Annals of neurology* **59**, 449-458, doi:10.1002/ana.20819 (2006).

354 Strong, M. J., Donison, N. S. & Volkening, K. Alterations in Tau Metabolism in ALS and ALS-FTSD. *Front Neurol* **11**, 598907, doi:10.3389/fneur.2020.598907 (2020).

355 Wszolek, Z. K. *et al.* Frontotemporal dementia and parkinsonism linked to chromosome 17 (FTDP-17). *Orphanet J Rare Dis* **1**, 30-30, doi:10.1186/1750-1172-1-30 (2006).
356 Groen, J. & Endtz, L. Hereditary Pick's disease: Second re-examination of a large family and discussion of other hereditary cases, with particular reference to electroencephalography and computerized tomography. *Brain* **105**, 443-459 (1982).
357 Braak, H., Alafuzoff, I., Arzberger, T., Kretzschmar, H. & Del Tredici, K. Staging of Alzheimer disease-associated neurofibrillary pathology using paraffin sections and immunocytochemistry. *Acta Neuropathol.* **112**, 389 (2006).
358 Zhang, H., Cao, Y., Ma, L., Wei, Y. & Li, H. Possible Mechanisms of Tau Spread and Toxicity in Alzheimer's Disease. *Frontiers in cell and developmental biology* **9**, 707268-707268, doi:10.3389/fcell.2021.707268 (2021).
359 Yu, M., Sporns, O. & Saykin, A. J. The human connectome in Alzheimer disease — relationship to biomarkers and genetics. *Nature Reviews Neurology* **17**, 545-563, doi:10.1038/s41582-021-00529-1 (2021).
360 Braak, H. & Del Tredici, K. Spreading of Tau Pathology in Sporadic Alzheimer's Disease Along Cortico-cortical Top-Down Connections. *Cereb Cortex* **28**, 3372-3384, doi:10.1093/cercor/bhy152 (2018).
361 Dujardin, S. & Hyman, B. T. Tau Prion-Like Propagation: State of the Art and Current Challenges. *Adv Exp Med Biol* **1184**, 305-325, doi:10.1007/978-981-32-9358-8_23 (2019).
362 Annadurai, N., De Sanctis, J. B., Hajdúch, M. & Das, V. Tau secretion and propagation: Perspectives for potential preventive interventions in Alzheimer's disease and other tauopathies. *Experimental neurology* **343**, 113756, doi:10.1016/j.expneurol.2021.113756 (2021).
363 Song, L., Wells, E. A. & Robinson, A. S. Critical Molecular and Cellular Contributors to Tau Pathology. *Biomedicines* **9**, doi:10.3390/biomedicines9020190 (2021).
364 d'Errico, P. & Meyer-Luehmann, M. Mechanisms of Pathogenic Tau and Aβ Protein Spreading in Alzheimer's Disease. *Front Aging Neurosci* **12**, 265, doi:10.3389/fnagi.2020.00265 (2020).
365 Quinn, J. P., Corbett, N. J., Kellett, K. A. & Hooper, N. M. Tau proteolysis in the pathogenesis of tauopathies: neurotoxic fragments and novel biomarkers. *Journal of Alzheimer's Disease* **63**, 13-33 (2018).
366 Cicognola, C. *et al.* Novel tau fragments in cerebrospinal fluid: relation to tangle pathology and cognitive decline in Alzheimer's disease. *Acta neuropathologica* **137**, 279-296 (2019).
367 Hasegawa, M., Arai, T. & Ihara, Y. Immunochemical evidence that fragments of phosphorylated MAP5 (MAP1B) are bound to neurofibrillary tangles in Alzheimer's disease. *Neuron* **4**, 909-918, doi:https://doi.org/10.1016/0896-6273(90)90144-5 (1990).
368 Kosik, K. S. *et al.* Microtubule-associated protein 2: monoclonal antibodies demonstrate the selective incorporation of certain epitopes into Alzheimer neurofibrillary tangles. *Proceedings of the National Academy of Sciences* **81**, 7941-7945 (1984).
369 Anderton, B. H. *et al.* Monoclonal antibodies show that neurofibrillary tangles and neurofilaments share antigenic determinants. *Nature* **298**, 84-86, doi:10.1038/298084a0 (1982).
370 Sinsky, J., Pichlerova, K. & Hanes, J. Tau Protein Interaction Partners and Their Roles in Alzheimer's Disease and Other Tauopathies. *International journal of molecular sciences* **22**, 9207 (2021).
371 Armstrong, R. A., Lantos, P. L. & Cairns, N. J. What determines the molecular composition of abnormal protein aggregates in neurodegenerative disease? *Neuropathology* **28**, 351-365 (2008).
372 Drummond, E. *et al.* P4-530: PHOSPHORYLATED TAU INTERACTOME IN THE HUMAN ALZHEIMER'S DISEASE BRAIN. *Alzheimer's & Dementia* **15**, P1517-P1517, doi:https://doi.org/10.1016/j.jalz.2019.08.077 (2019).
373 Minjarez, B. *et al.* Identification of Polypeptides in Neurofibrillary Tangles and Total Homogenates of Brains with Alzheimer's Disease by Tandem Mass Spectrometry. *Journal of Alzheimer's Disease* **34**, 239-262, doi:10.3233/JAD-121480 (2013).
374 Wang, Q. *et al.* Proteomic analysis of neurofibrillary tangles in Alzheimer disease identifies GAPDH as a detergent-insoluble paired helical filament tau binding protein. *FASEB J* **19**, 1-12, doi:https://doi.org/10.1096/fj.04-3210fje (2005).
375 Tsai, C. W. *et al.* An investigation of the correlation between the S-glutathionylated GAPDH levels in blood and Alzheimer's disease progression. *PloS one* **15**, e0233289, doi:10.1371/journal.pone.0233289 (2020).

376 Kadavath, H. *et al.* Tau stabilizes microtubules by binding at the interface between tubulin heterodimers. *Proceedings of the National Academy of Sciences* **112**, 7501-7506, doi:10.1073/pnas.1504081112 (2015).
377 Li, X.-H., Culver, J. A. & Rhoades, E. Tau Binds to Multiple Tubulin Dimers with Helical Structure. *Journal of the American Chemical Society* **137**, 9218-9221, doi:10.1021/jacs.5b04561 (2015).
378 Majewski, J. *et al.* Lipid membrane templated misfolding and self-assembly of intrinsically disordered tau protein. *Scientific reports* **10**, 13324, doi:10.1038/s41598-020-70208-6 (2020).
379 Eschmann, N. A. *et al.* Tau Aggregation Propensity Engrained in Its Solution State. *J Phys Chem B* **119**, 14421-14432, doi:10.1021/acs.jpcb.5b08092 (2015).
380 Ait-Bouziad, N. *et al.* Phosphorylation of the overlooked tyrosine 310 regulates the structure, aggregation, and microtubule- and lipid-binding properties of Tau. *The Journal of biological chemistry* **295**, 7905-7922, doi:10.1074/jbc.RA119.012517 (2020).
381 Friedhoff, P., von Bergen, M., Mandelkow, E.-M., Davies, P. & Mandelkow, E. A nucleated assembly mechanism of Alzheimer paired helical filaments. *Proceedings of the National Academy of Sciences* **95**, 15712-15717, doi:10.1073/pnas.95.26.15712 (1998).
382 Barghorn, S. *et al.* Structure, Microtubule Interactions, and Paired Helical Filament Aggregation by Tau Mutants of Frontotemporal Dementias. *Biochemistry* **39**, 11714-11721, doi:10.1021/bi000850r (2000).
383 Rossi, G. *et al.* New mutations in MAPT gene causing frontotemporal lobar degeneration: biochemical and structural characterization.
384 Strang, K. H. *et al.* Distinct differences in prion-like seeding and aggregation between Tau protein variants provide mechanistic insights into tauopathies. *The Journal of biological chemistry* **293**, 2408-2421, doi:10.1074/jbc.M117.815357 (2018).
385 Asherie, N. Protein crystallization and phase diagrams. *Methods* **34**, 266-272, doi:https://doi.org/10.1016/j.ymeth.2004.03.028 (2004).
386 Kashchiev, D. *Nucleation*. (Elsevier, 2000).
387 Oosawa, F. The effect of field fluctuation on a macromolecular system. *Journal of theoretical biology* **52**, 175-186 (1975).
388 Bramblett, G. T. *et al.* Abnormal tau phosphorylation at Ser396 in Alzheimer's disease recapitulates development and contributes to reduced microtubule binding. *Neuron* **10**, 1089 (1993).
389 Sengupta, A. *et al.* Maximal inhibition of tau binding to microtubules requires the phosphorylation of tau at both Thr 231 and Ser 262. *Neurobiology of aging* **19**, S124-S524 (1998).
390 Alonso, A., Mederlyova, A., Novak, M., Grundke-Iqbal, I. & Iqbal, K. Promotion of hyperphosphorylation by Frontotemporal dementia Tau mutations. *J. Biol. Chem.* **279**, 34873 (2004).
391 Liu, F. *et al.* Site-specific effects of tau phosphorylation on its microtubule assembly activity and self-aggregation. *The European journal of neuroscience* **26**, 3429-3436, doi:10.1111/j.1460-9568.2007.05955.x (2007).
392 Feijoo, C., Campbell, D. G., Jakes, R., Goedert, M. & Cuenda, A. Evidence that phosphorylation of the microtubule-associated protein Tau by SAPK4/p38delta at Thr50 promotes microtubule assembly. *J Cell Sci* **118**, 397-408, doi:10.1242/jcs.01655 (2005).
393 Duka, V. *et al.* Identification of the Sites of Tau Hyperphosphorylation and Activation of Tau Kinases in Synucleinopathies and Alzheimer's Diseases. *PloS one* **8**, e75025, doi:10.1371/journal.pone.0075025 (2013).
394 Köpke, E. *et al.* Microtubule-associated protein tau. Abnormal phosphorylation of a non-paired helical filament pool in Alzheimer disease. *Journal of Biological Chemistry* **268**, 24374-24384 (1993).
395 Grundke-Iqbal, I. *et al.* Abnormal phosphorylation of the microtubule-associated protein tau (tau) in Alzheimer cytoskeletal pathology. *Proceedings of the National Academy of Sciences* **83**, 4913-4917, doi:10.1073/pnas.83.13.4913 (1986).
396 Hanger, D. P., Betts, J. C., Loviny, T. L., Blackstock, W. P. & Anderton, B. H. New phosphorylation sites identified in hyperphosphorylated tau (paired helical filament-tau) from Alzheimer's disease brain using nanoelectrospray mass spectrometry. *Journal of neurochemistry* **71**, 2465-2476, doi:10.1046/j.1471-4159.1998.71062465.x (1998).
397 Malia, T. J. *et al.* Epitope mapping and structural basis for the recognition of phosphorylated tau by the anti-tau antibody AT8. *Proteins: Structure, Function, and Bioinformatics* **84**, 427-434 (2016).

398 Tosun, D. *et al.* Detection of β-amyloid positivity in Alzheimer's Disease Neuroimaging Initiative participants with demographics, cognition, MRI and plasma biomarkers. *Brain Communications* **3**, doi:10.1093/braincomms/fcab008 (2021).
399 Chen, Z. & Cole, P. A. Synthetic approaches to protein phosphorylation. *Curr Opin Chem Biol* **28**, 115-122, doi:10.1016/j.cbpa.2015.07.001 (2015).
400 Paleologou, K. E. *et al.* Phosphorylation at Ser-129 but not the phosphomimics S129E/D inhibits the fibrillation of alpha-synuclein. *The Journal of biological chemistry* **283**, 16895-16905, doi:10.1074/jbc.M800747200 (2008).
401 Alonso, A. D. *et al.* Phosphorylation of tau at Thr212, Thr231, and Ser262 combined causes neurodegeneration. *The Journal of biological chemistry* **285**, 30851-30860, doi:10.1074/jbc.M110.110957 (2010).
402 Chiki, A. *et al.* Site-Specific Phosphorylation of Huntingtin Exon 1 Recombinant Proteins Enabled by the Discovery of Novel Kinases. *Chembiochem* **22**, 217-231, doi:10.1002/cbic.202000508 (2021).
403 DeGuire, S. M. *et al.* N-terminal Huntingtin (Htt) phosphorylation is a molecular switch regulating Htt aggregation, helical conformation, internalization, and nuclear targeting. *The Journal of biological chemistry* **293**, 18540-18558, doi:10.1074/jbc.RA118.004621 (2018).
404 Fauvet, B. & Lashuel, H. A. in *Protein Amyloid Aggregation: Methods and Protocols* (ed David Eliezer) 3-20 (Springer New York, 2016).
405 Chen, Z. & Cole, P. A. Synthetic approaches to protein phosphorylation. *Curr Opin Chem Biol* **28**, 115-122, doi:https://doi.org/10.1016/j.cbpa.2015.07.001 (2015).
406 Guttmann, R. P., Erickson, A. C. & Johnson, G. V. Tau self-association: stabilization with a chemical cross-linker and modulation by phosphorylation and oxidation state. *Journal of neurochemistry* **64**, 1209-1215, doi:10.1046/j.1471-4159.1995.64031209.x (1995).
407 Mandelkow, E. M. *et al.* Microtubule-associated protein tau, paired helical filaments, and phosphorylation. *Annals of the New York Academy of Sciences* **695**, 209-216, doi:10.1111/j.1749-6632.1993.tb23054.x (1993).
408 Alonso, A., Zaidi, T., Novak, M., Grundke-Iqbal, I. & Iqbal, K. Hyperphosphorylation induces self-assembly of tau into tangles of paired helical filaments/straight filaments. *Proceedings of the National Academy of Sciences of the United States of America* **98**, 6923-6928, doi:10.1073/pnas.121119298 (2001).
409 Abraha, A. *et al.* C-terminal inhibition of tau assembly in vitro and in Alzheimer's disease. *J Cell Sci* **113**, 3737-3745 (2000).
410 Haase, C., Stieler, J. T., Arendt, T. & Holzer, M. Pseudophosphorylation of tau protein alters its ability for self-aggregation. *Journal of neurochemistry* **88**, 1509-1520, doi:10.1046/j.1471-4159.2003.02287.x (2004).
411 Schneider, A., Biernat, J., von Bergen, M., Mandelkow, E. & Mandelkow, E. M. Phosphorylation that detaches tau protein from microtubules (Ser262, Ser214) also protects it against aggregation into Alzheimer paired helical filaments. *Biochemistry* **38**, 3549-3558, doi:Doi 10.1021/Bi981874p (1999).
412 Drepper, F. *et al.* A combinatorial native MS and LC-MS/MS approach reveals high intrinsic phosphorylation of human tau but minimal levels of other key modifications. *Journal of Biological Chemistry*, jbc. RA120. 015882 (2020).
413 Takahashi, M. *et al.* Glycosylation of microtubule-associated protein tau in Alzheimer's disease brain. *Acta neuropathologica* **97**, 635-641 (1999).
414 Wang, J.-Z., Grundke-Iqbal, I. & Iqbal, K. Glycosylation of microtubule–associated protein tau: An abnormal posttranslational modification in Alzheimer's disease. *Nat Med* **2**, 871-875 (1996).
415 Aguilar, A. L., Hou, X., Wen, L., Wang, P. G. & Wu, P. A chemoenzymatic histology method for O-GlcNAc detection. *Chembiochem: a European journal of chemical biology* **18**, 2416 (2017).
416 Pinho, T. S., Correia, S. C., Perry, G., Ambrósio, A. F. & Moreira, P. I. Diminished O-GlcNAcylation in Alzheimer's disease is strongly correlated with mitochondrial anomalies. *Biochimica et Biophysica Acta (BBA)-Molecular Basis of Disease* **1865**, 2048-2059 (2019).
417 Wang, A. C., Jensen, E. H., Rexach, J. E., Vinters, H. V. & Hsieh-Wilson, L. C. Loss of O-GlcNAc glycosylation in forebrain excitatory neurons induces neurodegeneration. *Proceedings of the National Academy of Sciences* **113**, 15120-15125 (2016).

418 Arnold, C. S. *et al.* The microtubule-associated protein tau is extensively modified with O-linked N-acetylglucosamine. *Journal of Biological Chemistry* **271**, 28741-28744 (1996).
419 Robertson, L. A., Moya, K. L. & Breen, K. C. The potential role of tau protein O-glycosylation in Alzheimer's disease. *Journal of Alzheimer's Disease* **6**, 489-495 (2004).
420 Yuzwa, S. A. *et al.* Mapping O-GlcNAc modification sites on tau and generation of a site-specific O-GlcNAc tau antibody. *Amino acids* **40**, 857-868 (2011).
421 Liu, F. *et al.* Reduced O-GlcNAcylation links lower brain glucose metabolism and tau pathology in Alzheimer's disease. *Brain* **132**, 1820-1832 (2009).
422 Gong, C.-X., Liu, F., Grundke-Iqbal, I. & Iqbal, K. Impaired brain glucose metabolism leads to Alzheimer neurofibrillary degeneration through a decrease in tau O-GlcNAcylation. *Journal of Alzheimer's disease* **9**, 1-12 (2006).
423 Smet-Nocca, C. *et al.* Identification of O-GlcNAc sites within peptides of the Tau protein and their impact on phosphorylation. *Mol Biosyst* **7**, 1420-1429 (2011).
424 Lim, S. *et al.* Monitoring of intracellular tau aggregation regulated by OGA/OGT inhibitors. *International journal of molecular sciences* **16**, 20212-20224 (2015).
425 Schedin-Weiss, S. *et al.* Glycan biomarkers for Alzheimer disease correlate with T-tau and P-tau in cerebrospinal fluid in subjective cognitive impairment. *The FEBS journal* **287**, 3221-3234, doi:10.1111/febs.15197 (2020).
426 Yu, C. H. *et al.* O-GlcNAcylation modulates the self-aggregation ability of the fourth microtubule-binding repeat of tau. *Biochemical and biophysical research communications* **375**, 59-62, doi:10.1016/j.bbrc.2008.07.101 (2008).
427 Hart, G. W., Housley, M. P. & Slawson, C. Cycling of O-linked β-N-acetylglucosamine on nucleocytoplasmic proteins. *Nature* **446**, 1017-1022 (2007).
428 Di Domenico, F., Lanzillotta, C. & Tramutola, A. Therapeutic potential of rescuing protein O-GlcNAcylation in tau-related pathologies. *Expert review of neurotherapeutics* **19**, 1-3 (2019).
429 Cantrelle, F.-X. *et al.* Phosphorylation and O-GlcNAcylation of the PHF-1 Epitope of Tau Protein Induce Local Conformational Changes of the C-Terminus and Modulate Tau Self-Assembly Into Fibrillar Aggregates. *Frontiers in molecular neuroscience* **14**, doi:10.3389/fnmol.2021.661368 (2021).
430 Losev, Y. *et al.* Novel model of secreted human tau protein reveals the impact of the abnormal N-glycosylation of tau on its aggregation propensity. *Scientific reports* **9**, 2254 (2019). <http://europepmc.org/abstract/MED/30783169

https://doi.org/10.1038/s41598-019-39218-x

https://europepmc.org/articles/PMC6381127

https://europepmc.org/articles/PMC6381127?pdf=render>.
431 Maillard, L. C. Action des acides amines sur les sucres; formation des melanoidines par voie methodique. *Comptes R. Acad. Sci.(Paris)* **154**, 66-68 (1912).
432 Reily, C., Stewart, T. J., Renfrow, M. B. & Novak, J. Glycosylation in health and disease. *Nature Reviews Nephrology* **15**, 346-366 (2019).
433 Yan, S. *et al.* Glycated tau protein in Alzheimer disease: a mechanism for induction of oxidant stress. *Proceedings of the National Academy of Sciences* **91**, 7787-7791 (1994).
434 Smith, M. A. *et al.* Advanced Maillard reaction end products are associated with Alzheimer disease pathology. *Proceedings of the National Academy of Sciences* **91**, 5710-5714 (1994).
435 Sasaki, N. *et al.* Advanced glycation end products in Alzheimer's disease and other neurodegenerative diseases. *The American journal of pathology* **153**, 1149-1155 (1998).
436 Lüth, H.-J. *et al.* Age-and stage-dependent accumulation of advanced glycation end products in intracellular deposits in normal and Alzheimer's disease brains. *Cerebral Cortex* **15**, 211-220 (2005).
437 Batkulwar, K. *et al.* Advanced Glycation End Products Modulate Amyloidogenic APP Processing and Tau Phosphorylation: A Mechanistic Link between Glycation and the Development of Alzheimer's Disease. *ACS chemical neuroscience* **9**, 988-1000, doi:10.1021/acschemneuro.7b00410 (2018).

438 Necula, M. & Kuret, J. Pseudophosphorylation and glycation of tau protein enhance but do not trigger fibrillization in vitro. *J. Biol. Chem.* **279**, 49694 (2004).
439 Ledesma, M. D., Medina, M. & Avila, J. The in vitro formation of recombinant tau polymers: effect of phosphorylation and glycation. *Molecular and chemical neuropathology* **27**, 249-258, doi:10.1007/bf02815107 (1996).
440 Yuzwa, S. A. *et al.* Increasing O-GlcNAc slows neurodegeneration and stabilizes tau against aggregation. *Nature chemical biology* **8**, 393-399 (2012).
441 Yuzwa, S. A., Cheung, A. H., Okon, M., McIntosh, L. P. & Vocadlo, D. J. O-GlcNAc modification of tau directly inhibits its aggregation without perturbing the conformational properties of tau monomers. *Journal of molecular biology* **426**, 1736-1752, doi:10.1016/j.jmb.2014.01.004 (2014).
442 Irwin, D. J. *et al.* Acetylated tau, a novel pathological signature in Alzheimer's disease and other tauopathies. *Brain* **135**, 807-818, doi:10.1093/brain/aws013 (2012).
443 Lucke-Wold, B. *et al.* Role of Tau Acetylation in Alzheimer's Disease and Chronic Traumatic Encephalopathy: The Way Forward for Successful Treatment. *J Neurol Neurosurg* **4**, 140 (2017).
444 Min, S.-W. *et al.* Critical role of acetylation in tau-mediated neurodegeneration and cognitive deficits. *Nat Med* **21**, 1154-1162, doi:10.1038/nm.3951 (2015).
445 Tracy, Tara E. *et al.* Acetylated Tau Obstructs KIBRA-Mediated Signaling in Synaptic Plasticity and Promotes Tauopathy-Related Memory Loss. *Neuron* **90**, 245-260, doi:https://doi.org/10.1016/j.neuron.2016.03.005 (2016).
446 Tracy, T. E. & Gan, L. Acetylated tau in Alzheimer's disease: An instigator of synaptic dysfunction underlying memory loss. *Bioessays* **39**, 1600224, doi:10.1002/bies.201600224 (2017).
447 Choi, H. *et al.* Acetylation changes tau interactome to degrade tau in Alzheimer's disease animal and organoid models. *Aging Cell* **19**, e13081, doi:10.1111/acel.13081 (2020).
448 Kirchner, P. *et al.* Proteome-wide analysis of chaperone-mediated autophagy targeting motifs. *PLoS biology* **17**, e3000301 (2019).
449 Carlomagno, Y. *et al.* An acetylation–phosphorylation switch that regulates tau aggregation propensity and function. *Journal of Biological Chemistry* **292**, 15277-15286 (2017).
450 Min, S.-W. *et al.* Acetylation of tau inhibits its degradation and contributes to tauopathy. *Neuron* **67**, 953-966 (2010).
451 Fauvet, B. *et al.* Characterization of Semisynthetic and Naturally N^α-Acetylated α-Synuclein in Vitro and in Intact Cells: IMPLICATIONS FOR AGGREGATION AND CELLULAR PROPERTIES OF α-SYNUCLEIN *. *Journal of Biological Chemistry* **287**, 28243-28262, doi:10.1074/jbc.M112.383711 (2012).
452 Trzeciakiewicz, H. *et al.* A dual pathogenic mechanism links tau acetylation to sporadic tauopathy. *Scientific reports* **7**, 44102 (2017).
453 Cohen, T. J. *et al.* The acetylation of tau inhibits its function and promotes pathological tau aggregation. *Nat Commun* **2**, 252, doi:10.1038/ncomms1255 (2011).
454 Kamah, A. *et al.* Nuclear magnetic resonance analysis of the acetylation pattern of the neuronal Tau protein. *Biochemistry* **53**, 3020-3032, doi:10.1021/bi500006v (2014).
455 Ferreon, J. C. *et al.* Acetylation Disfavors Tau Phase Separation. *International journal of molecular sciences* **19**, doi:10.3390/ijms19051360 (2018).
456 David, D. C. *et al.* Proteasomal degradation of tau protein. *Journal of neurochemistry* **83**, 176-185 (2002).
457 Morishima, M. & Ihara, Y. Posttranslational modifications of tau in paired helical filaments. *Dement Geriatr Cogn Disord* **5**, 282-288 (1994).
458 Flach, K. *et al.* Axotrophin/MARCH7 acts as an E3 ubiquitin ligase and ubiquitinates tau protein in vitro impairing microtubule binding. *Biochimica et Biophysica Acta (BBA)-Molecular Basis of Disease* **1842**, 1527-1538 (2014).
459 Petrucelli, L. *et al.* CHIP and Hsp70 regulate tau ubiquitination, degradation and aggregation. *Human molecular genetics* **13**, 703-714 (2004).
460 Babu, J. R., Geetha, T. & Wooten, M. W. Sequestosome 1/p62 shuttles polyubiquitinated tau for proteasomal degradation. *Journal of neurochemistry* **94**, 192-203 (2005).

461 Shimura, H., Schwartz, D., Gygi, S. P. & Kosik, K. S. CHIP-Hsc70 complex ubiquitinates phosphorylated tau and enhances cell survival. *Journal of Biological Chemistry* **279**, 4869-4876 (2004).
462 Wang, P. *et al.* Tau interactome mapping based identification of Otub1 as Tau deubiquitinase involved in accumulation of pathological Tau forms in vitro and in vivo. *Acta neuropathologica* **133**, 731-749 (2017).
463 Hejjaoui, M., Haj-Yahya, M., Kumar, K. S. A., Brik, A. & Lashuel, H. A. Towards Elucidation of the Role of Ubiquitination in the Pathogenesis of Parkinson's Disease with Semisynthetic Ubiquitinated α-Synuclein. *Angewandte Chemie International Edition* **50**, 405-409, doi:https://doi.org/10.1002/anie.201005546 (2011).
464 Haj-Yahya, M. *et al.* Synthetic polyubiquitinated α-Synuclein reveals important insights into the roles of the ubiquitin chain in regulating its pathophysiology. *Proceedings of the National Academy of Sciences* **110**, 17726-17731, doi:10.1073/pnas.1315654110 (2013).
465 Barini, E. *et al.* Tau in the brain interstitial fluid is fragmented and seeding-competent. *Neurobiology of aging*, doi:https://doi.org/10.1016/j.neurobiolaging.2021.09.013 (2021).
466 Horowitz, P. M. *et al.* Early N-terminal changes and caspase-6 cleavage of tau in Alzheimer's disease. *Journal of Neuroscience* **24**, 7895-7902 (2004).
467 Ugolini, G., Cattaneo, A. & Novak, M. Co-localization of truncated tau and DNA fragmentation in Alzheimer's disease neurones. *Neuroreport* **8**, 3709-3712 (1997).
468 Rissman, R. A. *et al.* Caspase-cleavage of tau is an early event in Alzheimer disease tangle pathology. *J Clin Invest* **114**, 121-130, doi:10.1172/JCI200420640 (2004).
469 Mena, R., Edwards, P. C., Harrington, C. R., Mukaetova-Ladinska, E. B. & Wischik, C. M. Staging the pathological assembly of truncated tau protein into paired helical filaments in Alzheimer's disease. *Acta neuropathologica* **91**, 633-641 (1996).
470 Wischik, C. M. *et al.* Isolation of a fragment of tau derived from the core of the paired helical filament of Alzheimer disease. *Proceedings of the National Academy of Sciences* **85**, 4506, doi:10.1073/pnas.85.12.4506 (1988).
471 Wischik, C. M. *et al.* Structural characterization of the core of the paired helical filament of Alzheimer disease. *Proceedings of the National Academy of Sciences* **85**, 4884, doi:10.1073/pnas.85.13.4884 (1988).
472 Binder, L. I., Guillozet-Bongaarts, A. L., Garcia-Sierra, F. & Berry, R. W. Tau, tangles, and Alzheimer's disease. *Biochimica et Biophysica Acta (BBA) - Molecular Basis of Disease* **1739**, 216-223, doi:https://doi.org/10.1016/j.bbadis.2004.08.014 (2005).
473 Mondragón-Rodríguez, S. *et al.* Cleavage and conformational changes of tau protein follow phosphorylation during Alzheimer's disease. *International journal of experimental pathology* **89**, 81-90 (2008).
474 Wray, S., Saxton, M., Anderton, B. H. & Hanger, D. P. Direct analysis of tau from PSP brain identifies new phosphorylation sites and a major fragment of N-terminally cleaved tau containing four microtubule-binding repeats. *Journal of neurochemistry* **105**, 2343-2352, doi:10.1111/j.1471-4159.2008.05321.x (2008).
475 Jang, S. H. in *Traumatic Brain Injury - Pathobiology, Advanced Diagnostics and Acute Management* (InTech, 2018).
476 Yang, L. S. & Ksiezak-Reding, H. Calpain-induced proteolysis of normal human tau and tau associated with paired helical filaments. *European journal of biochemistry* **233**, 9-17 (1995).
477 Garg, S., Timm, T., Mandelkow, E.-M., Mandelkow, E. & Wang, Y. Cleavage of Tau by calpain in Alzheimer's disease: the quest for the toxic 17 kD fragment. *Neurobiology of aging* **32**, 1-14 (2011).
478 Paholikova, K. *et al.* N-terminal Truncation of Microtubule Associated Protein Tau Dysregulates its Cellular Localization. *Journal of Alzheimer's Disease* **43**, 915-926, doi:10.3233/JAD-140996 (2015).
479 Gamblin, T. C. *et al.* Caspase cleavage of tau: Linking amyloid and neurofibrillary tangles in Alzheimer's disease. *Proceedings of the National Academy of Sciences* **100**, 10032-10037, doi:10.1073/pnas.1630428100 (2003).
480 Corsetti, V. *et al.* Identification of a caspase-derived N-terminal tau fragment in cellular and animal Alzheimer's disease models. *Molecular and Cellular Neuroscience* **38**, 381-392, doi:10.1016/j.mcn.2008.03.011 (2008).
481 Amadoro, G. *et al.* NMDA receptor mediates tau-induced neurotoxicity by calpain and ERK/MAPK activation. *Proceedings of the National Academy of Sciences* **103**, 2892-2897 (2006).

482 Matsumoto, S. E. *et al.* The twenty-four KDa C-terminal tau fragment increases with aging in tauopathy mice: implications of prion-like properties. *Human molecular genetics* **24**, 6403-6416, doi:10.1093/hmg/ddv351 (2015).
483 Guo, T., Dakkak, D., Rodriguez-Martin, T., Noble, W. & Hanger, D. P. A pathogenic tau fragment compromises microtubules, disrupts insulin signaling and induces the unfolded protein response. *Acta Neuropathol Commun* **7**, 2, doi:10.1186/s40478-018-0651-9 (2019).
484 Zhao, X. *et al.* Caspase-2 cleavage of tau reversibly impairs memory. *Nat Med* **22**, 1268 (2016).
485 Zhang, Z. *et al.* Cleavage of tau by asparagine endopeptidase mediates the neurofibrillary pathology in Alzheimer's disease. *Nat Med* **20**, 1254-1262, doi:10.1038/nm.3700 (2014).
486 Sengupta, S. *et al.* Degradation of Tau Protein by Puromycin-Sensitive Aminopeptidase in Vitro†. *Biochemistry* **45**, 15111-15119, doi:10.1021/bi061830d (2006).
487 Sokolowski, J. D. *et al.* Caspase-mediated cleavage of actin and tubulin is a common feature and sensitive marker of axonal degeneration in neural development and injury. *Acta Neuropathol Commun* **2**, doi:10.1186/2051-5960-2-16 (2014).
488 Garcia-Sierra, F., Mondragon-Rodriguez, S. & Basurto-Islas, G. Truncation of tau protein and its pathological significance in Alzheimer's disease. *Journal of Alzheimer's Disease* **14**, 401-409 (2008).
489 Chesser, A. S., Pritchard, S. M. & Johnson, G. V. W. Tau Clearance Mechanisms and Their Possible Role in the Pathogenesis of Alzheimer Disease. *Front Neurol* **4**, doi:10.3389/fneur.2013.00122 (2013).
490 Friedrich, M. G. *et al.* Tau Is Truncated in Five Regions of the Normal Adult Human Brain. *International journal of molecular sciences* **22**, 3521 (2021).
491 Gendron, T. F. & Petrucelli, L. The role of tau in neurodegeneration. *Mol Neurodegener* **4**, 13 (2009).
492 Saito, M. *et al.* Tau phosphorylation and cleavage in ethanol-induced neurodegeneration in the developing mouse brain. *Neurochem Res* **35**, 651-659 (2010).
493 Rohn, T. T. *et al.* Caspase-9 activation and caspase cleavage of tau in the Alzheimer's disease brain. *Neurobiol Dis* **11**, 341-354 (2002).
494 Albrecht, S., Bogdanovic, N., Ghetti, B., Winblad, B. & LeBlanc, A. C. Caspase-6 Activation in Familial Alzheimer Disease Brains Carrying Amyloid Precursor Protein or Presenilin I or Presenilin II Mutations. *Journal of Neuropathology & Experimental Neurology* **68**, 1282-1293, doi:10.1097/nen.0b013e3181c1da10 (2009).
495 Fasulo, L. *et al.* The neuronal microtubule-associated protein tau is a substrate for caspase-3 and an effector of apoptosis. *Journal of neurochemistry* **75**, 624-633 (2000).
496 Guo, H. *et al.* Active Caspase-6 and Caspase-6-Cleaved Tau in Neuropil Threads, Neuritic Plaques, and Neurofibrillary Tangles of Alzheimer's Disease. *The American journal of pathology* **165**, 523-531, doi:10.1016/s0002-9440(10)63317-2 (2004).
497 Rissman, R. A. *et al.* Caspase-cleavage of tau is an early event in Alzheimer disease tangle pathology. *Journal of Clinical Investigation* **114**, 121-130, doi:10.1172/jci200420640 (2004).
498 Wai, M. S. M. *et al.* Co-localization of hyperphosphorylated tau and caspases in the brainstem of Alzheimer's disease patients. *Biogerontology* **10**, 457 (2009).
499 Park, S.-Y., Tournell, C., Sinjoanu, R. C. & Ferreira, A. Caspase-3-and calpain-mediated tau cleavage are differentially prevented by estrogen and testosterone in beta-amyloid-treated hippocampal neurons. *Neuroscience* **144**, 119-127 (2007).
500 Sinjoanu, R. C. *et al.* The novel calpain inhibitor A-705253 potently inhibits oligomeric beta-amyloid-induced dynamin 1 and tau cleavage in hippocampal neurons. *Neurochem Int* **53**, 79-88 (2008).
501 Adamec, E., Mohan, P., Vonsattel, J. P. & Nixon, R. A. Calpain activation in neurodegenerative diseases: confocal immunofluorescence study with antibodies specifically recognizing the active form of calpain 2. *Acta neuropathologica* **104**, 92-104 (2002).
502 Gamblin, T. C. *et al.* Caspase cleavage of tau: linking amyloid and neurofibrillary tangles in Alzheimer's disease. *Proceedings of the national academy of sciences* **100**, 10032-10037 (2003).
503 Niewiadomska, G., Niewiadomski, W., Steczkowska, M. & Gasiorowska, A. Tau Oligomers Neurotoxicity. *Life (Basel)* **11**, doi:10.3390/life11010028 (2021).

504 Manassero, G. *et al.* Dual Mechanism of Toxicity for Extracellular Injection of Tau Oligomers versus Monomers in Human Tau Mice. *Journal of Alzheimer's disease : JAD* **59**, 743-751, doi:10.3233/jad-170298 (2017).
505 Barthelemy, N. R. *et al.* Differential mass spectrometry profiles of tau protein in the cerebrospinal fluid of patients with Alzheimer's disease, progressive supranuclear palsy, and dementia with lewy bodies. *Journal of Alzheimer's Disease* **51**, 1033-1043 (2016).
506 Derisbourg, M. *et al.* Role of the Tau N-terminal region in microtubule stabilization revealed by newendogenous truncated forms. *Scientific Reports* **5**, doi:10.1038/srep09659 (2015).
507 Portelius, E. *et al.* Characterization of tau in cerebrospinal fluid using mass spectrometry. *The Journal of Proteome Research* **7**, 2114-2120 (2008).
508 Horowitz, P. M. Early N-Terminal Changes and Caspase-6 Cleavage of Tau in Alzheimer's Disease. *Journal of Neuroscience* **24**, 7895-7902, doi:10.1523/jneurosci.1988-04.2004 (2004).
509 Kanmert, D. *et al.* C-Terminally Truncated Forms of Tau, But Not Full-Length Tau or Its C-Terminal Fragments, Are Released from Neurons Independently of Cell Death. *Journal of Neuroscience* **35**, 10851-10865, doi:10.1523/jneurosci.0387-15.2015 (2015).
510 Sokolow, S. *et al.* Pre-synaptic C-terminal truncated tau is released from cortical synapses in Alzheimer's disease. *Journal of neurochemistry* **133**, 368-379, doi:10.1111/jnc.12991 (2015).
511 Pomin, V. H. & Mulloy, B. Glycosaminoglycans and Proteoglycans. *Pharmaceuticals (Basel)* **11**, 27, doi:10.3390/ph11010027 (2018).
512 Gupta, R. C., Lall, R., Srivastava, A. & Sinha, A. Hyaluronic Acid: Molecular Mechanisms and Therapeutic Trajectory. *Front Vet Sci* **6**, 192-192, doi:10.3389/fvets.2019.00192 (2019).
513 Logsdon, A. F. *et al.* Decoding perineuronal net glycan sulfation patterns in the Alzheimer's disease brain. *Alzheimer's & Dementia* **n/a**, doi:https://doi.org/10.1002/alz.12451.
514 Hayes, A. J. & Melrose, J. Glycans and glycosaminoglycans in neurobiology: key regulators of neuronal cell function and fate. *Biochem J* **475**, 2511-2545, doi:10.1042/bcj20180283 (2018).
515 Lindahl, U., Couchman, J., Kimata, K. & Esko, J. D. Proteoglycans and sulfated glycosaminoglycans. *Essentials of glycobiology* **3** (2015).
516 Couchman, J. R. & Pataki, C. A. An introduction to proteoglycans and their localization. *Journal of Histochemistry & Cytochemistry* **60**, 885-897 (2012).
517 Mah, D. *et al.* The Sulfation Code of Tauopathies: Heparan Sulfate Proteoglycans in the Prion Like Spread of Tau Pathology. *Front Mol Biosci* **8**, 671458-671458, doi:10.3389/fmolb.2021.671458 (2021).
518 Zhu, H. L. *et al.* Quantitative characterization of heparin binding to Tau protein: implication for inducer-mediated Tau filament formation. *The Journal of biological chemistry* **285**, 3592-3599, doi:10.1074/jbc.M109.035691 (2010).
519 Ramachandran, G. & Udgaonkar, J. B. Understanding the kinetic roles of the inducer heparin and of rod-like protofibrils during amyloid fibril formation by Tau protein. *The Journal of biological chemistry* **286**, 38948-38959, doi:10.1074/jbc.M111.271874 (2011).
520 Haque, M. M. *et al.* Inhibition of tau aggregation by a rosamine derivative that blocks tau intermolecular disulfide cross-linking. *Amyloid* **21**, 185-190, doi:10.3109/13506129.2014.929103 (2014).
521 Huvent, I. *et al.* A functional fragment of Tau forms fibers without the need for an intermolecular cysteine bridge. *Biochemical and biophysical research communications* **445**, 299-303, doi:10.1016/j.bbrc.2014.01.161 (2014).
522 Zhao, J. *et al.* Glycan Determinants of Heparin-Tau Interaction. *Biophysical journal* **112**, 921-932, doi:10.1016/j.bpj.2017.01.024 (2017).
523 Sarrazin, S., Lamanna, W. C. & Esko, J. D. Heparan sulfate proteoglycans. *Cold Spring Harb Perspect Biol* **3**, a004952 (2011).
524 Capila, I. & Linhardt, R. J. Heparin–protein interactions. *Angewandte Chemie International Edition* **41**, 390-412 (2002).
525 Aviezer, D. *et al.* Differential structural requirements of heparin and heparan sulfate proteoglycans that promote binding of basic fibroblast growth factor to its receptor. *Journal of Biological Chemistry* **269**, 114-121 (1994).

526 Herndon, M. E., Stipp, C. S. & Lander, A. D. Interactions of neural glycosaminoglycans and proteoglycans with protein ligands: assessment of selectivity, heterogeneity and the participation of core proteins in binding. *Glycobiology* **9**, 143-155 (1999).
527 Mukrasch, M. D. *et al.* Sites of tau important for aggregation populate β-structure and bind to microtubules and polyanions. *Journal of Biological Chemistry* **280**, 24978-24986 (2005).
528 Fichou, Y., Eschmann, N. A., Keller, T. J. & Han, S. in *Methods in cell biology* Vol. 141 (eds Stuart C. Feinstein & Nichole E. LaPointe) 89-112 (Academic Press, 2017).
529 von Bergen, M., Barghorn, S., Biernat, J., Mandelkow, E. M. & Mandelkow, E. *Biochim. Biophys. Acta* **1739**, 158 (2005).
530 Friedhoff, P., von Bergen, M., Mandelkow, E. M., Davies, P. & Mandelkow, E. A nucleated assembly mechanism of Alzheimer paired helical filaments. *Proceedings of the National Academy of Sciences of the United States of America* **95**, 15712-15717, doi:10.1073/pnas.95.26.15712 (1998).
531 Moreira, G. G. *et al.* Zinc Binding to Tau Influences Aggregation Kinetics and Oligomer Distribution. *International journal of molecular sciences* **20** (2019). <http://europepmc.org/abstract/MED/31783644

https://doi.org/10.3390/ijms20235979

https://europepmc.org/articles/PMC6928861

https://europepmc.org/articles/PMC6928861?pdf=render>.
532 Trzeciakiewicz, H., Esteves-Villanueva, J. O., Carlin, N. & Martić, S. Electrochemistry of heparin binding to tau protein on Au surfaces. *Electrochimica Acta* **162**, 24-30, doi:https://doi.org/10.1016/j.electacta.2014.08.101 (2015).
533 de Ancos, J. G., Correas, I. & Avila, J. Differences in microtubule binding and self-association abilities of bovine brain tau isoforms. *Journal of Biological Chemistry* **268**, 7976-7982 (1993).
534 Congdon, E. E. *et al.* Nucleation-dependent tau filament formation: the importance of dimerization and an estimation of elementary rate constants. *The Journal of biological chemistry* **283**, 13806-13816, doi:10.1074/jbc.M800247200 (2008).
535 Díaz-Nido, J., Wandosell, F. & Avila, J. Glycosaminoglycans and β-amyloid, prion and tau peptides in neurodegenerative diseases. *Peptides* **23**, 1323-1332, doi:https://doi.org/10.1016/S0196-9781(02)00068-2 (2002).
536 Seidler, P. M. *et al.* Structure-based inhibitors halt prion-like seeding by Alzheimer's disease-and tauopathy-derived brain tissue samples. *The Journal of biological chemistry* **294**, 16451-16464, doi:10.1074/jbc.RA119.009688 (2019).
537 Shipps, C. *et al.* Intrinsic electronic conductivity of individual atomically resolved amyloid crystals reveals micrometer-long hole hopping via tyrosines. *Proceedings of the National Academy of Sciences of the United States of America* **118**, doi:10.1073/pnas.2014139118 (2021).
538 Eisenberg, D. & Jucker, M. The amyloid state of proteins in human diseases. *Cell* **148**, 1188-1203 (2012).
539 Zhang, W. *et al.* (bioRxiv, 2018).
540 Dregni, A. J. *et al.* In vitro 0N4R tau fibrils contain a monomorphic β-sheet core enclosed by dynamically heterogeneous fuzzy coat segments. *Proceedings of the National Academy of Sciences of the United States of America* **116**, 16357-16366, doi:10.1073/pnas.1906839116 (2019).
541 Yang, J., Agnihotri, M. V., Huseby, C. J., Kuret, J. & Singer, S. J. A theoretical study of polymorphism in VQIVYK fibrils. *Biophysical journal* **120**, 1396-1416, doi:https://doi.org/10.1016/j.bpj.2021.01.032 (2021).
542 Huvent, I. *et al.* A functional fragment of Tau forms fibers without the need for an intermolecular cysteine bridge. *Biochemical and biophysical research communications* **445**, 299-303, doi:10.1016/j.bbrc.2014.01.161 (2014).
543 Bhattacharyya, R., Pal, D. & Chakrabarti, P. Disulfide bonds, their stereospecific environment and conservation in protein structures. *Protein Engineering, Design and Selection* **17**, 795-808, doi:10.1093/protein/gzh093 (2004).
544 Zhang, W. *et al.* Novel tau filament fold in corticobasal degeneration. *Nature* **580**, 283-287 (2020).
545 DeLano, W. L. (2002).

546 Hernández, F., Pérez, M., Lucas, J. J. & Avila, J. Sulfo-glycosaminoglycan content affects PHF-tau solubility and allows the identification of different types of PHFs. *Brain Res* **935**, 65-72, doi:10.1016/s0006-8993(02)02455-1 (2002).
547 Santa-Maria, I., Perez, M., Hernandez, F., Avila, J. & Moreno, F. J. Characteristics of the binding of thioflavin S to tau paired helical filaments. *Journal of Alzheimer's disease : JAD* **9**, 279-285, doi:10.3233/jad-2006-9307 (2006).
548 Carlson, S. W. *et al.* A complex mechanism for inducer mediated tau polymerization. *Biochemistry* **46**, 8838-8849, doi:10.1021/bi700403a (2007).
549 Shriver, Z., Capila, I., Venkataraman, G. & Sasisekharan, R. Heparin and heparan sulfate: analyzing structure and microheterogeneity. *Handb Exp Pharmacol*, 159-176, doi:10.1007/978-3-642-23056-1_8 (2012).
550 Kasai, M. & Oosawa, F. Removal of nucleotides from F-actin. *Biochim. Biophys. Acta* **75**, 223 (1963).
551 Mulloy, B. & Rider, C. C. Cytokine/Proteoglycan Interactions: a Biochemical Society Focused Meeting (Royal Holloway University of London). *The Biochemist* **28**, 37-38, doi:10.1042/bio02804037 (2006).
552 Rauch, J. N. *et al.* Tau Internalization is Regulated by 6-O Sulfation on Heparan Sulfate Proteoglycans (HSPGs). *Scientific reports* **8**, 6382 (2018). <http://europepmc.org/abstract/MED/29686391

https://doi.org/10.1038/s41598-018-24904-z

https://europepmc.org/articles/PMC5913225

https://europepmc.org/articles/PMC5913225?pdf=render>.
553 Pernègre, C., Duquette, A. & Leclerc, N. Tau Secretion: Good and Bad for Neurons. *Frontiers in neuroscience* **13**, doi:10.3389/fnins.2019.00649 (2019).
554 Brunello, C. A., Merezhko, M., Uronen, R.-L. & Huttunen, H. J. Mechanisms of secretion and spreading of pathological tau protein. *Cellular and Molecular Life Sciences* **77**, 1721-1744, doi:10.1007/s00018-019-03349-1 (2020).
555 Lewis, J. & Dickson, D. W. Propagation of tau pathology: hypotheses, discoveries, and yet unresolved questions from experimental and human brain studies. *Acta neuropathologica* **131**, 27-48, doi:10.1007/s00401-015-1507-z (2016).
556 Vogels, T. *et al.* Propagation of Tau Pathology: Integrating Insights From Postmortem and In Vivo Studies. *Biol Psychiatry* **87**, 808-818, doi:10.1016/j.biopsych.2019.09.019 (2020).
557 Holth, J. K. *et al.* The sleep-wake cycle regulates brain interstitial fluid tau in mice and CSF tau in humans. *Science*, eaav2546, doi:10.1126/science.aav2546 (2019).
558 Yamada, K. *et al.* Analysis of in vivo turnover of tau in a mouse model of tauopathy. *Mol Neurodegener* **10**, 55 (2015). <http://europepmc.org/abstract/MED/26502977

https://doi.org/10.1186/s13024-015-0052-5

https://europepmc.org/articles/PMC4621881

https://europepmc.org/articles/PMC4621881?pdf=render>.
559 Undin, T., Lind, S. B. & Dahlin, A. P. MS for investigation of time-dependent protein adsorption on surfaces in complex biological samples. *Future Sci OA* **1**, Fso32, doi:10.4155/fso.15.32 (2015).
560 Mawal-Dewan, M., Sen, P. C., Abdel-Ghany, M., Shalloway, D. & Racker, E. Phosphorylation of tau protein by purified p34cdc28 and a related protein kinase from neurofilaments. *The Journal of biological chemistry* **267**, 19705-19709 (1992).
561 Brandt, R., Lee, G., Teplow, D. B., Shalloway, D. & Abdel-Ghany, M. Differential effect of phosphorylation and substrate modulation on tau's ability to promote microtubule growth and nucleation. *The Journal of biological chemistry* **269**, 11776-11782 (1994).
562 Yang, S. D., Yu, J. S., Shiah, S. G. & Huang, J. J. Protein kinase FA/glycogen synthase kinase-3 alpha after heparin potentiation phosphorylates tau on sites abnormally phosphorylated in Alzheimer's disease brain. *Journal of neurochemistry* **63**, 1416-1425, doi:10.1046/j.1471-4159.1994.63041416.x (1994).

563 Goedert, M. *et al.* Phosphorylation of microtubule-associated protein tau by stress-activated protein kinases. *FEBS letters* **409**, 57-62 (1997).
564 Hasegawa, M. *et al.* Protein sequence and mass spectrometric analyses of tau in the Alzheimer's disease brain. *J. Biol. Chem.* **267**, 17047 (1992).
565 Iqbal, K. *et al.* Tau pathology in Alzheimer disease and other tauopathies. *Biochimica et Biophysica Acta (BBA) - Molecular Basis of Disease* **1739**, 198-210, doi:https://doi.org/10.1016/j.bbadis.2004.09.008 (2005).
566 Schröder, H. C., Bernd, A., Zahn, R. K. & Müller, W. E. Binding of polyribonucleotides and polydeoxyribonucleotides to bovine brain microtubule protein: age-dependent modulation via phosphorylation of high-molecular-weight microtubule-associated proteins and tau proteins. *Mechanisms of ageing and development* **24**, 101-117 (1984).
567 Zhang, X. *et al.* RNA stores tau reversibly in complex coacervates. *PLoS biology* **15**, e2002183, doi:10.1371/journal.pbio.2002183 (2017).
568 Ginsberg, S. D. *et al.* RNA sequestration to pathological lesions of neurodegenerative diseases. *Acta Neuropathol.* **96**, 487 (1998).
569 Ginsberg, S. D., Crino, P. B., Lee, V. M., Eberwine, J. H. & Trojanowski, J. Q. Sequestration of RNA in Alzheimer's disease neurofibrillary tangles and senile plaques. *Ann. Neurol.* **41**, 200 (1997).
570 Wang, X. S. *et al.* The proline-rich domain and the microtubule binding domain of protein tau acting as RNA binding domains. *Protein and peptide letters* **13**, 679-685 (2006).
571 Ambadipudi, S., Biernat, J., Riedel, D., Mandelkow, E. & Zweckstetter, M. Liquid-liquid phase separation of the microtubule-binding repeats of the Alzheimer-related protein Tau. *Nat Commun* **8**, 275 (2017). <http://europepmc.org/abstract/MED/28819146

https://doi.org/10.1038/s41467-017-00480-0

https://europepmc.org/articles/PMC5561136

https://europepmc.org/articles/PMC5561136?pdf=render>.
572 Darling, A. L. & Shorter, J. Combating deleterious phase transitions in neurodegenerative disease. *Biochim Biophys Acta Mol Cell Res* **1868**, 118984, doi:10.1016/j.bbamcr.2021.118984 (2021).
573 Zbinden, A., Pérez-Berlanga, M., De Rossi, P. & Polymenidou, M. Phase Separation and Neurodegenerative Diseases: A Disturbance in the Force. *Developmental Cell* **55**, 45-68, doi:https://doi.org/10.1016/j.devcel.2020.09.014 (2020).
574 Wegmann, S. in *Tau Biology* 341-357 (Springer, 2019).
575 Babinchak, W. M. & Surewicz, W. K. Liquid–Liquid Phase Separation and Its Mechanistic Role in Pathological Protein Aggregation. *Journal of molecular biology* **432**, 1910-1925, doi:https://doi.org/10.1016/j.jmb.2020.03.004 (2020).
576 Wegmann, S. *et al.* Tau protein liquid-liquid phase separation can initiate tau aggregation. *EMBO J* **37**, doi:10.15252/embj.201798049 (2018).
577 Lin, Y. *et al.* Narrow equilibrium window for complex coacervation of tau and RNA under cellular conditions. *eLife* **8** (2019). <http://europepmc.org/abstract/MED/30950394

https://doi.org/10.7554/eLife.42571

https://europepmc.org/articles/PMC6450672

https://europepmc.org/articles/PMC6450672?pdf=render>.
578 Lin, Y., Fichou, Y., Zeng, Z., Hu, N. Y. & Han, S. Electrostatically Driven Complex Coacervation and Amyloid Aggregation of Tau Are Independent Processes with Overlapping Conditions. *ACS chemical neuroscience* **11**, 615-627, doi:10.1021/acschemneuro.9b00627 (2020).
579 Boyko, S., Surewicz, K. & Surewicz, W. K. Regulatory mechanisms of tau protein fibrillation under the conditions of liquid–liquid phase separation. *Proceedings of the National Academy of Sciences*, 202012460, doi:10.1073/pnas.2012460117 (2020).

580 Reynolds, M. R., Berry, R. W. & Binder, L. I. Site-specific nitration and oxidative dityrosine bridging of the tau protein by peroxynitrite: implications for Alzheimer's disease. *Biochemistry* **44**, 1690 (2005).
581 Kanaan, N. M., Hamel, C., Grabinski, T. & Combs, B. Liquid-liquid phase separation induces pathogenic tau conformations in vitro. *Nat Commun* **11**, 2809, doi:10.1038/s41467-020-16580-3 (2020).
582 Soeda, Y. & Takashima, A. New Insights Into Drug Discovery Targeting Tau Protein. *Frontiers in molecular neuroscience* **13**, doi:10.3389/fnmol.2020.590896 (2020).
583 Gray, E. G., Paula-Barbosa, M. & Roher, A. *Neuropathol. Appl. Neurobiol.* **13**, 110 (1987).
584 Sparkman, D. R., Goux, W. J., Jones, C. M., White, C. L., III & Hill, S. J. *Biochem. Biophys. Res. Commun. 181, 771–779*. (1991).
585 Goux, W. J., Rodriguez, S. & Sparkman, D. R. *FEBS Lett.* **366**, 85 (1995).
586 Surridge, C. D. & Burns, R. G. *Biochemistry 33, 8051–8057*. (1994).
587 Bok, E. *et al.* Role of the Lipid Membrane and Membrane Proteins in Tau Pathology. *Frontiers in cell and developmental biology* **9**, 653815, doi:10.3389/fcell.2021.653815 (2021).
588 Talaga, D. *et al.* PIP2 Phospholipid-Induced Aggregation of Tau Filaments Probed by Tip-Enhanced Raman Spectroscopy. *Angewandte Chemie (International ed. in English)* **57**, 15738-15742, doi:10.1002/anie.201809636 (2018).
589 Georgieva, E. R., Xiao, S., Borbat, P. P., Freed, J. H. & Eliezer, D. Tau binds to lipid membrane surfaces via short amphipathic helices located in its microtubule-binding repeats. *Biophysical journal* **107**, 1441-1452, doi:10.1016/j.bpj.2014.07.046 (2014).
590 Barracchia, C. G. *et al.* Unsaturated Fatty Acid-Induced Conformational Transitions and Aggregation of the Repeat Domain of Tau. *Molecules* **25**, doi:10.3390/molecules25112716 (2020).
591 Fanni, A. M., Vander Zanden, C. M., Majewska, P. V., Majewski, J. & Chi, E. Y. Membrane-mediated fibrillation and toxicity of the tau hexapeptide PHF6. *The Journal of biological chemistry* **294**, 15304-15317, doi:10.1074/jbc.RA119.010003 (2019).
592 Ait-Bouziad, N. *et al.* Discovery and characterization of stable and toxic Tau/phospholipid oligomeric complexes. *Nat Commun* **8**, 1678, doi:10.1038/s41467-017-01575-4 (2017).
593 Pooler, A. M. *et al.* Dynamic association of tau with neuronal membranes is regulated by phosphorylation. *Neurobiology of aging* **33**, 431.e427-431.e438, doi:10.1016/j.neurobiolaging.2011.01.005 (2012).
594 Eidenmüller, J. *et al.* Phosphorylation-mimicking glutamate clusters in the proline-rich region are sufficient to simulate the functional deficiencies of hyperphosphorylated tau protein. *Biochemical Journal* **357**, 759-767 (2001).
595 Ekinci, F. J. & Shea, T. B. Phosphorylation of tau alters its association with the plasma membrane. *Cellular and molecular neurobiology* **20**, 497-508 (2000).
596 Maas, T., Eidenmüller, J. & Brandt, R. Interaction of tau with the neural membrane cortex is regulated by phosphorylation at sites that are modified in paired helical filaments. *Journal of Biological Chemistry* **275**, 15733-15740 (2000).
597 Nuebling, G. S. *et al.* Binding of Metal-Ion-Induced Tau Oligomers to Lipid Surfaces Is Enhanced by GSK-3β-Mediated Phosphorylation. *ACS chemical neuroscience* **11**, 880-887, doi:10.1021/acschemneuro.9b00459 (2020).
598 Shelton, S. B. & Johnson, G. V. Tau and HMW tau phosphorylation and compartmentalization in apoptotic neuronal PC12 cells. *J Neurosci Res* **66**, 203-213 (2001).
599 Usardi, A. *et al.* Tyrosine phosphorylation of tau regulates its interactions with Fyn SH2 domains, but not SH3 domains, altering the cellular localization of tau. *The FEBS journal* **278**, 2927-2937 (2011).
600 Merezhko, M. *et al.* Secretion of Tau via an Unconventional Non-vesicular Mechanism. *Cell reports* **25**, 2027-2035 e2024, doi:10.1016/j.celrep.2018.10.078 (2018).
601 Katsinelos, T. *et al.* Unconventional Secretion Mediates the Trans-cellular Spreading of Tau. *Cell reports* **23**, 2039-2055, doi:10.1016/j.celrep.2018.04.056 (2018).
602 Armstrong, R. A. On the'classification'of neurodegenerative disorders: discrete entities, overlap or continuum? *Folia neuropathologica* **50**, 201-218 (2012).
603 Serrano-Pozo, A., Frosch, M. P., Masliah, E. & Hyman, B. T. Neuropathological alterations in Alzheimer disease. *Cold Spring Harb Perspect Med* **1**, a006189 (2011).

604 Vasconcelos, B. *et al.* Heterotypic seeding of Tau fibrillization by pre-aggregated Abeta provides potent seeds for prion-like seeding and propagation of Tau-pathology in vivo. *Acta neuropathologica* **131**, 549-569, doi:10.1007/s00401-015-1525-x (2016).
605 Bennett, R. E. *et al.* Enhanced Tau Aggregation in the Presence of Amyloid β. *The American journal of pathology* **187**, 1601-1612, doi:10.1016/j.ajpath.2017.03.011 (2017).
606 Oddo, S. *et al.* Triple-transgenic model of Alzheimer's disease with plaques and tangles: intracellular Aβ and synaptic dysfunction. *Neuron* **39**, 409-421 (2003).
607 Götz, J., Chen, F. v., Van Dorpe, J. & Nitsch, R. Formation of neurofibrillary tangles in P301L tau transgenic mice induced by Aβ42 fibrils. *Science* **293**, 1491-1495 (2001).
608 He, Z. *et al.* Amyloid-β plaques enhance Alzheimer's brain tau-seeded pathologies by facilitating neuritic plaque tau aggregation. *Nat Med* **24**, 29-38, doi:10.1038/nm.4443 (2018).
609 Ciccone, L., Shi, C., di Lorenzo, D., Van Baelen, A.-C. & Tonali, N. The Positive Side of the Alzheimer's Disease Amyloid Cross-Interactions: The Case of the Aβ 1-42 Peptide with Tau, TTR, CysC, and ApoA1. *Molecules* **25**, 2439 (2020).
610 Hansen, L. *et al.* The Lewy body variant of Alzheimer's disease: a clinical and pathologic entity. *Neurology* **40**, 1-1 (1990).
611 McKeith, I. G. *et al.* Consensus guidelines for the clinical and pathologic diagnosis of dementia with Lewy bodies (DLB): report of the consortium on DLB international workshop. *Neurology* **47**, 1113-1124 (1996).
612 Spotorno, N. *et al.* Tau pathology associates with in vivo cortical thinning in Lewy body disorders. *Ann Clin Transl Neurol*.
613 Colom-Cadena, M. *et al.* Regional Overlap of Pathologies in Lewy Body Disorders. *Journal of Neuropathology & Experimental Neurology* **76**, 216-224, doi:10.1093/jnen/nlx002 (2017).
614 Giasson, B. I. *et al.* Initiation and synergistic fibrillization of tau and alpha-synuclein. *Science* **300**, 636-640 (2003).
615 Castillo-Carranza, D. L., Guerrero-Muñoz, M. J., Sengupta, U., Gerson, J. E. & Kayed, R. α-Synuclein Oligomers Induce a Unique Toxic Tau Strain. *Biol Psychiatry* **84**, 499-508, doi:10.1016/j.biopsych.2017.12.018 (2018).
616 Iljina, M. *et al.* Quantifying Co-Oligomer Formation by α-Synuclein. *ACS Nano* **12**, 10855-10866, doi:10.1021/acsnano.8b03575 (2018).
617 Bassil, F. *et al.* α-Synuclein modulates tau spreading in mouse brains. *Journal of Experimental Medicine* **218** (2020).
618 Williams, T., Sorrentino, Z., Weinrich, M., Giasson, B. I. & Chakrabarty, P. Differential cross-seeding properties of tau and α-synuclein in mouse models of tauopathy and synucleinopathy. *Brain Commun* **2**, fcaa090, doi:10.1093/braincomms/fcaa090 (2020).
619 Uemura, N., Uemura, M. T., Luk, K. C., Lee, V. M. Y. & Trojanowski, J. Q. Cell-to-Cell Transmission of Tau and α-Synuclein. *Trends in Molecular Medicine*, doi:https://doi.org/10.1016/j.molmed.2020.03.012 (2020).
620 Vacchi, E., Kaelin-Lang, A. & Melli, G. Tau and Alpha Synuclein Synergistic Effect in Neurodegenerative Diseases: When the Periphery Is the Core. *International journal of molecular sciences* **21**, 5030, doi:10.3390/ijms21145030 (2020).
621 McMillan, C. T. & Wolk, D. A. Presence of cerebral amyloid modulates phenotype and pattern of neurodegeneration in early Parkinson's disease. *Journal of Neurology, Neurosurgery & Psychiatry* **87**, 1112-1122 (2016).
622 Chung, D. C., Roemer, S., Petrucelli, L. & Dickson, D. W. Cellular and pathological heterogeneity of primary tauopathies. *Mol Neurodegener* **16**, 57, doi:10.1186/s13024-021-00476-x (2021).
623 Martin, L. *et al.* Tau protein kinases: Involvement in Alzheimer's disease. *Ageing Res Rev* **12**, 289-309, doi:https://doi.org/10.1016/j.arr.2012.06.003 (2013).
624 Braithwaite, S. P., Stock, J. B., Lombroso, P. J. & Nairn, A. C. Protein phosphatases and Alzheimer's disease. *Prog Mol Biol Transl Sci* **106**, 343-379 (2012).
625 Yadikar, H. *et al.* Screening of tau protein kinase inhibitors in a tauopathy-relevant cell-based model of tau hyperphosphorylation and oligomerization. *PloS one* **15**, e0224952, doi:10.1371/journal.pone.0224952 (2020).

626 Bhat, R. V. *et al.* The conundrum of GSK3 inhibitors: is it the dawn of a new beginning? *Journal of Alzheimer's Disease* **64**, S547-S554 (2018).
627 Sayas, C. L. & Ávila, J. GSK-3 and Tau: A Key Duet in Alzheimer's Disease. *Cells* **10**, doi:10.3390/cells10040721 (2021).
628 Yamaguchi, H. *et al.* Preferential labeling of Alzheimer neurofibrillary tangles with antisera for tau protein kinase (TPK) I/glycogen synthase kinase-3β and cyclin-dependent kinase 5, a component of TPK II. *Acta neuropathologica* **92**, 232-241 (1996).
629 Imahori, K. & Uchida, T. Physiology and pathology of tau protein kinases in relation to Alzheimer's disease. *The Journal of Biochemistry* **121**, 179-188 (1997).
630 Takashima, A. GSK-3 is essential in the pathogenesis of Alzheimer's disease. *Journal of Alzheimer's disease* **9**, 309-317 (2006).
631 Guo, T., Noble, W. & Hanger, D. P. Roles of tau protein in health and disease. *Acta neuropathologica* **133**, 665-704, doi:10.1007/s00401-017-1707-9 (2017).
632 Liu, M. *et al.* Beneficial effects of low-dose lithium on cognitive ability and pathological alteration of Alzheimer's disease transgenic mice model. *Neuroreport* **31** (2020).
633 Rubenstein, R. *et al.* Novel Mouse Tauopathy Model for Repetitive Mild Traumatic Brain Injury: Evaluation of Long-Term Effects on Cognition and Biomarker Levels After Therapeutic Inhibition of Tau Phosphorylation. *Front Neurol* **10**, 124, doi:10.3389/fneur.2019.00124 (2019).
634 Hong, M., Chen, D. C., Klein, P. S. & Lee, V. M.-Y. Lithium reduces tau phosphorylation by inhibition of glycogen synthase kinase-3. *Journal of Biological Chemistry* **272**, 25326-25332 (1997).
635 Lovestone, S. *et al.* Lithium reduces tau phosphorylation: effects in living cells and in neurons at therapeutic concentrations. *Biol Psychiatry* **45**, 995-1003 (1999).
636 Muñoz-Montaño, J. R., Moreno, F. J., Avila, J. & Díaz-Nido, J. Lithium inhibits Alzheimer's disease-like tau protein phosphorylation in neurons. *FEBS letters* **411**, 183-188 (1997).
637 Caccamo, A., Oddo, S., Tran, L. X. & LaFerla, F. M. Lithium reduces tau phosphorylation but not Aβ or working memory deficits in a transgenic model with both plaques and tangles. *The American journal of pathology* **170**, 1669-1675 (2007).
638 Leroy, K. *et al.* Lithium treatment arrests the development of neurofibrillary tangles in mutant tau transgenic mice with advanced neurofibrillary pathology. *Journal of Alzheimer's Disease* **19**, 705-719 (2010).
639 Tondo, L. *et al.* Clinical use of lithium salts: guide for users and prescribers. *International journal of bipolar disorders* **7**, 1-10 (2019).
640 Donix, M. & Bauer, M. Population studies of association between lithium and risk of neurodegenerative disorders. *Curr Alzheimer Res* **13**, 873-878 (2016).
641 Matsunaga, S. *et al.* Lithium as a Treatment for Alzheimer's Disease: A Systematic Review and Meta-Analysis. *Journal of Alzheimer's disease : JAD* **48**, 403-410, doi:10.3233/jad-150437 (2015).
642 Kessing, L. V. *et al.* Association of Lithium in Drinking Water With the Incidence of Dementia. *JAMA Psychiatry* **74**, 1005-1010, doi:10.1001/jamapsychiatry.2017.2362 (2017).
643 Parker, W. F. *et al.* Association between groundwater lithium and the diagnosis of bipolar disorder and dementia in the United States. *JAMA Psychiatry* **75**, 751-754 (2018).
644 Wilson, E. N. *et al.* NP03, a Microdose Lithium Formulation, Blunts Early Amyloid Post-Plaque Neuropathology in McGill-R-Thy1-APP Alzheimer-Like Transgenic Rats. *Journal of Alzheimer's Disease* **73**, 723-739, doi:10.3233/JAD-190862 (2020).
645 Noori, M. S. *et al.* Identification of a novel selective and potent inhibitor of glycogen synthase kinase-3. *American Journal of Physiology-Cell Physiology* **317**, C1289-C1303, doi:10.1152/ajpcell.00061.2019 (2019).
646 Tolosa, E. *et al.* A phase 2 trial of the GSK-3 inhibitor tideglusib in progressive supranuclear palsy. *Movement Disorders* **29**, 470-478 (2014).
647 Höglinger, G. U. *et al.* Tideglusib reduces progression of brain atrophy in progressive supranuclear palsy in a randomized trial. *Movement Disorders* **29**, 479-487 (2014).
648 Lee, G. *et al.* Phosphorylation of tau by fyn: Implications for Alzheimer's disease. *Journal of Neuroscience* **24**, 2304-2312, doi:10.1523/Jneurosci.4162-03.2004 (2004).

649 Kaufman, A. C. *et al.* F yn inhibition rescues established memory and synapse loss in A lzheimer mice. *Annals of neurology* **77**, 953-971 (2015).
650 Smith, L. M., Zhu, R. & Strittmatter, S. M. Disease-modifying benefit of Fyn blockade persists after washout in mouse Alzheimer's model. *Neuropharmacology* **130**, 54-61 (2018).
651 Nygaard, H. B. *et al.* A phase Ib multiple ascending dose study of the safety, tolerability, and central nervous system availability of AZD0530 (saracatinib) in Alzheimer's disease. *Alzheimers Res Ther* **7**, 1-11 (2015).
652 Van Dyck, C. H. *et al.* Effect of AZD0530 on cerebral metabolic decline in Alzheimer disease: a randomized clinical trial. *JAMA Neurol* **76**, 1219-1229 (2019).
653 Kimura, T., Ishiguro, K. & Hisanaga, S.-i. Physiological and pathological phosphorylation of tau by Cdk5. *Frontiers in molecular neuroscience* **7**, 65 (2014).
654 Schlatterer, S. D., Acker, C. M. & Davies, P. c-Abl in Neurodegenerative Disease. *Journal of Molecular Neuroscience* **45**, 445-452, doi:10.1007/s12031-011-9588-1 (2011).
655 Mórotz, G. M. *et al.* LMTK2 binds to kinesin light chains to mediate anterograde axonal transport of cdk5/p35 and LMTK2 levels are reduced in Alzheimer's disease brains. *Acta Neuropathol Commun* **7**, 73 (2019).
656 Melchior, B. *et al.* Tau pathology reduction with SM07883, a novel, potent, and selective oral DYRK1A inhibitor: A potential therapeutic for Alzheimer's disease. *Aging Cell* **18**, e13000, doi:10.1111/acel.13000 (2019).
657 Giacomini, C. *et al.* A new TAO kinase inhibitor reduces tau phosphorylation at sites associated with neurodegeneration in human tauopathies. *Acta Neuropathol Commun* **6**, 37, doi:10.1186/s40478-018-0539-8 (2018).
658 Fallacara, A. L., Trist, I. M. L., Schenone, S. & Botta, M. in *Alzheimer's Disease II* (ed Michael S. Wolfe) 119-158 (Springer International Publishing, 2017).
659 Schwab, C. *et al.* Casein kinase 1 delta is associated with pathological accumulation of tau in several neurodegenerative diseases. *Neurobiology of aging* **21**, 503-510 (2000).
660 Ferrer, I., Blanco, R., Carmona, M. & Puig, B. Phosphorylated mitogen-activated protein kinase (MAPK/ERK-P), protein kinase of 38 kDa (p38-P), stress-activated protein kinase (SAPK/JNK-P), and calcium/calmodulin-dependent kinase II (CaM kinase II) are differentially expressed in tau deposits in neurons and glial cells in tauopathies. *Journal of neural transmission* **108**, 1397-1415 (2001).
661 Pei, J.-J. *et al.* Up-regulation of mitogen-activated protein kinases ERK1/2 and MEK1/2 is associated with the progression of neurofibrillary degeneration in Alzheimer's disease. *Mol Brain Res* **109**, 45-55 (2002).
662 Vingtdeux, V., Davies, P., Dickson, D. W. & Marambaud, P. AMPK is abnormally activated in tangle-and pre-tangle-bearing neurons in Alzheimer's disease and other tauopathies. *Acta neuropathologica* **121**, 337-349 (2011).
663 Liu, F. *et al.* PKA modulates GSK-3β-and cdk5-catalyzed phosphorylation of tau in site-and kinase-specific manners. *FEBS letters* **580**, 6269-6274 (2006).
664 Taniguchi, T. *et al.* Phosphorylation of tau is regulated by PKN. *Journal of Biological Chemistry* **276**, 10025-10031 (2001).
665 Imahori, K. *et al.* Possible role of tau protein kinases in pathogenesis of Alzheimer's disease. *Neurobiology of aging* **19**, S93-S98 (1998).
666 Chin, J. Y. *et al.* Microtubule-affinity regulating kinase (MARK) is tightly associated with neurofibrillary tangles in Alzheimer brain: a fluorescence resonance energy transfer study. *Journal of Neuropathology & Experimental Neurology* **59**, 966-971 (2000).
667 Qian, W. *et al.* Activation of protein phosphatase 2B and hyperphosphorylation of Tau in Alzheimer's disease. *Journal of Alzheimer's Disease* **23**, 617-627 (2011).
668 Tanimukai, H., Grundke-Iqbal, I. & Iqbal, K. Up-regulation of inhibitors of protein phosphatase-2A in Alzheimer's disease. *The American journal of pathology* **166**, 1761-1771 (2005).
669 Liu, F., Iqbal, K., Grundke-Iqbal, I., Rossie, S. & Gong, C.-X. Dephosphorylation of tau by protein phosphatase 5: impairment in Alzheimer's disease. *Journal of Biological Chemistry* **280**, 1790-1796 (2005).
670 Wasik, U. *et al.* Calcyclin binding protein and Siah-1 interacting protein in Alzheimer's disease pathology: neuronal localization and possible function. *Neurobiology of aging* **34**, 1380-1388 (2013).

671 Graham, D. L. *et al.* Increased O-GlcNAcylation reduces pathological tau without affecting its normal phosphorylation in a mouse model of tauopathy. *Neuropharmacology* **79**, 307-313 (2014).
672 Hastings, N. B. *et al.* Inhibition of O-GlcNAcase leads to elevation of O-GlcNAc tau and reduction of tauopathy and cerebrospinal fluid tau in rTg4510 mice. *Mol Neurodegener* **12**, 1-16 (2017).
673 Borghgraef, P. *et al.* Increasing brain protein O-GlcNAc-ylation mitigates breathing defects and mortality of Tau. P301L mice. *PloS one* **8**, e84442 (2013).
674 Yu, Y. *et al.* Differential effects of an O-GlcNAcase inhibitor on tau phosphorylation. *PloS one* **7**, e35277 (2012).
675 Selnick, H. G. *et al.* Discovery of MK-8719, a potent O-GlcNAcase inhibitor as a potential treatment for tauopathies. *J Med Chem* **62**, 10062-10097 (2019).
676 Wang, X. *et al.* MK-8719, a Novel and Selective O-GlcNAcase Inhibitor That Reduces the Formation of Pathological Tau and Ameliorates Neurodegeneration in a Mouse Model of Tauopathy. *J Pharmacol Exp Ther* **374**, 252-263, doi:10.1124/jpet.120.266122 (2020).
677 VandeVrede, L., Boxer, A. L. & Polydoro, M. Targeting tau: Clinical trials and novel therapeutic approaches. *Neurosci Lett*, 134919 (2020).
678 Lee, H. E., Lim, D., Lee, J. Y., Lim, S. M. & Pae, A. N. (Future Science, 2019).
679 Shirakawa, K. *et al.* Salicylate, diflunisal and their metabolites inhibit CBP/p300 and exhibit anticancer activity. *eLife* **5**, e11156, doi:10.7554/eLife.11156 (2016).
680 Wang, Y. & Mandelkow, E. Degradation of tau protein by autophagy and proteasomal pathways. *Biochem Soc Trans* **40**, 644-652 (2012).
681 Cook, C., Stankowski, J. N., Carlomagno, Y., Stetler, C. & Petrucelli, L. Acetylation: a new key to unlock tau's role in neurodegeneration. *Alzheimers Res Ther* **6**, 29, doi:10.1186/alzrt259 (2014).
682 Cisek, K., Cooper, G. L., Huseby, C. J. & Kuret, J. Structure and mechanism of action of tau aggregation inhibitors. *Curr Alzheimer Res* **11**, 918-927, doi:10.2174/1567205011666141107150331 (2014).
683 Wischik, C., Edwards, P., Lai, R., Roth, M. & Harrington, C. Selective inhibition of Alzheimer disease-like tau aggregation by phenothiazines. *Proceedings of the National Academy of Sciences* **93**, 11213-11218 (1996).
684 Landau, M. *et al.* Towards a pharmacophore for amyloid. *PLoS biology* **9**, e1001080 (2011).
685 Li, W. *et al.* Inhibition of tau fibrillization by oleocanthal via reaction with the amino groups of tau. *Journal of neurochemistry* **110**, 1339-1351, doi:10.1111/j.1471-4159.2009.06224.x (2009).
686 Sinha, S. *et al.* Lysine-Specific Molecular Tweezers Are Broad-Spectrum Inhibitors of Assembly and Toxicity of Amyloid Proteins. *Journal of the American Chemical Society* **133**, 16958-16969, doi:10.1021/ja206279b (2011).
687 Akoury, E. *et al.* Inhibition of tau filament formation by conformational modulation. *Journal of the American Chemical Society* **135**, 2853-2862 (2013).
688 Dolai, S. *et al.* "Clicked" sugar–curcumin conjugate: modulator of amyloid-β and tau peptide aggregation at ultralow concentrations. *ACS chemical neuroscience* **2**, 694-699 (2011).
689 Fuse, S., Matsumura, K., Fujita, Y., Sugimoto, H. & Takahashi, T. Development of dual targeting inhibitors against aggregations of amyloid-β and tau protein. *European journal of medicinal chemistry* **85**, 228-234 (2014).
690 Klingstedt, T. & Nilsson, K. P. R. Luminescent conjugated poly-and oligo-thiophenes: optical ligands for spectral assignment of a plethora of protein aggregates. *Biochem Soc Trans* **40**, 704-710 (2012).
691 Congdon, E. E. & Sigurdsson, E. M. Tau-targeting therapies for Alzheimer disease. *Nature reviews. Neurology* **14**, 399-415, doi:10.1038/s41582-018-0013-z (2018).
692 Soeda, Y. *et al.* Methylene Blue Inhibits Formation of Tau Fibrils but not of Granular Tau Oligomers: A Plausible Key to Understanding Failure of a Clinical Trial for Alzheimer's Disease. *Journal of Alzheimer's disease : JAD* **68**, 1677-1686, doi:10.3233/jad-181001 (2019).
693 Crowe, A. *et al.* Aminothienopyridazines and methylene blue affect Tau fibrillization via cysteine oxidation. *The Journal of biological chemistry* **288**, 11024-11037, doi:10.1074/jbc.M112.436006 (2013).
694 Ballatore, C. *et al.* Aminothienopyridazine inhibitors of tau aggregation: evaluation of structure-activity relationship leads to selection of candidates with desirable in vivo properties. *Bioorg Med Chem* **20**, 4451-4461, doi:10.1016/j.bmc.2012.05.027 (2012).

695 Congdon, E. E. *et al.* Methylthioninium chloride (methylene blue) induces autophagy and attenuates tauopathy in vitro and in vivo. *Autophagy* **8**, 609-622 (2012).
696 Sun, W. *et al.* Attenuation of synaptic toxicity and MARK4/PAR1-mediated Tau phosphorylation by methylene blue for Alzheimer's disease treatment. *Scientific reports* **6**, 1-10 (2016).
697 Stack, C. *et al.* Methylene blue upregulates Nrf2/ARE genes and prevents tau-related neurotoxicity. *Human molecular genetics* **23**, 3716-3732, doi:10.1093/hmg/ddu080 (2014).
698 Williams, J. R. & Challis, F. E. Methylene blue as an antidote for anilin dye poisoning: case report with confirmatory experimental study. *The Journal of Laboratory and Clinical Medicine* **19**, 166-171 (1933).
699 STEELE, C. W. & SPINK, W. W. Methylene blue in the treatment of poisonings associated with methemoglobinemia. *New England Journal of Medicine* **208**, 1152-1153 (1933).
700 Jack Clifton, I. & Leikin, J. B. Methylene blue. *American journal of therapeutics* **10**, 289-291 (2003).
701 Guttmann, P. & Ehrlich, P. in *The Collected Papers of Paul Ehrlich* 9-14 (Elsevier, 1960).
702 Lu, G. *et al.* Efficacy and safety of methylene blue in the treatment of malaria: a systematic review. *BMC Med* **16**, 1-16 (2018).
703 Delport, A., Harvey, B. H., Petzer, A. & Petzer, J. P. Methylene blue and its analogues as antidepressant compounds. *Metabolic brain disease* **32**, 1357-1382 (2017).
704 Oz, M. *et al.* Methylene blue inhibits function of the 5-HT transporter. *Br J Pharmacol* **166**, 168-176 (2012).
705 Telch, M. J. *et al.* Effects of post-session administration of methylene blue on fear extinction and contextual memory in adults with claustrophobia. *Am J Psychiatry* **171**, 1091-1098, doi:10.1176/appi.ajp.2014.13101407 (2014).
706 Oz, M., Lorke, D. E., Hasan, M. & Petroianu, G. A. Cellular and molecular actions of Methylene Blue in the nervous system. *Med Res Rev* **31**, 93-117, doi:10.1002/med.20177 (2011).
707 Melis, V. *et al.* Effects of oxidized and reduced forms of methylthioninium in two transgenic mouse tauopathy models. *Behavioural Pharmacology* **26**, 353 (2015).
708 Harrington, C. R. *et al.* Cellular models of aggregation-dependent template-directed proteolysis to characterize tau aggregation inhibitors for treatment of Alzheimer disease. *Journal of Biological Chemistry* **290**, 10862-10875 (2015).
709 Colin, M. *et al.* From the prion-like propagation hypothesis to therapeutic strategies of anti-tau immunotherapy. *Acta neuropathologica* **139**, 3-25, doi:10.1007/s00401-019-02087-9 (2020).
710 Pizzarelli, R., Pediconi, N. & Di Angelantonio, S. Molecular Imaging of Tau Protein: New Insights and Future Directions. *Frontiers in molecular neuroscience* **13**, 586169, doi:10.3389/fnmol.2020.586169 (2020).
711 Shi, Y. *et al.* Cryo-EM structures of tau filaments from Alzheimer's disease with PET ligand APN-1607. *Acta neuropathologica*, doi:10.1007/s00401-021-02294-3 (2021).
712 Sandusky-Beltran, L. A. & Sigurdsson, E. M. Tau immunotherapies: Lessons learned, current status and future considerations. *Neuropharmacology* **175**, 108104, doi:https://doi.org/10.1016/j.neuropharm.2020.108104 (2020).
713 West, T. *et al.* Preclinical and Clinical Development of ABBV-8E12, a Humanized Anti-Tau Antibody, for Treatment of Alzheimer's Disease and Other Tauopathies. *J Prev Alzheimers Dis* **4**, 236-241, doi:10.14283/jpad.2017.36 (2017).
714 Bateman, R. J. *et al.* The DIAN-TU Next Generation Alzheimer's prevention trial: Adaptive design and disease progression model. *Alzheimers Dement* **13**, 8-19, doi:10.1016/j.jalz.2016.07.005 (2017).
715 Dunn, B., Stein, P. & Cavazzoni, P. Approval of Aducanumab for Alzheimer Disease—the FDA's Perspective. *JAMA internal medicine* (2021).
716 Alexander, G. C. *et al.* Revisiting FDA Approval of Aducanumab. *New England Journal of Medicine* **385**, 769-771 (2021).
717 Food & Administration, D.
718 Bussiere, T. *et al.* Differential in vitro and in vivo binding profiles of BIIB037 and other anti-abeta clinical antibody candidates. *Neurodegener Dis* **11** (2013).
719 Kontsekova, E., Zilka, N., Kovacech, B., Novak, P. & Novak, M. First-in-man tau vaccine targeting structural determinants essential for pathological tau–tau interaction reduces tau oligomerisation and neurofibrillary degeneration in an Alzheimer's disease model. *Alzheimers Res Ther* **6**, 1-12 (2014).

720 Theunis, C. *et al.* Efficacy and safety of a liposome-based vaccine against protein Tau, assessed in tau. P301L mice that model tauopathy. *PloS one* **8**, e72301 (2013).
721 Messer, A. & Butler, D. C. Optimizing intracellular antibodies (intrabodies/nanobodies) to treat neurodegenerative disorders. *Neurobiol Dis* **134**, 104619 (2020).
722 Visintin, M. *et al.* The intracellular antibody capture technology (IACT): towards a consensus sequence for intracellular antibodies11Edited by J. Karn. *Journal of molecular biology* **317**, 73-83, doi:https://doi.org/10.1006/jmbi.2002.5392 (2002).
723 Nisbet, R. M. *et al.* Combined effects of scanning ultrasound and a tau-specific single chain antibody in a tau transgenic mouse model. *Brain* **140**, 1220-1230 (2017).
724 Goodwin, M. S. *et al.* Anti-tau scFvs Targeted to the Cytoplasm or Secretory Pathway Variably Modify Pathology and Neurodegenerative Phenotypes. *Mol Ther* **29**, 859-872, doi:10.1016/j.ymthe.2020.10.007 (2021).
725 Danis, C. *et al.* Inhibition of Tau seeding by targeting Tau nucleation core within neurons with a single domain antibody fragment. *bioRxiv*, 2021.2003.2023.436266, doi:10.1101/2021.03.23.436266 (2021).
726 Wang, Y., Jiang, X., Feng, F., Liu, W. & Sun, H. Degradation of proteins by PROTACs and other strategies. *Acta Pharmaceutica Sinica B* **10**, 207-238, doi:https://doi.org/10.1016/j.apsb.2019.08.001 (2020).
727 Gao, H., Sun, X. & Rao, Y. PROTAC Technology: Opportunities and Challenges. *ACS medicinal chemistry letters* **11**, 237-240, doi:10.1021/acsmedchemlett.9b00597 (2020).
728 McCoull, W. *et al.* Development of a Novel B-Cell Lymphoma 6 (BCL6) PROTAC To Provide Insight into Small Molecule Targeting of BCL6. *ACS Chem. Biol.* **13**, 3131 (2018).
729 Popow, J. *et al.* Highly Selective PTK2 Proteolysis Targeting Chimeras to Probe Focal Adhesion Kinase Scaffolding Functions. *J. Med. Chem.* **62**, 2508 (2019).
730 Neklesa, T. *et al. ARV-110: an oral androgen receptor PROTAC degrader for prostate cancer*. (2019).
731 Flanagan, J. J. *et al. ARV-471, an oral estrogen receptor PROTAC protein degrader for breast cancer*. (2018).
732 Zorba, A. *et al.* Delineating the role of cooperativity in the design of potent PROTACs for BTK. *Proc. Natl. Acad. Sci. U. S. A.* **115**, E7285 (2018).
733 Bassi, Z. I. *et al.* Modulating PCAF/GCN5 Immune Cell Function through a PROTAC Approach. *ACS Chem. Biol.* **13**, 2862 (2018).
734 Nunes, J. *et al.* Targeting IRAK4 for Degradation with PROTACs. *ACS Med. Chem. Lett.* **10**, 1081 (2019).
735 Bai, L. *et al.* A Potent and Selective Small-Molecule Degrader of STAT3 Achieves Complete Tumor Regression In Vivo. *Cancer Cell* **36**, 498 (2019).
736 Chu, T.-T. *et al.* Specific Knockdown of Endogenous Tau Protein by Peptide-Directed Ubiquitin-Proteasome Degradation. *Cell Chem Biol* **23**, 453-461, doi:https://doi.org/10.1016/j.chembiol.2016.02.016 (2016).
737 Lu, M. *et al.* Discovery of a Keap1-dependent peptide PROTAC to knockdown Tau by ubiquitination-proteasome degradation pathway. *European journal of medicinal chemistry* **146**, 251-259, doi:https://doi.org/10.1016/j.ejmech.2018.01.063 (2018).
738 Kargbo, R. B. Treatment of Alzheimer's by PROTAC-Tau Protein Degradation. *ACS medicinal chemistry letters* **10**, 699-700, doi:10.1021/acsmedchemlett.9b00083 (2019).
739 Silva, M. C. *et al.* Targeted degradation of aberrant tau in frontotemporal dementia patient-derived neuronal cell models. *eLife* **8** (2019). <http://europepmc.org/abstract/MED/30907729

https://doi.org/10.7554/eLife.45457

https://europepmc.org/articles/PMC6450673

https://europepmc.org/articles/PMC6450673?pdf=render>.
740 Wang, W. *et al.* A novel small-molecule PROTAC selectively promotes tau clearance to improve cognitive functions in Alzheimer-like models. *Theranostics* **11**, 5279-5295, doi:10.7150/thno.55680 (2021).
741 Guo, J. L. *et al.* The Dynamics and Turnover of Tau Aggregates in Cultured Cells: INSIGHTS INTO THERAPIES FOR TAUOPATHIES. *The Journal of biological chemistry* **291**, 13175-13193, doi:10.1074/jbc.M115.712083 (2016).

742 Lee, M. J., Lee, J. H. & Rubinsztein, D. C. Tau degradation: the ubiquitin-proteasome system versus the autophagy-lysosome system. *Prog Neurobiol* **105**, 49-59, doi:10.1016/j.pneurobio.2013.03.001 (2013).
743 Chu, T.-T. *et al.* Clearance of the intracellular high level of the tau protein directed by an artificial synthetic hydrolase. *Mol Biosyst* **10**, 3081-3085 (2014).
744 Zhou, Y., Li, J., Nordberg, A. & Ågren, H. Dissecting the Binding Profile of PET Tracers to Corticobasal Degeneration Tau Fibrils. *ACS chemical neuroscience* **12**, 3487-3496, doi:10.1021/acschemneuro.1c00536 (2021).
745 Limorenko, G. & Lashuel, H. A. To target Tau pathologies, we must embrace and reconstruct their complexities. *Neurobiol Dis* **161**, 105536 (2021).
746 Golde, T. E. Alzheimer's disease - the journey of a healthy brain into organ failure. *Mol Neurodegener* **17**, 18, doi:10.1186/s13024-022-00523-1 (2022).
747 Goedert, M. *et al.* Assembly of microtubule-associated protein tau into Alzheimer-like filaments induced by sulphated glycosaminoglycans. *Nature* **383**, 550 (1996).
748 Horvath, I., Rocha, S. & Wittung-Stafshede, P. in *Amyloid Proteins* 73-83 (Springer, 2018).
749 Sasanian, N., Bernson, D., Horvath, I., Wittung-Stafshede, P. & Esbjörner, E. K. Redox-Dependent Copper Ion Modulation of Amyloid-β (1-42) Aggregation In Vitro. *Biomolecules* **10**, 924 (2020).
750 Azzam, S. K. *et al.* Inhibition of Human Amylin Aggregation and Cellular Toxicity by Lipoic Acid and Ascorbic Acid. *Molecular Pharmaceutics* **15**, 2098-2106, doi:10.1021/acs.molpharmaceut.7b01009 (2018).
751 Limorenko, G. & Lashuel, H. A. Revisiting the grammar of Tau aggregation and pathology formation: how new insights from brain pathology are shaping how we study and target Tauopathies. *Chem Soc Rev* (2022).
752 Linhardt, R. J., Murugesan, S. & Xie, J. Immobilization of heparin: approaches and applications. *Curr Top Med Chem* **8**, 80-100 (2008).
753 Holmes, B. B. *et al.* Proteopathic tau seeding predicts tauopathy in vivo. *Proceedings of the National Academy of Sciences of the United States of America* **111**, E4376-4385, doi:10.1073/pnas.1411649111 (2014).
754 Lo, C. H. Recent advances in cellular biosensor technology to investigate tau oligomerization. *Bioeng Transl Med* **6**, e10231, doi:10.1002/btm2.10231 (2021).
755 Furman, J. L. & Diamond, M. I. in *Tau Protein* 349-359 (Springer, 2017).
756 Manos, J. D. *et al.* Uncovering specificity of endogenous TAU aggregation in a human iPSC-neuron TAU seeding model. *iScience* **25**, 103658, doi:https://doi.org/10.1016/j.isci.2021.103658 (2022).
757 Farid, M., Corbo, C. P. & Alonso Adel, C. Tau binds ATP and induces its aggregation. *Microscopy research and technique* **77**, 133-137, doi:10.1002/jemt.22319 (2014).
758 Boyko, S. & Surewicz, W. K. Tau liquid–liquid phase separation in neurodegenerative diseases. *Trends in Cell Biology* (2022).
759 Hutton, M. *et al.* Association of missense and 5'-splice-site mutations in tau with the inherited dementia FTDP-17. *Nature* **393**, 702 (1998).
760 Roy, S. & Bhat, R. Suppression, disaggregation, and modulation of γ-Synuclein fibrillation pathway by green tea polyphenol EGCG. *Protein Sci* **28**, 382-402, doi:10.1002/pro.3549 (2019).
761 Andersen, C. B., Yoshimura, Y., Nielsen, J., Otzen, D. E. & Mulder, F. A. A. How epigallocatechin gallate binds and assembles oligomeric forms of human alpha-synuclein. *The Journal of biological chemistry* **296**, 100788, doi:10.1016/j.jbc.2021.100788 (2021).
762 Bae, E. J. *et al.* Lipid peroxidation product 4-hydroxy-2-nonenal promotes seeding-capable oligomer formation and cell-to-cell transfer of α-synuclein. *Antioxid Redox Signal* **18**, 770-783, doi:10.1089/ars.2011.4429 (2013).
763 Andersen, C. *et al.* Lipid Peroxidation Products HNE and ONE Promote and Stabilize Alpha-Synuclein Oligomers by Chemical Modifications. *Biochemistry* **60**, 3644-3658, doi:10.1021/acs.biochem.1c00478 (2021).
764 Qin, Z. *et al.* Effect of 4-hydroxy-2-nonenal modification on alpha-synuclein aggregation. *The Journal of biological chemistry* **282**, 5862-5870, doi:10.1074/jbc.M608126200 (2007).
765 Ehrnhoefer, D. E. *et al.* EGCG redirects amyloidogenic polypeptides into unstructured, off-pathway oligomers. *Nat Struct Mol Biol* **15**, 558-566, doi:10.1038/nsmb.1437 (2008).

766 Wischik, C. M., Edwards, P. C., Lai, R. Y., Roth, M. & Harrington, C. R. Selective inhibition of Alzheimer disease-like tau aggregation by phenothiazines. *Proceedings of the National Academy of Sciences of the United States of America* **93**, 11213-11218, doi:10.1073/pnas.93.20.11213 (1996).
767 Lövestam, S. *et al.* Assembly of recombinant tau into filaments identical to those of Alzheimer's disease and chronic traumatic encephalopathy. *bioRxiv*, 2021.2012.2016.472950, doi:10.1101/2021.12.16.472950 (2021).
768 Shi, Y. *et al.* Structure-based classification of tauopathies. *Nature* **598**, 359-363 (2021).
769 Abràmoff, M. D., Magalhães, P. J. & Ram, S. J. Image processing with ImageJ. *Biophotonics international* **11**, 36-42 (2004).
770 Mastronarde, D. N. Automated electron microscope tomography using robust prediction of specimen movements. *J Struct Biol* **152**, 36-51 (2005).
771 Biyani, N. *et al.* Focus: The interface between data collection and data processing in cryo-EM. *J Struct Biol* **198**, 124-133 (2017).
772 Punjani, A., Rubinstein, J. L., Fleet, D. J. & Brubaker, M. A. cryoSPARC: algorithms for rapid unsupervised cryo-EM structure determination. *Nature methods* **14**, 290-296 (2017).
773 Schrodinger, LLC. *The PyMOL Molecular Graphics System, Version 1.8* (2015).
774 Organization, W. H. (2020).
775 Forster, T. Energiewanderung und fluoreszenz. *Naturwissenschaften* **33**, 166-175 (1946).
776 Berney, C. & Danuser, G. FRET or no FRET: a quantitative comparison. *Biophysical journal* **84**, 3992-4010 (2003).
777 Algar, W. R., Hildebrandt, N., Vogel, S. S. & Medintz, I. L. FRET as a biomolecular research tool—understanding its potential while avoiding pitfalls. *Nature methods* **16**, 815-829 (2019).
778 Bajar, B. T., Wang, E. S., Zhang, S., Lin, M. Z. & Chu, J. A Guide to Fluorescent Protein FRET Pairs. *Sensors (Basel)* **16**, 1488, doi:10.3390/s16091488 (2016).
779 Drescher, M., Huber, M. & Subramaniam, V. Hunting the Chameleon: Structural Conformations of the Intrinsically Disordered Protein Alpha-Synuclein. *Chembiochem* **13**, 761-768, doi:https://doi.org/10.1002/cbic.201200059 (2012).
780 Mudher, A. *et al.* What is the evidence that tau pathology spreads through prion-like propagation? *Acta Neuropathol Commun* **5**, 99, doi:10.1186/s40478-017-0488-7 (2017).
781 Holmes, B. B. *et al.* Proteopathic Tau Seeding Predicts Tauopathy in Vivo. *Proc. Natl. Acad. Sci. U. S. A.* **111**, E4376 (2014).
782 Sanders, David W. *et al.* Distinct Tau Prion Strains Propagate in Cells and Mice and Define Different Tauopathies. *Neuron* **82**, 1271-1288, doi:https://doi.org/10.1016/j.neuron.2014.04.047 (2014).
783 Sharma, A. M., Thomas, T. L., Woodard, D. R., Kashmer, O. M. & Diamond, M. I. Tau monomer encodes strains. *eLife* **7** (2018). <http://europepmc.org/abstract/MED/30526844

https://doi.org/10.7554/eLife.37813

https://europepmc.org/articles/PMC6289568

https://europepmc.org/articles/PMC6289568?pdf=render>.
784 Ait-Bouziad, N. *et al.* Discovery and characterization of stable and toxic Tau/phospholipid oligomeric complexes. *Nat Commun* **8**, 1678, doi:10.1038/s41467-017-01575-4 (2017).
785 Ganesan, D. & Cai, Q. Understanding amphisomes. *Biochem J* **478**, 1959-1976, doi:10.1042/bcj20200917 (2021).
786 Addi, C. *et al.* The Flemmingsome reveals an ESCRT-to-membrane coupling via ALIX/syntenin/syndecan-4 required for completion of cytokinesis. *Nat Commun* **11**, 1941, doi:10.1038/s41467-020-15205-z (2020).
787 Chavrier, P., Parton, R. G., Hauri, H. P., Simons, K. & Zerial, M. Localization of low molecular weight GTP binding proteins to exocytic and endocytic compartments. *Cell* **62**, 317-329, doi:10.1016/0092-8674(90)90369-p (1990).
788 Jäger, S. *et al.* Role for Rab7 in maturation of late autophagic vacuoles. *J Cell Sci* **117**, 4837-4848, doi:10.1242/jcs.01370 (2004).

789 Goksu, E. I., Vanegas, J. M., Blanchette, C. D., Lin, W. C. & Longo, M. L. AFM for structure and dynamics of biomembranes. *Biochimica et biophysica acta* **1788**, 254-266, doi:10.1016/j.bbamem.2008.08.021 (2009).
790 Zhu, S. Y. *et al.* Lysosomal quality control of cell fate: a novel therapeutic target for human diseases. *Cell Death Dis* **11**, 817, doi:10.1038/s41419-020-03032-5 (2020).
791 Fowler, W. E. & Aebi, U. A consistent picture of the actin filament related to the orientation of the actin molecule. *J Cell Biol* **97**, 264-269 (1983).
792 Hochmair, J. *et al.* Molecular crowding and RNA synergize to promote phase separation, microtubule interaction, and seeding of Tau condensates. *EMBO J* **41**, e108882, doi:https://doi.org/10.15252/embj.2021108882 (2022).
793 Puangmalai, N. *et al.* Lysine 63-linked ubiquitination of tau oligomers contributes to the pathogenesis of Alzheimer’s disease. *Journal of Biological Chemistry* **298**, doi:10.1016/j.jbc.2022.101766 (2022).
794 Mann, C. N. *et al.* Astrocytic α2-Na+/K+ ATPase inhibition suppresses astrocyte reactivity and reduces neurodegeneration in a tauopathy mouse model. *Sci Transl Med* **14**, eabm4107 (2022).
795 Kolay, S. *et al.* The dual fates of exogenous tau seeds: Lysosomal clearance versus cytoplasmic amplification. *Journal of Biological Chemistry* **298**, doi:10.1016/j.jbc.2022.102014 (2022).
796 Polanco, J. C. *et al.* Genome-wide CRISPRi screening reveals regulators of Alzheimer's tau pathology shared between exosomal and vesicle-free tau seeds. *bioRxiv*, 2022.2004.2026.489622, doi:10.1101/2022.04.26.489622 (2022).
797 Helboe, L. *et al.* Highly Specific and Sensitive Target Binding by the Humanized pS396-Tau Antibody hC10.2 Across a Wide Spectrum of Alzheimer's Disease and Primary Tauopathy Postmortem Brains. *Journal of Alzheimer's Disease* **Preprint**, 1-22, doi:10.3233/JAD-220125 (2022).
798 Dodd, D. A. *et al.* Tau seeds translocate across the cell membrane to initiate aggregation. *bioRxiv*, 2022.2005.2010.491429, doi:10.1101/2022.05.10.491429 (2022).
799 LaCroix, M. S. *et al.* Tau seeding without tauopathy. *bioRxiv*, 2022.2002.2003.479049, doi:10.1101/2022.02.03.479049 (2022).
800 Choi, C.-S. *et al.* Cytotoxic tau released from lung microvascular endothelial cells upon infection with Pseudomonas aeruginosa promotes neuronal tauopathy. *Journal of Biological Chemistry* **298**, doi:10.1016/j.jbc.2021.101482 (2022).
801 Saroja, S. R., Sharma, A., Hof, P. R. & Pereira, A. C. Differential expression of tau species and the association with cognitive decline and synaptic loss in Alzheimer's disease. *Alzheimer's & Dementia* **n/a**, doi:https://doi.org/10.1002/alz.12518 (2021).
802 Danis, C. *et al.* Inhibition of Tau seeding by targeting Tau nucleation core within neurons with a single domain antibody fragment. *Molecular Therapy* **30**, 1484-1499 (2022).
803 Saroja, S. R., Gorbachev, K., TCW, J., Goate, A. M. & Pereira, A. C. Astrocyte-secreted glypican-4 drives APOE4-dependent tau pathology. *bioRxiv*, 2021.2007.2007.451493, doi:10.1101/2021.07.07.451493 (2021).
804 Annadurai, N. *et al.* Antitumour drugs targeting tau R3 VQIVYK and Cys322 prevent seeding of endogenous tau aggregates by exogenous seeds. *The FEBS journal* **289**, 1929-1949, doi:https://doi.org/10.1111/febs.16270 (2022).
805 Meisl, G. *et al.* In vivo rate-determining steps of tau seed accumulation in Alzheimer’s disease. *Sci Adv* **7**, eabh1448, doi:doi:10.1126/sciadv.abh1448 (2021).
806 Stopschinski, B. E. *et al.* Anatomic survey of seeding in Alzheimer's disease brains reveals unexpected patterns. *Acta Neuropathol Commun* **9**, 164, doi:10.1186/s40478-021-01255-x (2021).
807 Kaufman, S. K., Svirsky, S., Cherry, J. D., McKee, A. C. & Diamond, M. I. Tau seeding in chronic traumatic encephalopathy parallels disease severity. *Acta neuropathologica* **142**, 951-960, doi:10.1007/s00401-021-02373-5 (2021).
808 Leroux, E. *et al.* Extracellular vesicles: Major actors of heterogeneity in tau spreading among human tauopathies. *Molecular Therapy* **30**, 782-797, doi:https://doi.org/10.1016/j.ymthe.2021.09.020 (2022).
809 Patel, H. *et al.* Pathological tau and reactive astrogliosis are associated with distinct functional deficits in a mouse model of tauopathy. *Neurobiology of aging* **109**, 52-63, doi:https://doi.org/10.1016/j.neurobiolaging.2021.09.006 (2022).

810 Fernandes, A. R., Dujardin, S., Maté de Gérando, A., Hyman, B. T. & Frosch, M. P. Impact of Sterilization Methods on the Seeding Ability of Human Tau Proteopathic Seeds. *Journal of Neuropathology & Experimental Neurology* **80**, 912-921, doi:10.1093/jnen/nlab087 (2021).

811 Capano, L. S. *et al.* Recapitulation of endogenous 4R tau expression and formation of insoluble tau in directly reprogrammed human neurons. *Cell Stem Cell* **29**, 918-932.e918, doi:https://doi.org/10.1016/j.stem.2022.04.018 (2022).

CV

GALINA LIMORENKO
galina.lim@gmail.com

education and training

PhD Neuroscience *2018-2023*
H. Lashuel Lab, EPFL, Switzerland

thesis: Deconstructing and Reconstructing Complexity of Tau Pathology
nomination for Doctoral Thesis award 2023, top 8%

BSc Genetics *2013-2018*
V. Buchman Lab, Cardiff University, United Kingdom
professional training year in *Lund University, Sweden 2016-2017*

dissertation: Investigation of biochemical features and physiological effects of mutated human γ-synuclein variants *in vitro* and *in vivo*
winner of Biochemical Society Undergraduate Recognition Award 2018

post-secondary

2010-2013
- EQL Level 3 in British Horse Society PTT
- EQL Level 2 Award in the Principles of Coaching Sport
- IES Certificate Equine Business

Yale College/ Coleg Cambria, Wrexham, United Kingdom

2008-2010
Karaliaus Mindaugo Professional Education Centre, Lithuania

PhD courses
- electrochemical nano-bio-sensing and bio/CMOS interfaces
- the making of an innovative medicine
- 3D Electron microscopy and FIB-nanotomography
- videomaking for science communication

teaching assistance
- fundamentals of biosensors and electronic biochips selected topics in life sciences
- neuroscience: from molecular mechanisms to disease
- physiology lab

publications **ORCiD: 0000-0002-6319-0257**

conferences
- *AD/PD 2019, Lisbon, Portugal*
- *Synuclein 2018, EPFL, Switzerland*
- *20 years of a-synuclein, 2017, Athens, Greece*
- *Latsis Symposium 2022, EPFL, Switzerland*

experience

recombinant protein expression and purification
- DNA and RNA isolation/manipulation (CRISPR/Cas) liquid chromatography (RP-HPLC, UPLC)
- mass spectrometry (LC/MS/MS, MALDI)
- protein blots and aggregation assays (Western, ELISA, ThT/S)

cell cultures
- cell lines (HEK293, HeLa, C2C12)
- primary neuronal and retinal cultures (mouse, rat, embryonic, postnatal)
- cryopreservation of primary neurons (cost-efficient) microinjection into adherent cells
- laser-capture microdissection flow cytometry

animal models
- RESAL Module I training
- mouse stereotaxic brain injection and dissection behavioural tests (Rotarod, grip test, open field, CatWalk ™)
- 3D mouse brain imaging CLARITY

microscopy and imaging
- electron and atomic force microscopy immunohistochemistry, immunocytochemistry confocal, epifluorescent
- correlative light and electron microscopy (CLEM)
- live-cell (Operetta, Cellomics ™)
- super-resolution (FRET, FLIM, STED)
- Image processing and 3D reconstruction using ImageJ, NISelements© and open source tools

bioinformatics and data analysis
- Python, R, Microsoft Office Tools, GraphPad Prism advanced user of open-source and proprietary software (CellProfiler, MEGA, LDhot, Adobe Suite Tools, Fiji, QuPath, MaxQuant, genomic and proteomic databases)

social engagement
- science podcast host and producer
- contributing science writer
- eLife Ambassador 2019-2020
- OSiP2019 Summer School organizer and speaker @LashuelLab Twitter account manager
- snooker player, Cardiff University BUCS winning team, 2015
- endurance runner, hiker, Sarek National Park, Sweden, 2017
- armchair quantum physicist